AFML-TR-77-56

THE EFFECT OF MINOR ALLOYING ELEMENT ADDITIONS ON MECHANICAL PROPERTIES OF TITANIUM ALLOYS

ROCKWELL INTERNATIONAL SCIENCE CENTER
THOUSAND OAKS, CALIFORNIA 91360

MAY 1977

TECHNICAL REPORT AFML-TR-77-56
Final Report for Period December 1974 – December 1976

Approved for public release; distribution unlimited.

UNITED STATES AIR FORCE
AIR FORCE SYSTEMS COMMAND
AERONAUTICAL SYSTEMS DIVISION / PPMRR
WRIGHT-PATTERSON AIR FORCE BASE, OHIO 45433

NOTICE

When Government drawings, specifications, or other data are used for any purpose other than in connection with a definitely related Government procurement operation, the United States Government thereby incurs no responsibility nor any obligation whatsoever; and the fact that the government may have formulated, furnished, or in any way supplied the said drawings, specifications, or other data, is not to be regarded by implication or otherwise as in any manner licensing the holder or any other person or corporation, or conveying any rights or permission to manufacture, use or sell any patented invention that may in any way be related thereto.

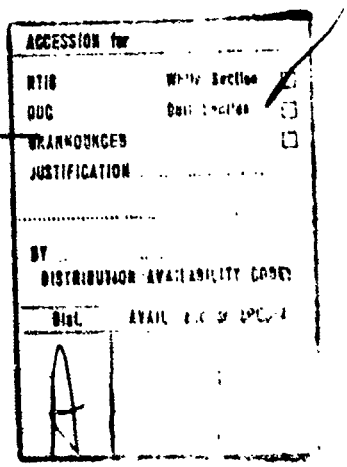

Paul J. Bania
Project Engineer

FOR THE COMMANDER

Nathan G. Tupper
NATHAN G. TUPPER
Acting Chief
Structural Metals Branch
Metals and Ceramics Division

Copies of this report should not be returned unless return is required by security consideration, contractual obligations, or notice on a specific document.

AIR FORCE/56780/31 October 1977 — 250

Unclassified

SECURITY CLASSIFICATION OF THIS PAGE (When Data Entered)

REPORT DOCUMENTATION PAGE	READ INSTRUCTIONS BEFORE COMPLETING FORM
1. REPORT NUMBER: AFML-TR-77-56	2. GOVT ACCESSION NO.
	3. RECIPIENT'S CATALOG NUMBER
4. TITLE (and Subtitle): THE EFFECT OF MINOR ALLOYING ELEMENT ADDITIONS ON MECHANICAL PROPERTIES OF TITANIUM ALLOYS	5. TYPE OF REPORT & PERIOD COVERED: Technical Report 12/15/74 thru 12/15/76
	6. PERFORMING ORG. REPORT NUMBER: SC5011.25TR
7. AUTHOR(s): M. W. Mahoney & N. E. Paton - Science Center, Rockwell International; W.M. Parris & J.A. Hall - TIMET	8. CONTRACT OR GRANT NUMBER(s): F33615-75-C-5089
9. PERFORMING ORGANIZATION NAME AND ADDRESS: Science Center, Rockwell International, 1049 Camino Dos Rios, Thousand Oaks, CA 91360	10. PROGRAM ELEMENT, PROJECT, TASK AREA & WORK UNIT NUMBERS: 7353-02-18
11. CONTROLLING OFFICE NAME AND ADDRESS: Air Force Materials Laboratory (LLS), Air Force Systems Command, Wright-Patterson AF Base, Ohio 45433	12. REPORT DATE: May 1977
	13. NUMBER OF PAGES: 196
14. MONITORING AGENCY NAME & ADDRESS(if different from Controlling Office): 243p.	15. SECURITY CLASS. (of this report): Unclassified
	15a. DECLASSIFICATION DOWNGRADING SCHEDULE

16. DISTRIBUTION STATEMENT (of this Report)

Approved for public release; distribution unlimited.

17. DISTRIBUTION STATEMENT (of the abstract entered in Block 20, if different from Report)

18. SUPPLEMENTARY NOTES

19. KEY WORDS (Continue on reverse side if necessary and identify by block number)

Creep, Fatigue, Fracture, Titanium, Mechanical Properties, Minor Element Additions to Composition, Alloy Partitioning, Microstructure, Effect of Si Additions.

20. ABSTRACT (Continue on reverse side if necessary and identify by block number)

This Technical Report describes a research program conducted jointly by the Science Center, Rockwell International, and TIMET, to study the effects of minor element additions on the mechanical properties of titanium alloys. The effect of additions of Si, B, Fe, S and O on mechanical properties of a base alloy of composition Ti-6Al-2Sn-2Zr-1Mo have been studied. In this Technical Report final results on tensile, creep, creep stability, alloy partitioning, fatigue, fracture, hot salt stress corrosion, and microstructural characterization of these alloys is presented.

DD FORM 1 JAN 73 1473 EDITION OF 1 NOV 65 IS OBSOLETE

Unclassified

SECURITY CLASSIFICATION OF THIS PAGE (When Data Entered)

389749

Foreword

This Technical Report covers a joint research program performed at the Science Center, Rockwell International, and at TIMET, Henderson, Nevada, under Contract No. F33615-75-C-5089. The program was initiated under Project No. 7353 and was administered under the direction of the Air Force Materials Laboratory, Air Force Systems Command, with Mr. Paul J. Ban'a as Project Engineer. Dr. L. Bidwell also assisted in administration of the program. In addition, Dr. H. Rosenberg of TIMET, contributed to the planning and initiation of tasks described herein.

This report covers the period December 15, 1974, to December 15, 1976, and was released by the Science Center, Rockwell International on January 14, 1977.

TABLE OF CONTENTS

Page

TABLES

FIGURE CAPTIONS

SECTION I
INTRODUCTION

The contribution of minor alloying element additions to the development of high temperature creep resistant titanium alloys is becoming increasingly more important in alloy design. For example, several newly developed Ti alloys have included silicon as a minor alloying addition.[1,2,3] However, the role that silicon plays in enhancing the creep strength of such alloys has been the subject of discussion in the literature. Anthony[4] has suggested that silicon plays two roles in such alloys, i) as a solid solution strengthener, and ii) as a means of providing a dispersion hardening silicide phase. However, it has been found that aging of such alloys generally degrades the creep strength[5] suggesting that (ii) is in fact not the case. This latter observation lends support to the views of Rosenberg[6] and Flower et al[7] who are of the opinion that the effect of Si is to provide an atmosphere drag on moving dislocations. This has been substantiated recently by Paton and Mahoney[5] who have shown that at low strain rates ($<10^{-4}$ Hr^{-1} at 1000F) silicon forms precipitates on moving dislocations, the motion of which is then restricted during creep. At strain rates above $\sim 10^{-4}$ Hr^{-1}, under the test conditions used, Paton et al[5] showed that a considerable enhancement in creep strength was still provided by Si additions and in this case the improvement was probably due to atmosphere drag (in agreement with the views of Rosenberg) since precipitates were no longer observed. Although the effect of Si has been examined in some detail, the general problem of systematically investigating the individual and combined effects of minor alloying element additions such as Si, Bi, S, Fe and O has not been studied to date. Thus, a more fundamental and precise understanding

of the effects of these minor alloying elements on the mechanical properties of titanium alloys is essential to continue alloy development along logical and economical paths. In addition, there is generally a lack of information on the effects of these elements on properties other than creep such as toughness and fatigue crack growth rate, particularly at elevated temperatures.

The purpose, therefore, of this program was to determine the effects that certain minor alloying elements might have on the creep, fracture, and mechanical properties of commercial titanium alloys. To this purpose, varying amounts of Si, O_2, Bi, Fe, Mo and S were added to a base alloy of composition Ti-6Al-2Sn-2Zr. The selection of this composition is based on results from various sources, but essentially the Al and Sn are added for solid solution strengthening, the Zr to promote uniform nucleation of silicides or Si bearing precipitates and improve stability, and the Mo to refine the microstructure and improve post-creep ductility. The composition is probably not optimum for maximum creep strength but is an ideal vehicle in which to study the effects of minor element additions. The base alloy composition is similar to a number of commercial alloys which should assist direct transfer of the results of this program to the development of future alloys.

Tests conducted on an extensive series of alloys included creep tests to determine both the effect of temperature and stress on steady state creep rate, tensile and compression properties, fracture toughness and fatigue crack growth rate. In addition to these studies, an investigation was made on the partitioning of elements between the α and β phases, with the objective being to assign the influence of a given element to a change in mechanical properties in the phase or phases to which it partitions. Lastly, an investigation was made of the diffusivity of Bi in Ti, the purpose being to see if a correlation might exist between the diffusivity of Bi and the apparent activation energy for creep of Bi containing alloys.

SECTION II

MATERIALS

Materials necessary for creep and tensile studies included button melts weighing approximately 0.5 lb., and 100 lb. ingots that were subsequently processed into 1/2-inch diameter bar stock. In addition, material from the 100 ingots was processed to 1¼-inch plate to be used for evaluation of toughness and fatigue properties.

Button melts were processed by arc melting a minimum of four times, turning between each melt so that the top and bottom faces of the button were exposed to the arc on the first two melts, and the sides on the subsequent two melts. Compositions were as listed in Tables I and II with EL90 sponge being used as a base. Table I itemizes those compositions used for evaluation of individual minor alloy addition effects, whereas Table II identifies alloy chemistries used to evaluate interaction effects due to multiple additions of minor elements. Except where indicated, oxygen aim for all heats was 0.1%. Buttons were then hot rolled to 1/2-inch round bar stock at 1950F (1338K) with reheating between each pass so that all deformation occurred in the beta field. Specimens for both creep and tensile testing were machined from these bars.

Generally, the button melts were not chemically analyzed but were assumed to have the nominal compositions. In the case of the alloys containing Bi and S, however, some anomalous test results were obtained so all of these buttons were analyzed for the element in question. Analyzed Bi and S contents of the buttons used for the work reported herein are given in Table III. In the case of the Bi alloys, only one of each pair of buttons was analyzed. These chemical results are for companion heats to those used for creep testing and indicate that all of the Bi containing heats have an actual Bi content approximately 30% lower than the nominal, possibly because of losses during melting due to the high vapor pressure of Bi.

Processing of five 100-lb ingots to bar was accomplished as follows:

1. Press forge from 8" dia. to 3" square from 2100F (1422K).
2. Press forge from 3" square to 1 1/2" square from 1950F (1338K).
3. Roll from 1 1/2" square to 1/2" dia. bar at 1950F (1338K) reheating between each rolling pass to assure full beta field processing.

To obtain plate stock from the 100-lb ingots, material was forged from an 8-inch diameter ingot to 2" x 5" x RL sheet bar at 2100F (1422K) and subsequently rolled to 1 1/4-inch thick at 1950F. Results from chemical analysis of these five 100-lb ingots are listed in Table IV. Except where indicated throughout the text, as a last processing step all bar and plate material was heat treated as follows: 1950F (1338K)/15 min, Air Cool + 1300F (978K)/2 hr, Air Cool.

SECTION III

TEST PROCEDURES

3.1 Mechanical Properties

Both tension and compression tests were utilized at times to evaluate mechanical properties of elongation, reduction in area, yield and ultimate strength and post-creep ductility. Tests were performed in air at a crosshead rate of 0.005 in/min to the 0.2% yield point and 0.05 in/min from yield to fracture. Round bar specimens with dimensions of 1.25 inch gauge and 0.25 inch diameter for tensile tests were used, while right circular cylinders of 0.5 inch length and 0.25 inch diameter were used for compression tests. To minimize sticking due to friction during testing in compression, Teflon was used at room temperature and molybdenum disulfide at elevated temperature to lubricate contacts between the specimens and the platens.

3.2 Creep Tests

Creep tests were conducted in air with either a continuous strip chart recording of strain versus time or with periodic high magnification optical monitoring of a strain-gauge spot welded to the specimen. Creep test procedures

included determination of creep strain at either constant applied load as a function of temperature or constant temperature as a function of applied load. For the former, a steady state creep rate was established at 1000F (811K) at which time the temperature was reduced to 975F (796K). At 975F (796K) a lower steady state creep rate was established. From the creep rate data and test temperature, it was possible to determine apparent activation energy. Apparent activation energy was also determined at 1100F (866K) using 1075F (854K) and 1100F (866K) test temperatures. Total duration of the creep tests was usually ~ 335 hours. Additionally, creep tests at a constant temperature of 1000F (811K) were conducted with periodic increases in stress of ~ 4 ksi. This type of test provides a convenient method for comparison of creep resistance for different alloys by determining creep rate just subsequent to the primary creep region. Time span over which creep rate was determined was 24-64 hours at each stress, with a total test duration ranging from 400 to 600 hours.

Metallurgical stability of the alloys was evaluated by post creep tensile testing the specimens used for the apparent activation energy work. Prior to tensile testing, 0.010-inch was machined off the gage length to remove spot welds where the creep extensometer was attached. This procedure also removed the oxide film and air contaminated metal from the surfaces so that the metallurgical stability is indicated here and does not include the influence of surface contamination which can be experienced under actual service conditions.

3.3 Alloy Partitioning

The following heats were used for this work:

Heat No.	Nominal Addition, %
B-2657	0.5 Si
B-2665	2.0 Bi(1)
B-2673	1.0 Fe

(1) Analyzed Bi content - 1.32%

Small samples of each heat were sealed in titanium capsules, heated for one hour at 1950F (1338K) and slow-cooled at 50F/hr. The capsules were water-quenched from temperatures between 1550 and 1800F (1116 to 1255K). Samples were removed from the capsules, reheated to the original quenching temperature, held 10-minutes and again water-quenched. The latter heat treatment was applied to remove any growth of the existing alpha phase which may have occurred during the relatively slow-quench in the titanium capsules. These samples were then prepared metallographically for microprobe analysis.

Precautions were taken to assure, as much as possible, that only the desired phase was being analyzed. Only areas of a particular phase with a width of at least five times the diameter of the beam were selected and several of these were given a preliminary analysis to find the two which gave either the highest or lowest value of the element in question. This procedure minimized the chance of analyzing an area so thin that the electron beam penetrated through the phase and excited radiation from the other phase beneath. The two selected areas were then quantitatively analyzed using a beta quenched sample of the same alloy as a standard. In each case, the composition of the standard was assumed to be the nominal composition.

3.4 Diffusivity of Bi

Half pound buttons nominally Ti-6Al-2Sn-2Zr-1Mo and Ti-6Al-2Sn-2Zr-1Mo-3Bi (analyzed at 2.7% Bi) were used for this work. These were hot rolled at 1850F (1283K) to about 1/4-inch thick. They were then descaled and pickled to remove all surface contamination. Diffusion couples were then formed by placing pieces of each alloy in a close fitting box made of commercially pure Ti, welding the assembly closed and hot rolling it to a 50% reduction after heating one hour at 1850F (1283K). Sections of the welded couple thus formed were encapsulated in Ti, given diffusion anneals for appropriate times at temperatures from 1900F (1311K) to 2200F (1477K) and water-quenched.

The Bi contents, determined at 50μm intervals within the diffusion zone, were determined by quantitative electron microprobe analysis. From these data, diffusion coefficients were determined using the Boltzmann-Matano method.[9] It should be noted that the Boltzmann-Matano analysis applies only to binary systems, and accordingly the analysis performed in this study on more complex alloys should not be considered as rigorous.

3.5 Fatigue and Fracture

Fatigue crack growth studies at 78 and 1000F (298 and 811K) utilized compact tension specimens complying with ASTM standards[8] except for a nominal thickness of 0.5-inch or all specimens. Specimens were precracked with a decreasing load schedule such that the final crack propagation was accomplished at a load equivalent to the test load. Crack propagation was achieved with a sine wave loading waveform at a frequency of 10 Hz. All load cycles were tension-tension with an R factor of 0.1 (R = minimum stress/maximum stress) and were chosen to preclude general yielding in the net section at test completion. Humidity during testing ranged from 40 to 50% unless otherwise noted. Crack growth rate (da/dN) was calculated for each increment of crack extension, and the corresponding stress intensity factor, K, was based on the average crack length for that increment. Stress intensity was calculated according to ASTM standards.[8]

Fracture toughness studies at 78 and 1000F (298 and 811K) also utilized compact tension specimens with a nominal thickness of 1.0-inch at 78F (298K) and 0.5-inch at 1000F (811K). Efforts were directed towards maintaining test variables such that valid fracture toughness[8] (K_{Ic}) results could be obtained. Where all requirements as set forth by ASTM standards[8] are maintained, a K_{Ic} value is reported, and where a valid fracture toughness result is not obtained a conditional fracture toughness (K_Q) is reported.

3.6 Hot Salt Stress Corrosion

Flat tensile specimens used for hot salt stress corrosion (HSSC) studies were coated with a slurry of reagent grade NaCl and distilled water and allowed to dry. Exposure conditions consisted of 48 hours at 850F (728K) under a constant stress. Following high temperature exposure, the specimens were pulled at ambient temperature at a strain rate of $\sim 1.1 \times 10^{-3}$ sec^{-1}. In this manner HSSC threshold stress was determined, i.e., the minimum applied stress where, after exposure to a HSSC environment, room temperature ductility is markedly reduced.

SECTION IV

RESULTS AND DISCUSSION

4.1 Tensile Properties - Button Materials

Room temperature tensile results for the 16 alloys listed in Table I are presented in Table V with elongation, yield strength and reduction in area results illustrated in Figures 1, 2 and 3, respectively. It is seen in Figure 1 that both Si and Bi decrease elongation with increasing quantities of element addition, although the relative change is small. However, with additions of 1 or 2 percent Fe to the base composition of Ti-6Al-2Sn-2Zr-1Mo, room temperature elongation decreases significantly. Corresponding reduction in area results, Table V and Figure 3, are unchanged over a significant composition range, but at the higher levels are more severely lowered. Yield strength, Figure 2 and Table V, and ultimate strength results, Table V, generally follow the reverse trend, i.e. yield strength and ultimate strength increase for element additions that reduce ductility.

Tensile results at 1000F (811K) for the alloys listed in Table I are also presented in Table V with elongation, yield strength and reduction in area results illustrated in Figs. 4, 5 and 6, respectively. Again, as was shown for room temperature tensile results, the relative change is small. Minor additions

of Fe for quantities greater than 0.5% proved to slightly increase the 1000F (811K) tensile elongation, whereas S over the range investigated had little effect. Again, at the higher levels of composition addition evaluated, Fig. 6 shows RA at 1000F (811K) to be reduced for all element additions except Fe. Additions of Si and Fe at the higher levels investigated resulted in moderate improvement in 1000F (811K) yield strength with yield strength continuously increasing with increasing element additions, as illustrated in Fig. 5. Additions of Bi and S had little effect.

In summary, changes in room temperature and 1000F tensile elongation results remain small for the range of element additions of Si, Bi, Fe and S examined, except for the isolated cases discussed above. Most important is the reduced reduction in area for the higher composition levels, especially the result at 0.5Si since this quantity of Si addition has been shown to significantly increase the creep resistance of Ti alloys.[5] Yield strength results generally showed the reverse trend increasing as ductility decreased.

The alloys listed in Table I and discussed above were designed to evaluate the individual effects of alloying additions on materials properties. Alloys listed in Table II were utilized to study interaction effects of multiple alloying additions on the same base alloy. Toward this purpose Table V presents 78 and 1000F tensile properties for a base alloy of Ti-6Al-2Sn-2Zr with a combination of additions of Mo, Si, Fe, O, and S.

In general, at 78F, additions of Fe, in quantities up to 2% in combination with Si or S, proved to reduce tensile elongation to unacceptable levels. At 1000 F (811K), however, 2% Fe proved to be embrittling when in combination with either Si or S. With additions of 2% Mo in concert with Si, tensile elongation takes a sharp drop at room temperature. However, Mo has been shown to be an important element in increasing creep resistance[5] and does not impair ductility to the extent of Fe additions.

At first it would appear that Si in combination with O_2 would impair ductility at 78F, however, when considering Si additions alone, it can be concluded that Si by itself reduces both elongation and reduction in area. The effects noted above are the most significant, although a number of less obvious effects might also be attributed to minor alloy element additions and elaborated upon. It is necessary, however, to establish the statistical significance of these effects. The remainder of this section, therefore, discusses the techniques used and results obtained from a statistical analysis of the tensile data presented in Table V.

The button melts to which two elements were added to the base composition (Table II) were designed to show effects of any interactions between the elements on properties. When combined with certain of the buttons having single element additions (Table I) they formed complete factorial designs which could, under the proper conditions, allow interactions as well as any effects of single additions to be evaluated statistically. To this end the yield strength and ductility (% RA) data from Table V have been statistically evaluated with a summary of the results of the analysis of variance tabulated in Table VI. A significance level of 0.05 was chosen as the level indicating a real effect or interaction.

Since there was no replication of the tensile tests on button melts, it was necessary to determine a test error variance separately in order to evaluate the possible significance of interactions between the alloy additions. This determination was carried out at both room temperature and 1000F using tensile results presented in Table VII. For each heat of a given nominal composition both a within heat variance and a between heat variance were determined by methods outlined by Brownlee.[9] These two variances were then combined to give a total error variance for each group of heats and the group variances were averaged to give the test error variance used in evaluating the factorial designs.

Considering first the alloys which had Fe and Si additions (Tables V and VI), it is apparent that each element individually increased strength and decreased ductility in RT tests. An interaction between the two elements on YS is also indicated. The fact that the latter attained significance statistically, however, was due almost entirely to the one low yield strength value for the 0 Fe-0.25 Si alloy. Otherwise, the results for the three Si levels plotted as a function of Fe content are nearly parallel indicating no interaction. Indeed, if a value of 125 ksi is substituted for the low 117.1 value and the analysis of variance repeated, the interaction is no longer statistically significant indicating that it may not really exist. At 1000F the effects are very similar to those at RT except that an interaction between Fe and Si is indicated for % RA. Here, the interaction is probably real since the data show an upward trend up to 0.5 Fe at 0 Si and a generally downward trend over this same range for the 0.25 and 0.5 Si alloys.

In the alloys to which Fe+S were added, only Fe affected strength significantly both at RT and 1000F. There was no apparent interaction between the two but their effects did show some indications of being additive, especially on ductility.

Mo+Si additions showed the expected first order effects of Si in increasing strength and decreasing ductility at both test temperatures. Mo also showed main effects on ductility at RT and strength at 1000F, decreasing the former and increasing the latter. The effect of Mo on RT strength was indicated to be in an interaction with Si. The trends suggest that increasing Mo was generally more effective in increasing strength at 0 Si than at the higher Si contents. The effects of the two elements were also generally additive.

Although apparently not statistically significant, possibly because of the large test error assumed, an interesting result is indicated in Figure 6 for

alloys containing 0.25 Si with variable additions of Mo (0 to 2%). As shown, an addition of 1 Mo improves RA above that for an alloy with no Mo. However, increasing the Mo level to 2% proves to lower RA below that obtained for 1 Mo. As will be seen later, this maximum in properties at 1% Mo also occurs for creep resistance.

In the Si+O_2 alloys Si exhibited the expected effects on both strength and ductility. Oxygen had no effect on RT ductility but appeared to be involved in an interaction with Si on RT strength. The results imply a decreasing effect of Si on strength as the O_2 content increases. Although O_2 shows no significant effect on ductility at RT, it decreased ductility at 1000F.

In summary, therefore, alloying additions of Fe, Si, S, Mo and O_2 all in some manner independently influenced room temperature and 1000F tensile properties of the alloy Ti-6Al-2Sn-2Zr. However, interaction effects between the elements when significant were so mostly in room temperature strength with the effects proving to be more often additive than interacting. A possible exception of interest involved additions of Mo to Si containing alloys even though the statistics in Table VI failed to show an interaction. As Table V shows, RA at 1000F (811K) was improved by an addition of 1% Mo but decreased with Mo additions up to 2%.

4.2 Compression Properties - Button Materials

In addition to tension tests, button melts listed in Table II were tested in compression at a strain rate of $6.7 \times 10^{-4} sec^{-1}$ over the temperature range of 78 to 1200F (298 to 921K) to determine the effect of element additions on the compressive yield strength. Results for these tests are illustrated in Figures 7-15. These figures show yield strength as a function of temperature and as a function of either Fe or Si additions for different base alloys. For example, Figures 11 and 12 illustrate the effect of Si additions on base alloys differing only in oxygen content. Base alloy variables included Si, S, O_2 and Mo.

Of interest in these figures are the two peaks in yield strength frequently evident at ~ 600F (588K) and ~ 1200F (921K). These peaks are most likely due to strain aging, but from the data, it is difficult to attribute either peak to any single element addition. In fact, for Ti-6Al-2Sn-2Zr with no additions (Fig. 13), although no strain aging peak is evident at 600F (588K) a peak does exist at 1200F (921K). This alloy does contain oxygen at some level <0.1 wt.% and if the 1200F (921K) peak was due to the presence of oxygen then one would expect a more pronounced effect for alloys with greater oxygen concentrations. However, for .12 O_2 (Fig. 11) no peak occurs at 1200F (921K) and the peak for .18 O_2 (Fig. 12) is less than that illustrated in Fig. 13 for an oxygen level <0.1.

Similarly, the strain aging peak at 600F (588K) cannot be definitely attributed to a single element from the available data. Figure 13 illustrates no strain aging peak at 600F (588K) in the absence of Si. However, in Fig. 12, a strain aging peak is evident at 600F (588K) for an alloy with no Si but only an addition of .18 O_2. Also, for all alloys, except Ti-6Al-2Sn-2Zr-.25Si (Fig. 13), a strain aging peak is evident at 600F (588K) when Si is an element addition and in all cases the greater the Si addition the more pronounced the strain aging peak. However, a strain aging peak is also evident in alloys containing only additions of Fe and S (Figs. 9 and 10) with the effect most pronounced with large additions of Fe.

Results are thus inconclusive in identifying a single element or combination of elements to which the apparent strain aging peaks could be attributed. The data do indicate that, except for the exceptions noted above, increased compressive yield strength at 600F (588K) is possibly due to oxygen and can be enhanced by the presence of Si. Also, the magnitude of the compressive yield strength is at times increased by minor alloying additions. Principally, a 2% Fe addition (Fig. 9) does increase compressive yield strength up to ~800F (700K), and a .02S addition (Fig. 10) extends this increase in strength up to ~ 1000F (811K). However, there appears to be no effect of S on compressive yield strength when coupled

with Fe additions of .25 and .5%. In addition to Fe, the effect of Mo on strength is evident from results illustrated in Fig. 15. As will be shown below, Mo also proves to be beneficial in creep strengthening at 1000F (811K), whereas in contrast to its effect on tensile and compressive strength properties, Fe proves to reduce creep resistance with increasing quantities of Fe.

4.3 Mechanical Properties - 100 lb. Ingots

Detailed results of the tensile tests on 1/2-inch diameter beta rolled bar from the five 100 lb. ingots are given in Table VIII. Two heat treatments are represented which will be referred to in the following discussion as the A and B treatments:

A - 1950F(15 Min)AC + 1300F(2 Hrs)AC
B - 1950F(15 Min)AC + 1100F(8 Hrs)AC

Average results of the tests at temperatures from 78 to 1200F (298 to 922K) are plotted in Figures 16 through 19.

In Figures 16 and 17, the effects of increasing Si content on tensile properties are shown for the two heat treatments. Generally, strength increased with increasing Si content over the entire temperature range. Concurrently, ductility generally decreased to very similar levels for both of the alloys containing Si. There were two exceptions to these ductility trends. First, the base alloy without Si given the B heat treatment, appeared to reach a peak in RA values at 600F (588K). At higher temperatures, values dropped to essentially the same or lower values than those of the Si containing heats. Second, the 0.5% Si heat in both conditions of heat treatment exhibited a relatively sharp increase in elongation at 1200F (922K) such that its values were appreciably higher than those of either the base alloy or the 0.25% Si heat.

The effects of increasing nominal oxygen content of the Ti-6Al-2Sn-2Zr-1Mo-0.25Si alloy from 0.06 to 0.18% are illustrated in Figures 18 and 19. As might

be expected, increasing oxygen content generally increased strength and decreased ductility over the whole temperature range. The magnitude of the effects, however, was small. It is interesting to note that the low oxygen heats, V-5128 and V-5130, given the B heat treatment showed a sharp increase in elongation at 1200F, similar to that shown by the 0.5% Si - 0.12% O_2 heat, V-5129.

The effects of the different heat treatments per se on the strength of this group of alloys was relatively small with the B heat treatment giving slightly higher strength than the A. The effects on ductility varied somewhat for different alloys but generally, the ductility of specimens given the B heat treatment was higher than that of the A.

The tensile properties of these heats at -320F are not shown in the figures but can be seen in Table VIII. Only specimens given the A heat treatment were tested at this temperature. Alloying effects were similar to those already described, that is, increasing either Si or O_2 content increased strength and reduced ductility.

Also for comparison purposes, Table IX lists tensile results at 78 and 1000F (298 and 811K) for the same melts fabricated into plate stock by the procedure described earlier. These results will be used to determine the validity of fracture toughness measurements discussed below. From these results it can be concluded that bar stock exhibits a significant and consistent increase in both strength and ductility as compared to plate material. Further investigation would be necessary to identify the reason for these differences.

Compression properties have also been evaluated for the 100 lb. ingot bar stock with results illustrated in Figs. 20 and 21 for additions of Si and O_2 as a function of temperature. From the results on button melts one might have expected a larger effect of oxygen or silicon on the strain aging peak. However, it is apparent that differences in compressive yield strength do exist between button versus 100 lb. melts for identical compositions, whereas discussed above,

differences in tensile properties were observed between bar and plate materials of the same composition. Fabrication and melting procedures thus have a significant effect on tensile properties with the strain aging behavior observed in compression decidedly reduced for the 100 lb. ingot material. Differences in creep properties have also been noted for different processing and melting procedures,[10] however, the reason has never been clearly identified, although it is possible that differences could be related to crystallographic texture. There are also differences in the composition of base materials, principally in Fe and S content which might contribute to the effects.

These data also illustrate the difference between tension and compression yield strengths for these alloys. At 78F (298K) yield strength in compression for Heat V-5129 (Fig. 21) is increased 23% or more above that determined in tension (Fig. 16). The contribution of friction in compression due to the applied stress has been calculated to be a maximum of 14 percent based on the assumption that the sample was sticking to the platens.[11] As noted previously, to minimize sticking due to friction, Teflon was used as a lubricant at room temperature and molybdenum disulfide at elevated temperature. However, the absence of any noticeable barreling suggested that sticking did not occur and that the effect of friction would then be less than 14%.

4.4 Creep Properties

4.4.1 Button Materials

4.4.1.1 Stress Dependence

Creep rate results established at 1000F (811K) are illustrated in Figs. 22-25 as a function of applied stress for the sixteen alloys listed in Table I. The results are best analyzed in terms of a comparison of each alloy to the creep properties of the base alloy and a comparison to the commercial alloy Ti-11 (Ti-6Al-2Sn-1.5Zr-1.0Mo-0.35Bi-0.1Si), already proven to possess good creep resistance. From the results illustrated in Fig. 22, it can be concluded that additions of Si to levels of 0.25 to 0.5 percent consistently increase the creep

resistance of the base alloy. At low stress levels creep rate was reduced by a factor of ~ 2 for a given stress, as compared to the base alloy, whereas at higher stresses the creep rate decreased by a factor of ~ 3. For applied stresses greater than 70 ksi the base alloy with additions of 0.25 or 0.5% had equivalent or better creep resistance than the commercial alloy Ti-11.

With regard to the quantity of Si added, Fig. 22 shows that an addition of 0.10 Si resulted in improved creep resistance for low applied stresses, but had little effect on creep resistance at applied stress levels greater than ~ 52 ksi. Also, Fig. 22 shows that creep resistance is approximately equivalent for additions of 0.25 and 0.5% Si. This was not the case for the less complex base alloy Ti-5Al-5Zr where additions of Si to levels greater than 0.25% further increased creep resistance.[5] Previously, it was shown for the Ti-5Al-5Zr base alloy that the probable cause for the observed effect of Si was that small precipitates, possibly Si clusters, formed along dislocations after creep.[5] These precipitates were apparently very effective in pinning dislocations. The mechanism whereby Si imparts creep resistance for the more complicated base alloy used in this study is discussed in more detail in the microstructure evaluation section below.

Figure 23 is a similar illustration depicting the effect of Bi additions to the base alloy. Results for Bi additions do not show a monotonic increase in creep resistance with Bi, i.e., nominal additions of 0.25, 1.0 and 2.0% consistently improve creep resistance for the range of stresses investigated whereas an addition of 0.5% Bi decreases the creep resistance. This inconsistency is possibly explained by the microstructure developed in the Ti-6Al-2Sn-2Zr-1Mo-0.5Si alloy. Microscopy results for this alloy revealed a microstructure with an abnormally high volume fraction of beta phase as compared to similar chemistries. This alloy was subsequently chemically analyzed for major alloying elements with the results providing no explanation for the observed

anomalous creep behavior or high volume fraction of beta. The Sn and Zr contents were slightly higher than the nominal but this alone would not be expected to produce the results observed. In addition, it is noted that a nominal addition of 2.0% Bi improved the creep resistance to a small degree as compared to 1.0% Bi, however, from Table V it is also seen that an addition of 2.0 Bi significantly reduced room temperature and 1000F (811K) reduction in area.

Figure 24 illustrates the effect of sulfur additions on creep resistance as a function of stress at 1000F (811K). Of interest is the result that the alloy with an addition of 0.005 S proved to have greater creep resistance than the base alloy (0.00085 S) and alloys with S additions of 0.01 and 0.02 wt.%. This result is not consistent however with creep results obtained for the activation energy work on S containing alloys (Table X). Here there was evidence that a maximum in 1000F (811K) creep resistance might exist at 0.005% S but the creep resistance at higher S contents, while lower than that at 0.005% S, was still appreciably higher than that of the base alloy.

Figure 25 illustrates creep results for Fe additions to the base alloy Ti-6Al-2Sn-2Zr-1Mo. Over the range of Fe additions, i.e., nominal 0.15 to 2.0 weight percent, a continuous increase in Fe content resulted in continuously decreasing creep resistance. These results are best illustrated by Fig. 26, where shear stress for a creep rate of 2×10^{-5} $Hr.^{-1}$ is plotted as a function of element additions to the base alloy. In this figure it can clearly be seen that increasing Fe additions resulted in a reduction in creep resistance, whereas increasing Si and Bi additions resulted in increased creep resistance.

In a like manner, Fig. 26 illustrates the effect of sulfur additions to the base alloy. It should be noted that the abscissa in Fig. 26 is drawn for two different scales due to the difference in magnitude between sulfur additions and the other elements evaluated. On this basis comparisons should be made accordingly.

Considering the four individual alloying additions investigated, it may be concluded that only Si and Bi impart a consistent improvement in creep resistance to the base alloy Ti-6Al-2Sn-2Zr-1Mo, whereas Fe additions continuously reduced creep resistance with increasing Fe up to 2% while S additions resulted in mixed results.

Similar creep rate-stress dependence results for materials with multiple alloying additions (Table II) are illustrated in Figs. 27 - 35. For individual additions it was shown that Si alone consistently increased creep resistance, whereas increases in Fe resulted in continuously decreasing creep resistance. It can be concluded from Figs. 27 and 28, where results for combined additions of Fe-Si are shown, that Fe-Si additions together exhibit no beneficial improvement in creep resistance. Silicon additions improve creep resistance when Fe is present, but continuously increasing Fe levels further degrade creep resistance. A consideration of data for Fe additions in combination with S, Figs. 29 and 30, results in the same conclusion. At no level of Fe addition, within the range investigated (.15 to 2 wt. %) has Fe, either individually or in combination with other elements, proven to be beneficial to creep resistance. In fact, in all cases increasing Fe content reduces creep resistance. It must be concluded from these results that when optimizing creep resistance in Ti alloys, Fe should be reduced to a practical minimum.

The next three figures, Figs. 31 - 33, should be considered jointly to evaluate any synergistic effect of $Si+O_2$ additions on creep resistance. Figure 33 illustrates that increasing oxygen content reduces creep resistance. However, when considering a base alloy containing .25Si (Figs. 31 and 32) it can be seen that a significant increase in creep resistance is obtained at the higher oxygen level (.18 vs. .12 wt. %). Conversely, at a Si level of 0.5, creep resistance for the two oxygen levels is identical. Apparently, if a synergistic relationship does exist, it is dependent upon the magnitude of each

ingredient and as such an addition of oxygen can prove to be either beneficial or detrimental to creep resistance depending upon the level of Si present.

The final two figures in this series, Figs. 34 and 35, illustrate the benefits of Si in a base alloy without Mo (Fig. 34) and the benefits of Mo additions without Si (Fig. 35). It is apparent from Fig. 34 that Mo is not necessary for increasing Si additions to impart an increasing creep resistance. However, an addition of 1Mo further improves on the benefits attained by Si. Similarly, Fig. 35 shows that an addition of 1Mo without Si greatly improves creep resistance. This benefit appears to peak out as indicated by the decrease in creep resistance for additions of 2Mo. From the results, it can be concluded that both Si and Mo individually increase creep resistance and when added in combination the benefits appear to be additive.

In summary, with regard to multiple additions of minor elements and considering their effect on creep resistance in a base alloy of composition Ti-6Al-2Sn-2Zr, [1] Fe content should at all times be kept to a minimum, [2] $Si-O_2$ combinations can be beneficial but the relationship is dependent on the magnitude of each element, [3] S appears to have no benefit in combination with other minor elements investigated, and [4] Mo-Si additions increase creep resistance with the benefits of each element being additive.

4.4.1.2 Apparent Activation Energy

In addition to evaluating the stress dependence of creep rate, apparent activation energy was determined for the alloys listed in Tables I and II at both 1000 and 1100 F (811 and 866K). Results of creep tests to determine the effect of minor alloying additions on apparent activation energy are listed in Table X. From these creep rate data and a phenomenological creep equation of the form

$$\dot{\epsilon} = A \exp \frac{-\Delta H}{RT}$$

where,
$\dot{\epsilon}$ = strain rate
ΔH = apparent activation energy
T = temperature (K)
R = gas constant
A = stress dependent constant,

it is possible to calculate apparent activation energy. This equation assumes apparent activation energy to be independent of stress and strain. The independence of apparent activation energy on strain has been established.[11] In fact, it has been shown that the apparent activation energy of creep in the transient part of the creep curve often is the same as that observed in the steady state part of the curve.[11] However, the dependence of apparent activation energy on applied stress is not as clear.

Before pursuing further, it should be noted that early work on specimens from the button melts showed wide variations in the apparent activation energy values obtained for duplicate specimens. It was not known whether this wide variation in apparent activation energies of duplicate specimens was primarily a function of material variables or minor test variables or both.

In order to clarify this question, a series of tests was initiated on 1/2-inch dia. bar stock from the 100 lb. Ti-6Al-2Sn-2Zr-1Mo-0.25Si ingot. Six specimen blanks were cut from a single bar and given the standard duplex heat treatment of 1950F (1338K)/15 min AC + 1300F (978K)/2 hrs AC. Results from these tests should be representative of material which is homogeneous both chemically and structurally. All possible precautions were taken to assure temperature uniformity and constancy during the tests.

Three specimens were tested at 40 Ksi and three at 50 Ksi stress. All tests were initially run at 1000F (811K) for one week. At the end of that time the temperature of the 40 Ksi tests was increased to 1025F (823K) and that of the 50 Ksi tests was decreased to 975F (798K). After a second week of testing, all temperatures were returned to 1000F (811K) and testing continued for a third week. During these tests, temperatures were maintained within $\pm$ 2 F and the temperature gradient over the length of the specimen was less than 2 F. Apparent activation energies were then calculated for both the increase and the decrease in temperature on each specimen. Complete results are shown in Table XI.

It is apparent that there is an inherent variability of considerable magnitude in these tests. The standard deviation for the 40 Ksi tests was ± 18% of the mean value and for the 50 Ksi tests ± 7% of the mean value. There were also appreciable differences in the two values of apparent activation energy determined on each specimen with no consistent trend as to whether the higher values were obtained by raising or lowering the temperature. These tests also showed an apparent stress effect, in that the average value at 50 Ksi was some 22 K/cal/mol higher than that obtained in the 40 Ksi tests.

From these results, it can be concluded that both material variables and test variables add to the scatter in magnitude of apparent activation energy results. The fact that the standard deviation was much less for specimens tested at 50 Ksi (Table XI) implies that a considerable portion of the error possibly rests in the measurement of low creep rate. That is, the percentage of error in test measurement or specimen anisotropy would be greatest for small creep strains and strain rates. Also, it should be realized that button melts are inherently less homogeneous than ingots. This could add further to the magnitude of test error, thus making detection of alloying effects difficult unless they are large.

With knowledge of the degree of scatter in apparent activation energy results, and realizing that the magnitude of apparent activation energy can be dependent on the magnitude of applied stress, it is now possible to realistically evaluate the apparent activation energy for creep. Like the tensile data for the button melts, creep data were arranged in factorial designs and subjected to analysis of variance to determine significant effects of the individual elements as well as possible interactions between them. When the raw data from Table X were used, however, the error variance determined from the duplicate creep tests was so large that none of the elements could be shown to have

statistically significant effects on apparent activation energy. Further examination of the data showed an apparent trend for the calculated activation energies to be lower in specimens which had shown high initial creep rates. In running these tests, stresses had been selected to give an estimated initial steady state creep rate in the range $3\text{-}7\text{x}10^{-5}$/hr. but the actual creep rates attained covered a much wider range. In view of the above, the data in Table X for each test temperature were subjected to regression analysis to determine whether a significant correlation existed between the initial creep rate and apparent activation energy. The best correlation for both temperatures was found to be an exponential relationship of the type:

$$\Delta H = K \exp^{b\dot{\varepsilon}}$$

where ΔH = apparent activation energy in Kcal/mol

$\dot{\varepsilon}$ = initial steady state creep rate

K = and b are constants

The values for K and b for the two test temperatures were found to be:

1000F K = 119.9

b = -0.04718

1100F K = 122.2

b = -0.0355

For the 1000F tests the statistical significance of the correlation was greater than 0.001 and for the 1100F data greater than 0.01. Plots of the data showing the best fit lines are shown in Figs. 36 and 37.

The slopes of the regression lines for each temperature were used to correct each of the activation energies in Table X for creep rate to a value of $5\text{x}10^{-5}$/hr.

Considering first the heats to which single alloying additions were made, average values for 1000F (811K) creep are plotted vs. alloy content in Figs. 38

and 39. These are corrected to $5x10^{-5}$/hr. creep rate. The only trends that are clear here are an apparent reduction of the apparent activation energies at the higher Fe contents and a modest increase with higher Bi additions. No clear trends were apparent for the Si and S additions. The data for the 1100F (866K) creep tests were not plotted because they failed to show clear trends for any of the alloying additions.

Apparent activation energy data (corrected for creep rate) for the heats which had multiple alloying additions formed complete factorial designs. Results of analysis of variance conducted on the data to determine statistically significant effects and interactions are summarized in Table XII. In this case, a level of 0.1% was chosen as indicating statistical significance because of the large scatter in the data. Evaluation of the significance of the effects utilized estimates of test error obtained from the duplicate 1000F (811K) tests. Since only single tests were run at 1100F (866K), such estimates could not be obtained so the error estimates obtained for the corresponding 1000F (811K) tests were used. The average effects of the various alloy additions and the interactions which were statistically significant to the 0.1 level or higher are plotted in Figs. 40 through 45.

The similarity between the significant effects of the Fe + Si and the Fe + S additions on the 1000F (811K) apparent activation energies is striking (Figs. 40 and 42.) In both cases a similar interaction between the two elements is indicated. At the lowest Fe level the effect of increasing Si content is indicated to be nil while S produces a small reduction in ΔH. At higher Fe contents, both Si and S produced a maximum in ΔH at the intermediate level of the element.

The indicated effects of these elements on 1100F (866K) creep were shown to be somewhat different (Figs. 41 and 43). The Fe + Si system did not have a significant interaction but rather showed independent effects for both elements.

The apparent activation energy decreased with increasing Si and decreased at Fe contents greater than 0.25%. The Fe + S system indicated an interaction between the two elements which is shown in Fig. 43. However, the trends shown are for single test results and the validity of the trends shown is open to question.

The Mo + Si system (Figs. 44 and 45) did not show significant interactions at either 1000 or 1100F (811K or 866K). Increasing Mo from 0 to 1% sharply lowered ΔH at both temperatures. Further increase to 2% Mo had only minor effects. The effect of Si was statistically significant only at 1100F (866K) where it exhibited a maximum at 0.25% similar to its effect in the Fe + Si system at 1000F (811K). Although the Si effect was not statistically significant at 1000F (811K), the data shows the same trend as the 1100F (866K) data, that is, a maximum ΔH at 0.25% Si.

No statistically significant effects were found in the Si + O_2 system.

In summary, all of the minor alloying elements, except oxygen, were indicated to have significant effects on the activation energy for creep in the 1000-1100F (811-866K) temperature range. Iron additions were involved in complex interactions with Si and S such that at higher Fe contents intermediate amounts of the former two elements produced a maximum ΔH. Increasing the Mo content of a Ti-6Al-2Sn-2Zr base from 0 to 1% sharply decreased activation energy, this in spite of the fact that creep strength was enhanced. This would suggest that Mo affected primarily the athermal component of the creep strength.

Activation energies for creep, in all cases were very much higher than would be expected in cases controlled by a normal diffusion mechanism. This latter case should reflect activation energies on the order of 40-50 Kcal/mole but in no case did the measured apparent activation energies decrease below 60 Kcal/mole and frequently were on the order of 120 Kcal/mole. Care, here, must be taken in interpreting these results since substructures were allowed to

stabilize after the change in temperature which then invalidates the pure interpretation of the activation energy so obtained. The latter generally presumes a constant structure. No work has been done to quantitatively characterize the substructures as the tests proceed, a necessary, and formidable, task toward an end of isolating the thermal component of the creep strength. The engineering significance leads one, then, to the possibility that the order of loading, in a block loading sequence or application environment may influence the instantaneous creep rate and perhaps the integrated life. Superposition, upon creep, of other loading schemes (fatigue, tensile, etc.) which, in themselves, influence substructure, further complicate the entire picture.

One last caution rests about the meaning of steady state creep results in engineering applications. Currently, materials specifications require no more than a certain maximum creep deformation in so many hours at a specified stress level. This adds primary creep to secondary creep for the total creep strain and since the latter is often much smaller than the former, alloy design aimed at the latter alone could possibly lead to improper choices.

4.4.1.3 Creep Stability

The term creep stability literally implies the degree to which the original mechanical properties are retained after a specified creep exposure. From a practical standpoint, this definition of stability has a serious shortcoming in that it says nothing about the level of the original properties. This program, however, is concerned prima ly with establishing effects of alloying additions with a view toward relating these to basic creep mechanisms, so that the actual change in properties during creep exposure regardless of the initial level would seem to be an appropriate parameter for evaluating the alloying effects. For this reason, the percentage of tensile ductility (expressed as reduction of area) retained after creep exposure was selected as the criterion of stability.

Complete results of the stability tests on button melt materials are given in Table XIII. The percentage of retained ductility after 1000F (811K) and 1100F (866K) for the heats to which single alloying additions were made are plotted as a function of such additions in Figs. 46 and 47. It is apparent that all of these heats retained at least 40% of their original ductility regardless of the alloy addition. It must be remembered, however, that the highest Si alloy and the higher Fe alloys had relatively low starting ductility so that their reasonably good retention of ductility would have little practical significance. Of significance here was the high percentage of retained ductility of the S heats as well as the lower Bi alloys, both of which had good starting ductility. The 0.25% Si alloy which also had good starting ductility retained 40-50% of it after creep exposure.

Subjecting these data to analyses of variance as was done for tensile and creep properties would be of little value because an estimate of test error variance was not available, so the significance of interactions could not be evaluated. However, the major trends with respect to alloy additions are readily apparent. The Fe + Si and Si + O_2 additions obviously have additive effects in decreasing stability, the former to the extent of producing completely brittle specimens at both Si levels containing 2% Fe after 1000F (811K) creep. Complete brittleness was also produced in the 0.5 Si alloys at all levels of Fe above 0.05% after 1100F (866K) creep.

The intermediate S level (0.005%) appeared to reduce stability of the 2% Fe alloy after both 1000 and 1100F (811 and 866K) creep in the Fe + S system. Beyond this one instance, S seemed to have little effect.

In the Mo + Si system the Mo additions seemed to have a stabilizing effect. In the Mo free alloy stability decreased sharply with increasing Si. At both

the 1% and 2% Mo levels, however, reasonably good stability was indicated at both Si levels.

Oxygen additions in combination with other element additions resulted in mixed results. For example, an increase in O_2 with .25 Si lowered stability, whereas an increase in O_2 with 1 Mo increased stability as shown in Table XIII.

4.4.2 100 lb. Ingots

4.4.2.1 Stress Dependence

A number of factors have been considered in evaluating the stress dependence of creep rate for the 100 lb. ingot materials listed in Table IV, e.g., minor element additions of Si + O_2, heat treatment, thermal aging with and without stress, and cyclic loading. Results of tests designed to evaluate these factors are presented and discussed below.

Creep rate data as a function of applied stress at 1000F (811K) for Si additions up to .5% and O_2 additions up to .18% are illustrated in Fig. 48 and 49. As expected, Si additions proved to increase creep resistance for a base alloy of Ti-6Al-2Sn-2Zr-1Mo-.12O_2. Similar to results from button materials, creep resistance appeared to be equivalent for additions of either 0.25 or 0.5 Si. This result has important implications when considering the fabricability of Si bearing alloys, since increases in Si content are accompanied by increased difficulties in workability. Considering variations in O_2 content (Fig. 49), no consistent trend is evident. It appears that the alloy containing .12 O_2 has superior creep resistance, however, when O_2 is increased to .18 O_2, creep rate is again reduced. Further investigations would be necessary before it could be concluded that these observations are indeed real and not simply an annomaly attributable to fluctuations in materials and test procedures.

With regard to fabrication procedures, comparing creep resistance of 100-lb. ingot materials to that of button melts (Figs. 50 and 51) reveals a significant difference, with the 100 lb. ingot materials exhibiting improved creep properties. In previous sections, tensile results were also shown to vary with fabrication procedures with the strain aging behavior reduced for the 100 lb. ingot materials. It is possible that the greater creep resistance of the 100 lb. ingot materials is due to the higher S content (~ 20 ppm vs. ~ 0). However, as before, further investigation would be necessary to clearly identify the reason for these differences.

Previously, it was shown that Si in solution, as opposed to precipitated silicides, resulted in increased creep resistance.[5] Below, in the microstructural characterization section of this report, it is noted that with the standard heat treatment used in this study (1950F/15 min/Air Cool + 1300F/2h/Air Cool), at times not all Si was in solution. Therefore, a heat treatment study was undertaken to optimize, both with regard to practical considerations and silicide morphology, the stabilization portion of the above heat treatment schedule. The resulting procedure consists of the same solution treatment plus a stabilization age of 1100F/8 hrs/Air Cool. Creep rate results for the Si containing 100 lb. ingots heat treated by this procedure are shown in Fig. 52. In comparison to the standard heat treatment (Fig. 48), creep resistance is only slightly influenced, showing an improvement in the .5Si alloy and little if any change in the results from other alloys. If the effect of this change in heat treatment is entirely due to its influence on Si morphology, then one would not expect to see a change in creep resistance for the base alloy which contains no Si. This is in fact what is observed.

Similarly, due to a potential effect on Si morphology and because this element has been shown to be important to creep resistance when in solution, studies were undertaken to determine if long-term exposures to temperature or temperature

with stress had a subsequent effect on creep resistance. To evaluate these possibilities, 100 lb. ingot materials were aged at 1000F/1000 h at zero stress and aged at 1000F/100 h at 30% of the 1000F (811K) yield strength. Results of this study are illustrated in Figs. 53 and 54. It is apparent that the age of 1000F/1000 h had little influence with only a small increase in creep resistance for Heat V-5130 and no effect on the other alloys. When considering a TTT curve (time-temperature-transformation) for precipitation of silicides in Ti materials (Ref. 5-Fig. 3) this result is not unexpected. However, at slightly higher temperatures the possibility exists that silicides could precipitate during long exposures, resulting in reduced creep resistance. Considering aging at a moderate stress, as Figure 54 shows in comparison to Figure 48, this procedure reduces creep resistance for all alloys examined. If Si were precipitated during the age, then one would expect a slight loss in creep resistance, but this does not explain the loss in creep resistance for the alloy with no Si (Heat V-5131). Further investigation would be necessary to explain these observations.

Increased creep resistance attributed to Si additions in Ti alloys has been shown to be due to silicide precipitation on mobile dislocations during creep[5]. It has also been shown that a stress pulse can free these pinned dislocations, resulting in a period of renewed primary creep and at times an increase in secondary creep rate.[10] However, it has not as yet been determined that a similar result will occur if, instead of a stress pulse for a short period, there is substituted a long period at zero stress. To this purpose specimens from the 100 lb. ingots were tested in a cyclic manner with stress periodically applied and removed in 24-hour increments. Both primary creep and secondary creep rate were monitored at each reloading. Results for all alloys proved remarkably repeatable and, except in one case, renewed primary creep was minimal while secondary creep rate remained constant.

The results discussed above help to establish the consistent effect of Si in improving high temperature creep resistance of Ti alloys. Indeed, the benefits ascribed to Si additions have proven to be non-transitory in nature resisting cyclically applied stress and age for long periods at 1000F (811K). Only an age at 1000F (811K) under a moderate stress proved to reduce creep resistance and it has not as yet been determined that this loss was due to a change in silicide morphology.

4.4.2.2 Apparent Activation Energy

Complete results of the creep tests on beta rolled bar stock from the 100 lb. ingots are given in Table XIV. Average apparent activation energies at both 1000 and 1100F (811 and 866K) are plotted as a function of Si and O_2 for two conditions of heat treatment in Fig. 55. It is evident that increasing either Si or O_2 in the ranges shown had only minor effects on the apparent activation energies. The data indicate slightly higher ΔH's for the 0.5% Si heat at both test temperatures. There is an indication also that the 0.18 O_2 heat given the B heat treatment had somewhat higher values of ΔH than the lower oxygen heats. The effect of Si and O_2 shown here is in agreement with the data obtained on the button melts. The latter indicated little or no effect of Si at the low Fe contents as is demonstrated with ingot materials.

Of some interest also is the apparent effect of heat treatment on the zero and 0.25% Si compositions tested at 1000F (811K). The heat treatment utilizing the 1100F (866K) age resulted in somewhat lower activation energies for both alloys than the one using the 1300F (977K) final treatment. From the standpoint of creep strength, the heat treatment effects were reversed for the 0.25 Si alloy, that is, the 1100F (866K) treatment gave higher strength. Heat treatment had little effect on the creep strength of the Si free composition. Since the thermal component of the creep strength of both alloys was apparently reduced by the 1100F (866K) treatment, this would imply that it's major effect was on the athermal component.

4.4.2.3 Creep Stability

Complete creep stability results for the ingot materials are presented in Table XV. Stability per se, is also plotted as a function of Si and O_2 content in Fig. 56. The trend is generally for decreased stability with increasing Si or O_2 contents. The magnitudes of the effects are, however, affected by both heat treatment and the creep exposure temperature.

The specific effects of increasing Si or O_2 on tensile ductility before and after creep exposure are shown in Figs. 57 and 58. The trend for decreased ductility with increasing amounts of either element both before and after creep exposure is evident.

4.5 Alloy Partitioning Between Phases

Complete results of phase partitioning studies on three button alloys are presented in Table XVI. The temperature ranges covered were somewhat limited due to the necessity of having particles of both phases sufficiently large to provide valid microprobe analyses with available equipment. The microstructures of the specimens analyzed are shown in Figs. 59 through 67. The trends shown provide a good picture of the partitioning behavior of the alloying elements between the alpha and beta phases so that their role in creep strengthening mechanisms may be better defined. The significant trends observed are described below.

The Al content of the alpha phase changed only slightly if at all over the temperature range investigated. The Al content of the beta phase, on the other hand, decreased markedly with decreasing temperature. Tin and zirconium partitioned moderately to the beta phase with Zr showing a slightly greater tendency than Sn. Changes in composition of either phase with temperature were small. Silicon also showed only a relatively small tendency to partition to the beta phase. The Si content of the alpha appeared to decrease somewhat with decreasing temperature while the trend for the Si content of the beta was not consistent. The latter

behavior may be simply analytical error because of the difficulty of analyzing the small concentrations involved. On the other hand, it may be associated with the precipitation of the Si compound which occurred at the lower temperature.

The three remaining elements, bismuth, molybdenum and iron, all partition strongly to the beta phase. The data of Table XVI indicate that the solubility in the alpha phase is highest for Bi, with Mo showing the next highest and Fe very low solubility. There is some metallographic indication that the Bi compound may form a fine precipitate on the alpha phase at lower temperatures (Figs. 63 and 64).

Ignoring morphological effects, the above trends indicate that the intrinsic creep strength of the alpha phase would change only slightly with heat treatment. The beta phase, on the other hand, would probably show large changes because of the large changes in alloy content with heat treatment. The results also suggest that the primary role of Mo and Bi in the Ti-11 alloy would be in strengthening the beta phase. Work described earlier on activation energies for creep indicates that the role of Mo would be to increase the athermal component of the creep strength. The role of the Bi at this point is not clear.

4.6 Diffusivity of Bi

The procedures for determining the diffusivity of Bi in a Ti-6Al-2Sn-2Zr-1Mo matrix were described earlier. Figure 68 shows a typical concentration vs. distance plot obtained by the microprobe analyses. The average diffusion coefficients determined at three temperatures are given in Table XVII. An Arrhenius plot of these values is shown in Fig. 69. From the latter, an activation energy of 39.4 Kcal/mole was obtained. Previously, unpublished research at TIMET has shown the activation energy for diffusion of Si in titanium alloys to be 44.1 kcal/mole. These values of activation energy, for both Bi and Si, are significantly

lower than the apparent activation energy determined for creep. Part of the difference could be due to the test technique used, wherein diffusivity measurements were made in the β range whereas creep studies were in the α range. Diffusivity could be different in the α phase as compared to the β phase.

4.7 Fatigue Crack Propagation

Using the 100 lb. ingot material of the compositions listed in Table IV, the effect of Si additions on crack growth rate (da/dn) at 78 and 1000F (298 and 811K) was studied with results illustrated in Fig. 70. At room temperature it is apparent that crack growth rate exhibits a great deal of scatter, which is most likely due to extensive crack branching and is characteristic of beta processed Ti alloys.[12] No consistent effect on crack growth rate can be attributed to Si additions, although if any conclusions can be reached it appears that the alloy containing 0.5 Si has the greatest crack growth resistance. Fractography results from each alloy, shown in Fig. 71, illustrate relatively coarse fracture features characteristic of the parent microstructures and an apparent lack of fatigue striations.

When comparing the base alloy da/dn results at 78F to similar results for Ti-6Al-4V, Fig. 72, it can be seen that crack growth rate for the base alloy falls below the scatter band for the microstructures of Ti-6Al-4V evaluated. Test parameters for the data shown in Fig. 70 include an R factor of 0.1 $\left(\frac{\text{minimum load}}{\text{maximum load}}\right)$, a frequency of 10 Hz with a relative humidity of 40 to 50%. The major difference in test variables for the Ti-6Al-4V study is a higher frequency (20 Hz) and dry air environment. Thus, the difference in test variables, if influential at all, would favor a more rapid crack growth rate for the Ti-6Al-2Sn-2Zr-1Mo-.12 O_2 alloy. That is, increased humidity and decreased frequency are test variables that increase da/dn in alloys sensitive to mildly aggressive enivronments at room temperature.

It can also be seen in Fig. 70 that da/dn results at 78 and 1000F (298 and

811K) converge at high growth rates. This observation implies an environmental effect at elevated temperature. For example, as the crack growth rate increases or as the cyclic frequency increases, the time for the environment to reduce crack propagation resistance decreases and thus the magnitude of the environmental effect decreases. Previously[13,14] it has been shown for austenitic stainless steels that in an inert environment the crack growth rate at elevated temperature is equivalent to crack growth rates at room temperature. In other words, the major effect of temperature on da/dn was to accelerate environmental effects, whereas the change in mechanical properties due to increased temperature was seemingly of minor importance in comparison. Again, no consistent effect of Si additions on fatigue crack growth rate was evident at the test temperature of 1000F (811K).

To pursue further the fracture characteristics of these creep resistant alloys, fatigue crack propagation tests were performed on a base alloy of Ti-6Al-2Sn-2Zr-1Mo-.25Si with separate additions of hydrogen and oxygen. Fatigue crack growth rate results as a function of hydrogen content at 78 F are illustrated in Fig. 73, whereas results of oxygen additions at 78 and 1000 F are presented in Figs. 74 and 75. It appears that hydrogen may have a small accelerating effect on da/dn (Fig. 73), particularly at intermediate growth rates (10^{-6}-10^{-5}in/cycle), whereas oxygen additions are not believed to have any significant effect on da/dn at 78 or 1000F (Figs. 74 and 75 respectively). Results in Figure 74 do show a deviation in da/dn at room temperature for the intermediate oxygen level, but this result cannot be attributed to additions of oxygen since a further increase to .18% O_2 does not result in an additional increase in da/dn.

An additional consideration with regard to fatigue crack propagation is the growth of a crack when hold times are superimposed upon the fatigue loading. In this study, hold time effects, with a 5-minute hold at maximum load, were investigated in a relatively dry environment (average relative humidity ≈ 10%) as a

function of hydrogen content and R ratio (R = .3 and .65). Results of this work are illustrated in Figure 76. Data are necessarily sparse on account of the long test times required; however it appears that there is little or no effect of 5-minute hold times on fatigue crack growth rate in the base alloy at either R = .3 or .65. Fatigue crack growth rate for a test frequency of 10 Hz without hold times are also shown for comparative purposes. This result is somewhat surprising when considering the tortuous fracture path developed in this material (Fig. 77). One might have expected a reduced average da/dn due to the large number of secondary cracks which effectively results in an extended crack length. In any case, neither a 5-minute hold time nor change in R ratio with hold periods proved to have any significant effect on da/dn in the base alloy.

However, when considering hold time testing in combination with additions of hydrogen, results shown in Fig. 76 illustrate a dramatic increase in da/dn. It is apparent from Fig. 76 that additions of hydrogen to levels of 150 and 350 ppm significantly increase hold time da/dn results above that obtained for the same alloy without hydrogen. This was not true for fatigue results with hydrogen additions up to 252 ppm when hold times were not considered. As Fig. 73 illustrates, additions of hydrogen up to 252 ppm resulted in little or no change in da/dn when testing at a frequency of 10 Hz. Unfortunately, data are insufficient to decipher an individual cause for the increase in da/dn at R = .65 with 350 ppm H (either R effect, increased hydrogen content or both). Further testing would be necessary to determine the influence of each of the variables.

Optical and transmission electron microscopy results, Figs. 78 and 79, offer a possible explanation for the increased da/dn associated with hold time testing of high hydrogen containing alloys. Optical microscopy, Fig. 78, illustrates the crack path on the surface of the specimen. The extreme secondary cracking illustrated in Fig. 77 for the as received material (~ 17 ppm H_2) is again observed for alloys containing hydrogen. However, as Fig. 78 shows, the cracking now takes on the appearance of a stepwise progression. Transmission electron

microscopy results in Fig. 79 indeed show that secondary cracks run in a direction parallel to possible basal hydrides (note arrows). These plates have not as yet been identified, but there is good reason to suspect that they are basal hydrides based on other recent work on hydride precipitation in similar alloys.[15]

These results lead to the hypothesis that the accelerated crack propagation may be directly caused by the formation of stress induced basal hydrides. Thus, the growth of a macroscopic crack under these test conditions could be visualized as a sequence of steps involving 1) a local stress concentration, 2) accumulation of hydrogen by diffusion in sufficient quantities to form stress induced basal hydrides, and 3) fracture associated with individual basal hydrides. This cracking process could now repeat and continue as long as necessary ingredients were available, i.e., diffusible hydrogen, a stress concentration, and time. This model accounts for both the increase in da/dn and the stepwise appearance of surface cracks.

4.8 Fracture Toughness

Fracture toughness results for Ti-6Al-2Sn-2Zr-1Mo-.12 O_2 with additions of Si up to 0.5% at 78 and 1000F (298 and 811K) are tabulated in Table XVIII and illustrated as a function of Si content in Fig. 80. Test results and variables in two tests were sufficient to meet ASTM requirements[8] for a valid fracture toughness (K_{Ic}) measurement. Valid K_{Ic} results are indicated in Table XVIII. Also listed in Table XVIII for each material and temperature is the value of $2.5\left(\frac{K_Q}{\text{Yield Stress}}\right)$ which determines the thickness of material required to attain a valid K_{Ic}. Valid K_{Ic} measurements were possible for Si bearing alloys at room temperature, due to both the increase in yield strength and the decrease in fracture toughness attendant with Si additions. As illustrated in Figure 80, an addition of 0.5 Si decreases the room temperature fracture toughness from ~ 112 to ~ 71 ksi$\sqrt{\text{in}}$.

Macroscopically, specimens with Si additions failed in plane strain with a relatively smooth and flat fracture surface, whereas for the base alloy the fracture surface exhibited large shear lips and a rough fracture surface. Figure 81 shows fractographic features at low magnification illustrating islands of tear ridges (Fig. 81a and 81c) that essentially fail by ductile tearing (Fig. 81d) for specimens with additions of Si. These ridges are widely spaced with a smooth fracture appearance between. These islands of tear ridges are surrounded by a very fine dimple fracture morphology. For the base alloy, without Si, Fig. 81b illustrates a coarse fracture morphology, where at higher magnification dimple fracture and finely spaced tearing to a thin edge predominate.

Since valid measurements were unattainable for tests performed at 1000F (811K) these results are best compared using a new quantity defined in ASTM-E399-72[8] as specimen strength ratio (R_{SC}). For a compact tension specimen R_{SC} is defined as follows:

$$R_{SC} = \frac{2\,P_{max}(2w+a)}{B(w-a)^2\sigma_{YS}}$$

where

P_{max} = maximum load that the specimen could sustain

B = thickness of specimen

w = width of specimen

a = crack length

σ_{YS} = yield strength

For the materials tested, R_{SC} varies from 2.63 to 1.77 to 1.40 for 0 Si, .25 Si and .5 Si additions, respectively. From the form of the equation it is apparent that the higher value indicates a greater sharp-notch strength. It can then be concluded that increasing additions of Si reduce sharp-notch strength at 1000F (811K). Unfortunately, since R_{SC} is a relatively new quantity, further comparison of this strength parameter to additional alloys tested with the same geometry is

not possible at this time. However, R_{SC} does serve as a comparative measure of toughness for the compositions tested.

4.9 Susceptibility to Hot Salt Stress Corrosion

Work performed on this task was funded entirely by the Rockwell International Research and Development Program using materials supplied under Contract F33615-75-C-5089.

Previous investigators[16,17] have shown that susceptibility to hot-salt-stress-corrosion (HSSC) cracking can be related to creep resistance. That is, as creep resistance is improved by changes in the microstructure, susceptibility to HSSC cracking increases.[16] To evaluate this observation for the high temperature creep resistant alloys used in this program, HSSC tests were performed on Si bearing alloys heat treated to develop different creep rates. For example, Fig. 82 shows the creep rates at 1000F (811K) for Ti-6Al-2Sn-2Zr-1Mo-.5Si heat treated by the standard heat treatment of 1950F (1338K)/15 min, AC + 1300F (978K)/2 hr. AC and heat treated at 1950F (1338K)/15 min, AC + 1470F (1072K)/18 hr. AC. This second heat treatment was designed to reduce creep resistance by precipitating silicides, and as Fig. 82 shows, the creep rate is significantly increased at higher stress levels. It is important to note, however, that an extrapolation of the data in Fig. 82 would result in the conclusion that creep rates at lower stress levels ($\lesssim$ 30 ksi) are approximately equal for the two heat treatments. Also, specimens containing variable quantities of silicon were exposed to a HSSC environment and tested as described in the experimental section to determine the HSSC threshold stress. Figure 83 illustrates the creep rate for these specimens and again it is apparent that creep rates are approximately equal at low stress levels ($\lesssim$ 30 ksi).

Figure 84 illustrates room temperature residual elongation after exposure to a hot salt environment for the two heat treatments and for the alloys with

variable silicon content discussed above. No distinct threshold stress is observed, however, a rapid decrease in residual elongation occurs even for low exposure stresses (15 ksi). Scatter in a corrosion experiment can be large, however, it appears that if there is an affect of Si on HSSC susceptibility, it would be to increase the vulnerability to embrittlement. There may be an affect of the high temperature age, however, the data are insufficient to draw firm conclusions.

It should be remembered that exposure to the salt environment occurred at 850F (728K) whereas the creep curves developed for these alloys and heat treatments (Figs. 82 and 83) were obtained at 1000F (811K). Thus, for the hot salt exposure conditions it would be expected that creep rates for the materials tested would be extremely low and essentially equivalent. It may be concluded, therefore, that the materials and test conditions were insufficient to obtain a relationship between creep resistance and susceptibility to HSSC embrittlement. However, the important point to be made is that at very low stresses, relative to the creep resistance of these alloys, HSSC embrittlement can occur in a short period of time. In fact, after exposure for 48 hours at 15 ksi, a crack was observed in the Ti-6Al-2Sn-2Zr-1Mo-.12 O_2 alloy and after 48 hours at 30 ksi, cracks were observed in all alloys. These stress levels are sufficiently low to be considered in the working range of these creep resistant alloys.

4.10 Evaluation of Microstructures

4.10.1 Pre-Creep Microstructural Characterization

Optical and transmission electron microscopy results for the alloys listed in Table I and II are illustrated in Figs. 85 through 106. All alloys were beta rolled to 1/2" round bar at 1950F (1338K) and heat treated 1950F (1338K)/15 min AC + 1300F (978K)/2 hr. AC. The resulting microstructure from this β processing, as illustrated in Fig. 85a for the base alloy composition, consists entirely of

Widmanstätten $\alpha+\beta$. Electron microscopy of the same structure, Figs. 85b and 85c, reveals thin strips of β between the α-phase plates. The region near the α/β interphase boundaries has been termed "interface phase." These regions have been shown to consist of fine particles of α-phase which nucleate at the interface and grow into the primary α.[18] This interface phase was found to be very common in the microstructures of this study. Additional results, Figs. 86 through 106, for the base alloy with single and multiple minor alloy additions, similarly illustrate the Widmanstätten $\alpha+\beta$ structure with strips of β between the α-phase plates. The existence of the interface phase is clearly established between the α/β boundaries.

Only two departures from the structure described above occurred for the button materials listed in Tables I and II. First, for additions of 0.5 Bi thin foil results, Fig. 88d, revealed what appeared to be an increase in the volume fraction of β phase. Figures 88a and 88b illustrate the microstructure for an addition of 0.25 Bi to the base alloy and it can be concluded that it is relatively similar to that previously illustrated for other minor additions. This is also true for additions of 1.0 and 2.0 Bi, Figs. 89b, 89c, and Fig. 90b. Thus, it is not believed that the morphology change in the alloy containing .5 Bi is due to the alloy addition since greater additions of Bi do not produce this structure. It is speculated that this structure is possibly due to anomalies during fabrication. The resulting poor creep properties determined for this alloy should therefore be suspect. The second departure from the structure described above occurred for alloys without additions of molybdenum (Figs. 104 a & b, 105 a & b, and 106 a & b). These figures do not show a Widmanstätten structure, but illustrate a coarse grained prior-β structure relatively devoid of internal detail. As noted earlier, the Mo additions are necessary for both refinement of the microstructure and improvement in post-creep ductility and as such these alloys do exhibit lower post-creep ductility than other alloys.

In addition, some thin foil results indicate the presence of silicide precipitates (Figs. 97d, 102b, and 105b). The removal of silicon from solution, by heat treatment, to form precipitates, would be expected to reduce creep resistance. This has been demonstrated in both commercial alloys and in model Ti-Si alloys,[5] and results from the requirement for Si to be in solution in order to achieve improvements in creep strength. As discussed above in the section on creep properties of 100 lb. ingots, this problem of precipitated silicides can at least be partially alleviated by reducing the temperature used for stabilization from 1300F (977K) to 1100F (866K). This also results in an attendant increase in creep resistance.

4.10.2. Post-Creep Microstructures

Samples of alloys containing additions of Bi, Fe and Si were examined after creep to investigate the possibility of precipitation on dislocations occurring during the creep process. Neither the Bi nor the Fe containing alloys showed any evidence of precipitation on dislocations. An example of an alloy containing Ti-6Al-2Sn-2Zr-1Mo-1.0Fe is shown in Fig. 107, and the absence of precipitation is evident. However, in the alloy containing .5% Si, a considerable amount of precipitation on dislocations after extended creep exposure at strain rates of less than $\sim 1 \times 10^{-4}$ h^{-1} was observed. Figures 108 (a) and (b) are a pair of micrographs of a Ti-6Al-2Sn-2Zr-1Mo-0.5Si alloy strained 1.5% at an average strain rate of 6×10^{-4} h^{-1}. Although discrete precipitation on dislocations such as were observed by Paton and Mahoney in a previous study[5] of a Ti-5Al-0.5Si alloy are not present, strong residual contrast is present at locations in Fig. 108 (b), where no contrast should be apparent with the 0002 reflection used to form this image. Another example of this strong residual contrast is shown in Fig. 109 for the same alloy as Fig. 108, but at a higher magnification. At even slower strain rates, more pronounced evidence of precipitation on

dislocations was observed. Figure 110 shows a sample strained at 2×10^{-5} hr^{-1} at 1000F, and the strong residual contrast (arrowed) is typical of the alloys containing 0.5 Si strained at lower strain rates. Examination of alloys containing either no silicon, 0.25 Si, or any of the other minor additions investigated in this program, did not show any residual contrast on $\vec{a}$ dislocations when imaged under the same conditions as used in Figs. 108 through 110. This is taken as evidence that the high supersaturation of Si available at the 0.5% level is probably responsible for the observed interaction with mobile $\vec{a}$ dislocations, and the consequent improvement in creep strength.

SECTION V

SUMMARY

In this report, baseline data have been established at room and elevated temperatures characterizing the effect of minor element alloying additions on materials performance. A base alloy of Ti-6Al-2Sn-2Zr with individual and multiple element additions of Mo, Si, S, Fe, Bi, and O_2 was evaluated with regard to mechanical properties, creep, fatigue, fracture, hot salt stress corrosion, diffusivity of Bi, element partitioning, and microstructure. Results from each of these catagories is discussed below: except where indicated throughout the text, as a last processing step all bar and plate material was heat treated as as follows: 1950F (1338K)/15 min, air cool + 1300F (978K)/2 h, air cool.

5.1 Tensile Properties

All of the above noted elements were found to have independent effects on room and elevated temperature tensile properties. Additions of Fe proved generally to have an undesirable effect on properties showing a decrease in ductility with increasing Fe content at room temperature, while strength parameters increased moderately both at 78 and 1000F. Interactions between the elements were seldom significant with the effects more often proving to be additive than interacting.

Compression yield strength results as a function of temperature on these same interaction alloys, have identified two peaks at ~ 600F (588K) and 1200F (921K) most likely due to strain aging. It was not possible to identify any single element responsible for the peaks.

5.2 Creep Properties

Creep properties were more significantly influenced by minor alloying additions than tensile properties. Considering the individual elements investigated, it may be concluded that only Si and Bi imparted a consistent improvement to creep resistance. Iron additions continuously reduced creep resistance while S, Mo and O_2 additions resulted in mixed results. With regard to interaction effects, Si-O_2 combinations were shown to be beneficial with the improvement in creep resistance dependent on the magnitude of each element, S appeared to have no benefit in combination with added minor elements, and Mo-Si additions increased creep resistance with the benefits of each element being additive.

Evaluation of alloying effects on apparent activation energy for creep proved difficult because of a large test error. However, a correlation was found between activation energy and creep rate which allowed correction of the observed energies for creep rate thus reducing test scatter sufficiently and thereby allowing evaluation to be carried out. All elements except O_2 had significant effects on apparent activation energy, either independently or as an interaction with a second element. Significant interactions between Fe and S and Fe and Si were found. Interestingly, Mo additions sharply reduced the apparent activation energy for creep despite the fact that they increased creep strength. The effects of Mo additions were thus indicated to be most influential on the athermal component of the creep strength. Activation energies in all cases were much higher than would be expected if creep were controlled by a simple diffusion mechanism.

All of the elements, except Mo, involved in this study were shown to have deleterious effects on creep stability. In most cases where two elements were present the effects were additive. The exceptions to this were Mo which, when added with Si, decreased the pronounced effect of the latter element on stability, and S, which seemingly had no influence on creep stability.

5.3 Alloy Partitioning

Phase partitioning studies indicated that the composition of the alpha phase and hence its intrinsic creep strength changed only a small amount during heat treatment. Sn, Zr, and Si were found to partition very moderately to the beta phase. Partitioning of Bi, Mo and Fe to the beta phase was pronounced, suggesting that the role of Bi in improving the alloy's creep strength may be associated with improving creep strength in this phase. Iron improves the strength of the β phase, whereas iron additions decrease creep resistance. Therefore, increased strength does not necessarily lead to an increase in creep strength.

5.4 Diffusivity of Bi

The diffusivity of Bi in a Ti-6Al-2Sn-2Zr-1Mo matrix was determined. The activation energy for diffusion was 39.4 Kcal/mole, and did not correspond to the apparent activation energy for creep of the Bi containing alloys.

5.5 Fatigue and Fracture

Studies have determined that additions of Si to a base alloy of Ti-6Al-2Sn-2Zr-1Mo-.12 O_2 have no consistent measurable effect on crack growth rate, whereas fracture toughness is significantly decreased with increasing Si content. These conclusions are true at both 78 and 1000F (298 and 811K). Further, crack growth rate is increased by a factor of ten for crack propagation at 1000F (811K) versus 78F (298K) at low stress intensities with rates tending to converge at higher stress intensities. This convergence implies an environmental effect on fatigue crack growth rate. In general, compared to Ti-6Al-4V, alloys of composition

Ti-6Al-2Sn-2Zr-1Mo-.12 O_2 with additions of Si exhibit a comparatively low crack growth rate for equivalent stress intensities.

Fatigue crack growth rate behavior at 78 and 1000F (298 and 811K) was also evaluated for an alloy of Ti-6Al-2Sn-2Zr-1Mo-.25Si with additions of O_2. From these results it can be concluded that O_2 additions up to 0.18 wt.% have no significant effect on fatigue crack growth rate. In a similar manner, the effect of hydrogen additions was evaluated, resulting in the conclusion that hydrogen up to 350 ppm increased da/dN only a small amount. However, when testing in fatigue with 5-minute hold times at the maximum applied load, additions of hydrogen increased crack growth rates by approximately an order of magnitude. This result is possibly due to cracks progressing parallel to what appears to be basal hydrides.

5.6 Hot Salt Stress Corrosion

Susceptibility to hot salt stress corrosion at 850F (727K) was evaluated for an alloy of composition Ti-6Al-2Sn-2Zr-1Mo with additions of Si up to 0.5 wt. %. No conclusion could be reached with regard to the effect of Si on susceptibility. However, it was shown that for very low stresses, relative to the creep resistance of these alloys, hot salt stress corrosion embrittlement could occur in a short period of time.

5.7 Pre- and Post Creep Microstructures

The predominant starting microstructure evaluated consisted entirely of Widmanstätten $\alpha+\beta$ with thin strips of β between the α-phase plates. Also, regions near the α/β interphase boundaries termed "interface phase" were clearly identified in most alloys. In general, only alloys without Mo showed a departure from this description.

Post-creep microscopy of alloys containing .5% Si has revealed considerable precipitation on dislocations after extended creep exposure for strain rates less than $\sim 1 \times 10^{-4} h^{-1}$. It is this silicide precipitation on mobile dislocations

during creep that imparts increased creep resistance to Si containing Ti alloys. Neither the Bi nor the Fe containing alloys showed any evidence of precipitation on dislocations.

SECTION VI

SUGGESTIONS FOR FURTHER WORK

One of the important conclusions that can be drawn from this work is that it is very difficult to examine the contribution of minor element additions using button-size heats. The anticipated effects on mechanical properties are generally small, and multiple tests are required to provide the required level of confidence in the results. Buttons do not provide sufficient material for multiple tests and in addition segregation problems are generally more severe with buttons than with ingots. It is therefore recommended that any future program along these lines should use ingots as starting material for all experimental work.

Although numerous individual and interaction effects were examined in this study, one interaction effect which was not included was that of Bi-Si. This was omitted in an effort to limit the size of the program, but since both of these elements showed individual effects which were beneficial, it would probably be worthwhile to study interactions also.

Several individual element effects which were not investigated in the current program should be studied in any future effort. Principal among these are nitrogen, which might be expected to improve strength without impairing toughness; carbon and germanium additions might also be worth investigation as an additional means of improving creep strength.

In the current program pre-aging was found to have significant effects on creep, particularly at low stress levels. This effect should certainly

be studied more extensively since so many independent variables are involved (stress, time, temperature) and since the effect would be very important in service. This should probably be investigated along with specimen size and environment effects, which have also been shown to be extremely important in influencing creep in Ti alloys. Size appears to have an influence through not only the exposed surface to volume ratio during creep, but also through the cooling rate experienced during heat treatment, and the consequent effect on microstructure. The effect of texture on creep is also known to be important[16] but has not been studied in any detail for creep resistant alloys.

One of the most important results to have come out of this program is the demonstration of a significant hold time effect in these alloys, particularly at high hydrogen concentrations. However, the effect of oxygen, Si and heat treatment (microstructure) was not studied, and the individual effects and interactions between these variables should be studied in detail.

Finally, the program has shown some benefits of going to higher Si contents than conventionally used in creep resistant Ti alloys. Since 0.5% Si is probably too high a Si content for a commercial alloy, optimizing the Si content for a given base alloy is still necessary. A series of alloys with Si compositions spaced at closer intervals than those used here would be required, with a final optimum composition probably being in the range of 0.2 to 0.4% Si, depending on the base alloy.

TABLE I

Heat Numbers and Nominal Alloy Addition to Button Melts of Base Composition Ti-6Al-2Sn-2Zr-1Mo

Heat No.	Alloy Addition to Ti-6Al-2Sn-2Zr-1Mo
B-2650, B-2651	No Addition
B-2652, B-2653	0.1 Si
B-2654, B-2655	0.25 Si
B-2656, B-2657	0.5 Si
B-2658, B-2659	0.25 Bi
B-2660, B-2661	0.5 Bi
B-2662, B-2663	1.0 Bi
B-2664, B-2665	2.0 Bi
B-2666, B-2667	0.15 Fe
B-2668, B-2669	0.25 Fe
B-2670, B-2671	0.5 Fe
B-2672, B-2673	1.0 Fe
B-2674, B-2675	2.0 Fe
B-2982, B-2983	0.005 S
B-3053, B-3054	0.010 S
B-3055, B-3056	0.020 S

Oxygen aim for all heats was 0.1%

TABLE II

Heat Numbers and Nominal Alloy Addition to Button Melts of Base Composition Ti-6Al-2Sn-2Zr

Heat No.	Alloy Addition to Ti-6Al-2Sn-2Zr
B-2986, B-2987	1Mo-.25Si-.25Fe
B-2988, B-2989	1Mo-.25Si-.5Fe
B-2990, B-2991	1Mo-.25Si-2.0Fe
B-2992, B-2993	1Mo-.5Si-.25Fe
B-2994, B-2995	1Mo-.5Si-.5Fe
B-2996, B-2997	1Mo-.5Si-2.0Fe
B-3080, B-3081	1Mo-.005S-.25Fe
B-3082, B-3083	1Mo-.005S-.5Fe
B-3008, B-3009	1Mo-.005S-2.0Fe
B-3061, B-3062	1Mo-.02S-.25Fe
B-3063, B-3064	1Mo-.02S-.5Fe
B-3065, B-3066	1Mo-.02S-2.0Fe
B-3010, B-3011	1Mo-.12 O_2
B-3012, B-3013	1Mo-.12 O_2-.25Si
B-3014, B-3015	1Mo-.12 O_2-.5Si
B-3016, B-3017	1Mo-.18 O_2
B-3018, B-3019	1Mo-.18 O_2-.25Si
B-3020, B-3021	1Mo-.18 O_2-.5Si
B-3022, B-3023	No Additions
B-3024, B-3025	2Mo
B-3026, B-3027	.25Si
B-3028, B-3051	2Mo-.25Si
B-3030, B-3031	.5Si
B-3032, B-3033	2Mo-.5Si

TABLE III ANALYZED Bi AND S CONTENTS OF BUTTON MELTS USED

Heat No.	Nominal Addition (1)	Actual Analysis % Bi	% S
B-2659	0.25 Bi	0.17	-
B-2661	0.5 Bi	0.32	-
B-2663	1.0 Bi	0.75	-
B-2665	2.0 Bi	1.32	-
B-2982	0.005 S	-	0.0065
B-2983	"	-	0.0063
B-3053	0.010 S	-	0.0132
B-3054	"	-	0.0119
B-3055	0.02 S	-	0.0207
B-3056	"	-	0.0212
B-3080	0.25 Fe - 0.005 S	-	0.0042
B-3081	" "	-	0.0044
B-3082	0.5 Fe "	-	0.0044
B-3083	" "	-	0.0050
B-3008	2.0 Fe "	-	0.0046
B-3009	" "	-	0.0045
B-3061	0.25 Fe - 0.02 S	-	0.0218
B-3062	" "	-	0.0177
B-3063	0.50 Fe - "	-	0.0179
B-3064	" "	-	0.0181
B-3065	2.0 Fe "	-	0.0202
B-3066	" "	-	0.0200

(1) To a Ti-6Al-2Sn-2Zr-1Mo base

TABLE IV

Chemical Analyses of 100-Pound Ingots

Heat No.	Al	Sn	Zr	Mo	Si	S	Fe	N	O
V-5129 (Ti-6Al-2Sn-2Zr -1Mo-0.5Si-0.12 O_2)	5.99	2.17	2.28	1.05	0.49	.0024	0.054	0.008	0.131
V-5130 (Ti-6Al-2Sn-2Zr -1Mo-0.25Si-0.12 O_2)	5.90	2.26	2.34	1.07	0.25	.0023	0.063	0.009	0.139
V-5131 (Ti-6Al-2Sn-2Zr -1Mo-0.12 O_2)	5.98	2.25	2.22	1.12	0.025	.0018	0.057	0.008	0.134
V-5128 (Ti-6Al-2Sn-2Zr -1Mo-0.25Si-0.06 O_2)	5.96	2.21	2.14	1.03	0.22	.0018	0.050	0.009	0.088
V-5132 (Ti-6Al-2Sn-2Zr -1Mo-0.25Si-0.18 O_2)	6.00	2.20	2.11	1.06	0.22	.0019	0.047	0.008	0.191

TABLE V

Tensile Properties of Button Melts

Heat No.[2]	Nominal Addition, %[1]	Room Temperature Tests UTS, Ksi	YS, Ksi	% RA	% El	1000F Tests UTS, Ksi	YS, Ksi	% RA	% El
B-2651	1 Mo	127.7	115.6	28.4	13	79.0	65.4	50.0	16
B-2653	1 Mo-0.1Si	130.5	122.2	26.8	14	83.9	65.9	47.7	18
B-2655	1 Mo-0.25Si	136.8	117.1	22.7	10	90.0	67.9	46.8	17
B-2657	1 Mo-0.5Si	144.9	135.7	12.5	10	97.1	74.1	39.5	17
B-2659	1 Mo-0.25Bi	127.1	115.6	26.9	13	80.9	62.4	49.4	17
B-2661	1 Mo-0.5Bi	130.4	121.3	27.7	13	77.0	59.0	46.0	17
B-2663	1 Mo-1.0Bi	130.6	121.3	26.2	10	82.2	65.7	43.7	16
B-2665	1 Mo-2.0Bi	132.7	120.0	19.8	11	86.7	64.1	27.2	15
B-2667	1 Mo-0.15Fe	132.7	124.5	28.3	11	86.5	65.9	52.2	20
B-2669	1 Mo-0.25Fe	130.2	121.6	23.8	11	82.3	63.7	56.2	19
B-2671	1 Mo-0.5Fe	136.7	125.7	25.0	16	93.4	71.1	60.2	29
B-2673	1 Mo-1.0Fe	142.4	132.2	10.5	7	95.3	71.8	48.4	21
B-2675	1 Mo-2.0Fe	140.5	138.8	3.0	2	98.4	73.7	46.3	28
B-2982	1 Mo-0.005S	130.5	119.2	29.4	14	88.5	68.2	46.0	15
B-3053	1 Mo-0.010S	132.3	120.5	27.1	14	87.6	65.8	47.5	19
B-3055	1 Mo-0.02S	131.6	121.6	16.5	10	87.6	66.9	40.1	16
B-2986	1 Mo-0.25Fe-0.25Si	145.3	131.2	11.6	5	97.8	82.9	37.8	17
B-2988	1 Mo-0.5Fe-0.25Si	147.9	133.5	11.8	4	100.8	80.8	32.8	19
B-2990	1 Mo-2.0Fe-0.25Si	161.0	154.8	6.2	0	111.4	94.5	30.9	8
B-2992	1 Mo-0.25Fe-0.5Si	152.4	138.5	5.3	15	107.8	90.8	47.1	19
B-2994	1 Mo-0.5Fe-0.5Si	158.1	144.6	7.6	3	109.7	82.4	25.4	14
B-2996	1 Mo-2.0Fe-0.5Si	165.2	165.2	1.6	0	126.7	112.3	20.9	7
B-3087	1 Mo-0.25Fe-0.005S	128.6	119.0	28.9	13	88.9	69.3	53.8	23
B-3083	1 Mo-0.5Fe-0.005S	131.5	121.7	21.3	13.5	90.3	79.4	45.1	21
B-3008	1 Mo-2.0Fe-0.005S	150.8	136.4	6.2	0	106.5	88.6	35.1	18
B-3061	1 Mo-0.25Fe-0.02S	132.6	124.5	22.0	10	90.5	69.2	43.7	19.5
B-3063	1 Mo-0.5Fe-0.02S	133.3	122.7	14.3	9	90.5	69.7	35.0	15
B-3065	1 Mo-2.0Fe-0.02S	147.0	137.6	3.0	2	105.9	86.1	28.7	18
B-3010	1 Mo-0.12 O_2	129.5	119.1	29.9	12	78.0	63.4	45.8	15
B-3012	1 Mo-0.25Si-0.12 O_2	138.4	125.9	19.3	12	86.7	69.9	35.0	13

TABLE V : Tensile Properties of Button Melts - (Continued)

Heat No.(2)	Nominal Addition, %(1)	Room Temperature Tests				1000F Tests			
		UTS, Ksi	YS, Ksi	% RA	% El	UTS, Ksi	YS, Ksi	% RA	% El
B-3014	1 Mo-0.5Si-0.12 O_2	149.2	134.7	10.9	6	99.3	78.7	28.6	14
B-3016	1 Mo-0.18 O_2	140.4	133.9	24.1	12	80.6	65.7	50	14
B-3018	1 Mo-0.25Si-0.18 O_2	140.8	127.5	21.8	8	93.5	74.2	34.4	14
B-3020	1 Mo-0.5Si-0.18 O_2	156.6	138.5	11.0	8	104.4	80.5	28.6	17
B-3022	None	115.7	102.5	35.1	20	63.0	51.2	46.6	21
B-3024	2 Mo	134.4	115.7	25.5	15	89.2	70.1	54.0	15
B-3026	0.25Si	125.3	116.1	26.1	19	69.5	58.5	37.9	17
B-3028	2Mo-0.25Si	141.5	122.5	14.6	10	93.6	73.9	40.2	15
B-3030	0.5Si	135.7	126.6	21.6	15	79.2	65.1	33.3	15
B-3032	2Mo-0.5Si	146.2	128.7	10.4	8	103.7	80.9	31.8	17

(1) Added to a Ti-6Al-2Sn-2Zr Base; Nominal O_2 content is 0.10 unless otherwise specified.

(2) One-half inch dia. beta rolled bar. Heat treated 1950F (15 min) AC + 1300F (2 hrs) AC.

TABLE VI

Results of Analysis of Variance on the Effects of Minor Alloying Additions to a Base Alloy of Ti-6Al-2Sn-2Zr

Alloy Addition	Temperature (F)	Materials Property[1]	Statistical Significance[2]
Fe	RT	YS	<0.001
Si	"	"	<0.001
S	"	"	<0.2>0.01
Mo	"	"	<0.2>0.1
O_2	"	"	<0.2>0.1
Fe	RT	RA	<0.001
Si	"	"	<0.001
S	"	"	<0.01>0.005
Mo	"	"	<0.005>0.001
O_2	"	"	>0.2
Fe	1000	YS	<0.001
Si	"	"	<0.001
S	"	"	>0.2
Mo	"	"	<0.001
O_2	"	"	>0.2
Fe	1000	RA	<0.2>0.1
Si	"	"	<0.025>0.01
S	"	"	<0.001
Mo	"	"	>0.2
O_2	"	"	<0.05>0.025
Fe-Si	RT	YS	<0.025>0.01
Fe-S	"	"	>0.2
Mo-Si	"	"	<0.01>0.005
O_2-Si	"	"	<0.005>0.001
Fe-Si	RT	RA	<0.1>0.05
Fe-S	"	"	>0.2
Mo-Si	"	"	>0.2
O_2-Si	"	"	>0.2
Fe-Si	1000	YS	<0.1>0.05
Fe-S	"	"	>0.2
Mo-Si	"	"	>0.2
O_2-Si	"	"	>0.2
Fe-Si	1000	RA	<0.025>0.01
Fe-S	"	"	>0.2
Mo-Si	"	"	>0.2
O_2-Si	"	"	>0.2

1) YS = Yield Strength; RA = Reduction of Area
2) Probability that observed effects were due to chance. A level of 0.05 or less was considered to indicate a real effect.

TABLE VII

Tensile Data Used to Determine Test Error Variance

Normal Composition	Temp F	Heat No.	UTS,Ksi	0.2%YS,Ksi	% RA	% El
Ti-6Al-2Sn-2Zr-1Mo-0.25Fe	RT	B-2998	134.9	126.9	26.9	14
			135.5	126.9	25.7	14
		B-2999	135.9	126.6	27.3	17
			133.0	125.9	22.0	14
		B-3005	131.7	124.9	27.0	15
			130.3	124.7	28.4	17
	1000	B-2998	82.9	72.5	44.5	14
			91.5	77.0	52.0	10
		B-2999	83.4	69.9	44.9	16
			84.7	68.9	45.1	14
		B-3005	86.0	67.7	48.4	19
			89.1	66.4	42.9	17
Ti-6Al-2Sn-2Zr-1Mo-0.5Fe	RT	B-3000	140.2	131.3	15.3	10
			137.3	128.3	21.8	15
		B-3001	138.7	128.0	21.0	14
			137.1	127.0	25.7	13
		B-3006	138.3	128.8	26.7	14
			136.5	126.6	22.2	14
		B-3007	137.9	129.3	23.2	15
			137.2	129.5	19.9	14
	1000	B-3000	92.8	74.1	45.3	18
			96.3	76.3	42.8	21
		B-3001	95.3	72.1	43.0	19
			96.5	75.4	48.9	22.5
		B-3006	93.4	71.4	45.7	20
			93.3	73.2	47.1	17
		B-3007	93.8	72.4	39.9	17
			93.9	73.1	43.0	18
Ti-6Al-2Sn-2Zr-1Mo-2.0Fe	RT	B-3002	155.1	142.8	8.6	4
			154.6	141.1	10.1	7
		B-3003	154.5	145.6	6.3	3
			153.4	145.1	4.8	3

TABLE VIII

Tensile Properties of 100-Pound Ingot Material[1]

Heat No.	Nominal Composition[2] % Si	% O_2	Test Temp F	1950 (15 Min)AC + 1300F (2 Hrs)AC UTS,Ksi	YS,Ksi	% RA	% Elong	1950F (15 Min)AC + 1100F (8 Hrs)AC UTS,Ksi	YS,Ksi	% RA	% Elong
V-5131		0.12	-320	207.3	193.5	5.7	5.5	-	-	-	-
				213.4	194.4	16.7	10	-	-	-	-
			Ave.	210.4	194.0	11.2	7.8				
			RT	140.3	124.6	16.8	11	140.4	123.8	21.0	15
				139.4	125.2	21.7	13	141.6	121.4	16.8	14
			Ave.	139.9	124.9	19.3	12	141.0	122.6	18.9	14.5
			300	114.5	95.5	33.4	14	120.2	98.4	28.8	14
				116.2	95.2	28.9	13.5	120.1	98.6	27.3	15
			Ave.	115.4	95.4	31.2	14	120.2	98.5	28.1	14.5
			600	99.8	89.7	36.8	16	102.5	78.1	33.2	15
				100.3	78.7	30.3	15	103.8	76.6	34.7	15
			Ave.	100.1	84.2	33.6	15.5	103.2	77.4	34.0	15
			800	94.1	75.5	40.9	14.5	94.7	72.2	20.8	18
				94.6	74.2	37.2	15	94.9	71.8	27.9	16
			Ave.	94.4	74.9	39.1	15	94.8	72.0	24.4	17
			1000	88.6	68.9	36.4	16	89.6	70.6	20.1	13.5
				87.7	68.7	37.9	15	90.0	65.9	19.4	15
			Ave.	88.2	68.8	37.2	15.5	89.8	68.3	19.8	14.5
			1200	70.1	60.8	20	9	74.5	61.1	18.7	14.5
				75.3	62.8	17.1	11	73.0	58.3	15.6	14.0
			Ave.	72.7	61.8	18.6	10	73.8	59.7	17.2	14.5
V-5130	0.25	0.12	-320	222.8	201.7	5.4	4.5	-	-	-	-
				222.9	201.2	7.9	5	-	-	-	-
			Ave.	222.9	201.5	4.7	4.8				
			RT	150.0	133.5	14.5	9	153.3	133.0	14.3	13
				149.0	132.8	10.4	7	152.6	133.4	17.9	13
			Ave.	149.5	133.2	12.5	8	153.0	133.2	16.1	13
			300	122.1	103.7	13.6	10	129.5	106.3	19.7	12
				125.3	105.6	16.7	10	132.6	102.2	17.9	15
			Ave.	123.7	104.7	15.2	10	131.1	104.3	18.8	13.5

TABLE VIII (Continued)

Tensile Properties of 100-Pound Ingot Material[1]

Heat No.	Nominal Composition[2] % Si	% O_2	Test Temp F	1950 (15 Min)AC + 1300F (2 Hrs)AC UTS,Ksi	YS,Ksi	% RA	% Elong	1950F (15 Min)AC + 1100F (8 Hrs)AC UTS,Ksi	YS,Ksi	% RA	% Elong
			600	109.7	88.7	15.9	11.5	113.8	83.7	21.6	13.5
				108.6	85.9	20.7	10	113.3	84.7	26.7	12
			Ave.	109.2	87.3	18.3	11	113.6	84.2	24.2	13
V-5130	0.25	0.12	800	103.5	83.2	21.6	13	108.0	79.0	25.4	12.5
				101.7	82.5	15.0	7 BOGL	107.3	80.6	27.7	15
			Ave.	102.6	82.9	18.3	13	107.7	79.8	26.6	14
			1000	94.9	76.0	24.2	15	100.8	74.9	28.4	13
				96.7	76.6	27.8	14.5	101.6	73.5	30.1	14
			Ave.	95.8	76.3	26.0	15	101.2	74.2	29.3	13.5
			1200	76.6	65.4	15.5	11.0	80.8	62.3	17.5	16
				78.3	63.9	15.6	9 BOGL	81.2	63.2	14.6	13
			Ave.	77.5	64.7	15.6	11	81.0	62.8	16.1	14.5
V-5129	0.50	0.12	-320	226.4	204.9	4.7	2	-	-	-	-
				228.9	206.5	5.1	3	-	-	-	-
			Ave.	227.7	205.7	4.9	2.5				
			RT	153.2	141.1	10.1	9	156.0	134.9	12.4	10
				154.4	139.6	9.1	7	156.7	137.9	9.6	10
			Ave.	153.8	140.4	9.6	8	156.4	136.4	11.0	10
			300	130.3	104.4	12.9	8	136.5	112.0	17.2	12
				129.5	106.7	7.8	8	134.6	109.6	16.0	12
			Ave.	129.9	105.7	10.4	8	135.6	110.8	16.6	12
			600	113.5	88.9	19.9	10	119.3	89.1	21.7	12.5
				114.1	89.5	15.8	11	120.6	90.1	20.3	11
			Ave.	113.8	89.2	17.9	10.5	120.0	89.6	21.0	12
			800	108.7	87.9	16.3	11	115.5	88.5	23.8	13
				107.8	85.4	19.8	11	113.4	84.6	22.9	13
			Ave.	108.3	86.7	18.1	11	114.5	86.6	23.4	13
			1000	103.1	80.1	24.3	13	106.0	79.8	23.6	13.5
				102.9	87.4	25.1	12	107.1	80.3	28.8	15

TABLE VIII (Continued)

Tensile Properties of 100-Pound Ingot Material[1]

Heat No.	Nominal Composition[2] % Si	% O_2	Test Temp F	1950 (15 Min)AC + 1300F (2 Hrs)AC UTS,Ksi	YS,Ksi	% RA	% Elong	1950F (15 Min)AC + 1100F (8 Hrs)AC UTS,Ksi	YS,Ksi	% RA	% Elong
				103.0	83.8	24.7	12.5	106.6	80.1	26.2	14.5
			1200	82.6	76.3	16.2	15	84.9	62.2	19.8	17
			Ave.	84.8	72.8	25.1	17	86.2	61.1	22.2	20.5
				83.7	74.6	20.7	16	85.6	61.7	21.0	19
V-5128	0.25	0.06	-320	214.7	195.0	9.7	8	-	-	-	-
			Ave.	215.3	194.7	7	5	-	-	-	-
				215.0	194.9	8.4	6.5				
			RT	144.3	129.8	13.6	12	145.9	118.8	20.7	13
			Ave.	140.6	128.2	15.1	12	146.1	125.6	21.0	12
				142.5	129.0	14.4	12	146.0	122.2	20.9	12.5
			300	121.3	101.3	16.8	13	127.7	100.7	22.5	14
			Ave.	122.1	99.8	15.9	10	127.6	100.6	24.5	14
				121.7	100.6	16.4	11.5	127.7	100.7	23.5	14
			600	106.0	79.3	23.0	11	109.2	82.0	27.6	12
			Ave.	105.9	80.1	21.7	12	109.3	79.4	28.9	12
				106.0	79.7	22.4	11.5	109.3	80.7	28.3	12
			800	100.8	75.2	22.7	13	106.3	79.2	31.4	12
			Ave.	98.0	73.2	24.4	13	105.1	77.4	34.3	15
				99.4	74.2	23.6	13	105.7	78.3	32.9	13.5
			1000	93.9	74.3	31.4	16	98.3	73.6	39.2	15
			Ave.	93.4	70.8	34.8	18	98.4	67.6	35.6	15.5
				93.7	72.6	33.1	17	98.4	70.6	37.4	15.5
			1200	77.2	58.9	15.7	12	82.1	58.3	28.3	18
			Ave.	77.6	62.2	17.4	14	74.9	56.6	30.3	30
				77.4	60.6	16.6	13	78.5	57.5	29.3	24
V-5132	0.25	0.18	-320	226.8	(3)	3.8	4	-	-	-	-
			Ave.	226.1	204.2	6	3	-	-	-	-
				226.5	204.2	4.9	3.5				
			RT	153.4	136.6	12.8	10	156.0	138.5	16.9	14.5

TABLE VIII (Continued)

Tensile Properties of 100-Pound Ingot Material[1]

Heat No.	Nominal Composition[2] % Si	% O_2	Test Temp F	1950 (15 Min)AC + 1300F (2 Hrs)AC UTS,Ksi	YS,Ksi	% RA	% Elong	1950F (15 Min)AC + 1100F (8 Hrs)AC UTS,Ksi	YS,Ksi	% RA	% Elong
				151.7	135.2	13.9	10	157.0	138.1	13.4	12
				152.6	135.9	13.4	10	156.5	138.3	15.2	13.5
			300 Ave.	126.6	105.4	9.9	5 BOPM	132.7	109.7	20.5	15
				127.4	105.3	18.0	12	134.1	106.8	14.4	12
				127.0	105.4	18	12	133.4	108.3	17.5	13.5
V-5132	0.25	0.18	600 Ave.	109.8	84.9	21.3	12	113.9	88.3	29.0	13
				108.4	84.6	20.4	12	113.6	84.1	24.2	11.5
				109.1	84.8	20.9	12	113.8	86.2	26.6	12.5
			800 Ave.	101.9	77.4	23.6	13	109.7	80.7	31.9	17
				101.7	73.5	25.6	10	106.6	75.9	31.5	13.5
				101.8	75.5	24.6	11.5	108.2	78.3	31.7	15.3
			1000 Ave.	93.5	70.9	28.1	13	99.4	75.5	33.0	14.5
				98.0	75.6	19.4	12	100.0	71.9	34.2	15
				95.8	73.3	23.8	12.5	99.7	73.7	33.6	15
			1200 Ave.	78.2	61.4	14.9	12	81.6	67.4	18.9	13.5
				79.2	59.9	10.6	10	83.4	68.8	20.9	14
				78.7	60.7	12.8	11	82.5	68.1	19.9	14

(1) Tests made on 1/2-inch dia. beta rolled bar.
(2) Added to a Ti-6Al-2Sn-2Zr-1Mo base
(3) Extensometer malfunctioned - YS was not obtained.

BOGL = Broke outside gage length.
BOPM = Broken on punch mark.

TABLE IX

Tensile Properties of Ti-6Al-2Sn-2Zr-1Mo-.12 O_2 Plate at 78 and 1000F as a Function of Si Additions

Heat No.	Nominal Addition of Si (%)	Temperature F	Elong.(1) (%)	YS(1) (psi)	UTS(1) (psi)
V-5131	0	78	7.82	106,950	126,520
"	"	1000	11.85	54,342	77,887
V-5130	.25	78	6.96	118,806	140,755
"	"	1000	10.17	65,560	85,822
V-5129	.5	78	3.53	118,846	143,011
"	"	1000	6.96	71,092	93,684

(1) Average of two tests

TABLE X CREEP PROPERTIES OF BUTTON MELTS

Nominal[1] Additions, %	Heat No.	Stress Ksi	Creep Rate x10^{-5}/hr at 1000F	975F	$RT^2 \frac{\delta \ln \dot{\epsilon}}{\delta T}(\sigma)$ Kcal/Mol	Heat No.	Stress Ksi	Creep Rate x10^{-5}/hr at 1100F	1075F	$RT^2 \frac{\delta \ln \dot{\epsilon}}{\delta T}(\sigma)$ Kcal/Mol
1Mo	B-2651	47	6.39	2.89	-73.3	B-2650	25	4.64	1.92	-93.4
		47	8.90	3.30	-91.7					
1Mo-0.1 Si	B-2653	51	9.76	5.14	-59.6	B-2652	25	3.69	1.20	-119.0
		46	8.29	4.12	-64.7					
1Mo-0.25 Si	B-2655	58	8.83	4.61	-60.1	B-2654	25	1.66	0.318	-174.4
		53	7.73	2.78	-94.7		28	2.97	1.07	-107.9
1Mo-0.5 Si	B-2657	56	1.51	0.366	-131.1	B-2656	25	0.652	0.191	-129.5
		56	3.56	1.38	-87.7					
1Mo-0.25 Bi	B-2659	50	9.03	3.68	-82.9	B-2658	25	3.15	1.01	-120.3
		47	7.66	4.39	-51.4					
1Mo-0.5 Bi	B-2661	47	6.27	1.97	-106.8	B-2660	25	4.80	1.85	-100.6
		47	6.59	2.39	-93.7					
1Mo-1.0 Bi	B-2663	52	4.74	1.20	-127.2	B-2662	25	4.64	1.92	-93.4
		52	4.35	1.59	-93.0					
1Mo-2.0 Bi	B-2665	54	6.69	2.77	-81.6	B-2664	25	2.50	0.704	-133.8
		54	2.92	0.812	-118.2					
1Mo-0.15 Fe	B-2667	37	2.89	0.879	-110.0	B-2666	22	5.66	1.96	-112.0
		40	6.33	1.97	-107.9					
1Mo-0.25 Fe	B-2669	35	3.39	1.26	-91.5	B-2668	20	10.22	3.42	-115.7
		35	4.35	1.76	-83.6					
1Mo-0.5 Fe	B-2671	25	0.993	0.358	-94.2	B-2670	20	8.88	3.25	-106.1
		30	4.24	2.28	-57.3					
1Mo-1.0 Fe	B-2673	30	5.32	2.81	-59.0	B-2956	15	2.67	0.97	-106.5
		25	1.91	0.71	-91.9					
1Mo-2.0 Fe	B-2675	25	3.88	1.63	-80.2	B-2674	15	11.65	5.48	-79.6
		26	5.43	2.31	-79.0					
1Mo-0.005 S	B-2982	52	3.93	1.51	-88.1	B-2983	25	1.14	0.303	-139.6
1Mo-0.01 S	B-3054	50	8.835	4.027	-72.6	B-3275	25	1.52	0.78	-70.5
		50	3.41	0.870	-126.0		28	2.89	1.00	-112.1

SC5011.26TR

TABLE X CREEP PROPERTIES OF BUTTON MELTS (Continued)

Nominal[1] Additions, %	Heat No.	Stress Ksi	Creep Rate $\times 10^{-5}$/hr at 1000F	975F	$RT^2 \frac{\partial \ln \dot{\varepsilon}}{\partial T(\sigma)}$ Kcal/Mol	Heat No.	Stress Ksi	Creep Rate $\times 10^{-5}$/hr at 1100F	1075F	$RT^2 \frac{\partial \ln \dot{\varepsilon}}{\partial T(\sigma)}$ Kcal/Mol
1Mo-0.020 S	B-3055	50	3.85	1.69	-76.3	B-3056	25	2.62	0.999	-101.9
		50	5.41	2.22	-82.3					
1Mo-0.25 Fe-0.25 Si	B-2986	40	4.12	1.14	-118.7	B-2986	20	1.09	0.305	-134.7
		40	4.26	1.25	-113.3					
1Mo-0.5 Fe 0.25 Si	B-2988	35	2.24	0.508	-137.0	B-2988	15	0.360	0.126	-110.9
	B-2989	35	2.80	0.830	-112.5	B-2989	20	1.40	0.365	-142.0
1Mo-2.0 Fe-0.25 Si	B-2990	30	7.90	2.62	-101.9	B-2990	10	0.483	0.167	-112.1
		25	9.24	2.94	-106.0	B-2991	15	1.93	0.958	-73.8
1Mo-0.25 Fe-0.5 Si	B-2993	50	7.95	2.97	-91.0	B-3100	25	1.77	0.71	-97.0
		50	12.7	6.43	-62.9					
1Mo-0.5 Fe-0.5 Si	B-2994	35	1.37	0.597	-76.9	B-2994	25	3.96	1.70	-89.3
	B-2995	38	2.99	1.31	-76.4					
1Mo-2.0 Fe-0.5 Si	B-2996	25	2.18	0.680	-107.5	B-3410	20	11.27	7.65	-40.9
	B-2997	28	2.87	1.05	-93.1					
1Mo-0.25 Fe-0.005 S	B-3080	40	5.92	1.95	-102.7	B-3081	22	5.78	2.12	-105.8
	B-3081	40	6.51	2.49	-89.0					
1Mo-0.5 Fe-0.005 S	B-3082	38	10.63	4.78	-73.8	B-3083	18	2.99	1.19	-103.9
	B-3083	35	5.53	1.76	-106.0					
1Mo-2.0 Fe-0.005 S	B-3008	28	7.46	3.07	-82.2	B-3008	15	6.34	3.06	-76.8
		25	5.27	1.93	-92.8					
1Mo-0.25 Fe-0.02 S	B-3061	38	6.06	2.62	-77.4	B-3061	22	12.32	4.14	-115.1
	B-3062	40	6.75	2.57	-89.3					
1Mo-0.5 Fe-0.02 S	B-3063	30	1.30	0.363	-117.8	B-3063	18	2.52	0.995	-98.1
		35	8.30	3.55	-78.6					

TABLE X CREEP PROPERTIES OF BUTTON MELTS (Continued)

Nominal(1) Additions, %	Heat No.	Stress Ksi	Creep Rate x10^{-5}/hr at 1000F	975F	$RT^2 \frac{\delta \ln \dot{\varepsilon}}{\delta T}(\sigma)$ Kcal/Mol	Heat No.	Stress Ksi	Creep Rate x10^{-5}/hr at 1100F	1075F	$RT^2 \frac{\delta \ln \dot{\varepsilon}}{\delta T}(\sigma)$ Kcal/Mol
1Mo-0.12 O_2	B-3010	47	5.39	2.04	-90.0	B-3010	25	3.12	1.33	-90.3
	B-3011	47	11.67	4.64	-85.3					
1Mo-0.25 Si-0.12 O_2	B-3012	54	5.92	2.05	-98.2	B-3012	27	1.90	0.548	-131.3
	B-3013	54	5.86	1.71	-113.9					
1Mo-0.5 Si-0.12 O_2	B-3014	58	4.56	1.18	-125.2	B-3014	30	1.31	0.352	-139.0
	B-3015	58	4.69	1.45	-108.9					
1Mo-0.18 O_2	B-3016	47	4.12	1.35	-103.2	B-3016	25	2.89	1.15	-97.7
	B-3017	47	4.75	1.63	-09.6					
1Mo-0.25 Si-0.18 O_2	B-3018	54	3.50	1.11	-106.1	B-3018	30	0.784	0.267	-113.8
	B-3019	54	4.90	1.43	-113.8		33	6.78	2.97	-87.2
1Mo-0.5 Si-0.18 O_2	B-3020	58	3.31	1.19	-94.8	B-3021	33	1.70	0.546	-120.0
	B-3021	58	4.55	1.68	-91.8					
None	B-3022	30	2.84	0.702	-129.3	B-3022	17	5.82	1.30	-158.2
	B-3023	30	3.43	0.916	-121.9					
2Mo	B-3024	42	4.43	1.31	-112.6	B-3024	22	5.00	2.01	-96.3
	B-3025	45	6.28	2.38	-89.8					
0.25 Si	B-3026	38	1.77	0.269	-174.2	B-3027	23	1.42	0.213	-200.4
	B-3027	38	2.63	0.395	-175.2					
2Mo-0.25 Si	B-3028	47	4.26	1.69	-85.2	B-3029	25	2.81	0.849	-126.4
	B-3029	47	5.44	1.84	-100.2					
0.5 Si	B-3030	48(2)	4.78	1.55	-104.1	B-3102	30	2.49	0.878	-110.1
	B-3031	48(2)	4.69	1.58	-100.6					
2Mo-0.5 Si	B-3032	50	2.57	0.608	-133.4	B-3032	25	0.820	0.376	-82.4
	B-3033	50	1.90	0.807	-79.2					

(1) Added to Ti-6Al-2Sn-2Zr Base
(2) Tests run for 770 hours instead of the usual 335

SC5011.261R

TABLE XI

Apparent Activation Energy Results for Creep at 1000F
for Ti-6Al-2Sn-2Zr-1Mo-0.25Si (Heat V-5130)

Stress Ksi	Temp F	Rate x 10^{-5}	$RT^2 \frac{\partial \ln \dot{\varepsilon}}{\partial T}\Big\|_\sigma$ K cal/mol
40	1000	1.119	- 73.7
	1025	2.418	- 64.8
	1000	1.228	
40	1000	0.863	- 66.3
	1025	1.725	- 72.2
	1000	0.811	
40	1000	0.926	- 83.1
	1025	2.207	-103.6
	1000	0.747	
		Average	- 77.3
		Standard dev. σ =	± 14.4
50	1000	5.265	- 94.8
	975	1.888	-103.8
	1000	5.801	
50	1000	3.399	- 87.4
	975	1.321	-104.9
	1000	4.111	
50	1000	5.454	-106.5
	975	1.723	-100.1
	1000	5.091	
		Average	- 99.6
		Standard dev. σ =	± 7.3

(1) One-half inch dia. beta rolled bar heat treated:
1950F (15 min) AC + 1300F (2 hrs) AC

TABLE XII

RESULTS OF ANALYSIS OF VARIANCE ON THE EFFECTS
OF MINOR ALLOYING ADDITIONS ON THE APPARENT ACTIVATION ENERGY FOR CREEP

Alloy (1) Addition	Temperature (F)	Statistical (2) Significance
Fe	1000	>0.2
Si	1000	<0.1 >0.05
Fe-Si	1000	0.1
Fe	1000	>0.2
S	1000	>0.2
Fe-S	1000	<0.1 >0.05
Mo (3)	1000	<0.5 >0.025
Si (3)	1000	>0.2
Mo-Si (3)	1000	<0.2 >0.1
O_2	1000	>0.2
Si	1000	>0.2
O_2-Si	1000	>0.2
Fe	1100	<0.1 >0.05
Si	1100	<0.1 >0.05
Fe-Si	1100	>0.2
Fe	1100	<0.2 >0.1
S	1100	>0.2
Fe-S	1100	0.05
Mo (3)	1100	<0.025 >0.01
Si (3)	1100	<0.1 >0.05
Mo-Si (3)	1100	>0.2
O_2	1100	>0.2
Si	1100	>0.2
O_2-Si	1100	>0.2

(1) Added to a base alloy of Ti-6Al-2Sn-2Zn-1Mo

(2) Probability that the observed effects were due to chance

(3) Added to a base alloy of Ti-6Al-2Sn-2Zr

TABLE XIII

Creep-Stability Properties of Button Melts

Alloy Addition[1]	Creep Test[2]	Heat[5] No.	UTS,Ksi	YS,Ksi	% RA	% Elong	Percent RA Retained after Creep[3]
1Mo	None	B-2651	127.7	115.6	28.4	13	
	1000F - 47 Ksi	B-2651	132.4	131.7	20.9	12	
	1000F - 47 Ksi	B-2651	132.4	126.5	24.0	15	79
	1100F - 25 Ksi	B-2650	127.4	120.5	26.5	15	93
1Mo-0.1Si	None	B-2653	130.5	122.2	26.8	14	
	1000F - 51 Ksi	B-2653	139.1	132.9	17.8	12.5	
	1000F - 46 Ksi	B-2653	136.9	129.9	17.1	13	65
	1100F - 25 Ksi	B-2652	131.7	123.8	18.5	12	69
1Mo-0.25Si	None	B-2655	136.8	117.1	22.7	10	
	1000F - 58 Ksi	B-2655	145.2	137.6	9.0	4	
	1000F - 53 Ksi	B-2655	143.6	133.7	12.4	10	47
	1100F - 28 Ksi	B-2654	140.6	130.8	9.4	8	41
1Mo-0.5Si	None	B-2657	144.9	135.7	12.5	10	
	1000F - 56 Ksi	B-2657	151.5	142.4	9.1	6	
	1000F - 56 Ksi	B-2657	150.8	140.6	9.1	7	73
	1100F - 25 Ksi	B-2656	149.1	139.4	8.0	4	64
1Mo-0.25Bi	None	B-2659	127.1	115.6	26.9	13	
	1000F - 50 Ksi	B-2659	134.3	126.4	21.7	13	
	1000F - 47 Ksi	B-2659	135.3	125.2	26.0	11	89
	1100F - 25 Ksi	B-2658	130.7	123.5	22.4	12.5	83
1Mo-0.50Bi	None	B-2661	130.4	121.3	27.7	13	
	1000F - 50 Ksi	B-2661	137.4	130.9	21.1	11	
	1000F - 47 Ksi	B-2661	135.5	128.9	22.5	13	79
	1100F - 25 Ksi	B-2660	130.1	121.7	22.7	17	82
1Mo-1Bi	None	B-2663	130.6	121.3	26.2	10	
	1000F - 52 Ksi	B-2663	137.5	128.2	16.5	10.5	
	1000F - 52 Ksi	B-2663	135.2	127.9	21.5	7.5	73
	1100F - 25 Ksi	B-2662	131.2	124.2	19.8	13.5	76

TABLE XIII (Continued)

Creep-Stability Properties of Button Melts

Alloy Addition[1]	Creep Test[2]	Heat[5] No.	UTS,Ksi	YS,Ksi	% RA	% Elong	Percent RA Retained after Creep[3]
1Mo-2Bi	None	B-2665	132.7	120.0	19.8	11	
	1000F - 54 Ksi	B-2665	138.5	127.3	5.4	1[4]	
	1000F - 54 Ksi	B-2665	136.0	128.6	14.4	2[4]	50
	1100F - 25 Ksi	B-2664	137.4	128.2	12.5	8	63
1Mo-0.15Fe	None	B-2667	132.7	124.5	28.3	11	
	1000F - 40 Ksi	B-2667	140.3	131.3	20.0	10	
	1000F - 40 Ksi	B-2667	138.8	130.8	21.2	13	73
	1100F - 22 Ksi	B-2666	134.6	125.2	16.0	12	57
1Mo-0.25Fe	None	B-2669	130.2	121.6	23.8	11	
	1000F - 35 Ksi	B-2669	137.8	127.2	19.1	7	
	1000F - 35 Ksi	B-2669	140.1	127.5	21.6	10	86
	1100F - 20 Ksi	B-2668	129.9	119.6	18.8	16	79
1Mo-0.5Fe	None	B-2671	136.7	125.7	25.0	16	
	1000F - 30 Ksi	B-2671	145.5	133.1	14.4	5.5	
	1000F - 25 Ksi	B-2671	139.5	125.5	16.4	6	62
	1100F - 20 Ksi	B-2670	141.3	132.2	10.3	9	41
1Mo-1Fe	None	B-2673	142.4	132.2	10.5	7	
	1000F - 25 Ksi	B-2673	147.9	137.2	6.7	3.5	69
	1000F - 30 Ksi	B-2673	150.3	138.7	7.8	3.5	89
	1100F	B-2956					
1Mo-2Fe	None	B-2675	140.5	138.8	3.0	2	
	1000F - 25 Ksi	B-2675	155.4	144.9	2.2	0	
	1000F - 28 Ksi	B-2675	155.3	145.1	4.8	2	100
	1100F - 15 Ksi	B-2674	155.7	144.9	5.2	3	100
1Mo-0.005S	None	B-2982	130.5	119.2	29.4	14	
	1000F - 52 Ksi	B-2982	134.9	127.6	22.2	15	
	1000F - 50 Ksi	B-2982	133.9	128.0	22.7	13	76
	1100F - 25 Ksi	B-2983	141.3	129.9	11.9	13	40

TABLE XIII (Continued)

Creep-Stability Properties of Button Melts

Alloy Addition[1]	Creep Test[2]	Heat[5] No.	UTS,Ksi	YS,Ksi	% RA	% Elong	Percent RA Retained after Creep[3]
1Mo-0.010S	None	B-3053	132.3	120.5	27.1	14	
	1000F - 50 Ksi	B-3054	136.0	129.5	17.9	14	
	1000F - 50 Ksi	B-3275	132.0	124.3	19.9	13	70
	1100F - 25 Ksi	B-3275	131.1	121.9	19.6	15.5	72
1Mo-0.020S	None	B-3055	131.6	121.6	16.5	10	
	1000F - 50 Ksi	B-3055	136.5	129.7	12.8	12	
	1000F - 50 Ksi	B-3056	136.4	128.6	14.1	10.5	82
	1100F - 25 Ksi	B-3056	134.3	125.3	13.9	12	84
1Mo-0.25Si-0.25Fe	None	B-2986	145.3	131.2	11.6	5	
	1000F - 40 Ksi	B-2986	149.0	140.5	4.6	2.5	
	1000F - 40 Ksi	B-2987	144.1	141.8	2.1	1	29
	1100F - 20 Ksi	B-2986	150.4	141.3	4.7	2	41
1Mo-0.25Si-0.5Fe	None	B-2988	147.9	133.5	11.8	4	
	1000F - 35 Ksi	B-2988	152.2	146.1	1.7	2	
	1000F - 35 Ksi	B-2989	155.0	145.6	3.9	1	24
	1100F - 20 Ksi	B-2989	153.8	142.6	3.1	2	26
1Mo-0.25Si-2Fe	None	B-2990	161.0	154.8	6.2	0	
	1000F - 30 Ksi	B-2990	Broke in threads				
	1000F - 25 Ksi	B-2991	Broke before yield				
	1100F - 15 Ksi	B-2991	Broke in threads				
1Mo-0.5Si-0.25Fe	None	B-2992	152.4	138.5	5.3	1.5	
	1000F - 50 Ksi	B-2993	Broke before yield				
	1000F - 50 Ksi	B-3100	156.2	150.0	2.4	1.5	23
	1100F - 25 Ksi	B-3100	Broke in threads				
1Mo-0.5Si-0.5Fe	None	B-2994	158.1	144.6	7.6	3	
	1000F - 35 Ksi	B-2994	161.2	152.8	2.8	2	
	1000F - 35 Ksi	B-2995	154.6	150.5	2.6	0	36
	1100F - 25 Ksi	B-2995	Broke in threads				

TABLE XIII (Continued)

Creep-Stability Properties of Button Melts

Alloy Addition[1]	Creep Test[2]	Heat[5] No.	UTS,Ksi	YS,Ksi	% RA	% Elong	Percent RA Retained after Creep[3]
1Mo-0.5Si-2Fe	None	B-2996	165.2	165.2	1.6	2	
	1000F - 25 Ksi	B-2996	Broke in threads				
	1100F - 28 Ksi	B-2997	Broke before yield				
	1100F - 20 Ksi	B-3410	Broke in threads				
1Mo at $0.12O_2$	None	B-3010	129.5	119.1	29.9	12	
	1000F - 47 Ksi	B-3010	133.6	129.4	24.4	10	
	1000F - 47 Ksi	B-3011	139.0	133.4	15.3	9.5	66
	1100F - 25 Ksi	B-3010	130.1	124.0	22.7	17.5	76
1Mo-0.25Si at $0.12O_2$	None	B-3012	138.4	125.9	19.3	12	
	1000F - 54 Ksi	B-3012	141.4	136.1	7.1	3	
	1000F - 54 Ksi	B-3013	142.5	140.8	4.8	2	31
	1100F - 27 Ksi	B-3012	138.2	131.1	9.5	7.5	49
1Mo-0.5Si at $0.12O_2$	None	B-3014	149.2	134.7	10.9	6	
	1000F - 58 Ksi	B-3014	147.8	146.5	1.1	0	
	1000F - 58 Ksi	B-3015	153.9	148.5	3.8	2	22
	1100F - 30 Ksi	B-3014	154.1	145.7	5.6	2.5	57
1Mo at $0.18O_2$	None	B-3016	140.4	133.9	24.1	12	
	1000F - 47 Ksi	B-3016	142.8	135.1	21.6	14	
	1000F - 47 Ksi	B-3017	143.0	137.4	19.7	14	86
	1100F - 25 Ksi	B-3016	141.0	134.1	20.3	10.5	84
1Mo-0.25Si at $0.18O_2$	None	B-3018	140.8	127.5	21.8	8	
	1000F - 54 Ksi	B-3018	148.5	144.1	5.1	1	
	1000F - 54 Ksi	B-3019	150.0	139.3	4.1	3	21
	1100F - 28 Ksi	B-3018	152.7	143.9	5.6	3	26
1Mo-0.5Si at $0.18O_2$	None	B-3020	156.6	138.5	11	8	
	1000F - 58 Ksi	B-3020	Broke before yield				
	1000F - 58 Ksi	B-3021	Broke in threads				
	1100F - 33 Ksi	B-3021	Broke in threads				

TABLE XIII (Continued)

Creep-Stability Properties of Button Melts

Alloy Addition[1]	Creep Test[2]	Heat[5] No.	UTS,Ksi	YS,Ksi	% RA	% Elong	Percent RA Retained after Creep[3]
None	None	B-3022	115.7	102.5	35.1	20	
	1000F - 35 Ksi	B-3022	119.1	114.0	20.4	13.5	
	1000F - 30 Ksi	B-3023	120.1	115.8	23.1	14	62
	1100F - 17 Ksi	B-3022	118.8	109.8	27.9	20	79
2Mo	None	B-3024	134.4	115.7	25.5	15	
	1000F - 42 Ksi	B-3024	138.3	126.4	15.7	13.5	
	1000F - 45 Ksi	B-3025	137.8	127.6	20.5	14.5	71
	1100F - 22 Ksi	B-3024	137.7	127.8	16.1	13	63
0.25Si	None	B-3026	125.3	116.1	26.1	19	
	1000F - 38 Ksi	B-3026	132.2	126.0	8.8	5	
	1000F - 38 Ksi	B-3027	131.6	126.9	3.9	2	24
	1100F - 23 Ksi	B-3027	133.3	123.5	12.5	7.5	48
2Mo-0.25Si	None	B-3028	141.5	122.5	14.6	10	
	1000F - 47 Ksi	B-3028	144.7	134.6	9.8	6.5	
	1000F - 47 Ksi	B-3029	144.3	134.8	9.5	7.5	66
	1100F - 25 Ksi	B-3029	146.3	135.8	8.1	7	55
0.5Si	None	B-3030	135.7	126.6	21.6	15	
	1000F - 48 Ksi[4]	B-3030	132.2	121.9	1,8	2.5	
	1000F - 48 Ksi[4]	B-3030	130.2	124.8	2.1	4	9
	1100F - 30 Ksi	B-3030	132.0	122.5	9.3	5	43
2Mo-0.5Si	None	B-3032	146.2	128.7	10.4	8	
	1000F - 50 Ksi	B-3032	152.3	143.7	5.2	5	
	1000F - 50 Ksi	B-3033	150.5	139.4	7.1	4	59
	1100F - 25 Ksi	B-3032	151.5	141.0	4.4	4	42
1Mo-0.005S-0.25Fe	None	B-3081	128.6	119.0	28.9	13	
	1000F - 40 Ksi	B-3081	136,0	126.6	18	14	
	1000F - 40 Ksi	B-3080	135.4	126.6	19	11.5	64
	1100F - 22 Ksi	B-3081	131.4	119.5	17.9	13	62

TABLE XIII (Continued)

Creep-Stability Properties of Button Melts

Alloy Addition[1]	Creep Test[2]	Heat[5] No.	UTS,Ksi	YS,Ksi	% RA	% Elong	Percent RA Retained after Creep[3]
1Mo-0.005S-0.5Fe	None	B-3083	131.5	121.7	21.3	13.5	
	1000F - 35 Ksi	B-3083	141.3	132.3	17.2	10.5	
	1000F - 38 Ksi	B-3082	139.4	131.1	14.8	11	75
	1100F - 18 Ksi	B-3083	138.5	124.3	14	11.5	66
1Mo-0.005S-2Fe	None	B-3008	150.8	136.4	6.2	0	
	1000F - 35 Ksi	B-3008	154.5	146.7	1.5	2	
	1000F - 25 Ksi	B-3009	158.1	148.2	1.7	1.5	26
	1100F - 15 Ksi	B-3008	155.7	148.8	3.5	2	56
1Mo-0.02S-0.25Fe	None	B-3061	132.6	124.5	22.0	10	
	1000F - 38 Ksi	B-3061	139.1	130.8	12.3	11	
	1000F - 40 Ksi	B-3062	138.9	130.5	11.5	8	54
	1100F - 22 Ksi	B-3061	137.5	126.3	15.4	14.5	70
1Mo-0.02S-0.5Fe	None	B-3063	133.3	122.7	14.3	9	
	1000F - 30 Ksi	B-3063	142.5	130.9	10.4	9	
	1000F - 35 Ksi	B-3064	143.8	135.4	10.4	7	73
	1100F - 18 Ksi	B-3063	140.1	128.5	11.6	10	81
1Mo-0.02S-2Fe	None	B-3065	147.0	137.6	3.0	2	
	1000F - 25 Ksi	B-3065	154.2	145.9	2.8	2	
	1000F - 27 Ksi	B-3066	154.3	148.1	1.4	1.5	70
	1100F - 15 Ksi	B-3065	154.3	143.5	3.2	3	100

(1) Made to a Ti-6Al-2Sn-2Zr base; Nominal O_2 content is 0.10 unless otherwise specified.
(2) Test duration was 335 hours unless otherwise noted.
(3) Results of the 1000F creep exposures were averaged.
(4) Test duration was 765 hours.
(5) One-half inch diameter beta rolled bar; heat-treated 1950F (15 min) AC + 1300F (2 hrs) AC.

TABLE XIV

Creep Data Obtained on Ingot Material[1]

Heat No.	Nominal Composition[2] % Si	% O_2	Heat Treatment	Stress Ksi	Creep Rate x 10^{-5} 1000F	975F	$RT^2 \frac{\partial/n\dot{\epsilon}}{\partial T}\Big\|_\sigma$ KCal/Mol	Stress Ksi	Creep Rate x 10^{-5} 1100F	1025	$RT^2 \frac{\partial/n\dot{\epsilon}}{\partial T}\Big\|_\sigma$ KCal/Mol
V-5131	0	0.12	A	53	8.54	2.83	-102.1	28	4.49	1.85	- 93.7
				53	7.89	2.79	- 96.1	28	4.74	2.06	- 88.0
								28	3.79	1.61	- 90.5
			B	53	7.64	3.17	- 81.3	28	3.94	1.69	- 89.4
				53	6.68	2.80	- 80.4				
V-5130	0.25	0.12	A	53	9.15	3.51	- 88.6	32	10.6	5.31	- 73.0
				50	5.27	1.89	- 94.8	30	8.47	3.39	- 96.7
			B	55	2.04	0.894	- 76.3	30	6.50	2.63	- 95.6
				58	3.35	0.460	- 76.8	30	6.89	2.95	- 89.6
V-5129	0.50	0.12	A	55	3.88	1.34	- 98.3	32	3.36	1.25	-104.4
				57	6.09	2.09	- 98.9	34	5.36	2.19	- 94.6
			B	57	2.18	0.670	-109.1	32	3.31	1.23	-104.6
				61	4.03	1.47	-93.2	32	4.07	1.59	- 99.3
V-5128	0.25	0.06	A	51	7.11	2.61	- 92.6	28	4.92	2.20	- 85.0
				53	9.94	3.95	- 85.3	28	5.45	2.02	-104.8
			B	53	2.07	0.697	-100.6	28	4.92	2.04	- 93.0
				58	3.63	1.64	- 73.4	30	8.22	3.38	- 93.9
V-5132	0.25	0.18	A	53	7.01	2.56	- 93.1	30	6.57	2.50	-102.0
				53	7.89	2.89	- 92.8	30	5.42	2.29	- 91.0
			B	53	1.23	0.466	- 89.7	28	3.72	1.25	-115.2
				56	2.05	0.832	- 83.4	28	4.10	1.46	-109.1

TABLE XIV (Continued)

(1) 1/2-inch diameter beta rolled bar.
(2) Base composition: Ti-6Al-2Sn-2Zr-1Mo

A = 1950(15 Min)AC + 1300F(2 Hrs)AC
B = 1950(15 Min)AC + 1100F(8 Hrs)AC

TABLE XV

Creep Stability of Ingot Materials[1]

Heat No.	Nominal Addition[2]	Heat Treatment	Creep Exposure[3]	UTS, Ksi	YS, Ksi	% RA	% Elong	Percent RA Retained After Creep
V-5131	None	A	None	140.3	124.6	16.8	11	
			None	139.4	125.2	21.7	13	
			1000F - 53 Ksi	144.0	138.1	6.9	4.5	44
			1000F - 53 Ksi	142.7	137.2	10.2	5	
			1100F - 28 Ksi	141.9	131.4	16.8	12	70
			1100F - 28 Ksi	141.8	129.9	10.3	7[4]	
		B	None	140.4	123.8	21.0	15	
			None	141.6	121.4	16.8	14	
			1000F - 53 Ksi	144.7	136.9	15.1	10	67
			1000F - 53 Ksi	145.0	137.9	10.3	3.5[5]	
			1100F - 28 Ksi	144.1	133.4	23.5	15	100
			1100F - 28 Ksi	141.7	132.0	17.4	13	
V-5130	0.25Si	A	None	150.0	133.5	14.5	9	
			None	149.0	132.8	10.4	7	
			1000F - 55 Ksi	Broke before yield				
			1000F - 53 Ksi	153.1	147.0	3.0	2	27
			1100F - 30 Ksi	151.5	142.9	6.8	5	50
			1100F - 32 Ksi	151.3	141.3	5.6	5	
		B	None	153.3	133.0	14.3	13	
			None	152.6	133.4	17.9	13	
			1000F - 55 Ksi	153.9	146.0	3.0	3	19
			1000F - 58 Ksi	153.3	146.7	3.0	2	
			1100F - 30 Ksi	153.7	142.6	6.4	5	30
			1100F - 30 Ksi	152.9	144.3	3.4	3	
V-5129	0.5Si	A	None	153.2	141.1	10.1	9	
			None	154.4	139.6	9.1	7	
			1000F - 50 Ksi	157.6	147.7	4.5	2	37
			1000F - 57 Ksi	157.1	147.6	2.6	2	
			1100F - 32 Ksi	155.7	144.9	2.6	2	27
			1100F - 32 Ksi	156.8	145.9	2.6	2	

TABLE XV (Continued)

Creep Stability of Ingot Materials[1]

Heat No.	Nominal Addition[2]	Heat Treatment	Creep Exposure[3]	UTS, Ksi	YS, Ksi	% RA	% Elong	Percent RA Retained After Creep
V-5129	0.5Si	B	None	156.0	134.9	12.4	10	
			None	156.7	137.9	9.6	10	
			1000F - 57 Ksi	154.6	148.1	Broke in threads		12
			1000F - 61 Ksi	155.0	150.2	2.6	1	
			1100F - 32 Ksi	157.2	146.4	5.1	2	44
			1100F - 32 Ksi	158.6	147.0	4.5	3.5	
V-5128	0.25Si at 0.06 O_2	A	None	144.3	129.8	13.6	12	
			None	140.6	128.2	15.1	12	
			1000F - 51 Ksi	147.9	141.1	5.6	3.5	34
			1000F - 53 Ksi	146.1	138.6	4.3	2	
			1100F - 28 Ksi	146.1	134.5	10.0	8	73
			1100F - 28 Ksi	146.9	136.0	10.9	10	
		B	None	145.9	118.8	20.7	13	
			None	146.1	125.6	21.0	12	
			1000F - 53 Ksi	148.6	139.8	7.7	6	34
			1000F - 58 Ksi	147.3	136.8	6.4	1.5[5]	
			1100F - 30 Ksi	147.8	137.2	11	6	46
			1100F - 30 Ksi	148.1	136.9	8.1	6	
V-5132	0.25Si at 0.18 O_2	A	None	153.4	136.6	12.8	10	
			None	151.7	135.2	13.9	10	
			1000F - 53 Ksi	Broke before yield				16
			1000F - 53 Ksi	147.9	146.6	4.3	3	
			1100F - 30 Ksi	150.9	144.6	3.9	1[5]	29
			1100F - 30 Ksi	154.0	144.4	3.9	3	
		B	None	156.0	138.5	16.9	14.5	
			None	157.0	138.1	13.4	12	
			1000F - 53 Ksi	155.9	144.2	6.4	5	40
			1000F - 56 Ksi	158.5	148.7	5.6	4	
			1100F - 28 Ksi	156.5	146.4	7.3	2.5	40
			1100F - 28 Ksi	155.4	145.1	4.7	5	

TABLE XV (Continued)

(1) 1/2-inch dia. beta rolled bar.
(2) Addition to a Ti-6Al-2Sn-2Zr-1Mo base - nominal O_2 level is 0.12% except where otherwise specified.
(3) Exposure time - 335 hours
Gage length was machined prior to tensile testing.
(4) Fracture contained a flaw.
(5) Broke outside gage length.

A = 1950F(15 Min)AC + 1300F(2 Hrs)AC
B = 1950F(15 Min)AC + 1100F(8 Hrs)AC

TABLE XVI - RESULTS OF PHASE PARTITIONING STUDIES ON THREE ALLOYS

Addition	Heat No.	Temperature (F)	Phase	Al	Sn	Zr	Mo	Si	Bi	Fe
0.5 Si	B-2657	1775	α	7.46	1.78	1.57	0.15	0.479	-	-
			β	5.44	2.14	2.20	1.69	0.567	-	-
		1700	α	6.80	1.76	1.64	0.18	0.448	-	-
			β	4.89	2.21	2.44	2.31	0.600	-	-
		1600	α	6.86	1.81	1.55	0.14	0.437	-	-
			β	3.78	2.47	2.55	5.14	0.578	-	-
1 Fe	B-2673	1725	α	7.43	1.95	1.72	0.19	-	-	0.05
			β	5.80	2.06	2.30	1.24	-	-	1.44
		1675	α	7.08	1.94	1.60	0.14	-	-	0.06
			β	4.75	2.12	2.20	1.98	-	-	1.89
		1550	α	7.31	1.87	1.89	0.15	-	-	0.03
			β	4.19	2.10	2.46	3.02	-	-	3.63
1.32 Bi	B-2665	1775	α	7.06	1.84	1.66	0.20	-	0.63	-
			β	5.46	2.17	2.27	1.68	-	1.59	-
		1750	α	7.10	1.79	1.64	0.22	-	0.73	-
			β	4.88	2.15	2.49	2.05	-	2.27	-
		1650	α	7.08	1.77	1.67	0.20	-	6.78	-
			β	3.86	2.32	2.78	4.09	-	3.08	-

TABLE XVII DIFFUSION COEFFICIENTS FOR Bi DIFFUSION IN A Ti-6Al-2Sn-2Zr-1Mo MATRIX

Temperature	Diffusion Coefficient, cm^2/sec
1900F (1311K)	2.54×10^{-9}
" "	2.34×10^{-9}
2000F (1366K)	3.84×10^{-9}
" "	4.17×10^{-9}
2200F (1477K)	1.32×10^{-8}
" "	1.28×10^{-8}

TABLE XVIII

Fracture Toughness of Ti-6Al-2Sn-2Zr-1Mo-.12 O_2
With Additions of Si at 78 and 1000F

Heat No.	Alloy Addition (%)	Test Temperature (F)	Conditional Fracture Toughness K_Q (ksi$\sqrt{in}$)	$2.5\left(\frac{K_Q}{YS}\right)^2$
V-5131	None	78	112.26	1.97
"	"	1000	104.29	9.21
V-5130	0.25Si	78	84.78(1)	0.9
"	"	1000	89.20	4.63
V-5129	0.5Si	78	70.92(1)	0.62
"	"	1000	87.60	3.8

(1) Valid K_{Ic}

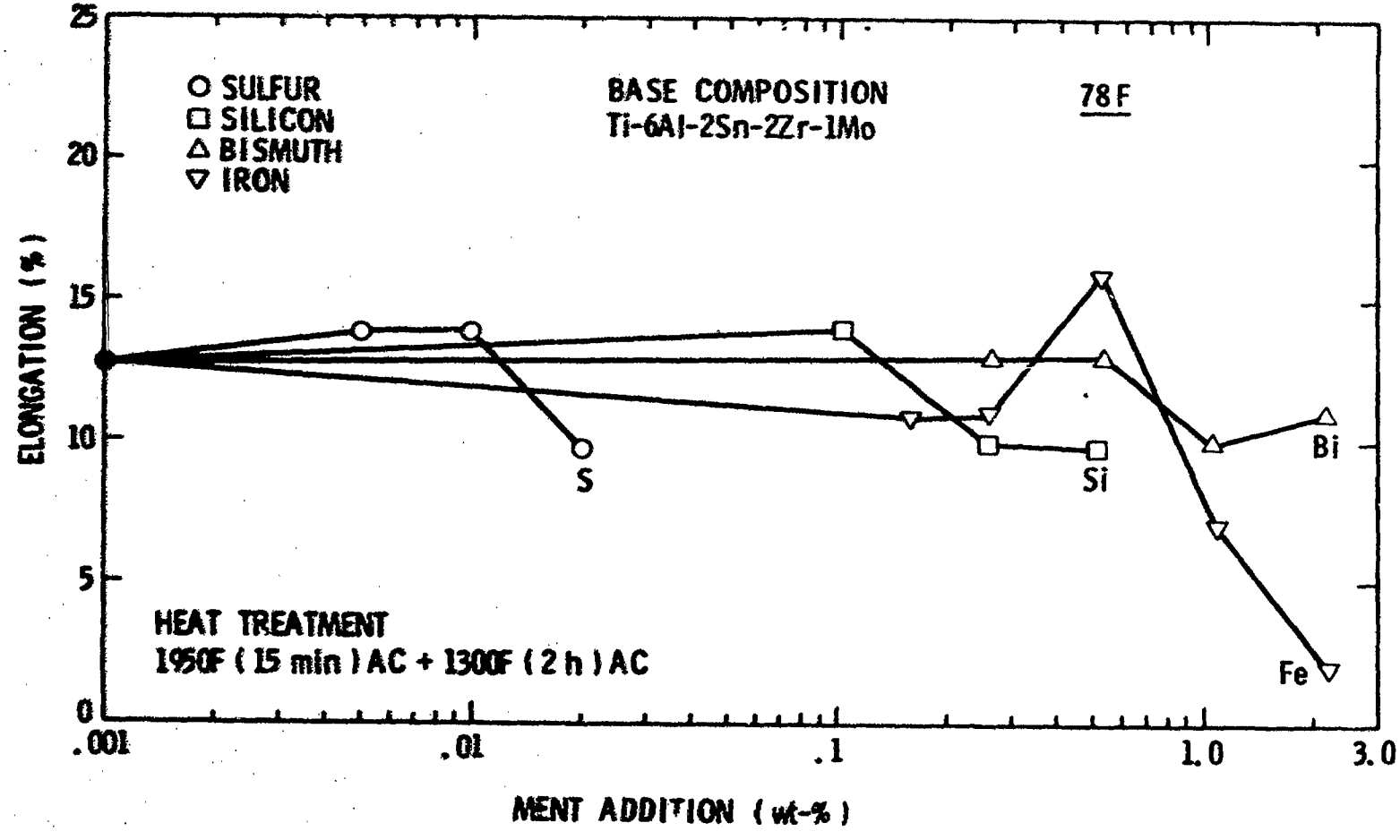

Figure 1 Room temperature tensile elongation results for button melts of composition Ti-6Al-2Sn-2Zr-1Mo with element additions of Si, Bi, Fe and S as a function of WGT-% addition.

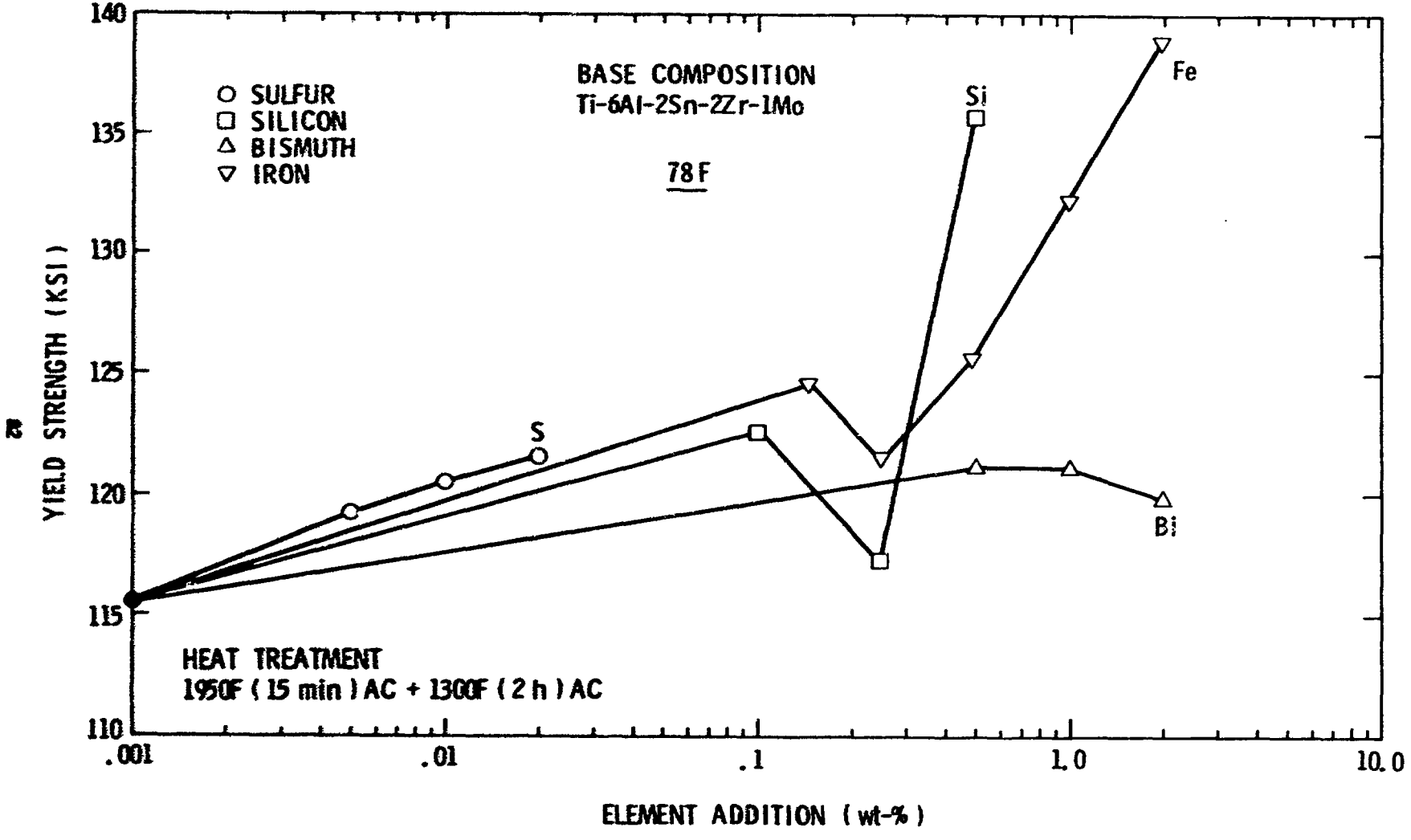

SC5011.26TR

Figure 2 Room temperature yield strength results for button melts of composition Ti-6Al-2Sn-2Zr-1Mo with element additions of Si, Bi, Fe and S as a function of WGT-% addition.

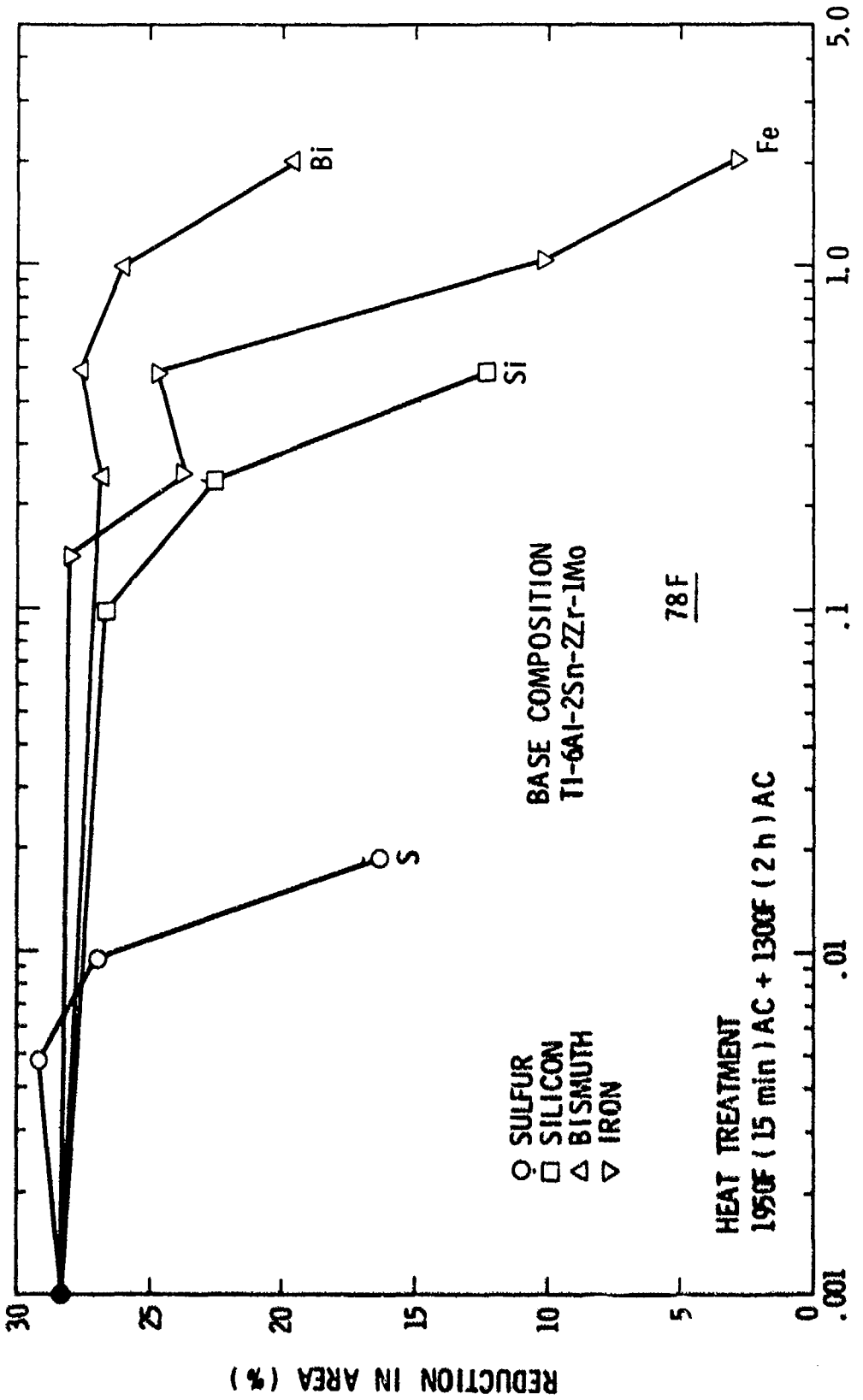

Figure 3 Room temperature reduction in area results for button melts of composition Ti-6Al-2Sn-2Zr-1Mo with additions of Si, Bi, Fe and S as a function of WGT-% addition.

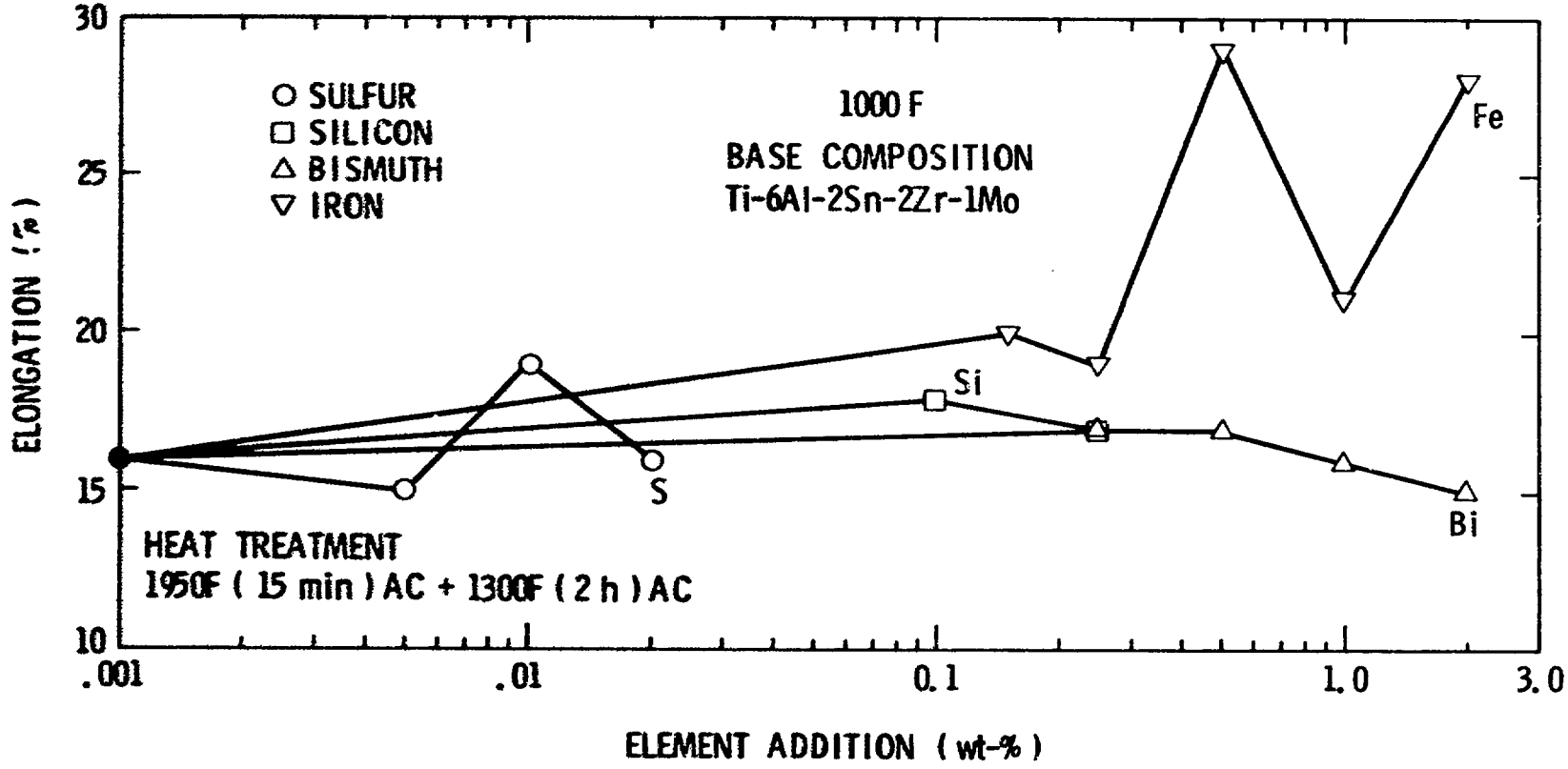

SC5011.26TR

Figure 4 High temperature (1000F) tensile elongation results for button melts of composition Ti-6Al-2Sn-2Zr-1Mo with element additions of Si, Bi, Fe and S as a function of WGT-% addition.

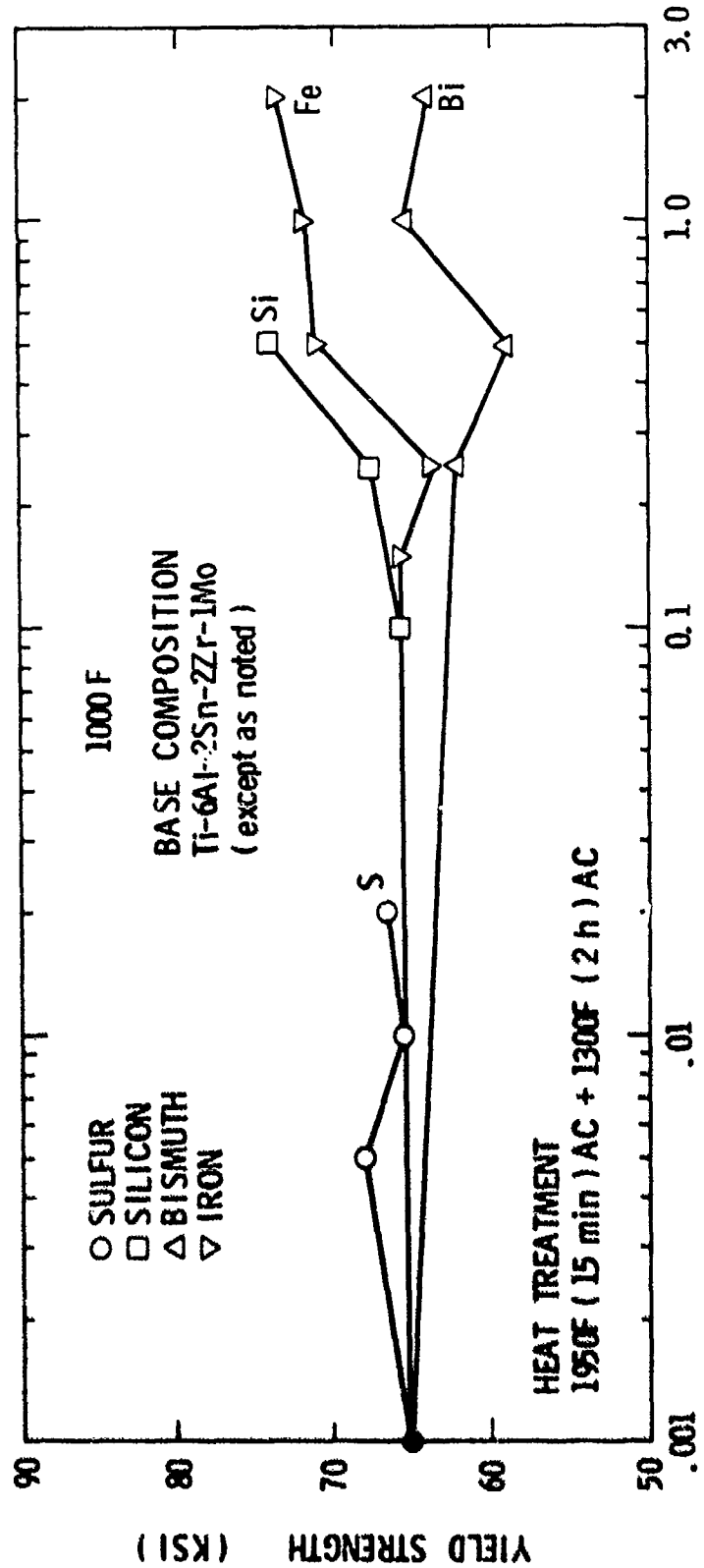

Figure 5 High temperature (1000F) yield strength results for button melts of composition Ti-6Al-2Sn-2Zr-1Mo with element additions of Si, Bi, Fe and S as a function of WST-% addition.

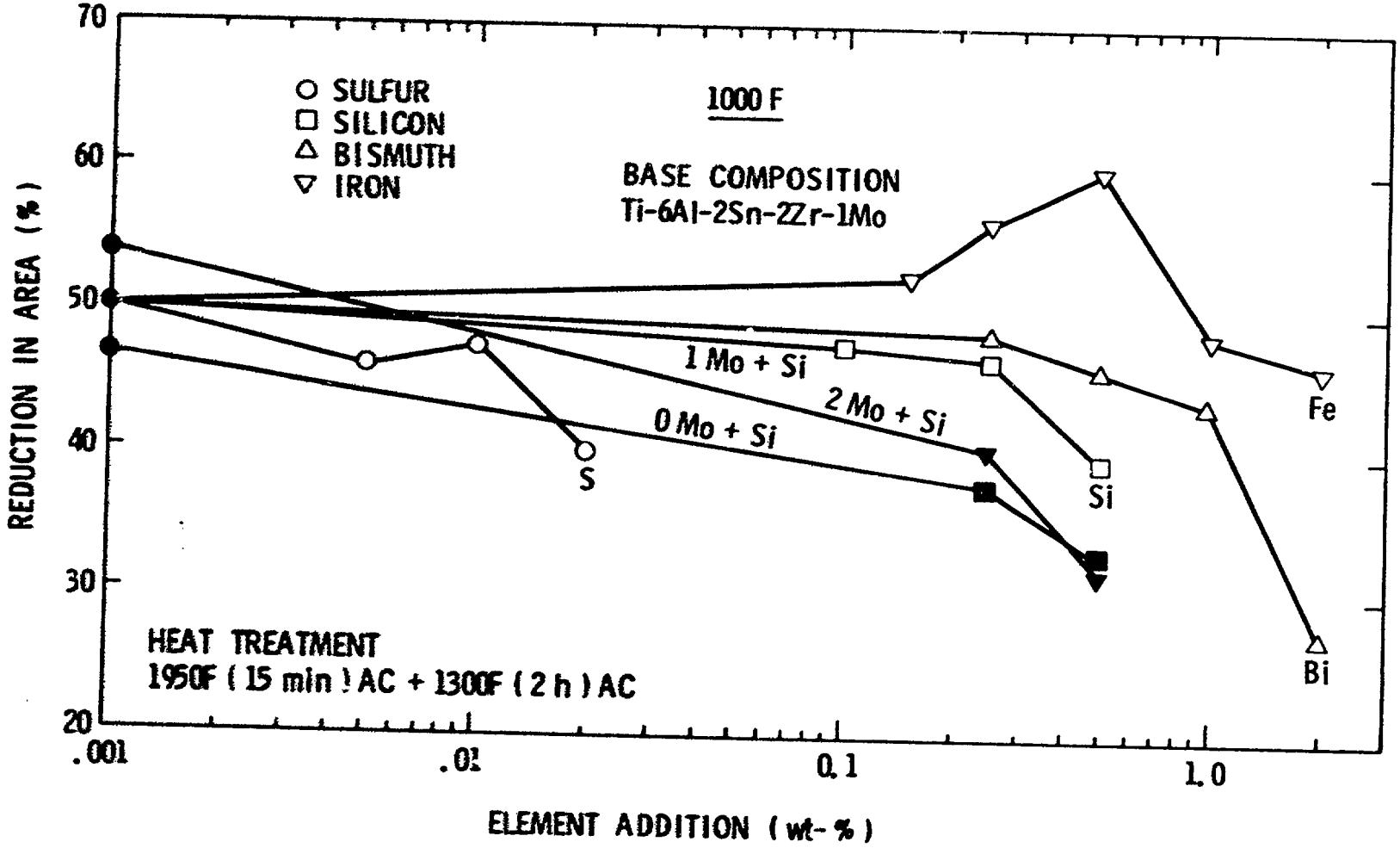

Figure 6 High temperature (1000F) reduction in area results for button melts of composition Ti-6Al-2Sn-2Zr-1Mo with additions of Si, Bi, Fe and S as a function of WGT-% addition.

SC5011.26TR

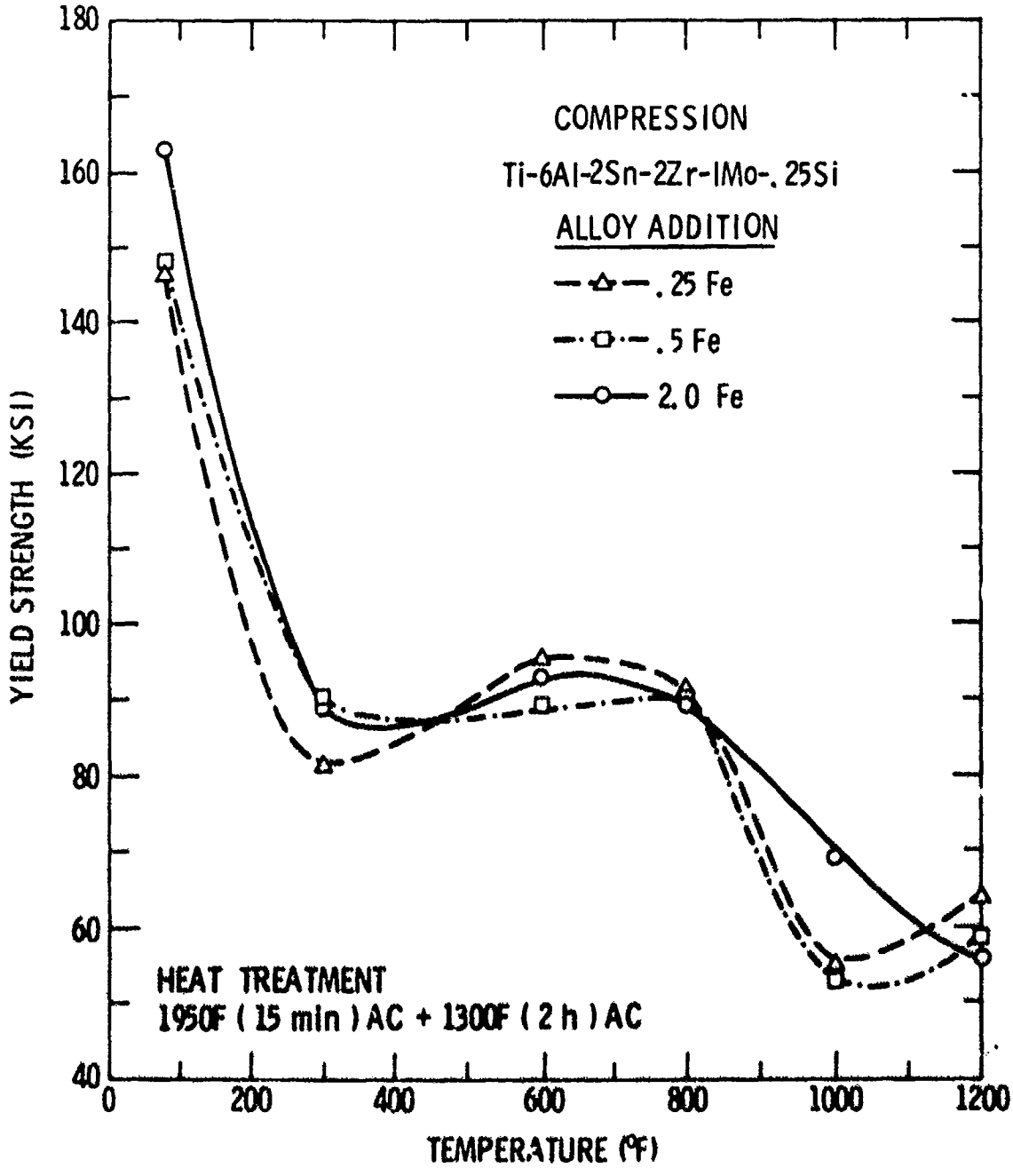

Figure 7 Compressive yield strength of button melts of composition Ti-6Al-2Sn-2Zr-1Mo-.25Si with additions of Fe as a function of temperature.

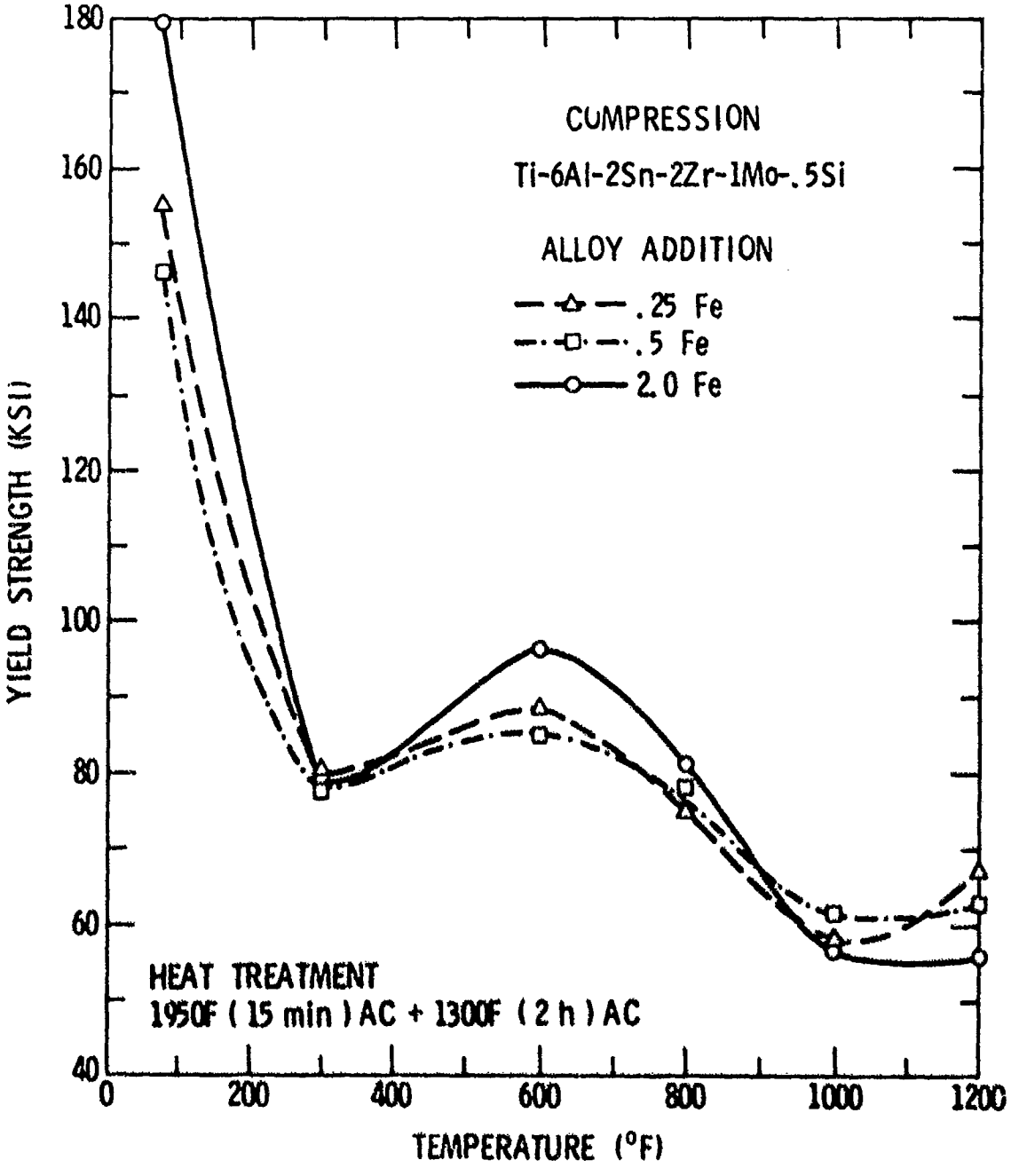

Figure 8 Compressive yield strength of button melts of composition Ti-6Al-2Sn-2Zr-1Mo-.5Si with additions of Fe as a function of temperature.

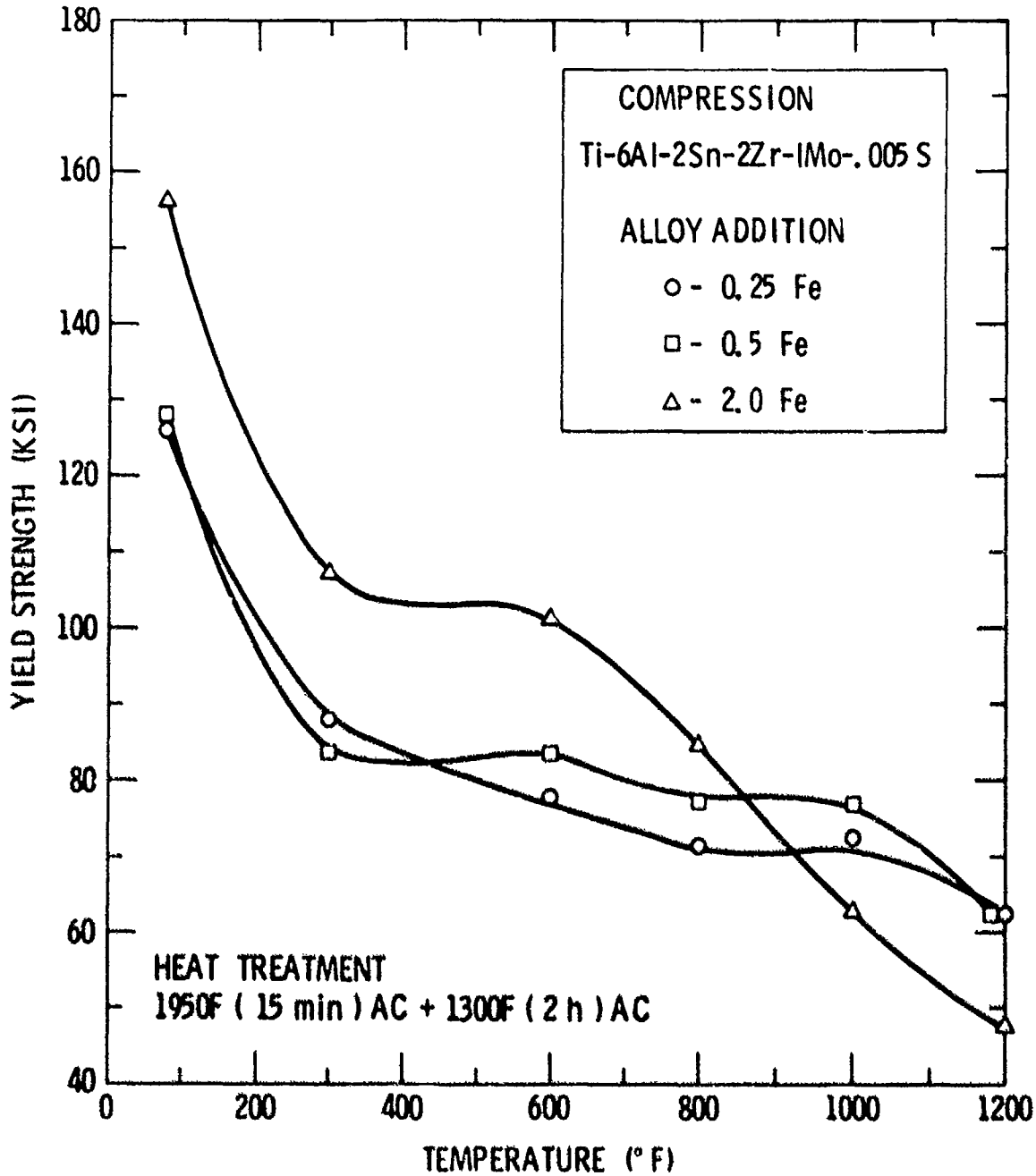

Figure 9 Compressive yield strength of button melts of composition Ti-6Al-2Sn-2Zr-1Mo-.005S as a function of Fe content and temperature.

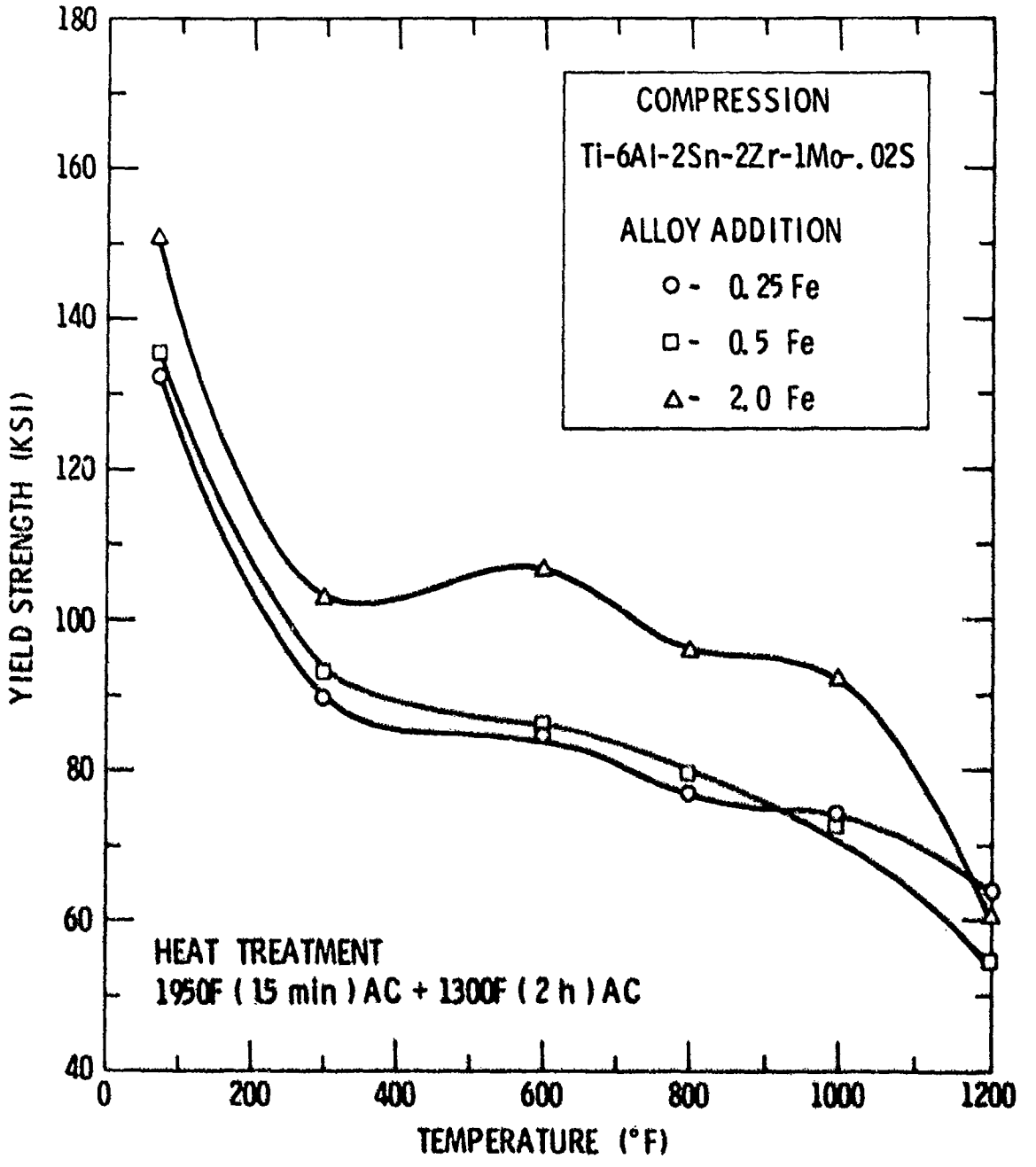

Figure 10 Compressive yield strength of button melts of composition Ti-6Al-2Sn-2Zr-1Mo-.02S as a function of Fe content and temperature.

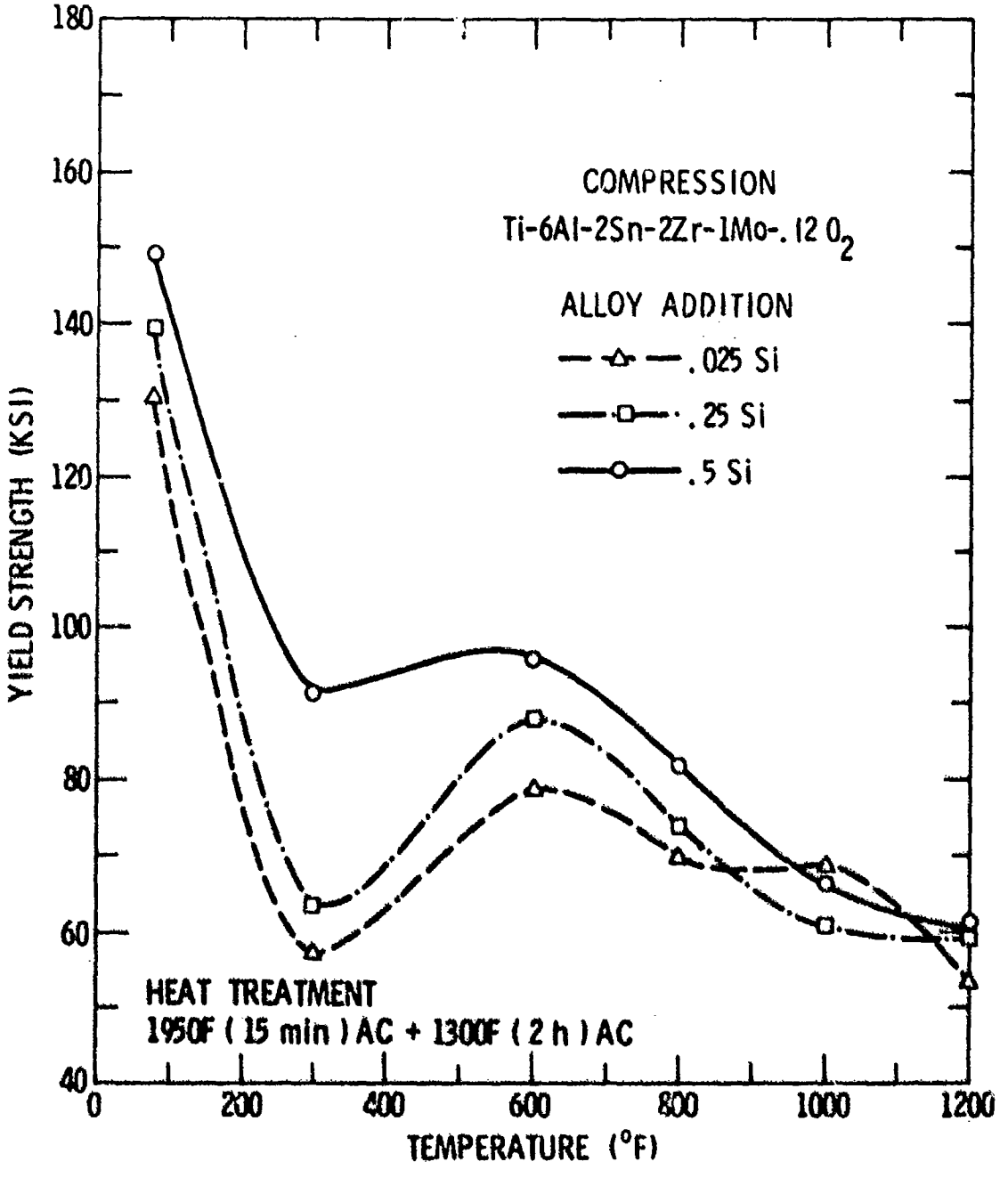

Figure 11 Compressive yield strenyth of button melts of composition Ti-6Al-2Sn-2Zr-1Mo-.12 O_2 with additions of Si as a function of temperature.

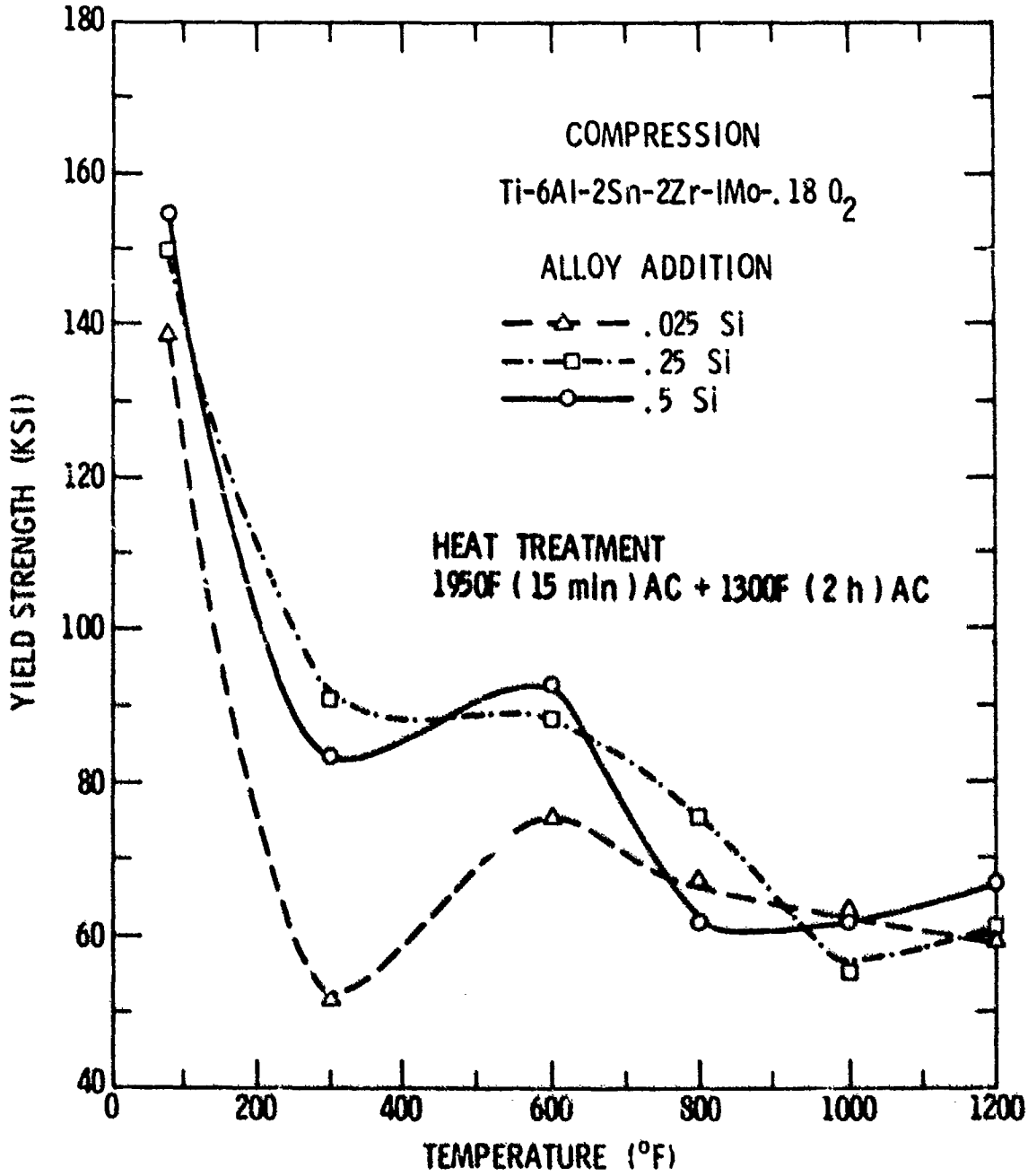

Figure 12 Compressive yield strength of button melts of composition Ti-6Al-2Sn-2Zr-1Mo-.18O_2 with additions of Si as a function of temperature.

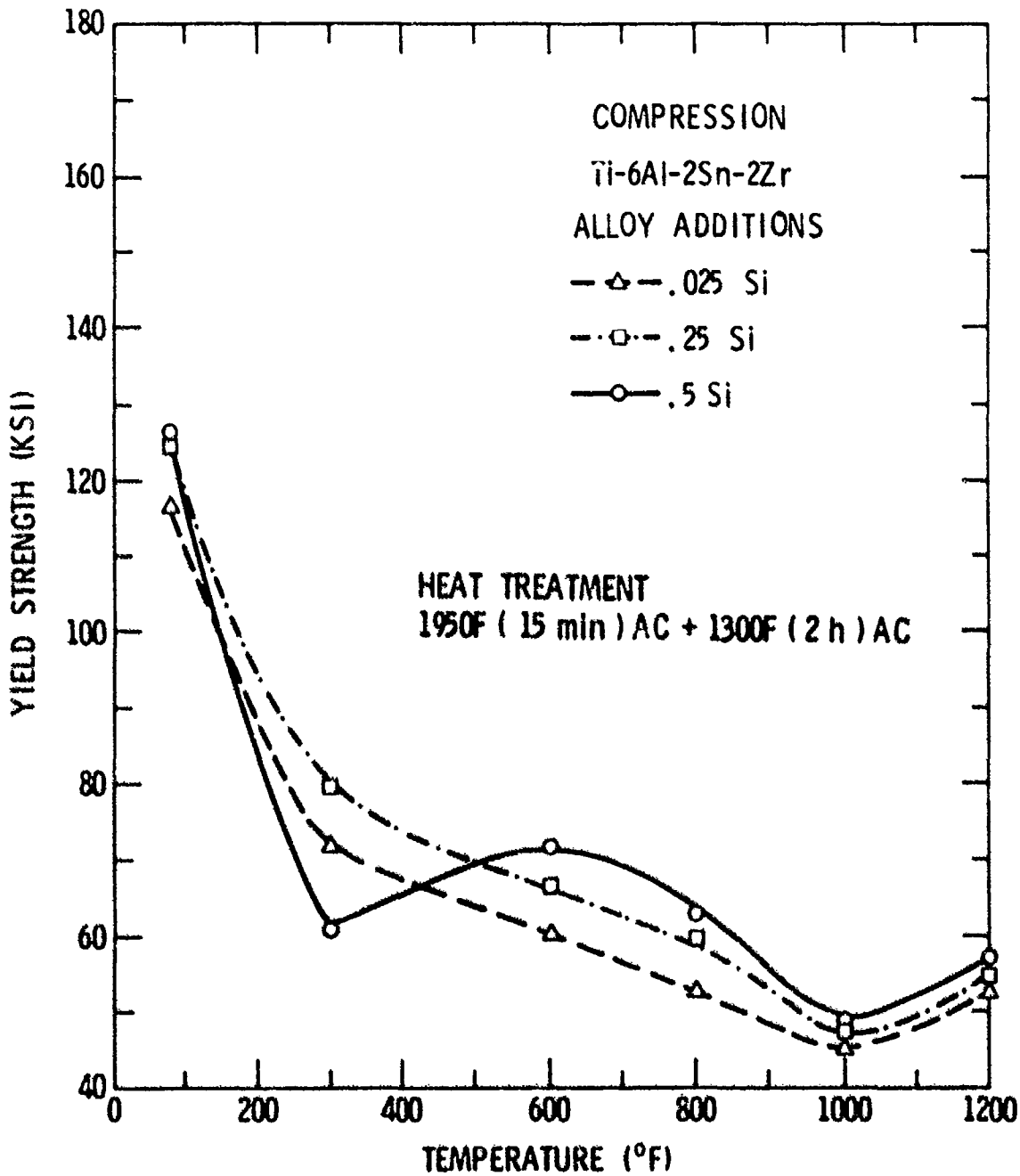

Figure 13 Compressive yield strength of button melts of composition Ti-6Al-2Sn-2Zr with additions of Si as a function of temperature.

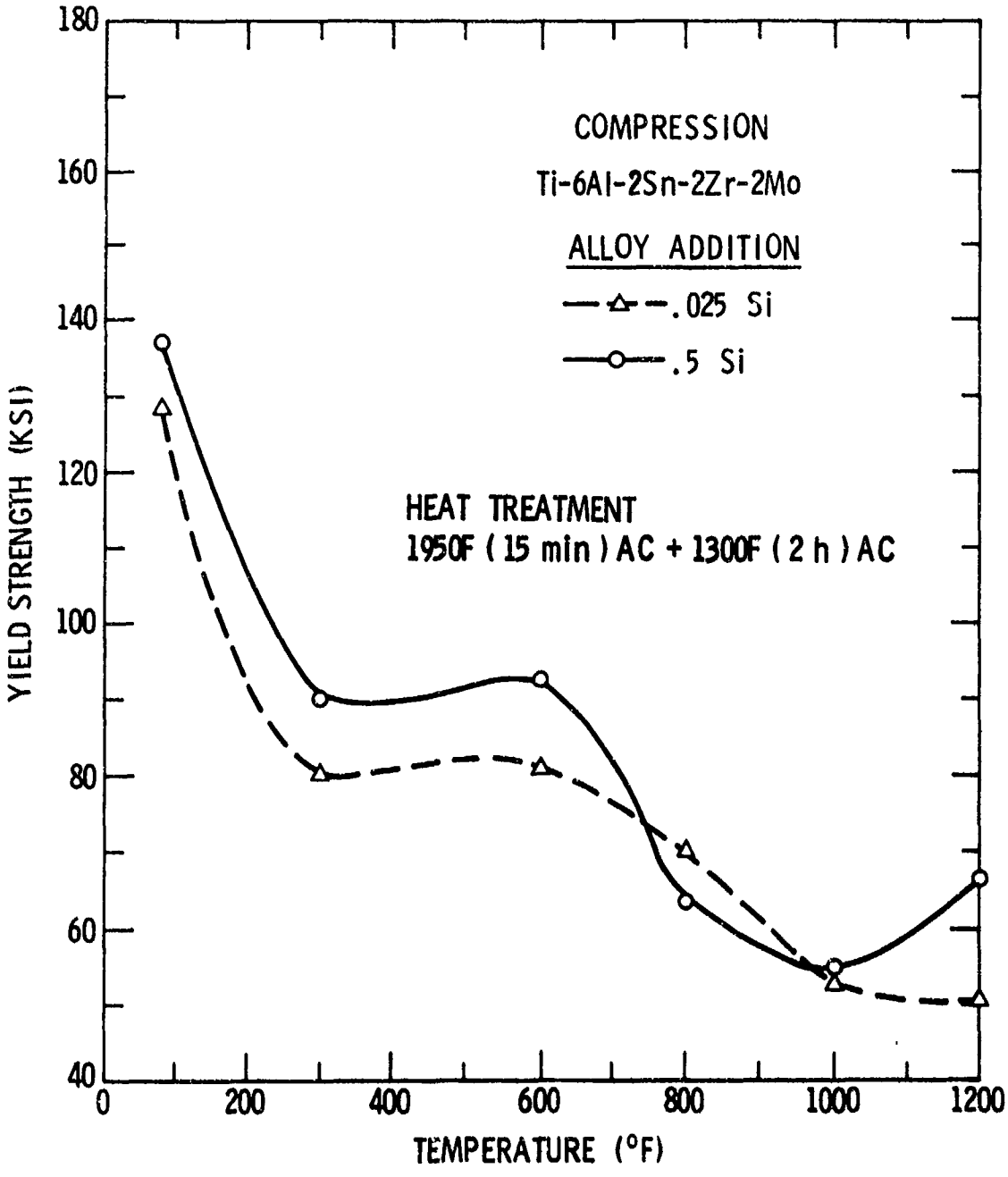

Figure 14 Compressive yield strength of button melts of composition Ti-6Al-2Sn-2Zr-2Mo with additions of Si as a function of temperature.

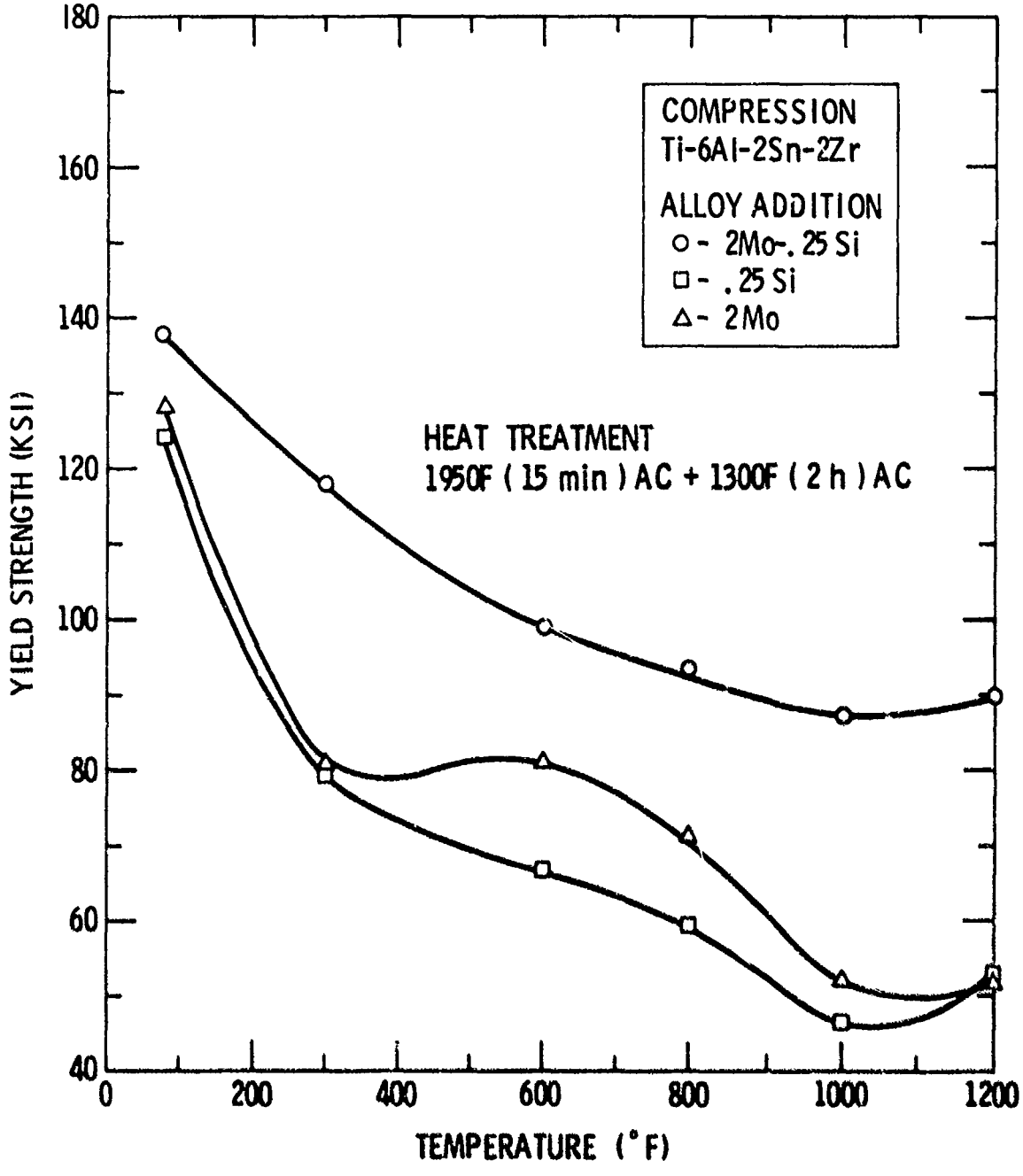

Figure 15 Compressive yield strength of button melts of composition Ti-6Al-2Sn-2Zr with additions of Mo and Si as a function of temperature.

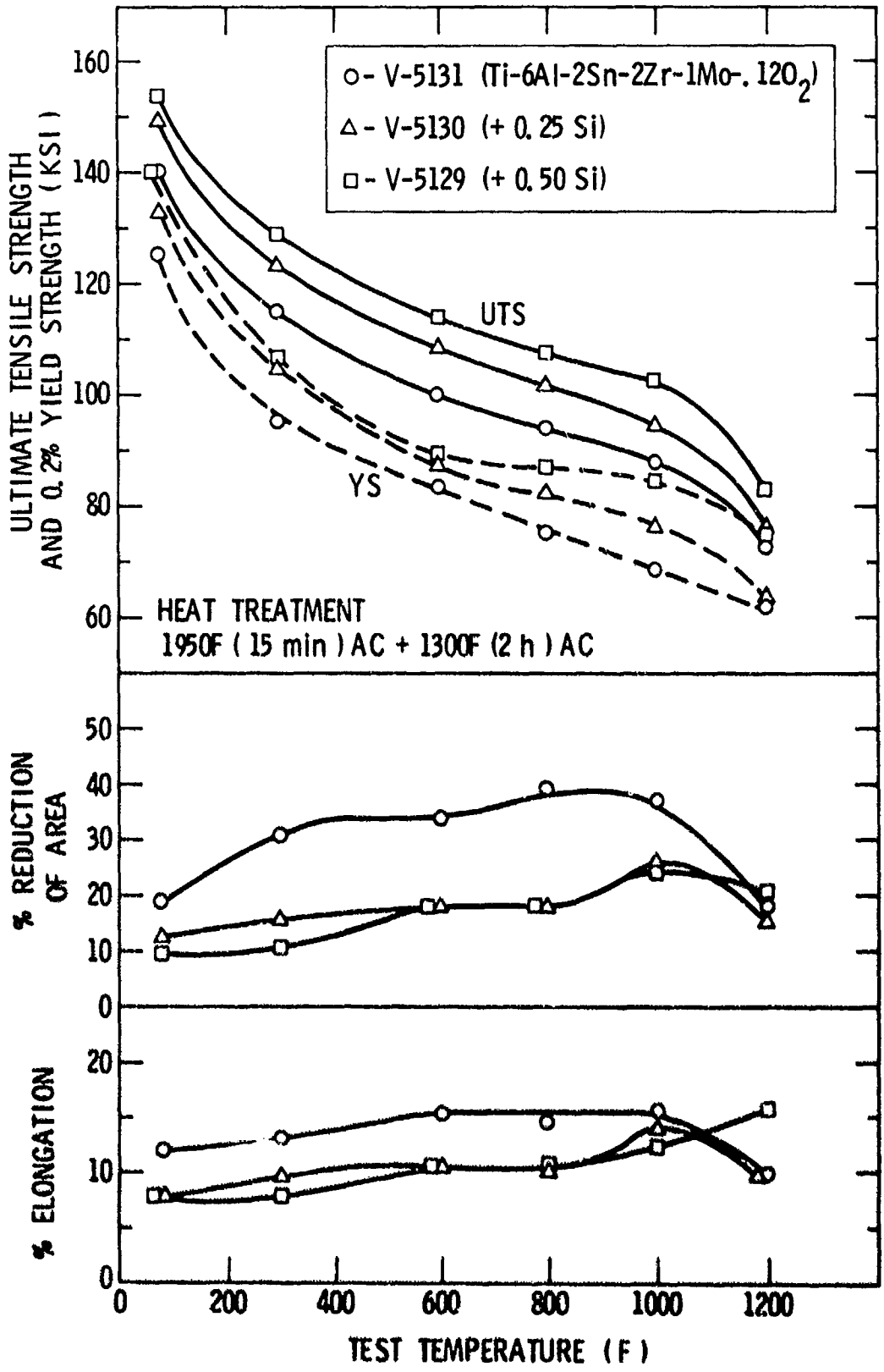

Figure 16 Mechanical properties of 100 lb. ingot materials of composition Ti-6Al-2Sn-2Zr-1Mo-.12O_2 - (<.05, .25, and .50 Si) as a function of temperature.

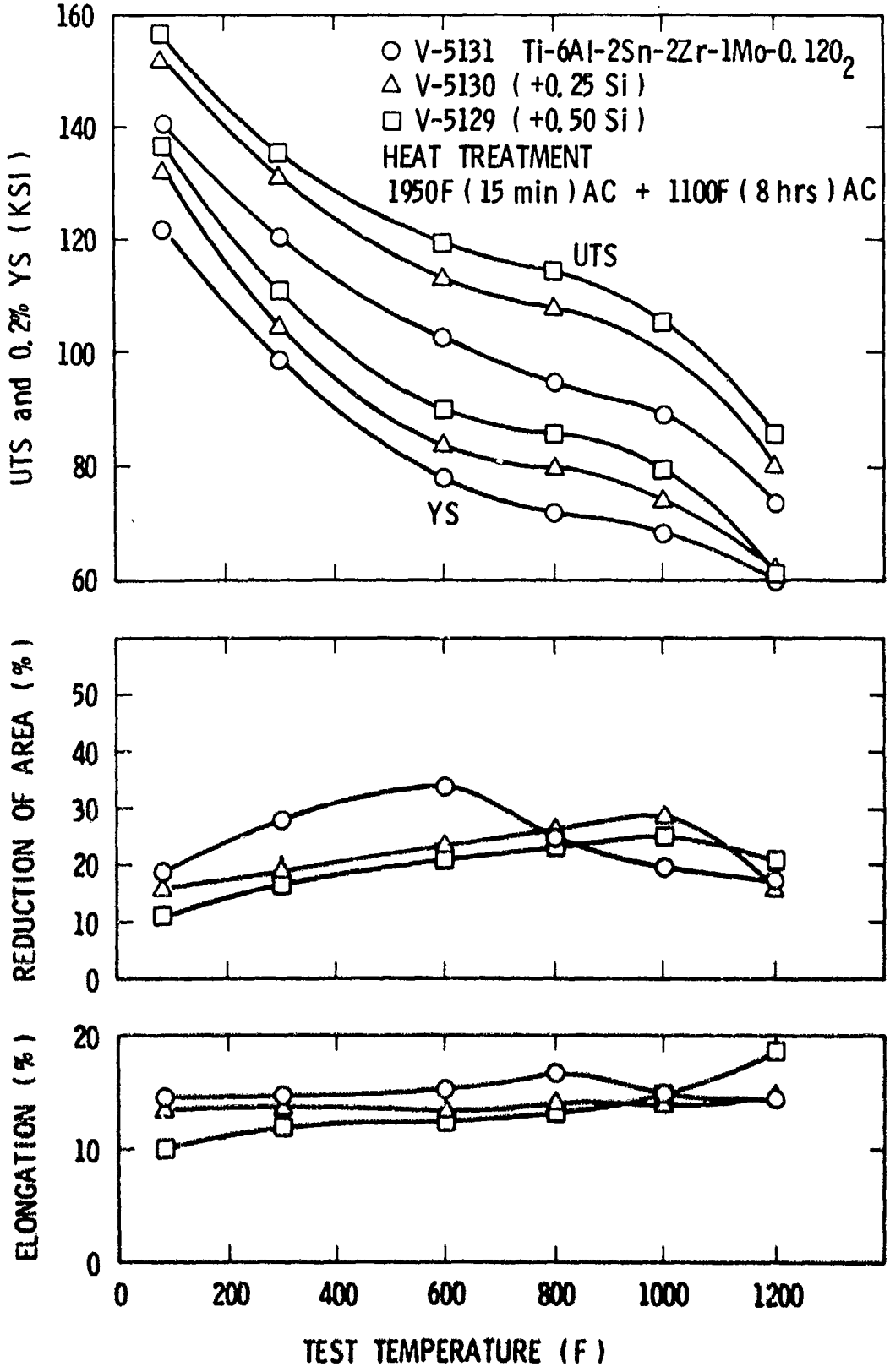

Figure 17 Effect of Si additions on the tensile properties of 100 lb. ingots of composition Ti-6Al-2Sn-2Zr-1Mo as a function of temperature.

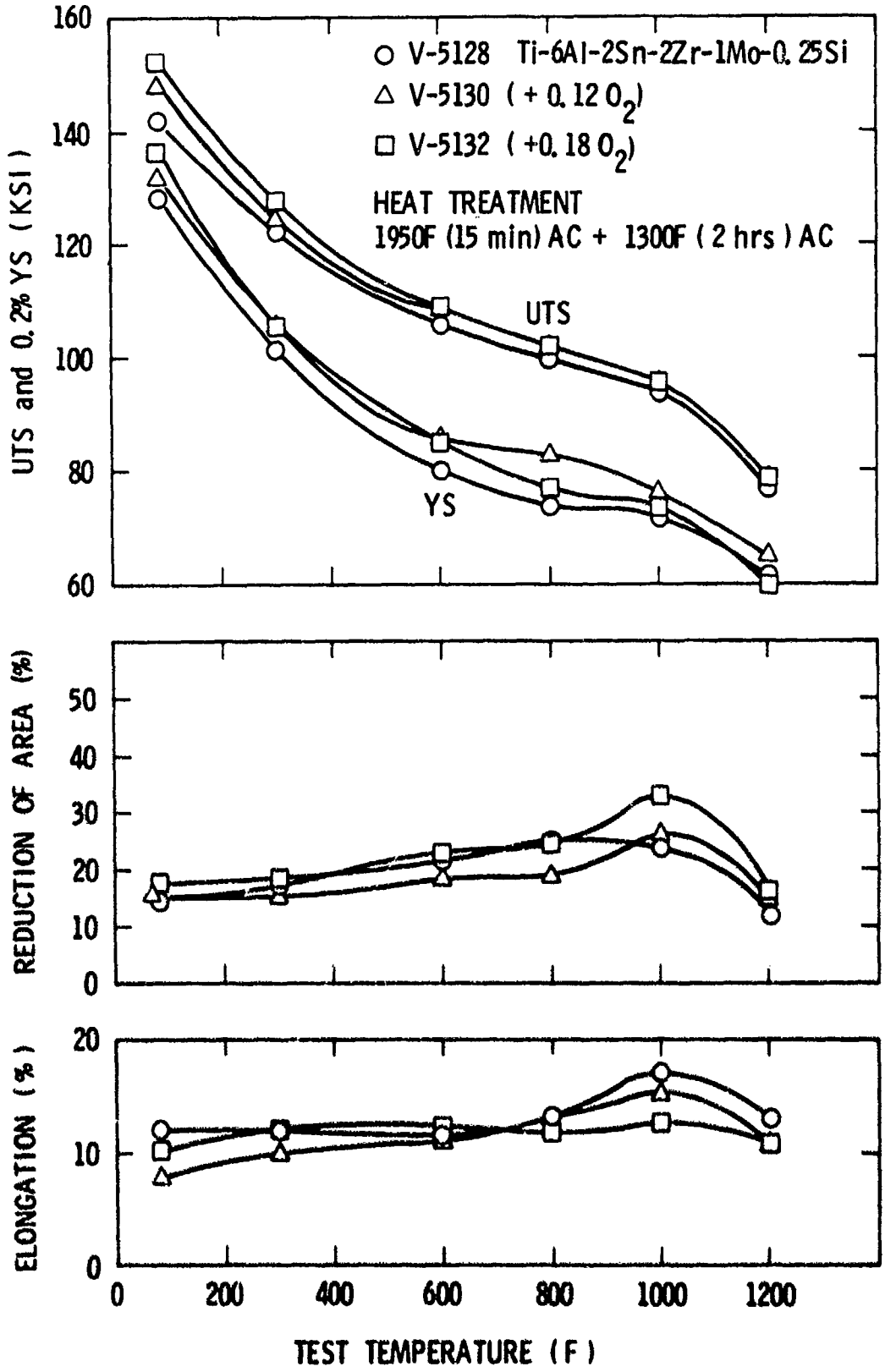

Figure 18 Effect of O_2 content on the tensile properties of 100 lb. ingots of composition Ti-6Al-2Sn-2Zr-1Mo-.25Si as a function of temperature.

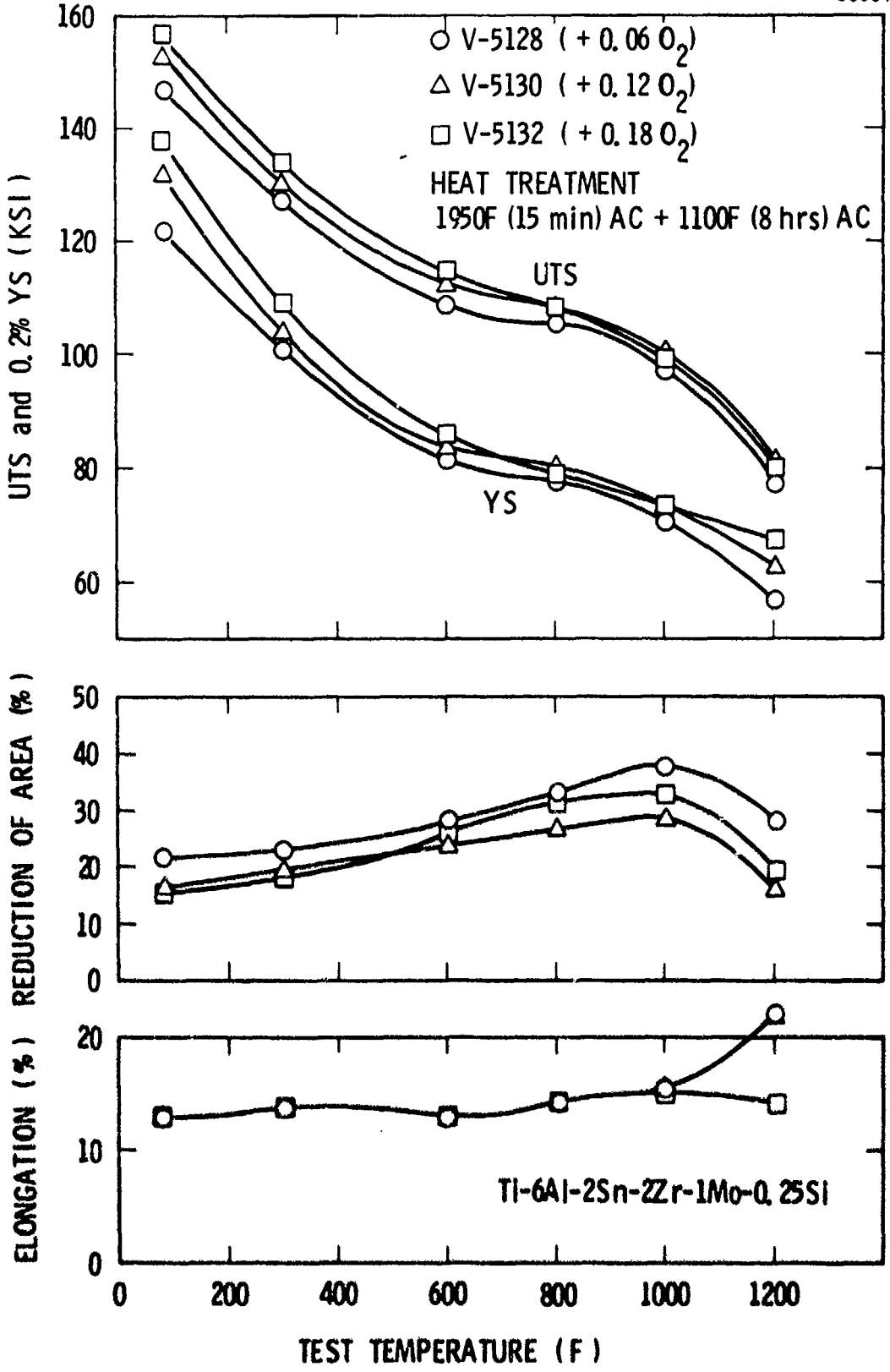

Figure 19 Effect of O_2 content on the tensile properties of 100 lb. ingots of composition Ti-6Al-2Sn-2Zr-1Mo-.25Si as a function of temperature utilizing a stabilization heat treatment of 1100F/8 hrs/AC.

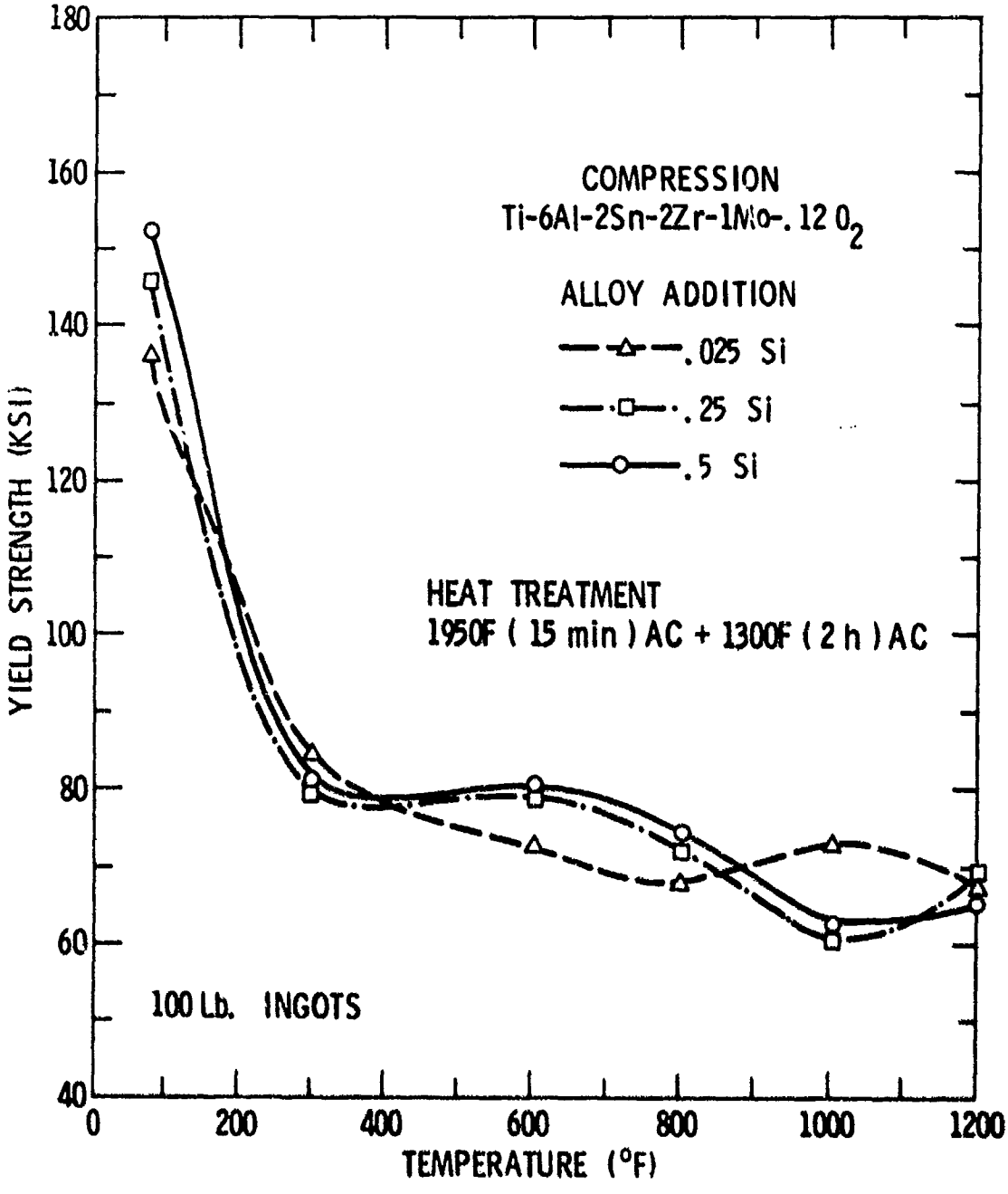

Figure 20 Compressive yield strength of 100 lb. ingots of base composition Ti-6Al-2Sn-2Zr-1Mo-.12 O_2 with additions of Si as a function of temperature.

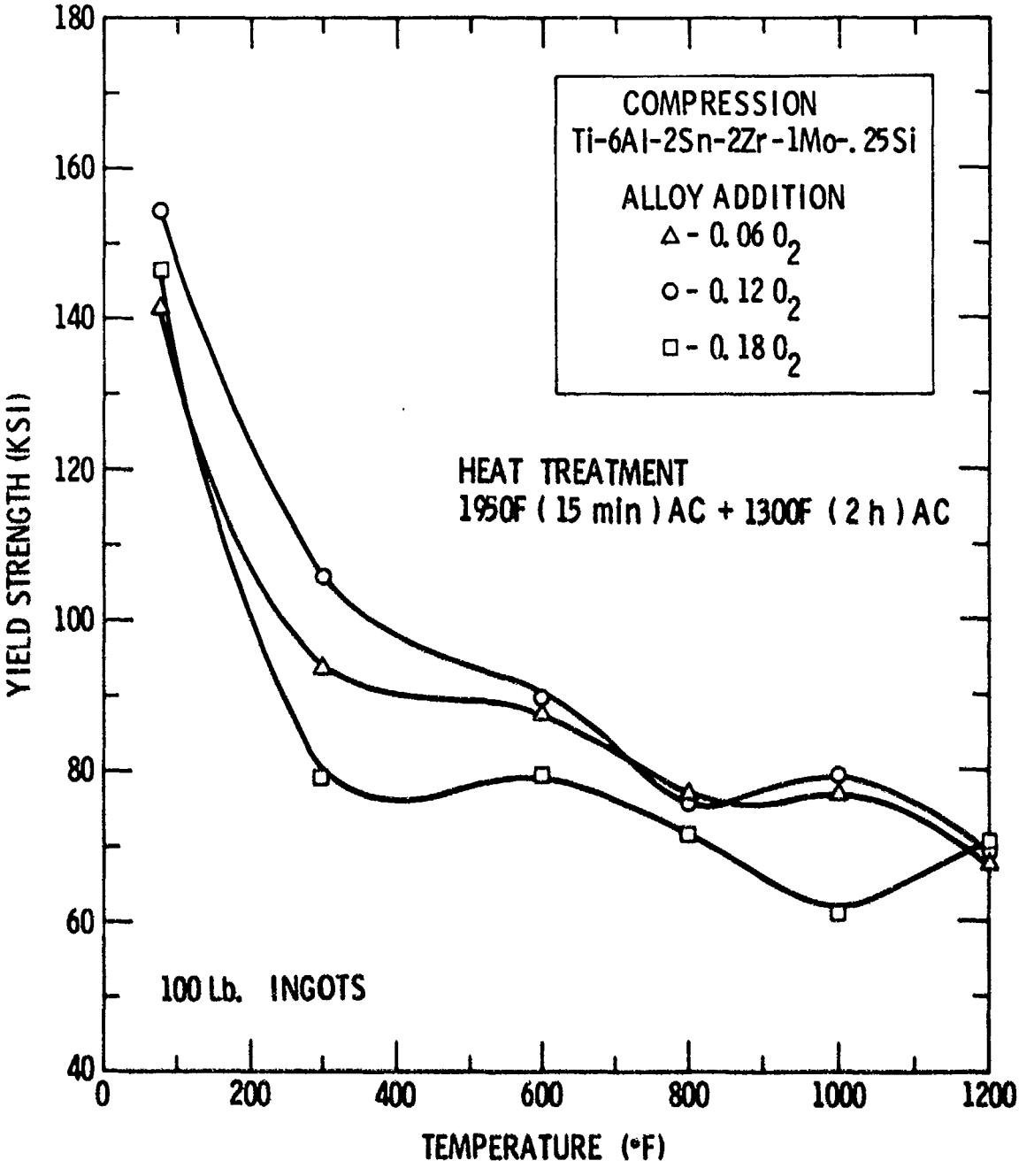

Figure 21 Compressive yield strength of 100 lb. ingots of base composition Ti-6Al-2Sn-2Zr-1Mo-.25Si as a function of O_2 content and temperature.

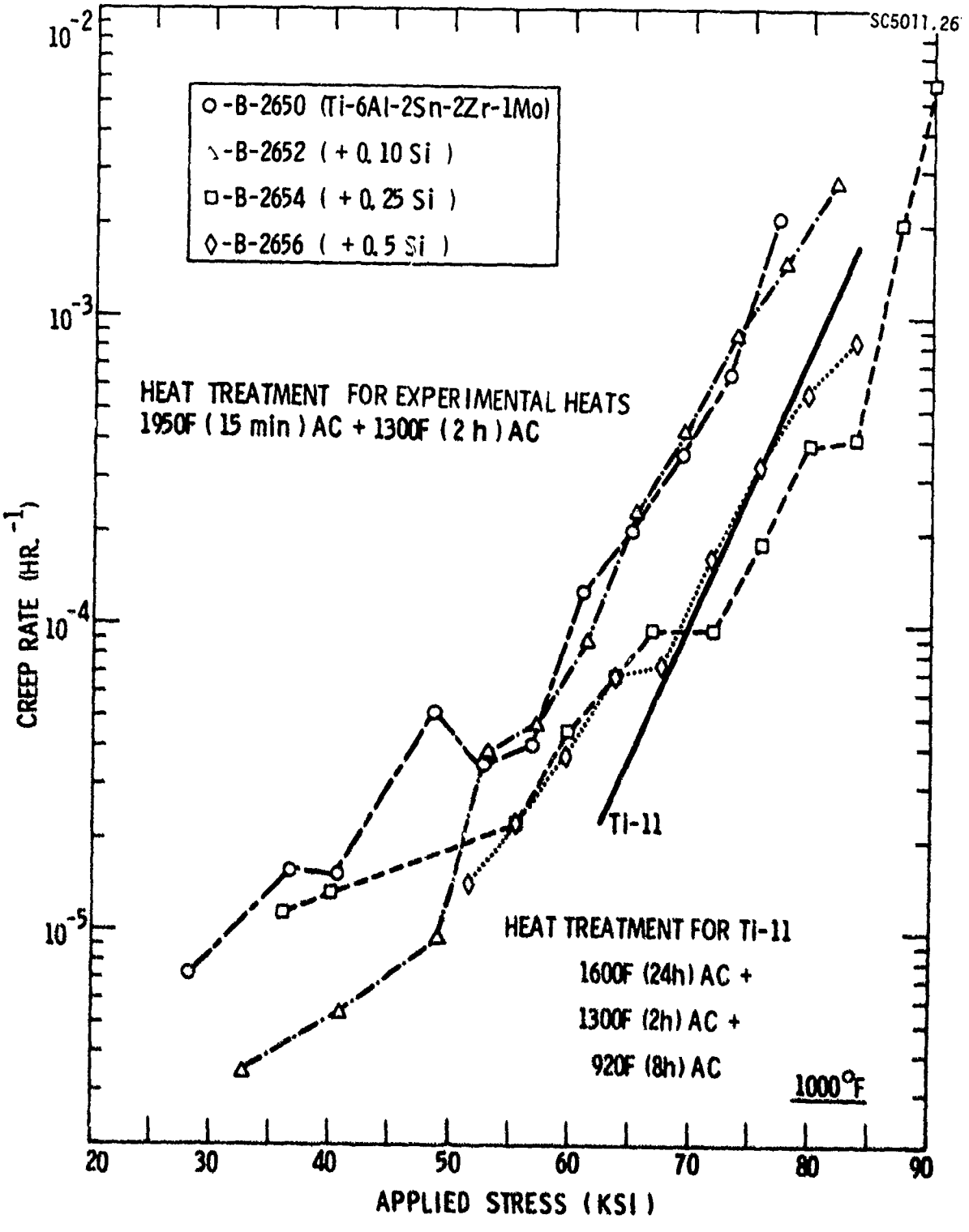

Figure 22 Creep rate as a function of applied stress at 1000F for button melts of composition Ti-6Al-2Sn-2Zr-1Mo with additions of Si.

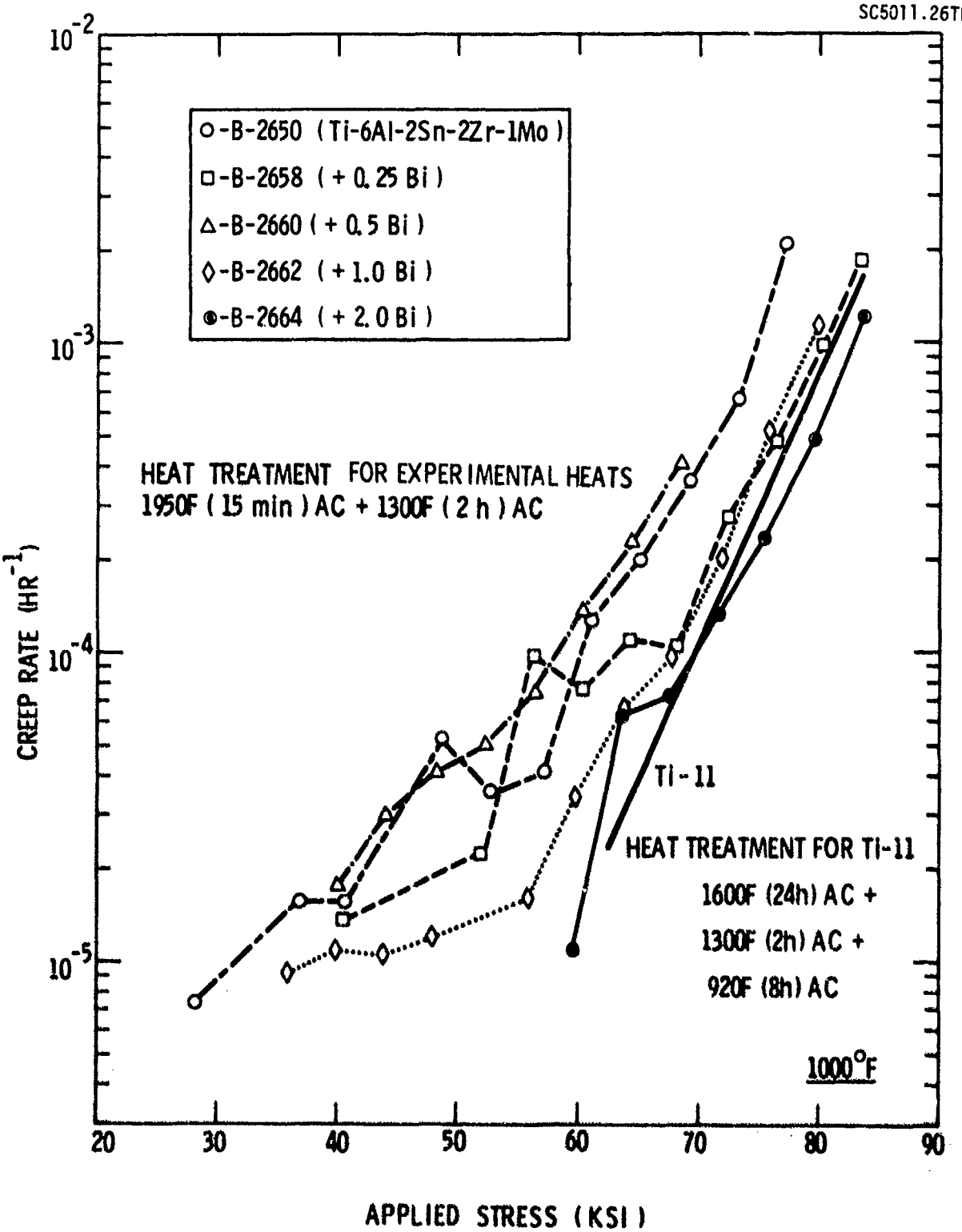

Figure 23 Creep rate as a function of applied stress at 1000F for button melts of composition Ti-6Al-2Sn-2Zr-1Mo with additions of Bi.

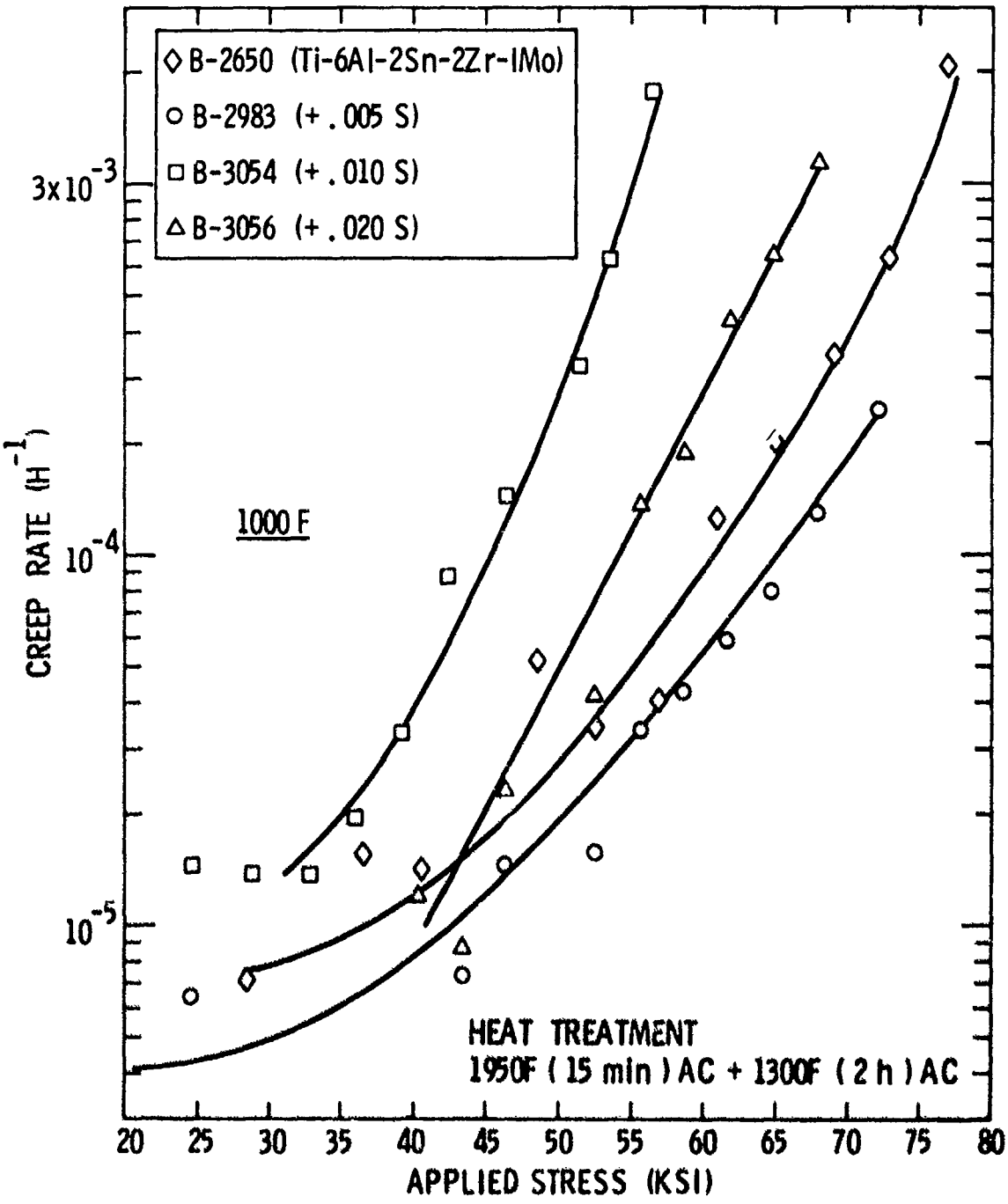

Figure 24 Creep rate as a function of applied stress at 1000F for button melts of composition Ti-6Al-2Sn-2Zr-1Mo with additions of S.

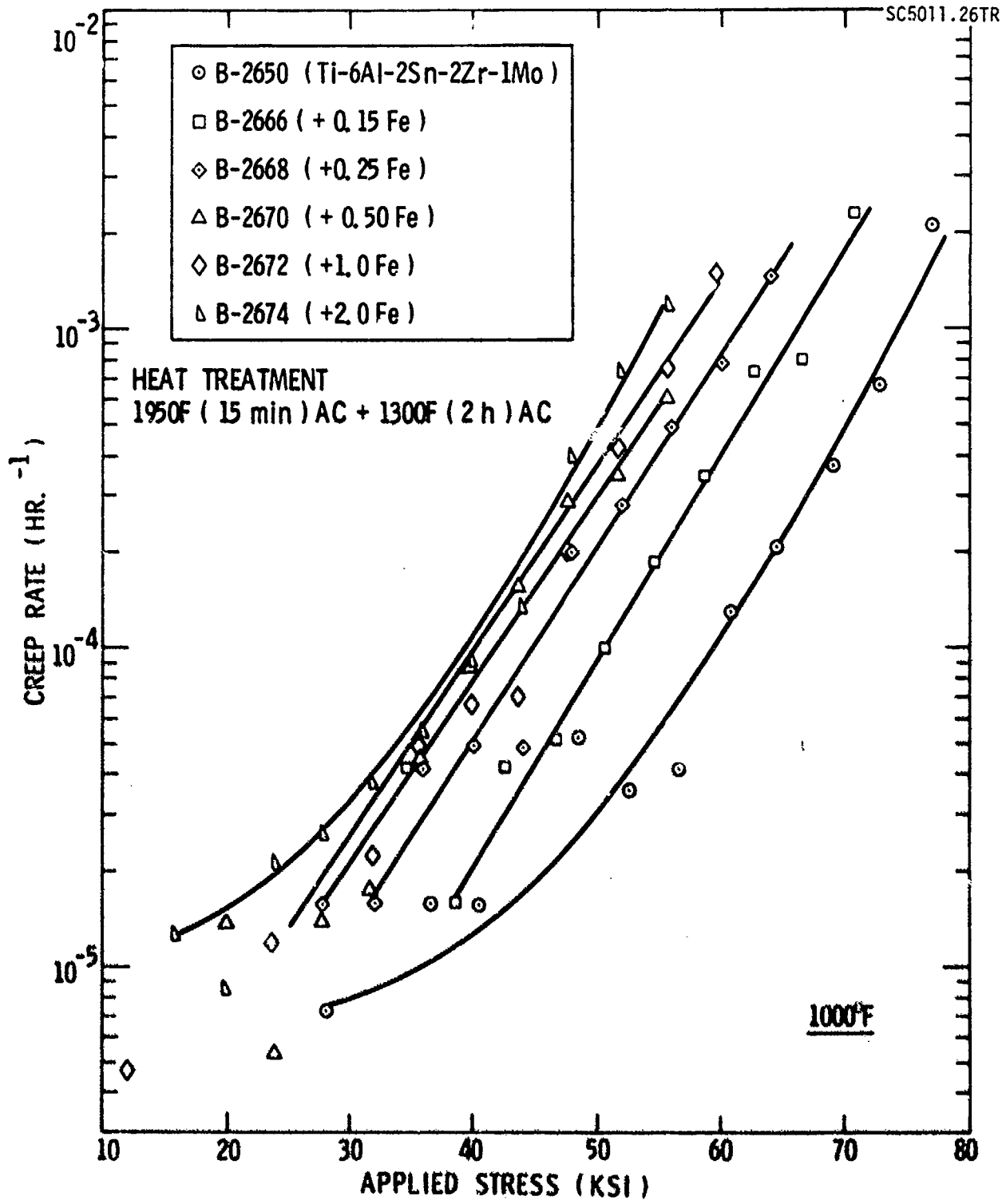

Figure 25 Creep rate as a function of applied stress at 1000F for button melts of composition Ti-6Al-2Sn-2Zr-1Mo with additions of Fe.

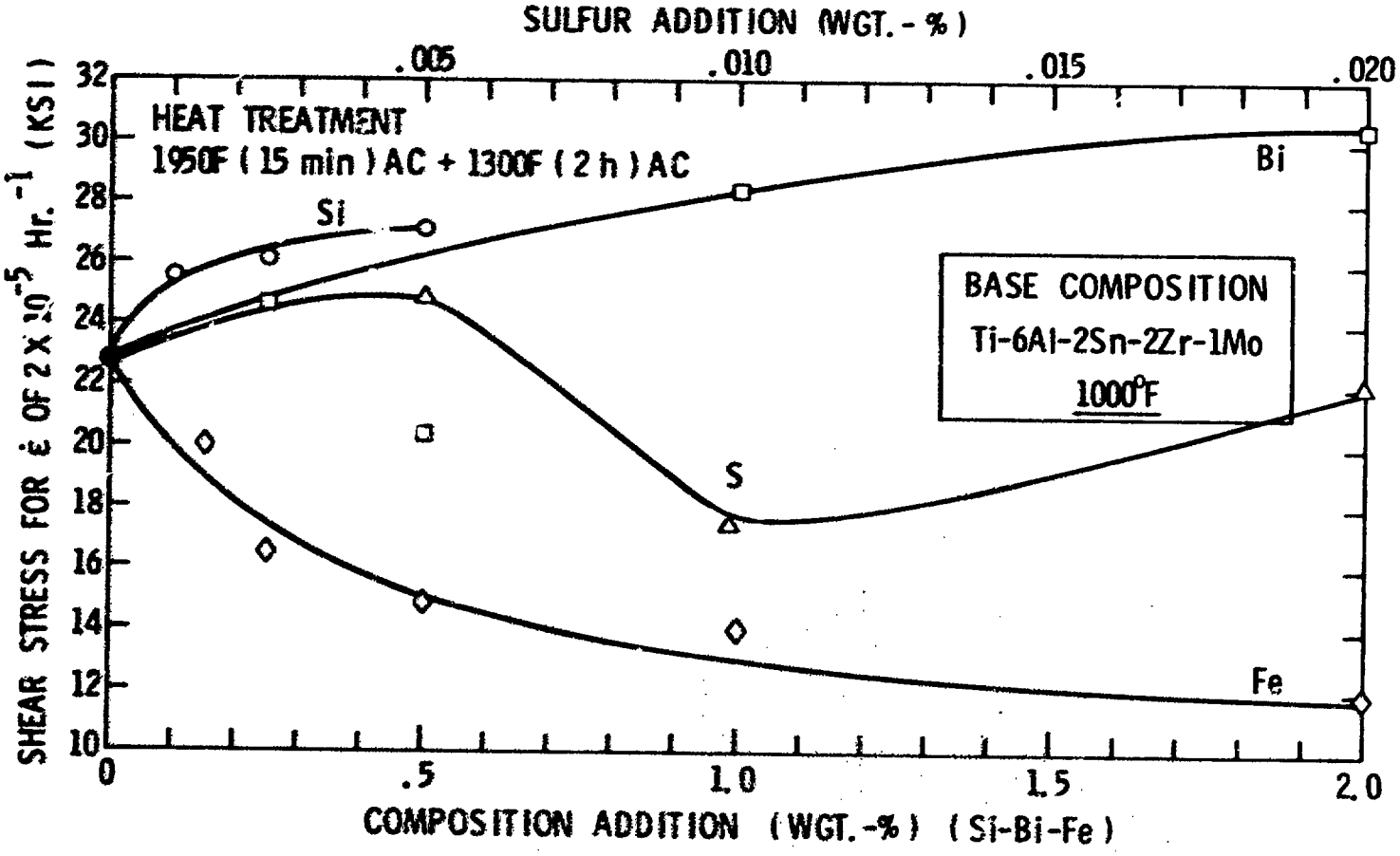

Figure 26 Shear stress for a creep rate of 2×10^{-5} Hr^{-1} as a function of WGT-% additions of Si, Bi, Fe, and S for button melts of base composition Ti-6Al-2Sn-2Zr-1Mo at 1000F.

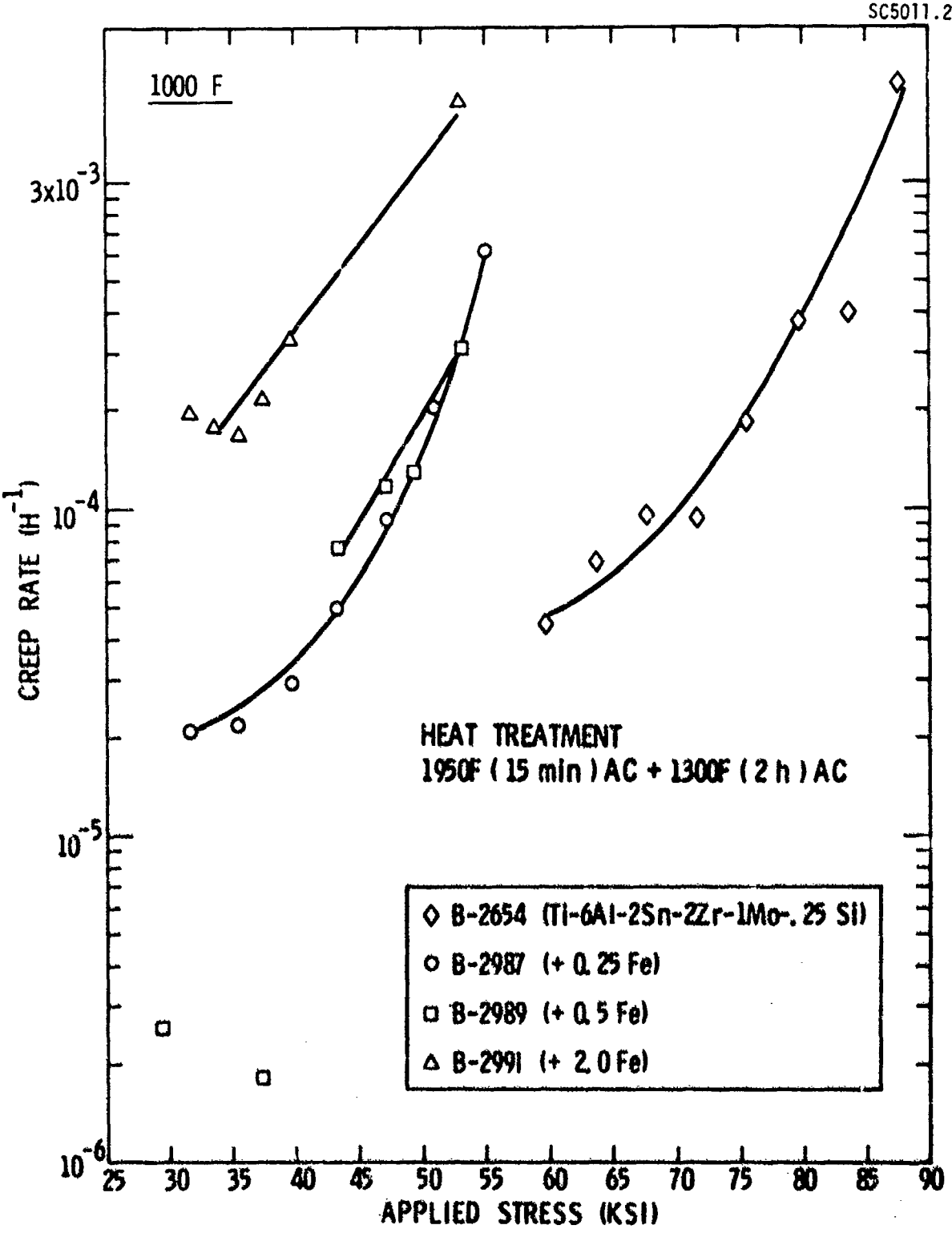

Figure 27 Creep rate as a function of applied stress at 1000F for button melts of composition Ti-6Al-2Sn-2Zr-1Mo-.25Si with additions of Fe.

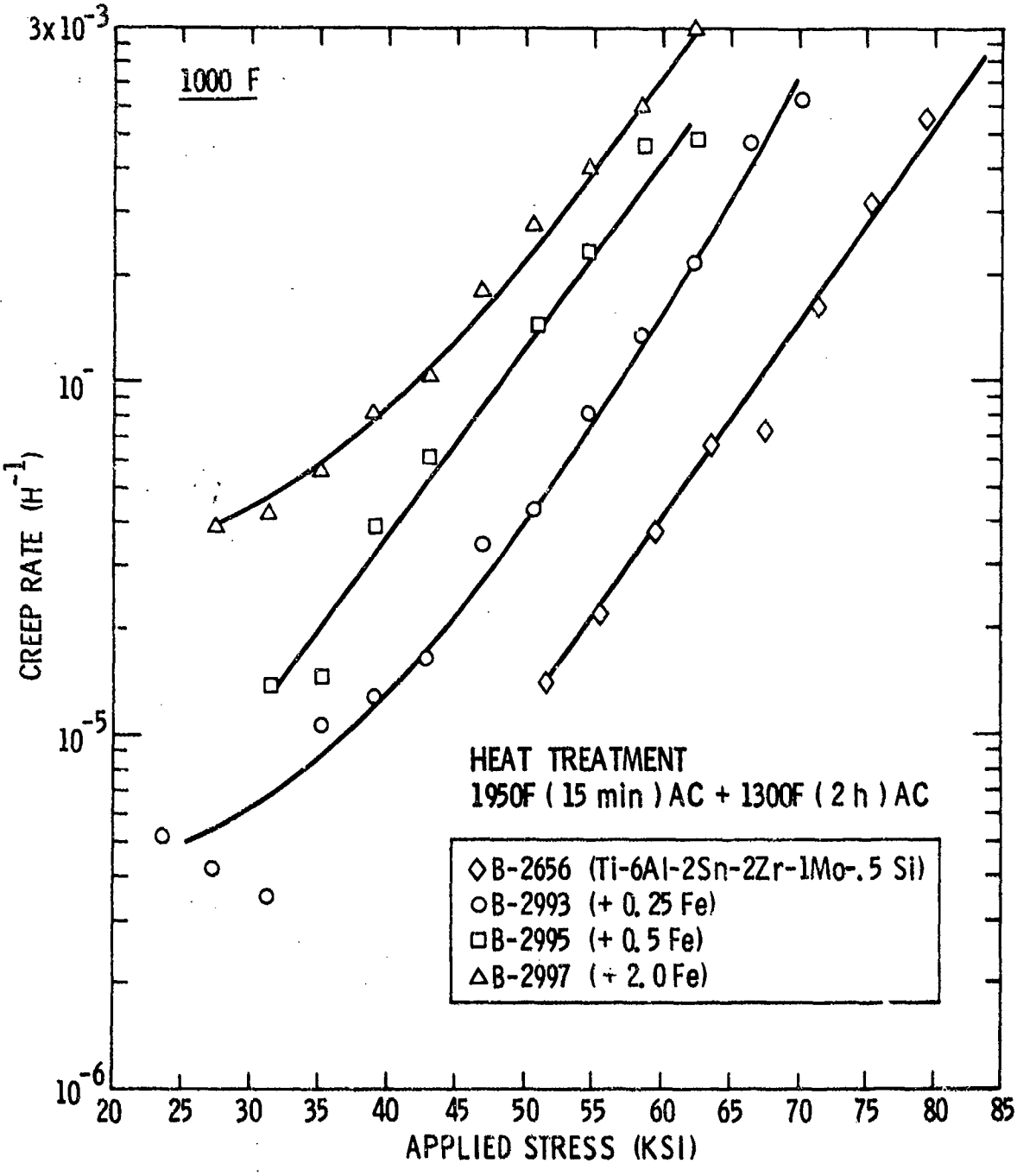

Figure 28 Creep rate as a function of applied stress at 1000F for button melts of composition Ti-6Al-2Sn-2Zr-1Mo-.5Si with additions of Fe.

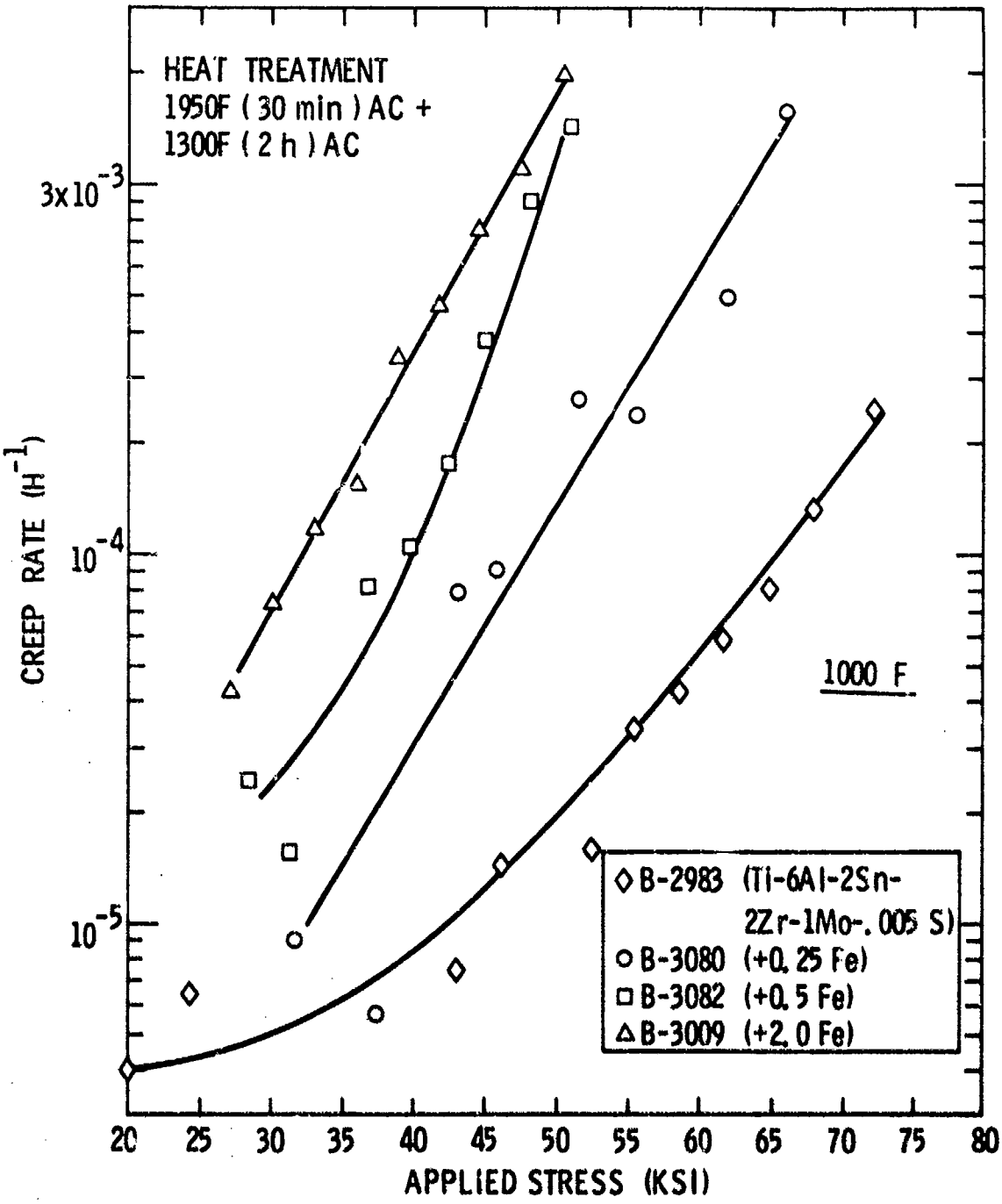

Figure 29 Creep rate as a function of applied stress at 1000F for button melts of composition Ti-6Al-2Sn-2Zr-1Mo-.005Si with additions of Fe.

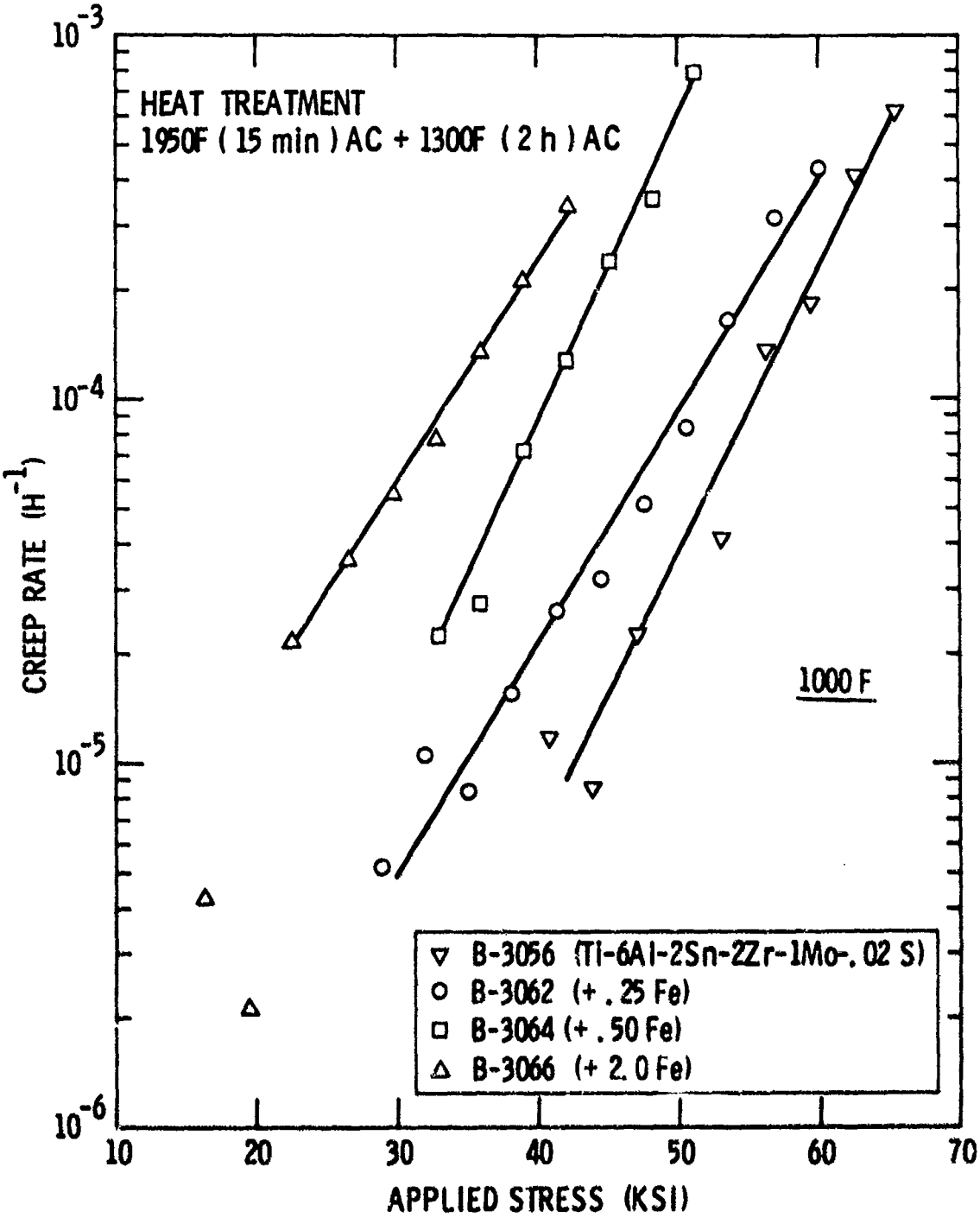

Figure 30 Creep rate as a function of applied stress at 1000F for button melts of composition Ti-6Al-2Sn-2Zr-1Mo-.02S with additions of Fe.

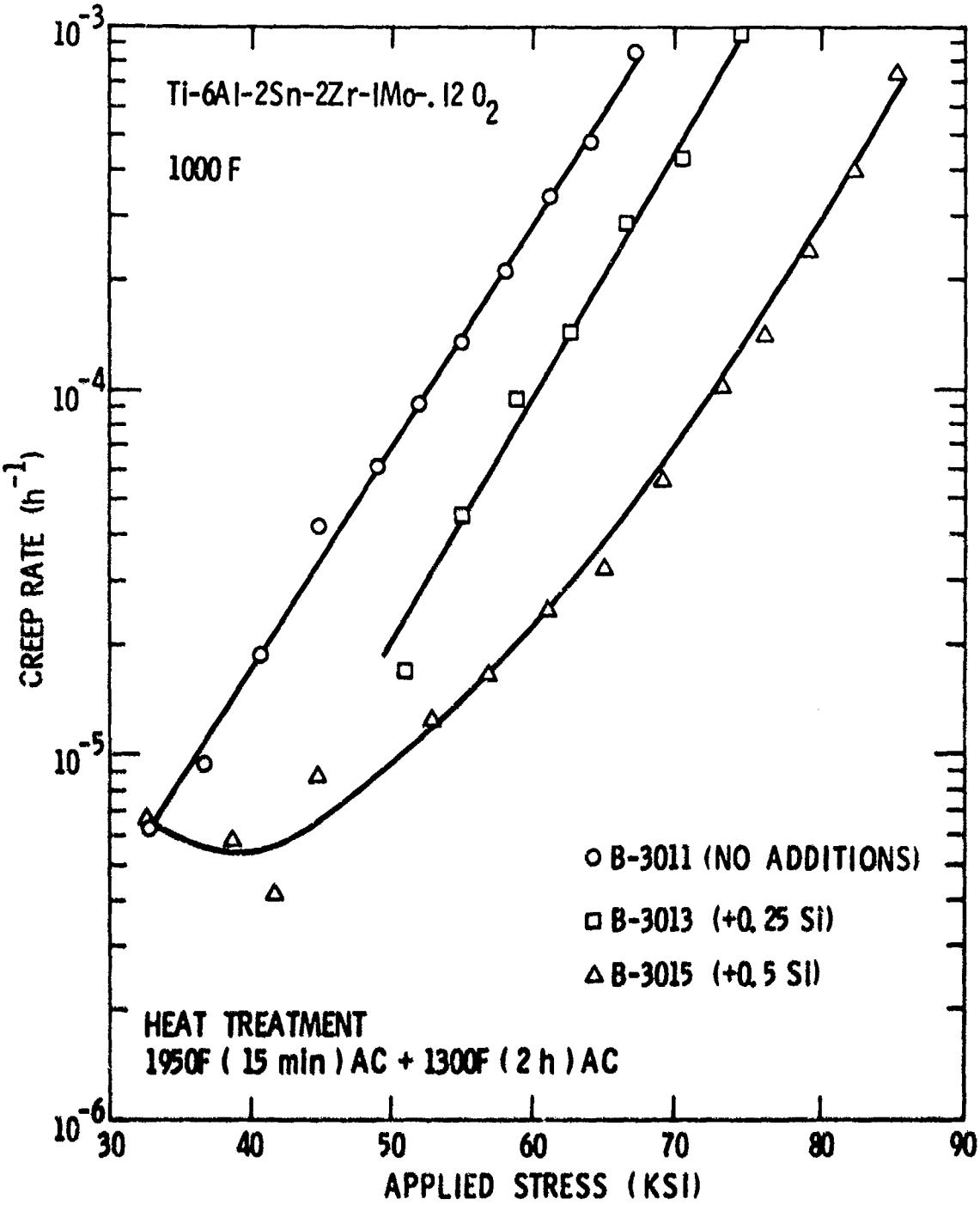

Figure 31 Creep rate as a function of applied stress at 1000F for button melts of composition Ti-6Al-2Sn-2Zr-1Mo-.12 O_2 with additions of Si.

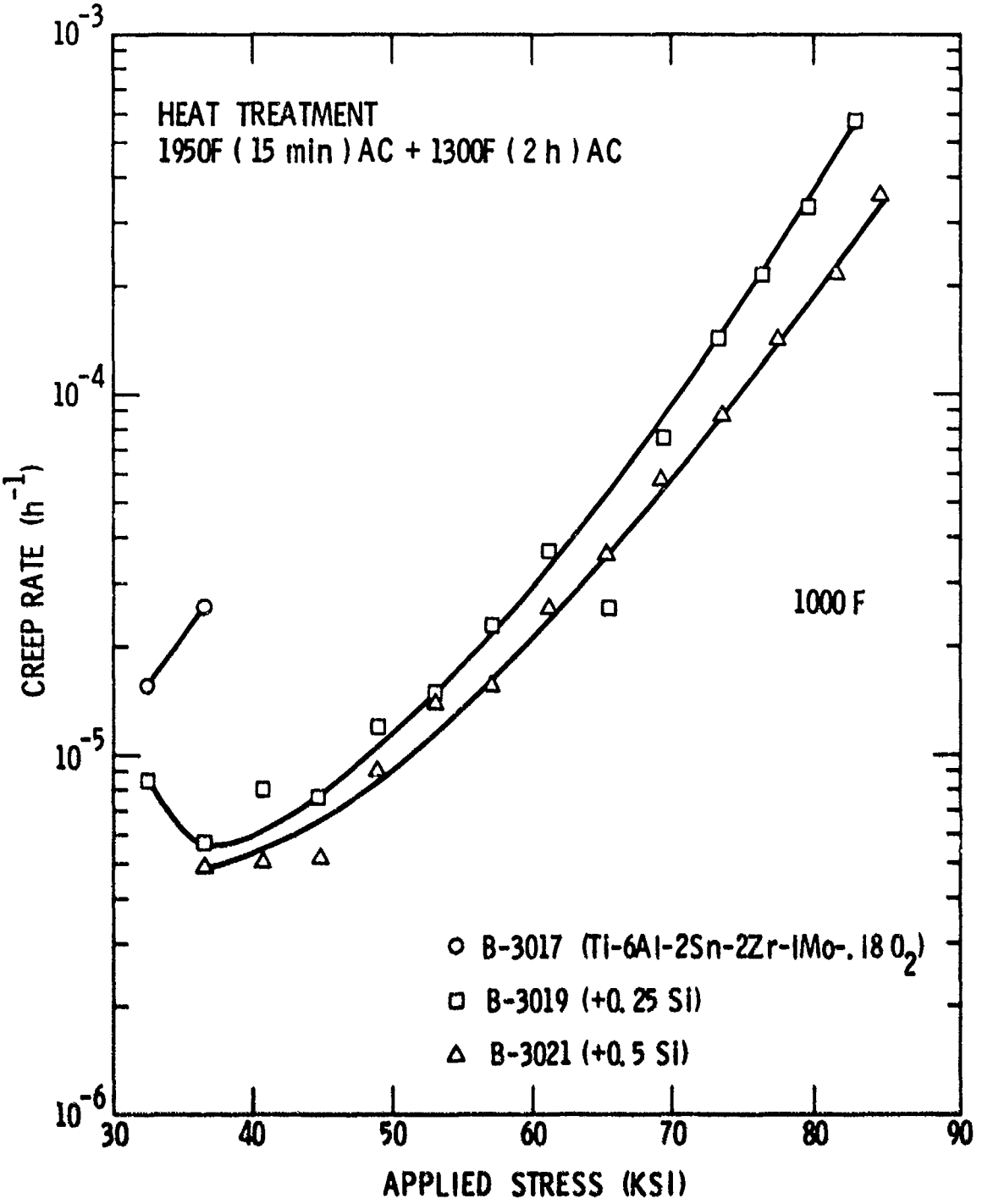

Figure 32 Creep rate as a function of applied stress at 1000F for button melts of composition Ti-6Al-2Sn-2Zr-1Mo-.18O_2 with additions of Si.

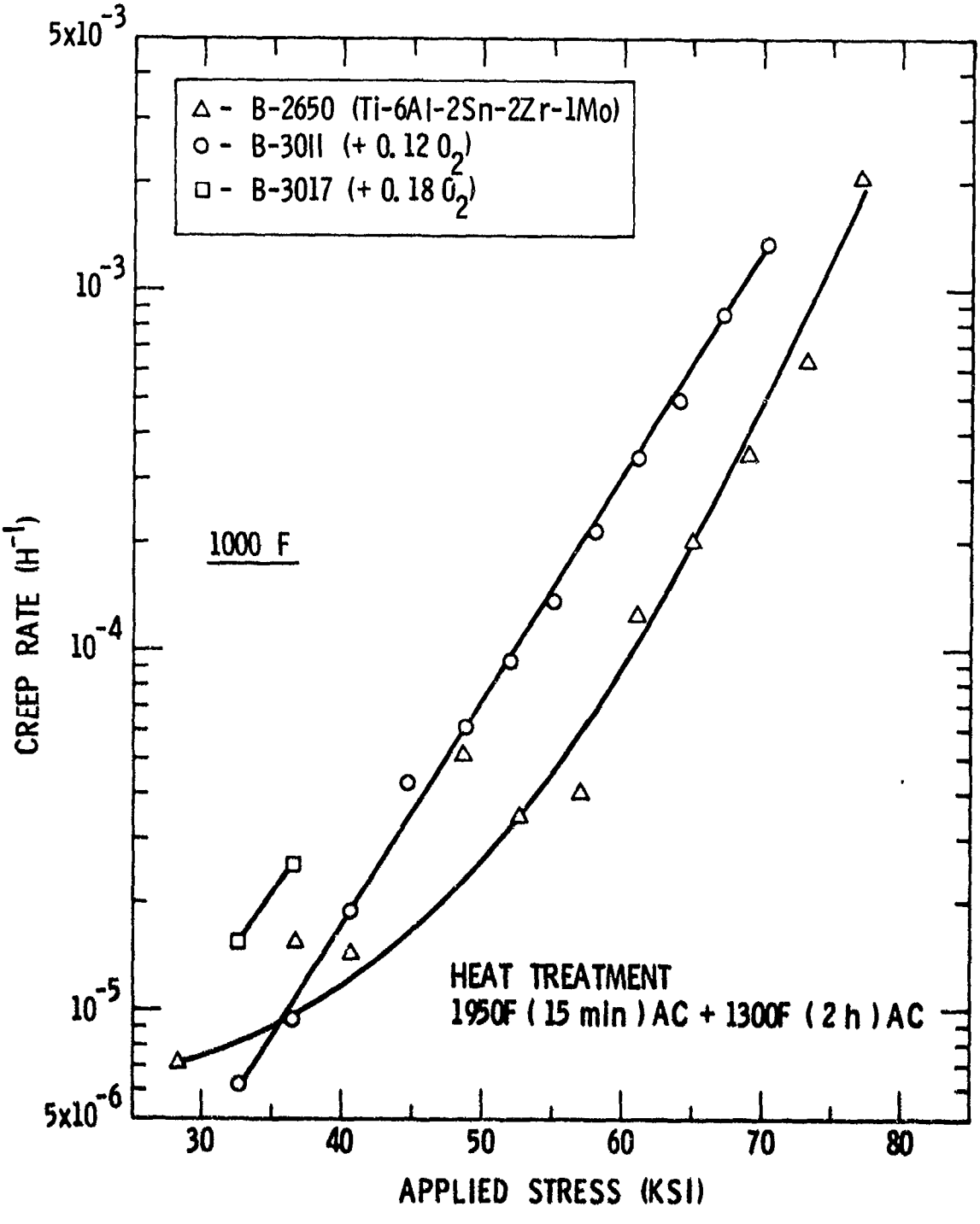

Figure 33 Creep rate as a function of applied stress at 1000F for button melts of composition Ti-6Al-2Sn-2Zr-1Mo with additions of O_2.

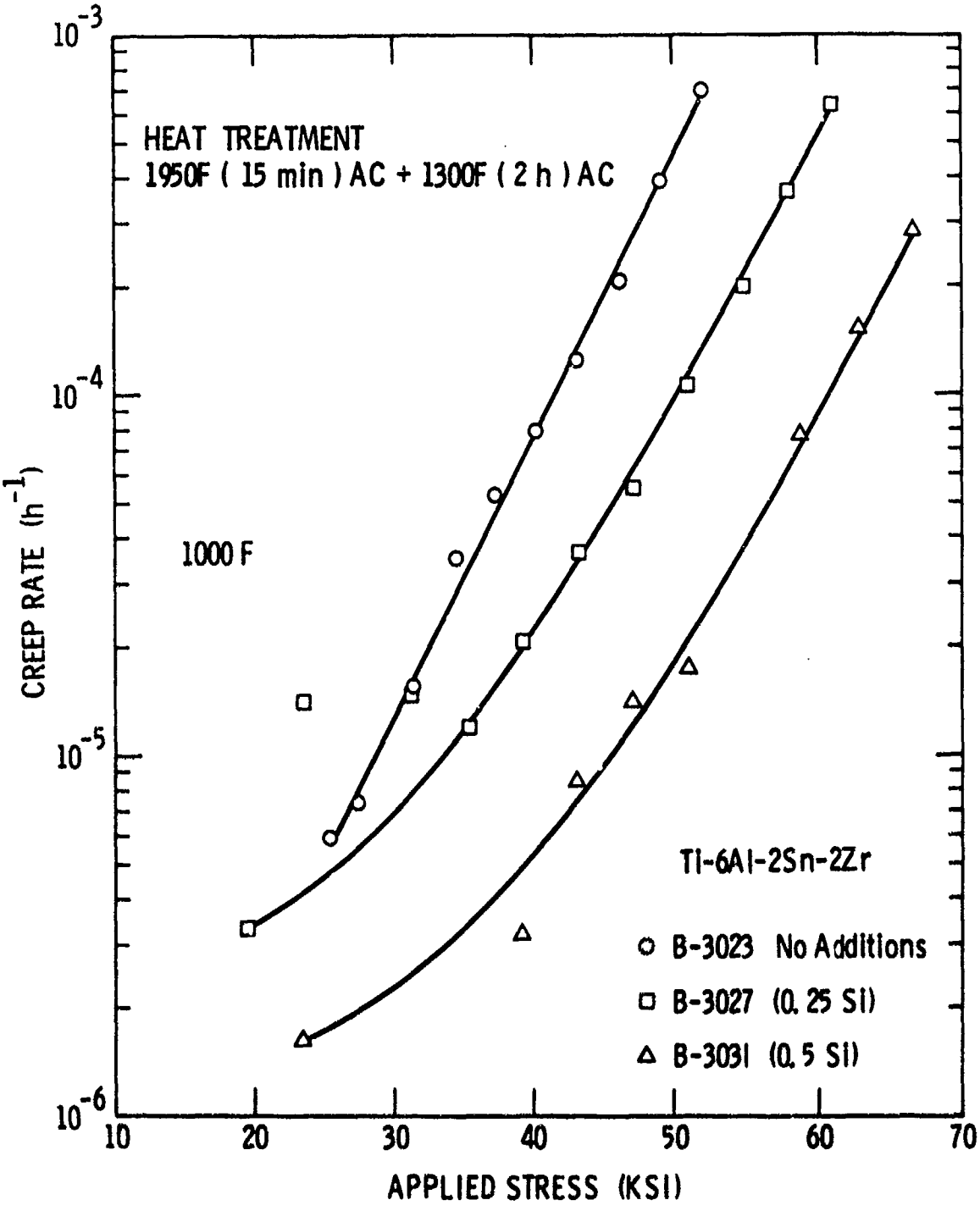

Figure 34 Creep rate as a function of applied stress at 1000F for button melts of composition Ti-6Al-2Sn-2Zr with additions of Si.

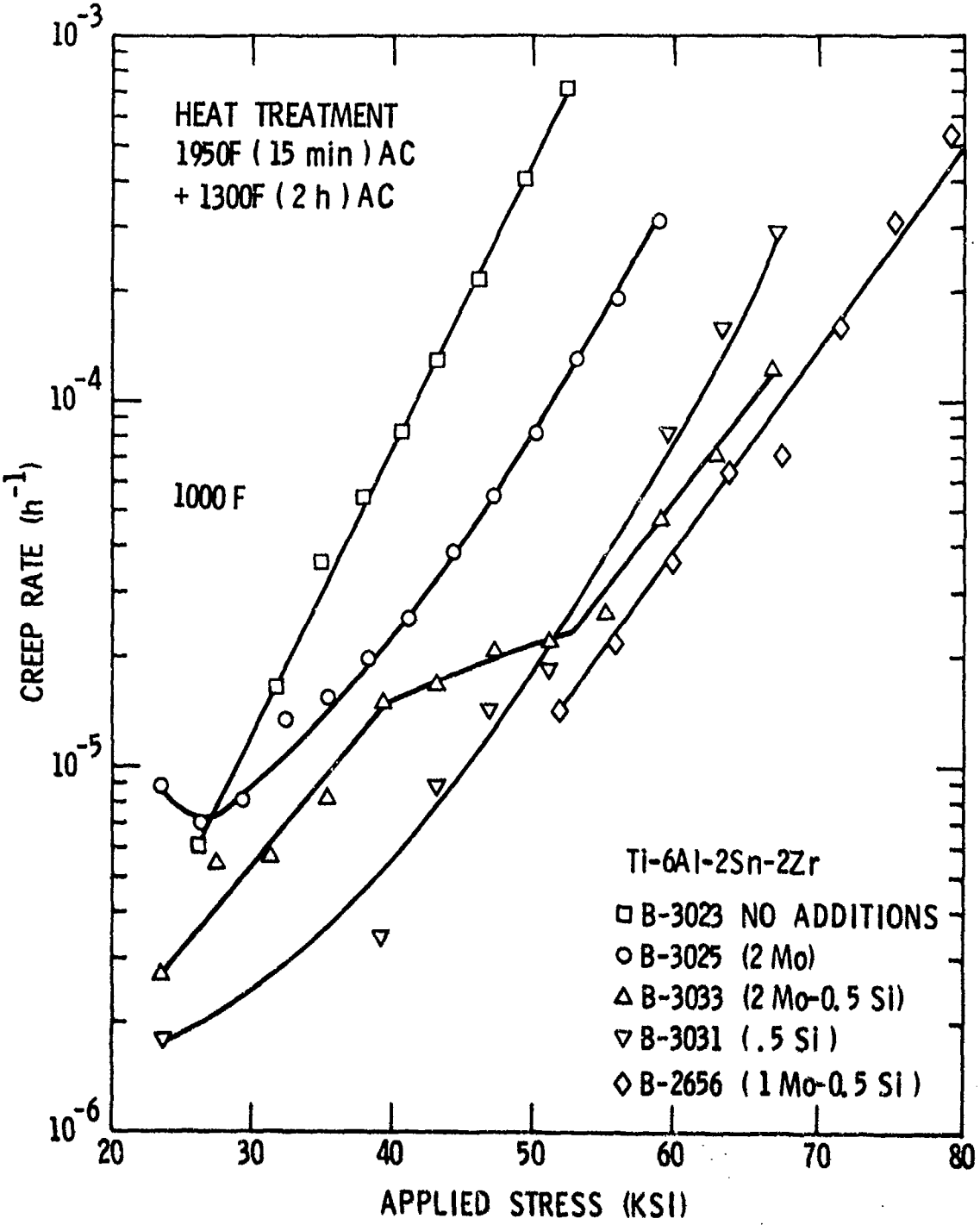

Figure 35 Creep rate as a function of applied stress at 1000F for button melts of composition Ti-6Al-2Sn-2Zr with additions of Mo and Si.

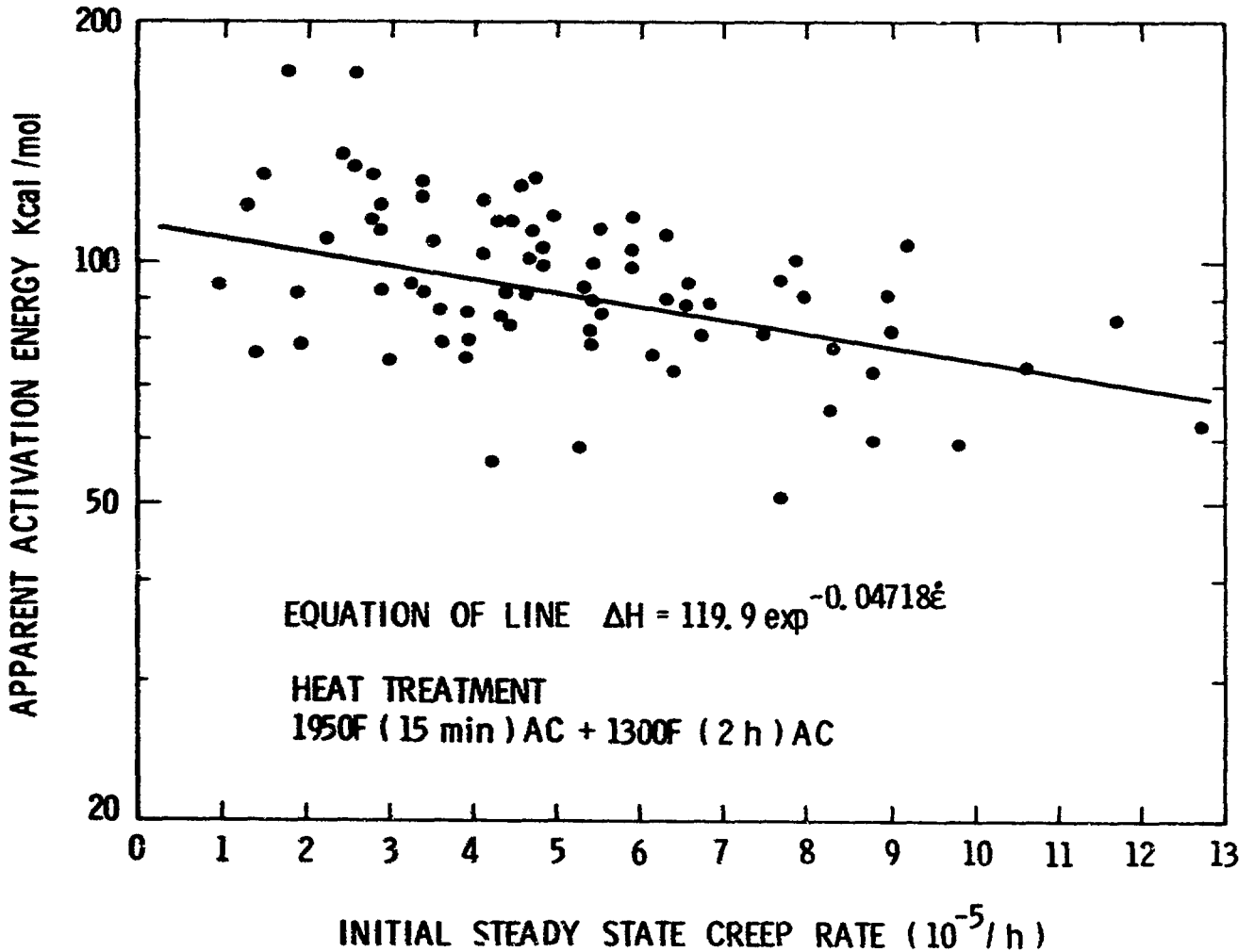

Figure 36 Apparent activation energy versus creep rate for 1000F tests on button melts showing best fit line.

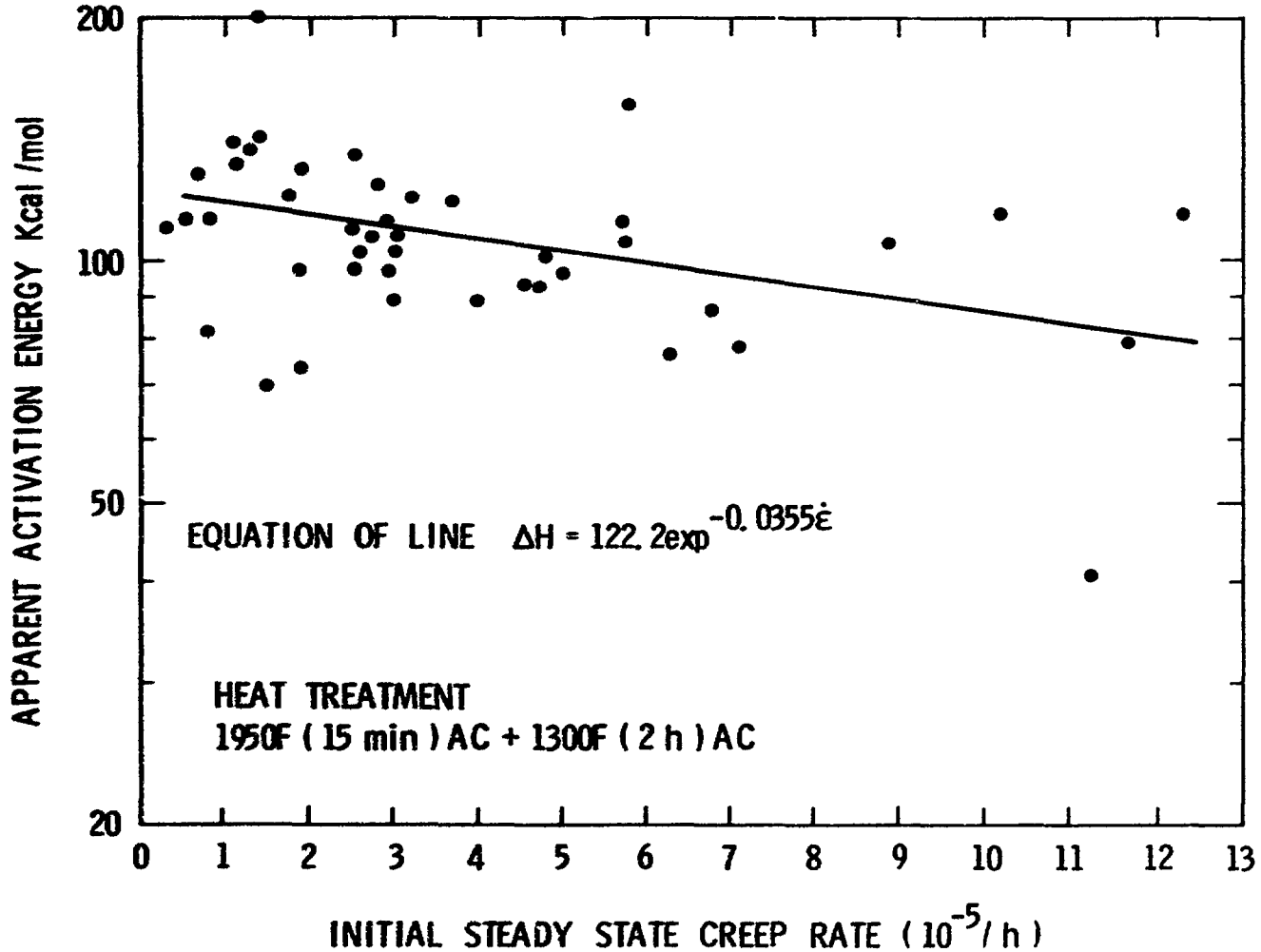

Figure 37 Apparent activation energy versus creep rate for 1100F tests on button melts showing best fit line.

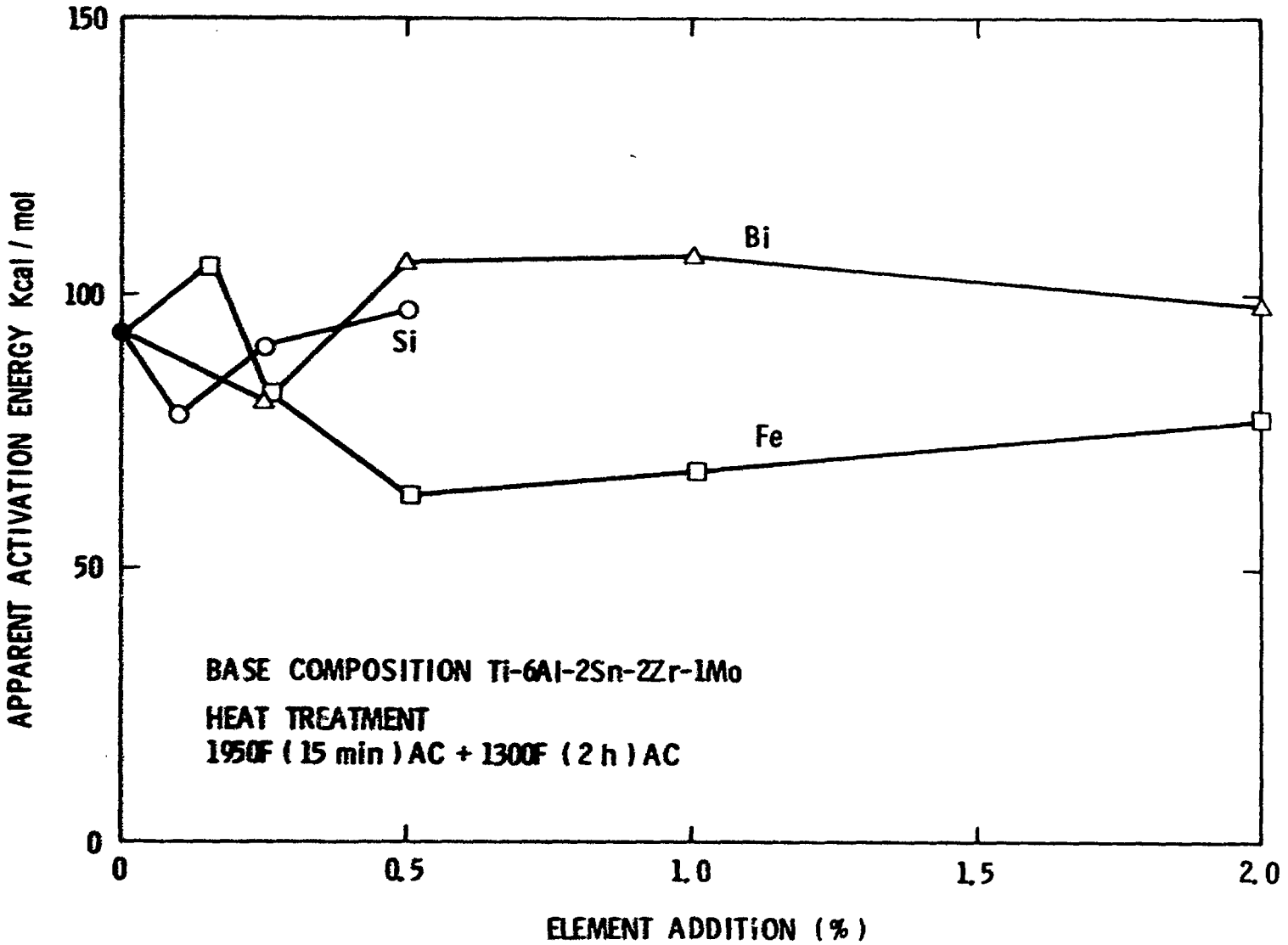

Figure 38 Effects of element additions of Bi, Si and Fe on the apparent activation energy for creep at 1000F in a button melt of base composition Ti-6Al-2Sn-2Zr-1Mo.

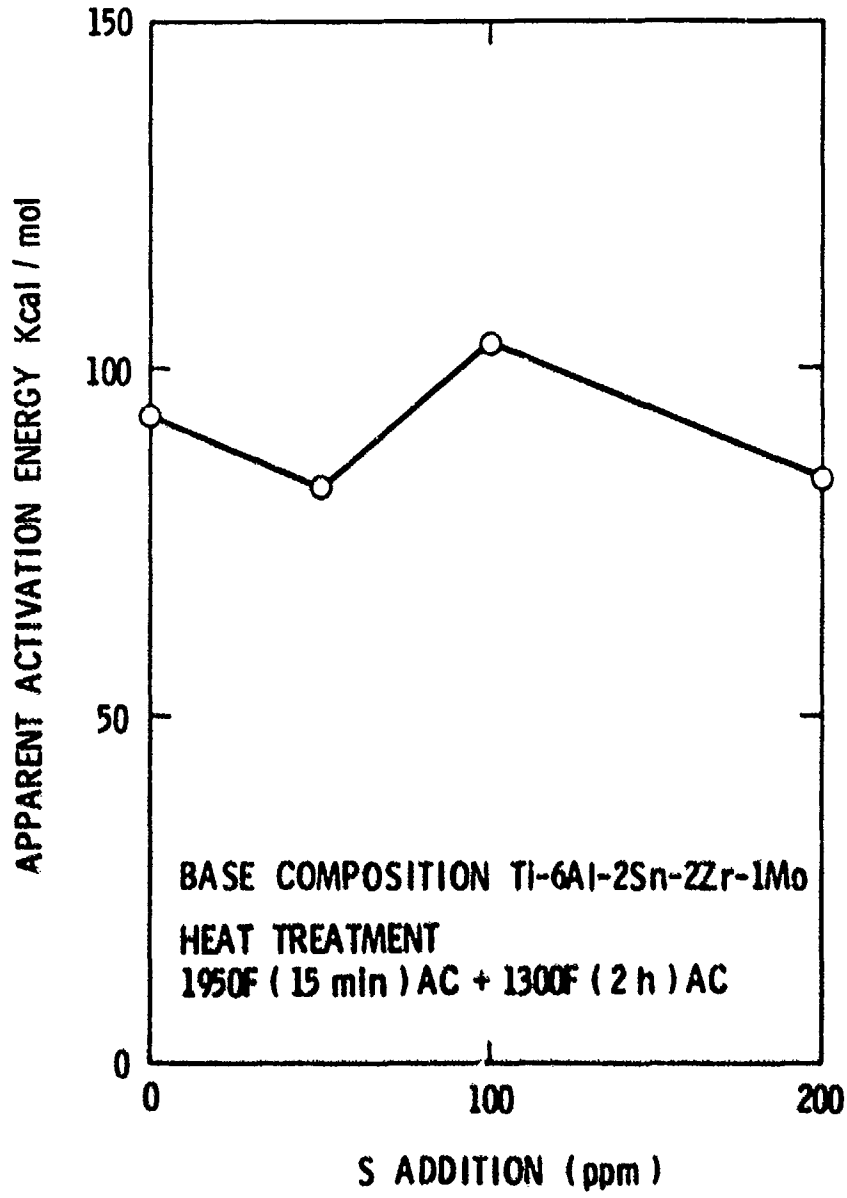

Figure 39 Effects of S additions on the apparent activation energy for creep at 1000F in a button melt of base composition Ti-6Al-2Sn-2Zr-1Mo.

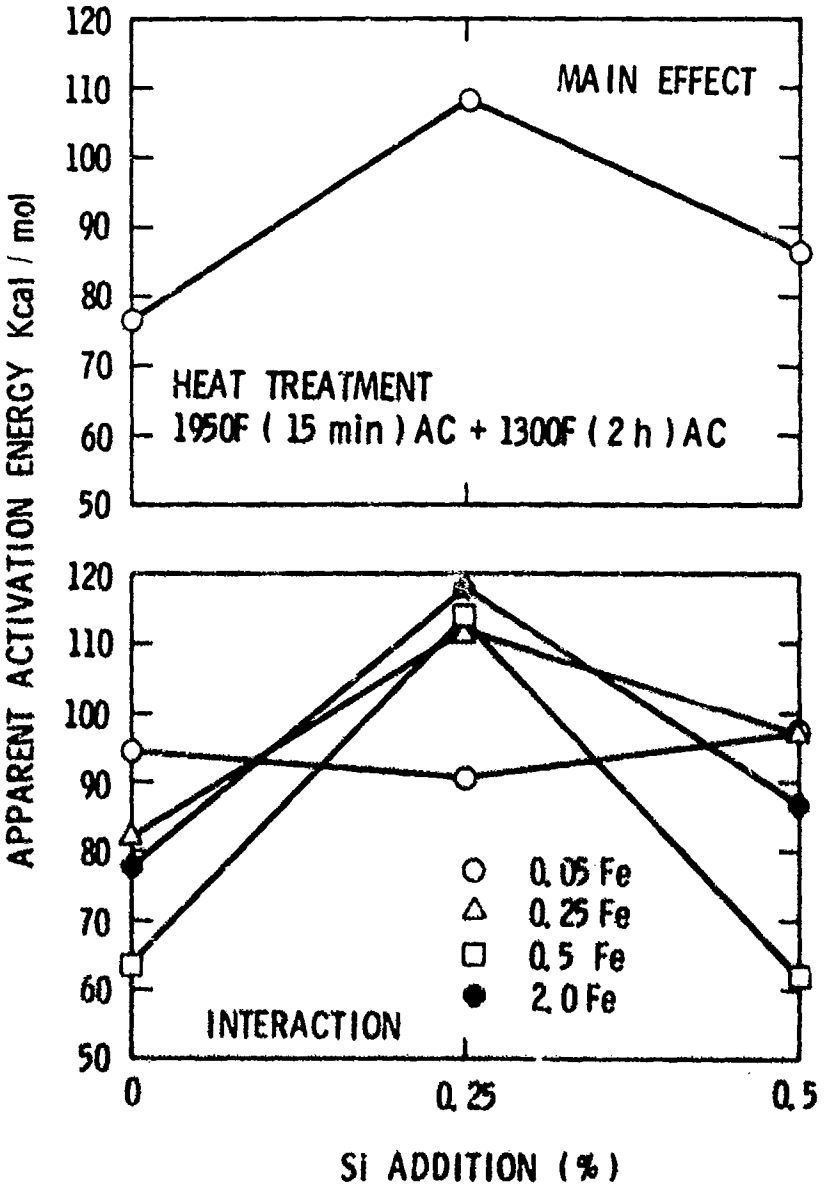

Figure 40 Statistically significant effects due to additions of Fe and Si on apparent activation energy for creep at 1000F in a button melt of base composition Ti-6Al-2Sn-2Zr-1Mo.

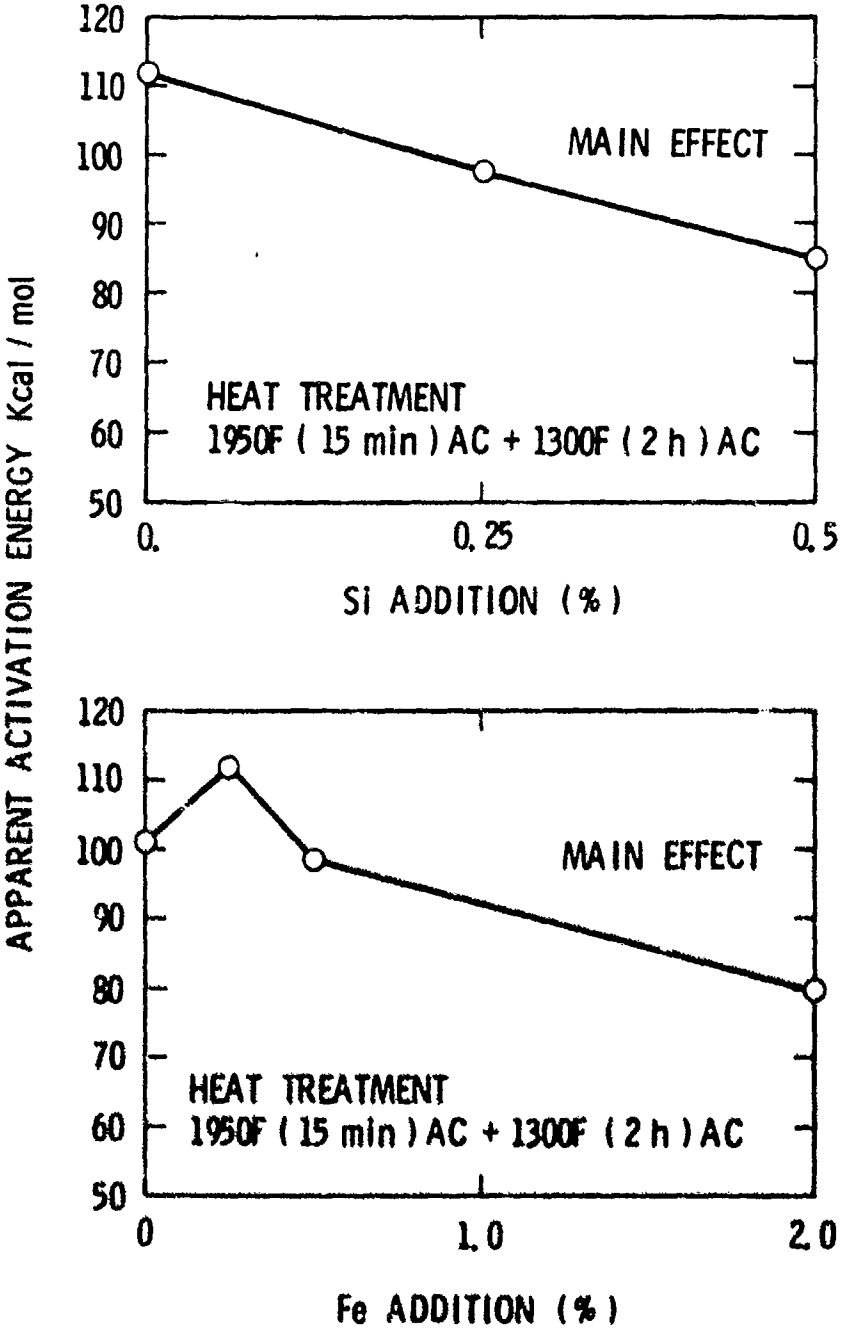

Figure 41 Statistically significant effects due to additions of Fe + Si on apparent activation energy for creep at 1100F in a button melt of base composition Ti-6Al-2Sn-2Zr-1Mo.

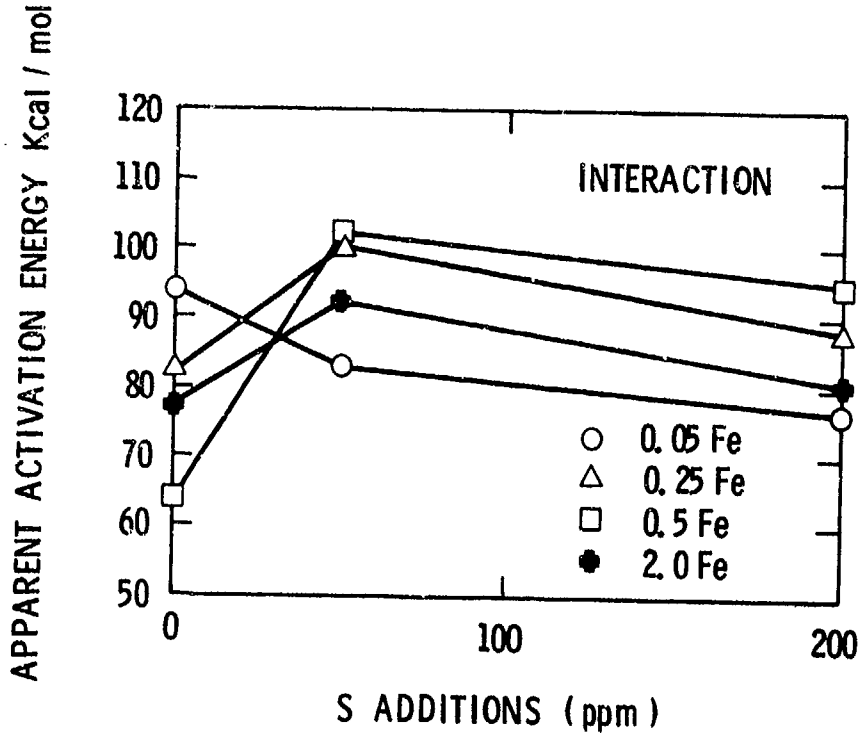

Figure 42 Statistically significant effects due to additions of Fe + S on apparent activation energy for creep at 1000F in a button melt of base composition Ti-6Al-2Sn-2Zr-1Mo.

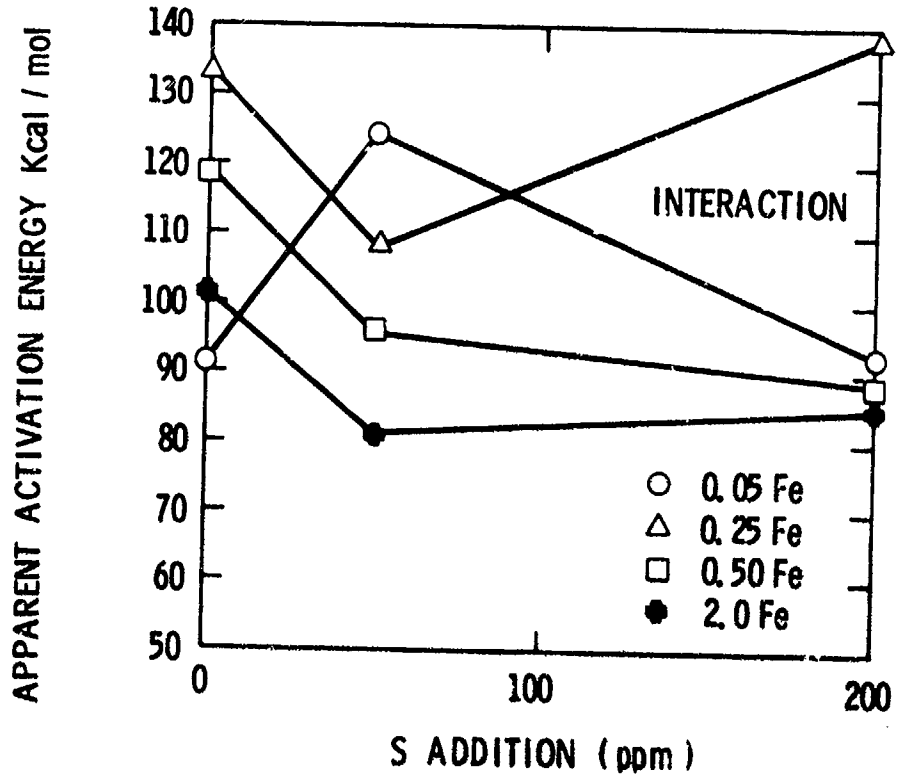

Figure 43 Statistically significant effects due to additions of Fe + S on apparent activation energy for creep at 1100F in a button melt of base composition Ti-6Al-2Sn-2Zr-1Mo.

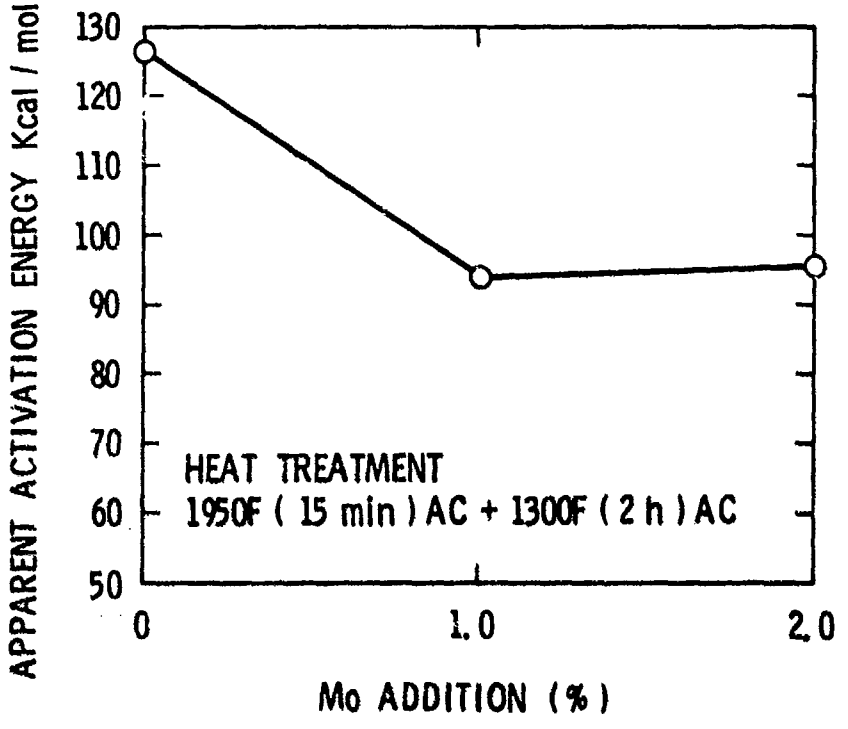

Figure 44 Scatistically significant effects due to additions of Mo + Si on apparent activation energy for creep at 1000F in a button melt of base composition Ti-6Al-2Sn-2Zr-1Mo.

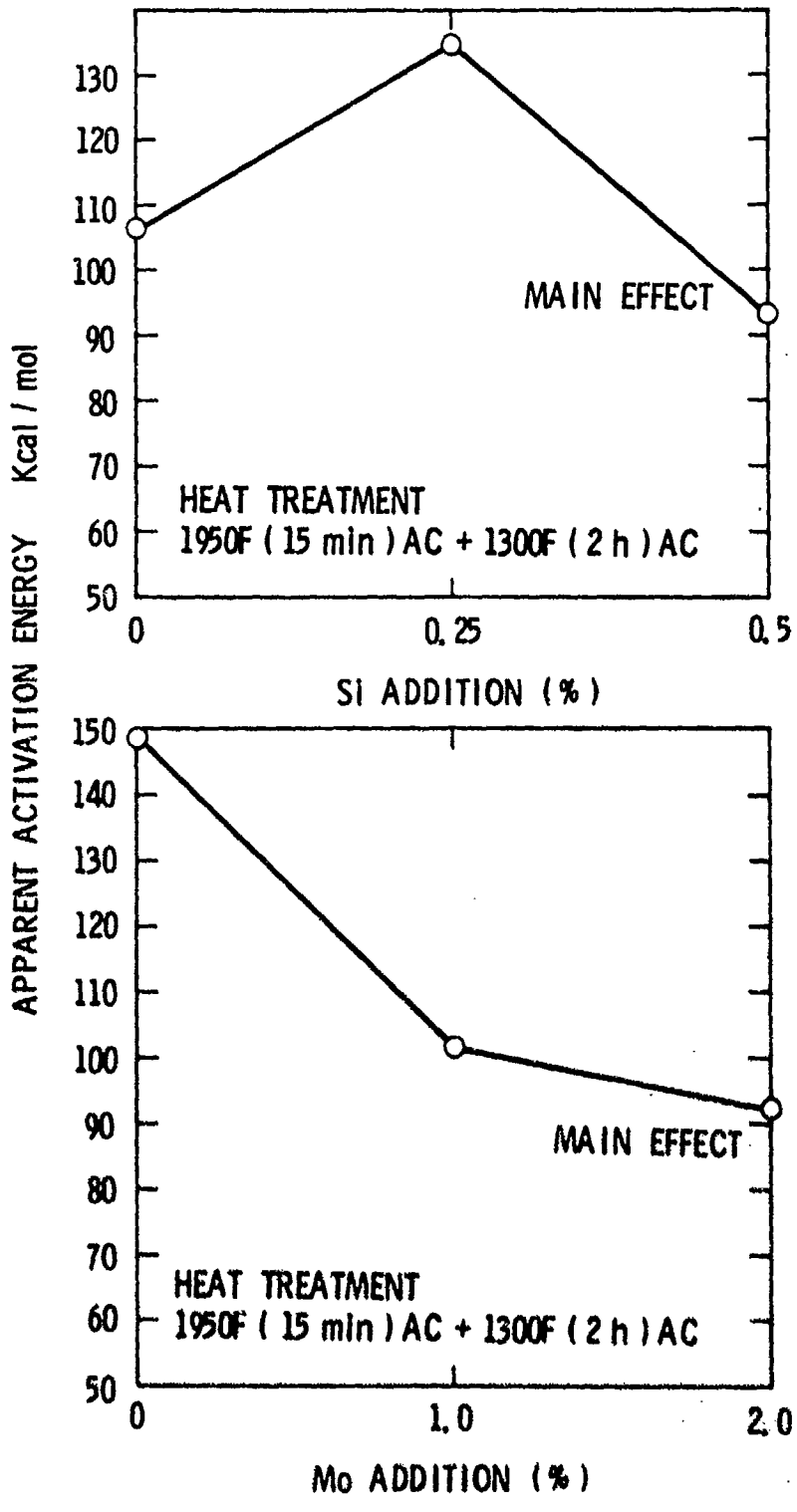

Figure 45 Statistically significant effects due to additions of Mo + Si on apparent activation energy for creep at 1100F in a button melt of base composition Ti-6Al-2Sn-2Zr-1Mo.

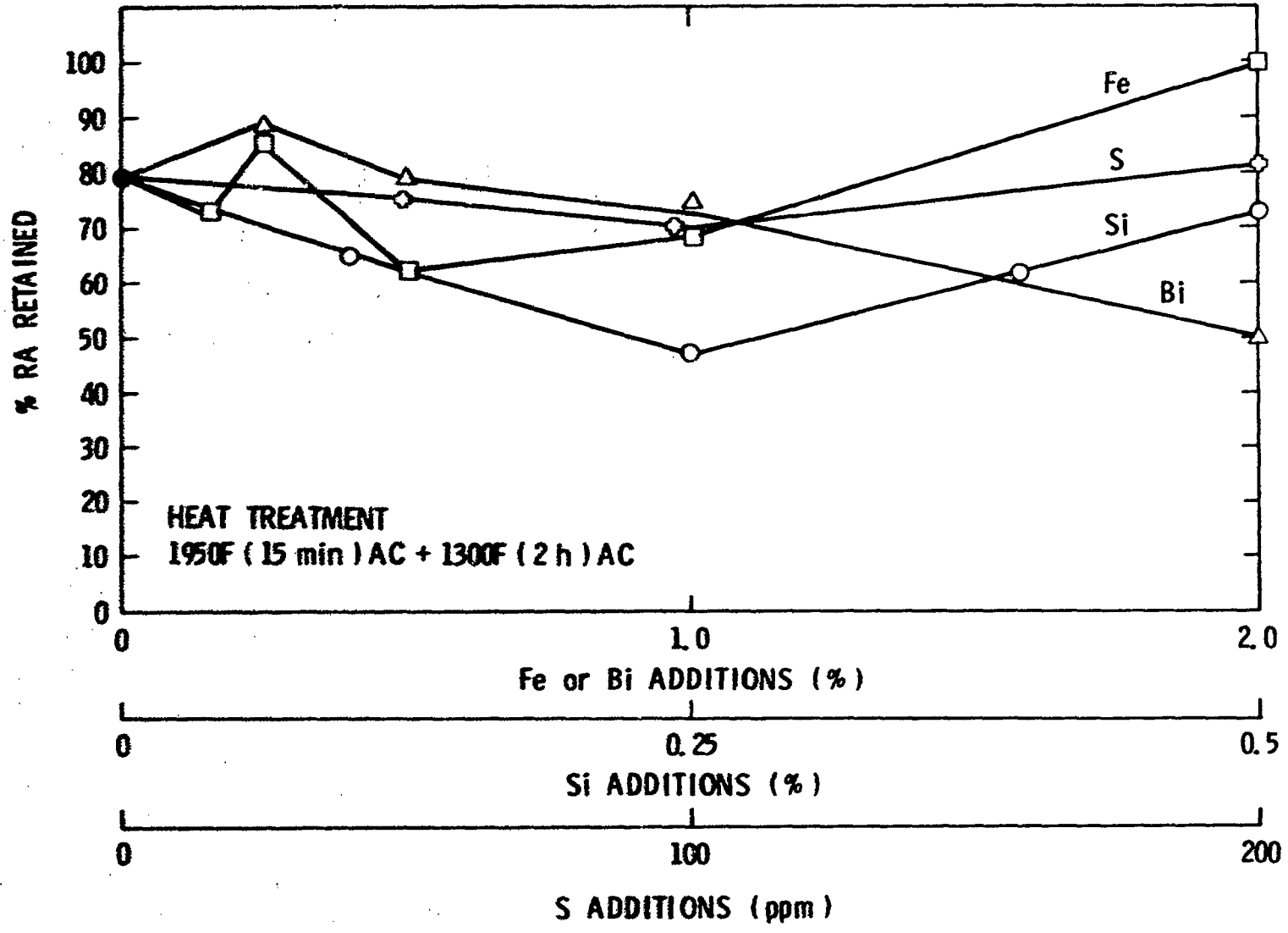

Figure 46 Percent reduction in area retained after creep exposure at 1000F for single alloy additions of Si, Bi, Fe and S to button melts of composition Ti-6Al-2Sn-2Zr-1Mo.

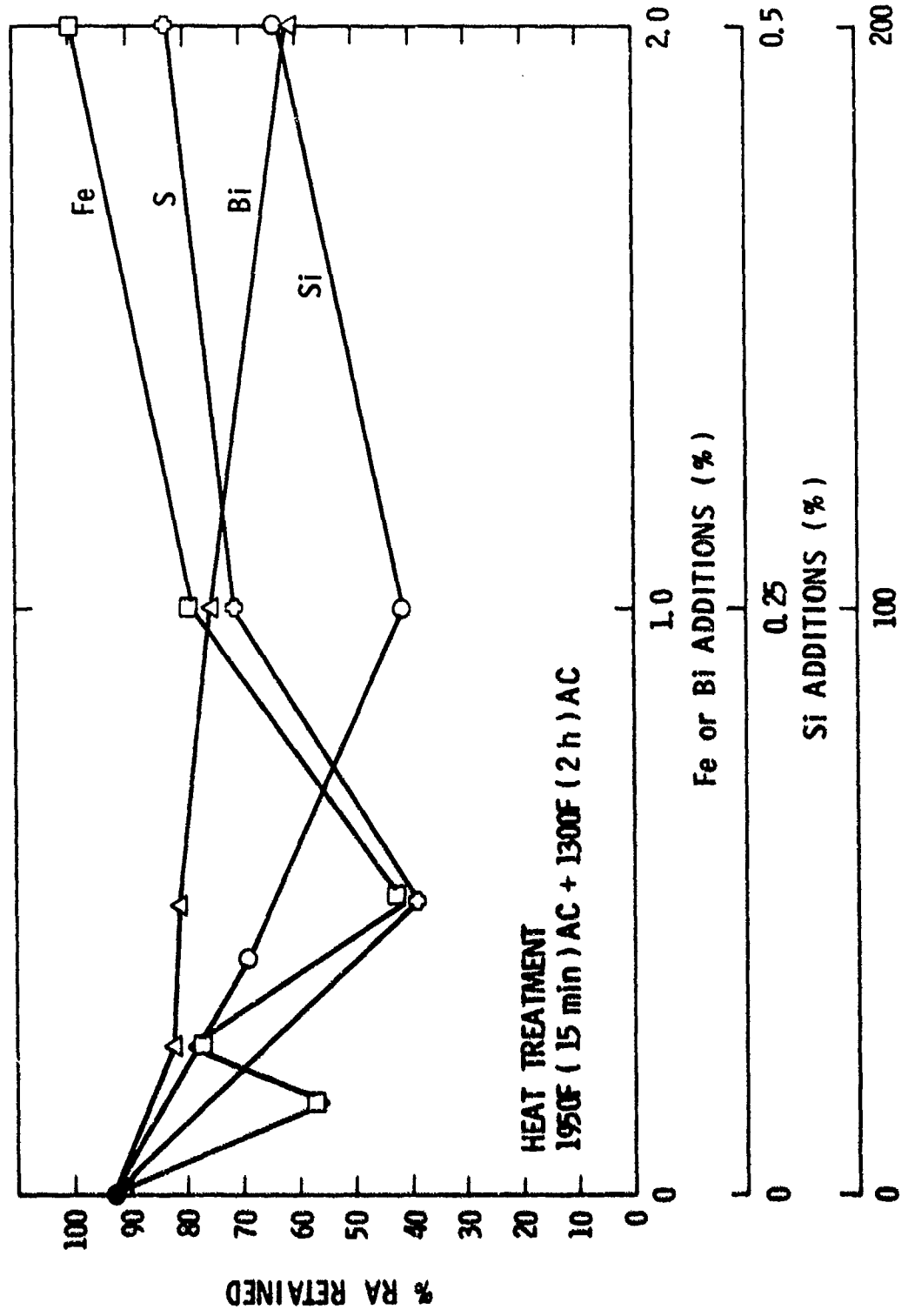

Figure 47 Percent reduction in area retained after creep exposure at 1100F for single alloy additions of Si, Bi, Fe and S to button melts of composition Ti-6Al-2Sn-2Zr-1Mo.

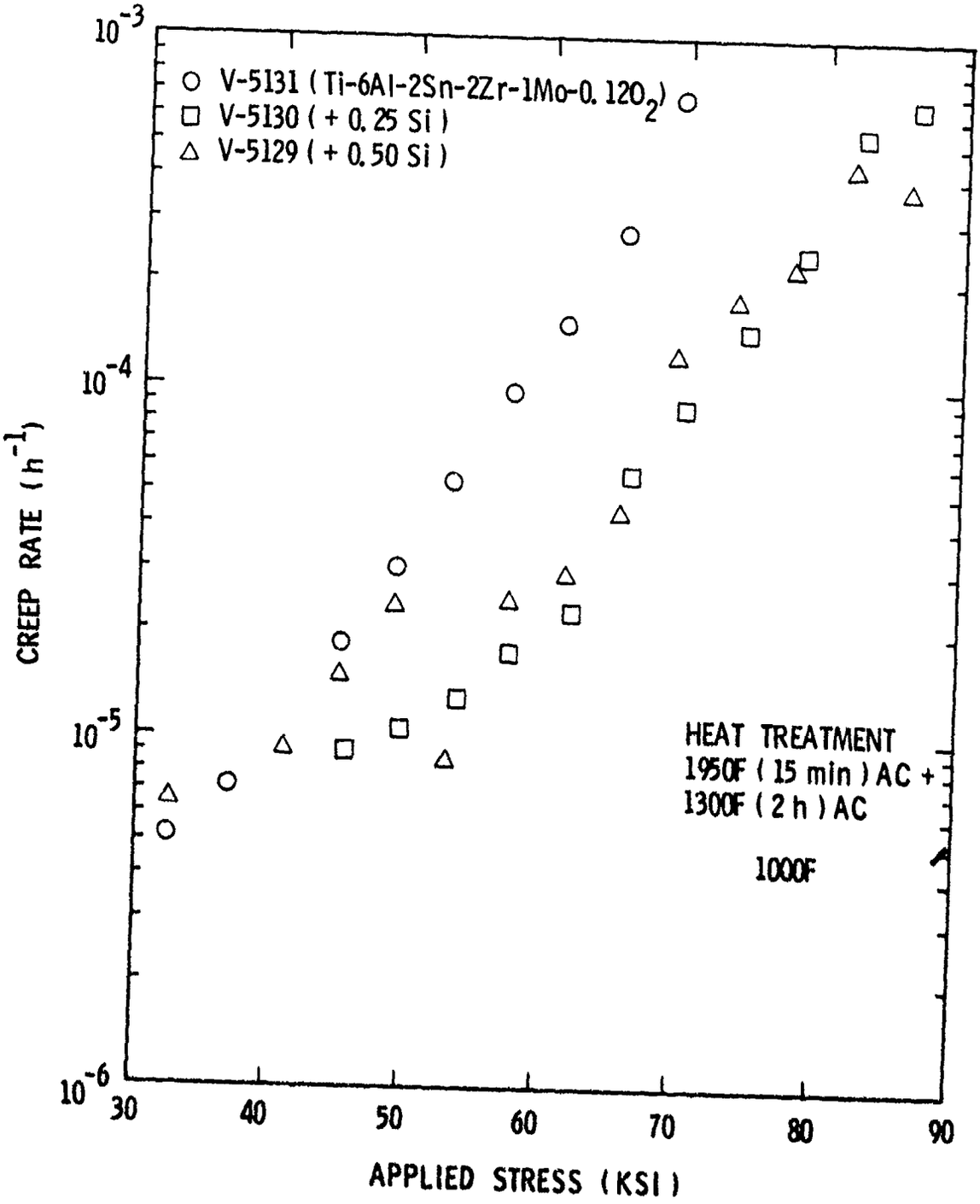

Figure 48 Creep rate at 1000F as a function of applied stress for 100 lb. ingot materials of composition Ti-6Al-2Sn-2Zr-1Mo-.12 O_2 with additions of Si.

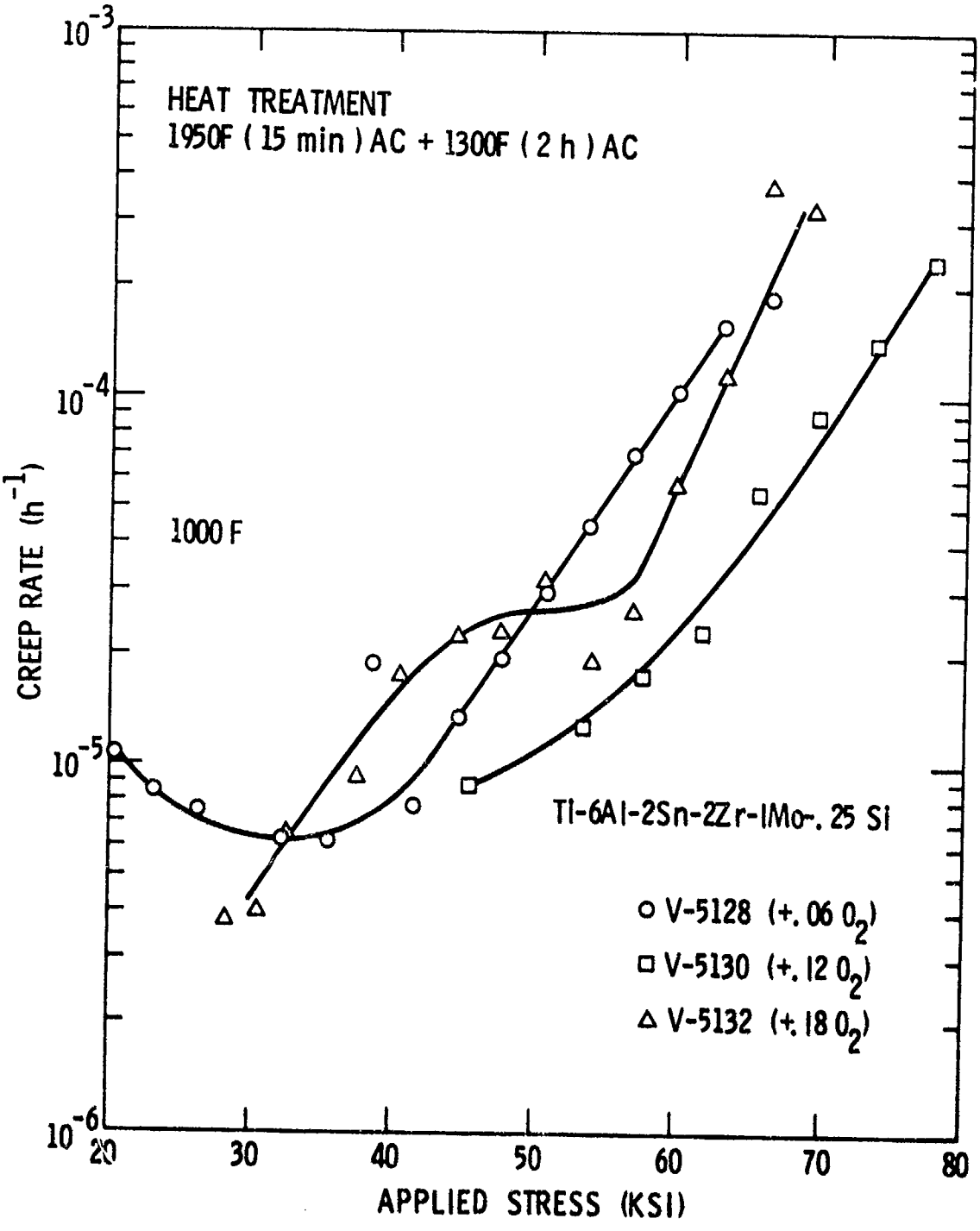

Figure 49 Creep rate at 1000F as a function of applied stress for 100 lb. ingot materials of composition Ti-6Al-2Sn-2Zr-1Mo-.25Si with additions of O_2.

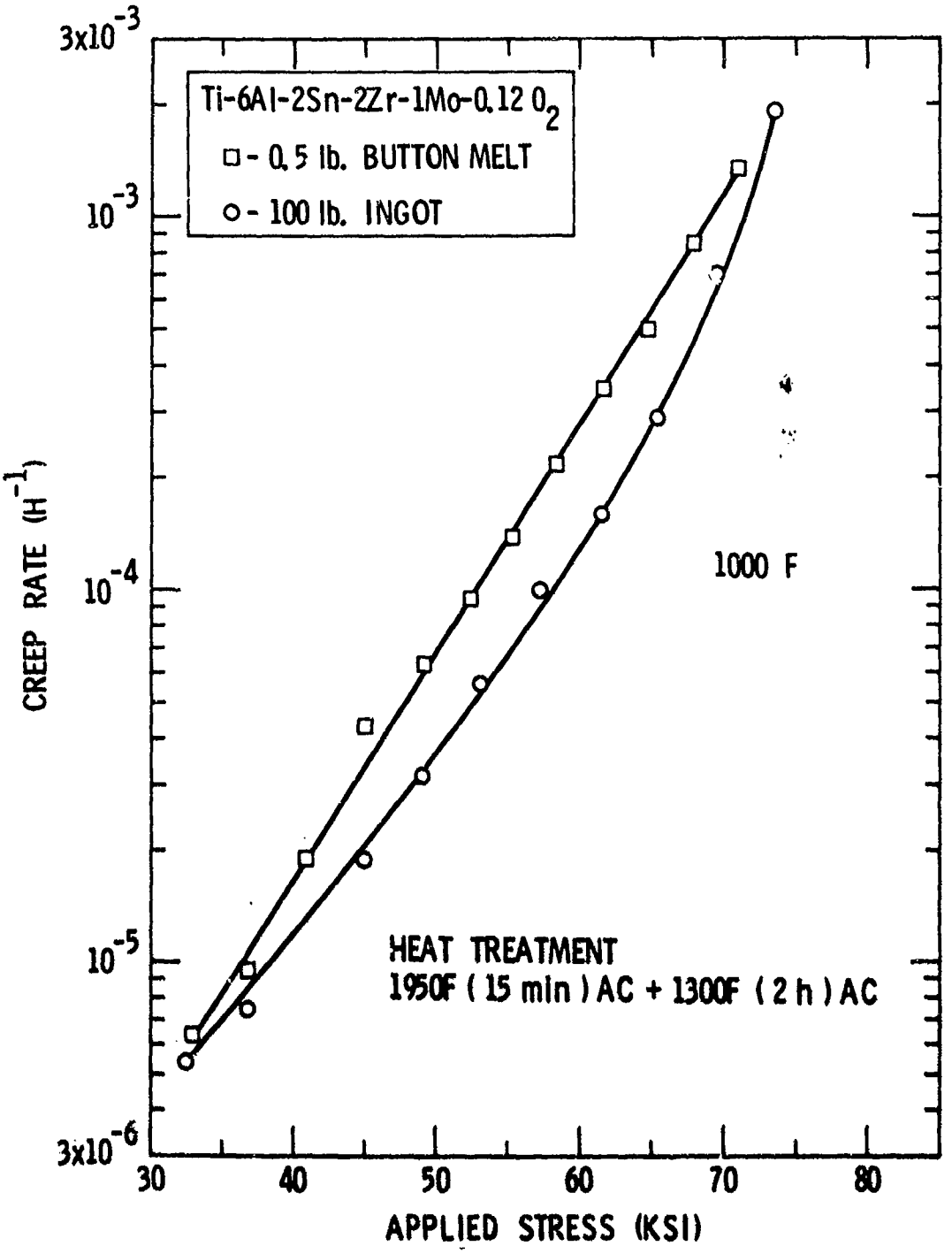

Figure 50 Comparison of creep rates at 1000F for a button melt and ingot material of composition Ti-6Al-2Sn-2Zr-1Mo-0.12 O_2.

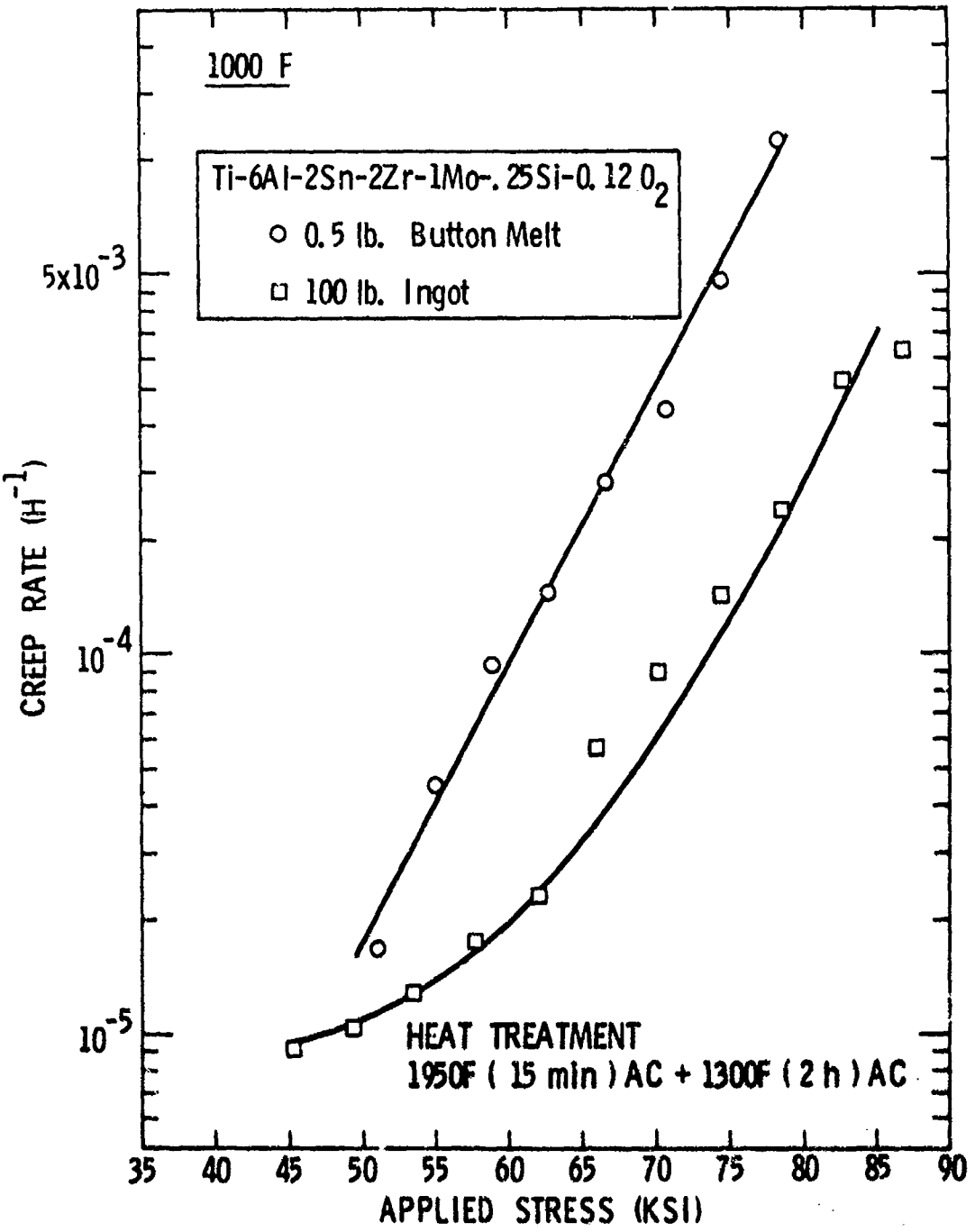

Figure 51 Comparison of creep rates at 1000F for a button melt and ingot material of composition Ti-6Al-2Sn-2Zr-1Mo-.25Si-0.12 O_2.

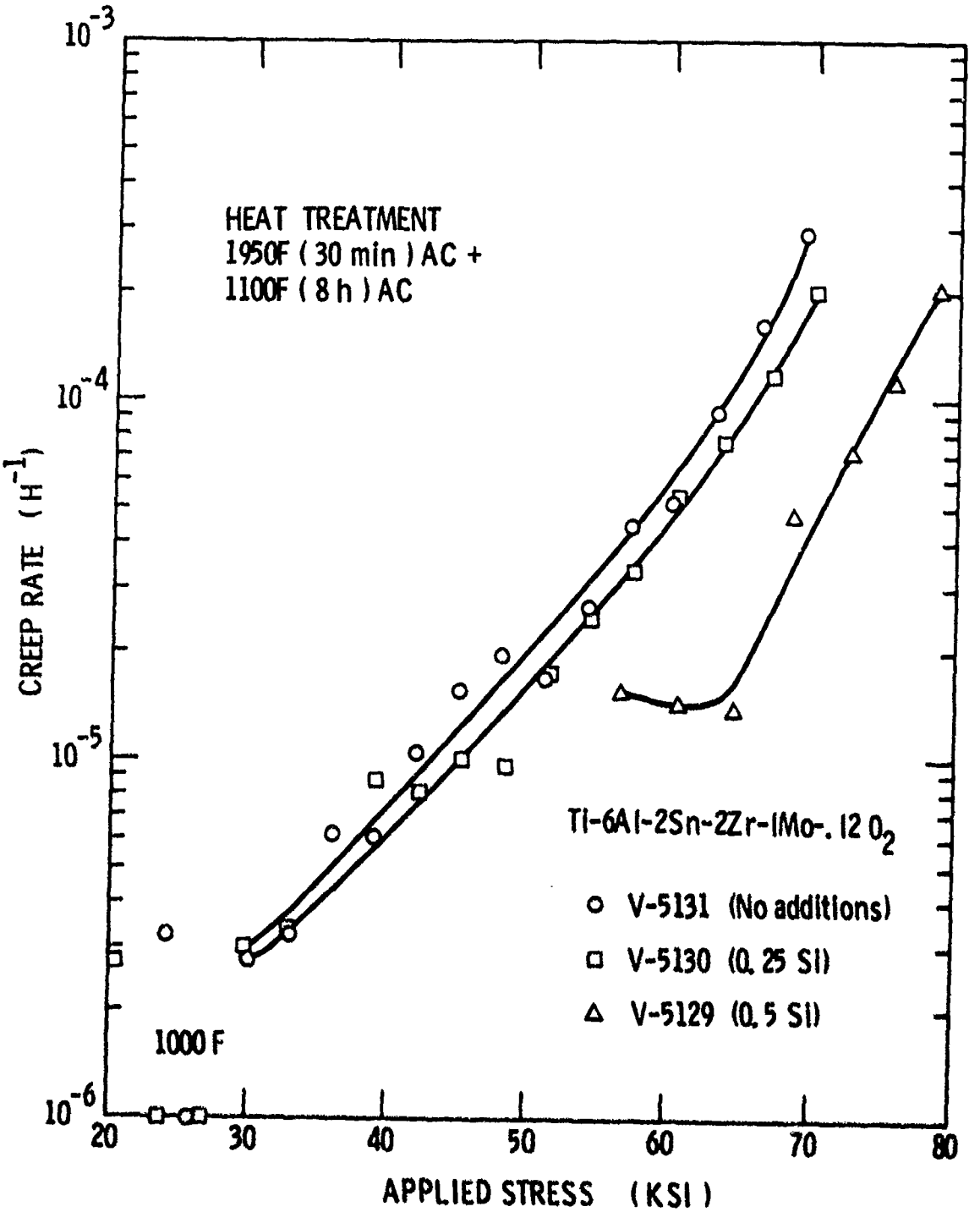

Figure 52 Creep rate at 1000F as a function of applied stress for 100 lb. ingot materials of composition Ti-6Al-2Sn-2Zr-1Mo-.12 O_2 with additions of Si and stabilized at 1100F/8 hrs.

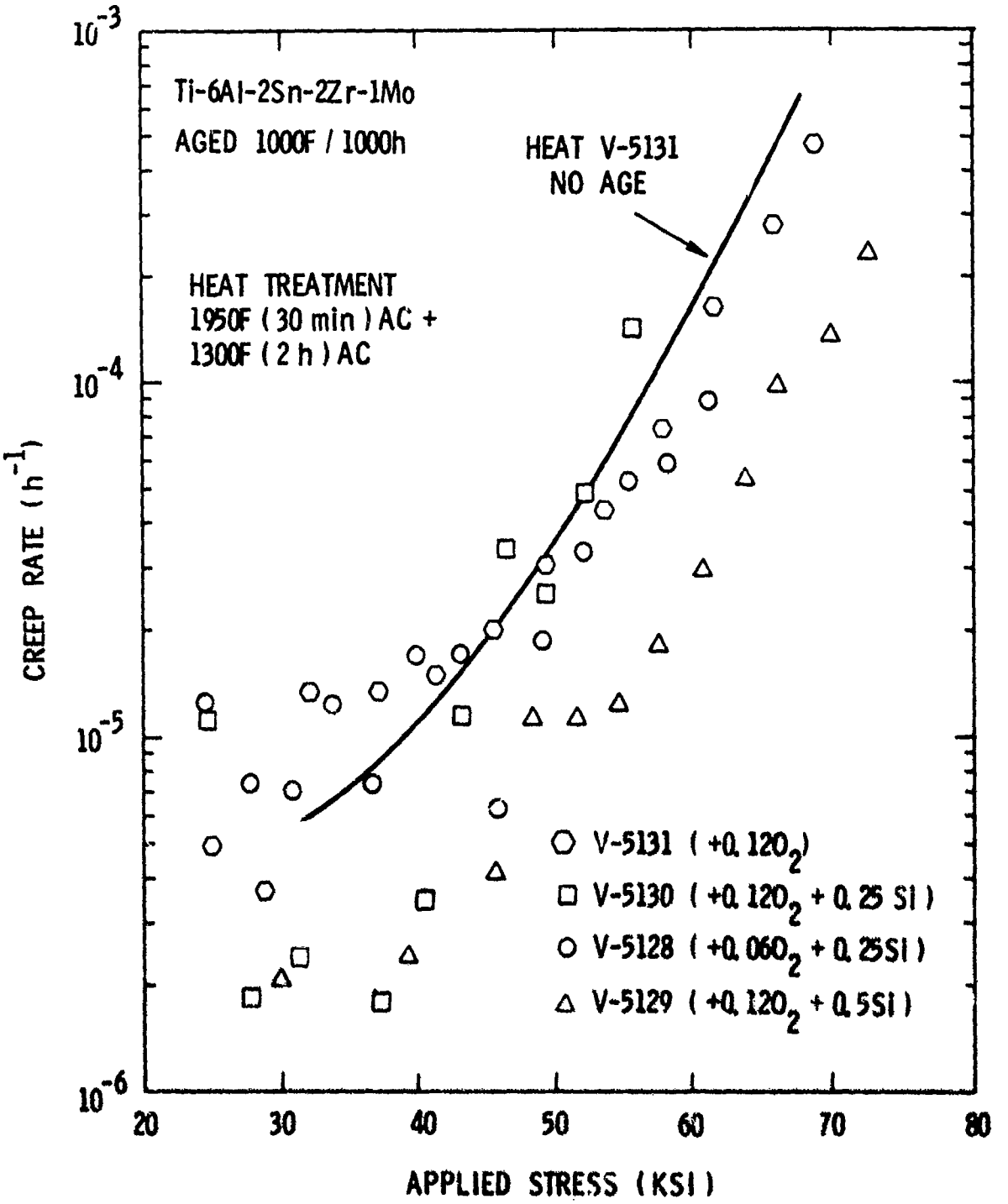

Figure 53 Creep rate at 1000F as a function of applied stress for 100 lb. ingot materials of base composition Ti-6Al-2Sn-2Zr-1Mo with additions of Si and O_2 following an age for 100h at 1000F.

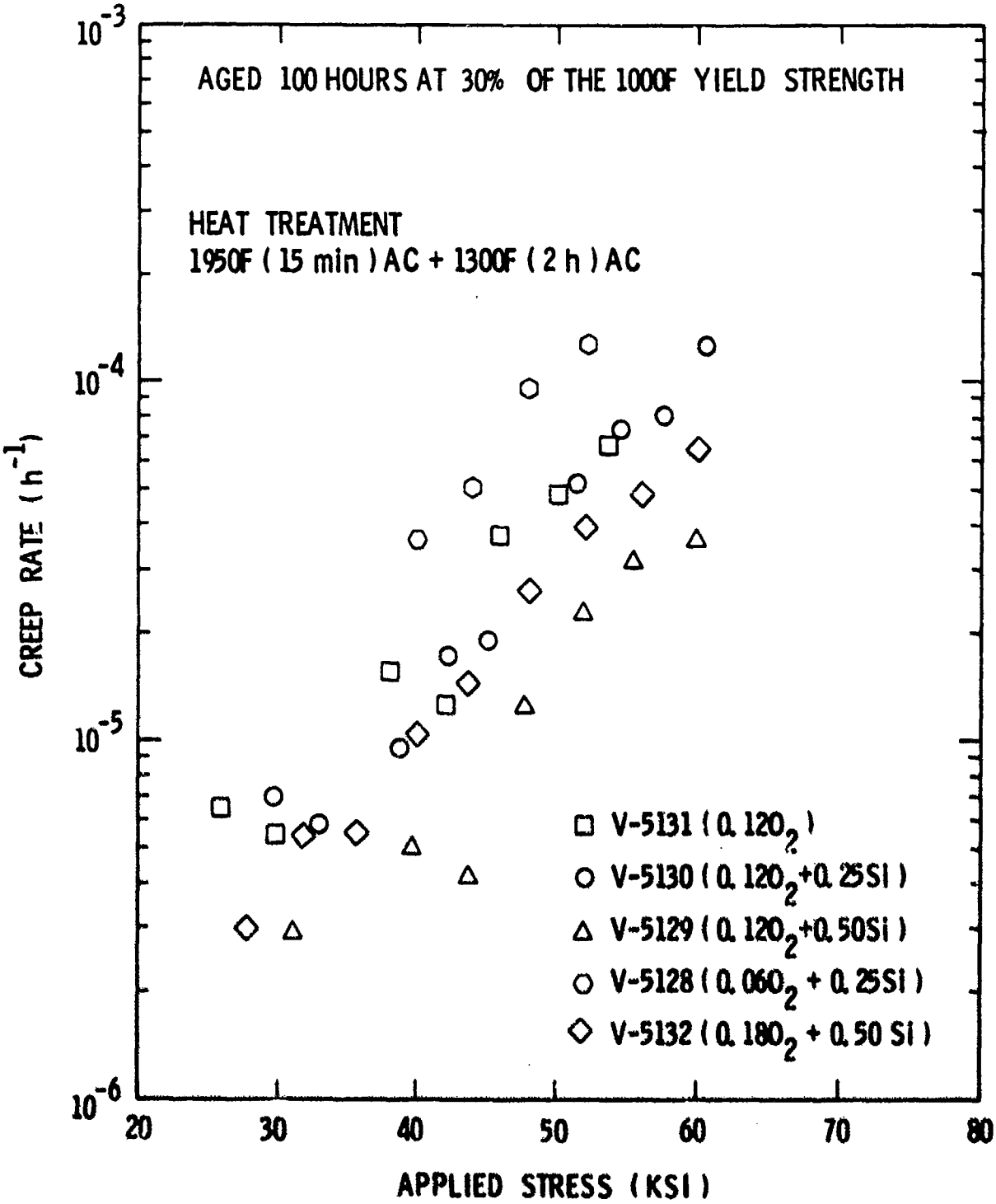

Figure 54 Creep rate at 1000F as a function of applied stress for 100 lb. ingot materials of base composition Ti-6Al-2Sn-2Zr-1Mo with additions of Si and O_2 following an age at a stress equal to 30% of the 1000F yield strength for 100 h at 1000F.

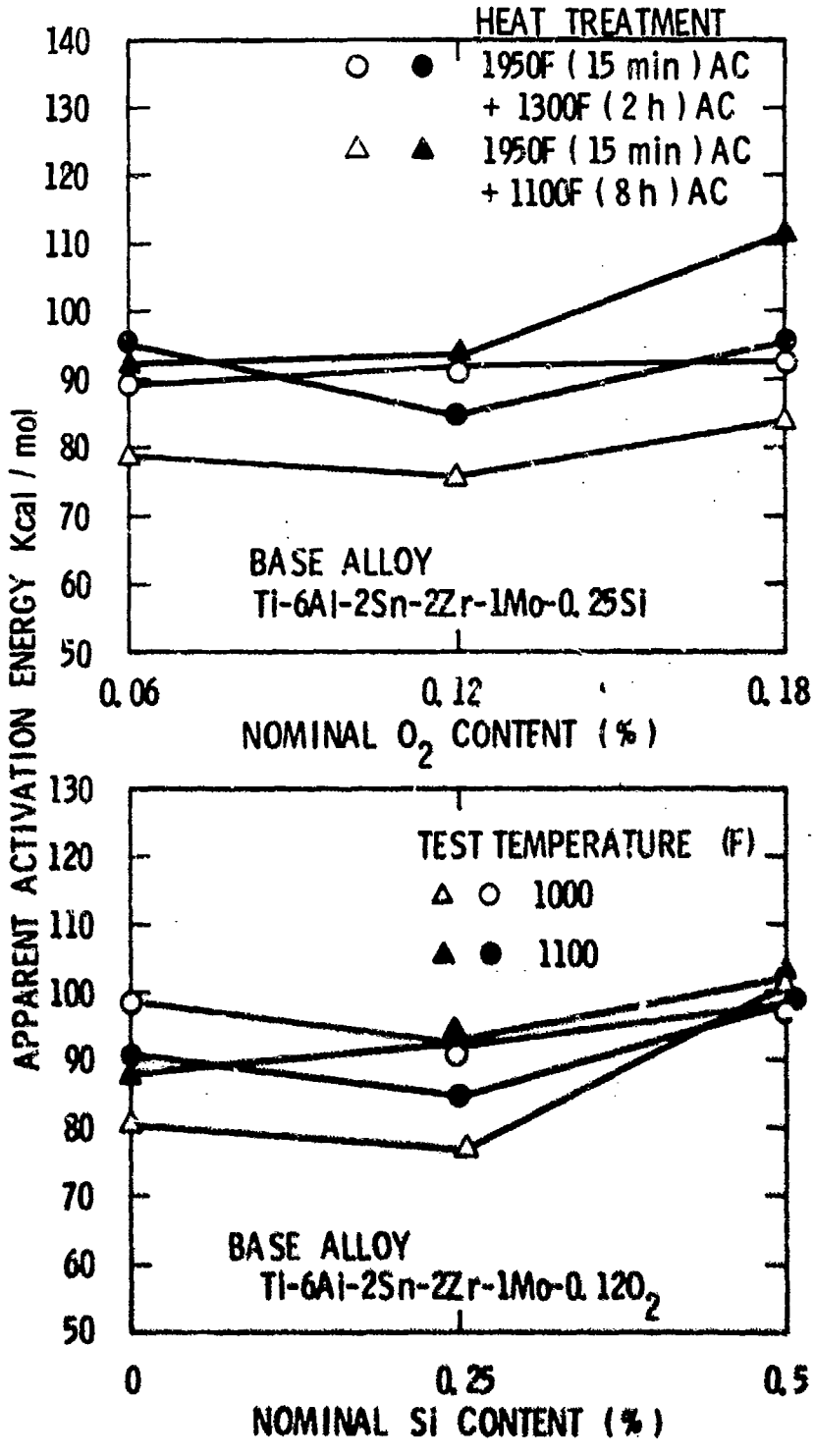

Figure 55 Effects of Si and O_2 content and heat treatment on apparent activation energy for creep at 1000F and 1100F in 100 lb. ingot materials.

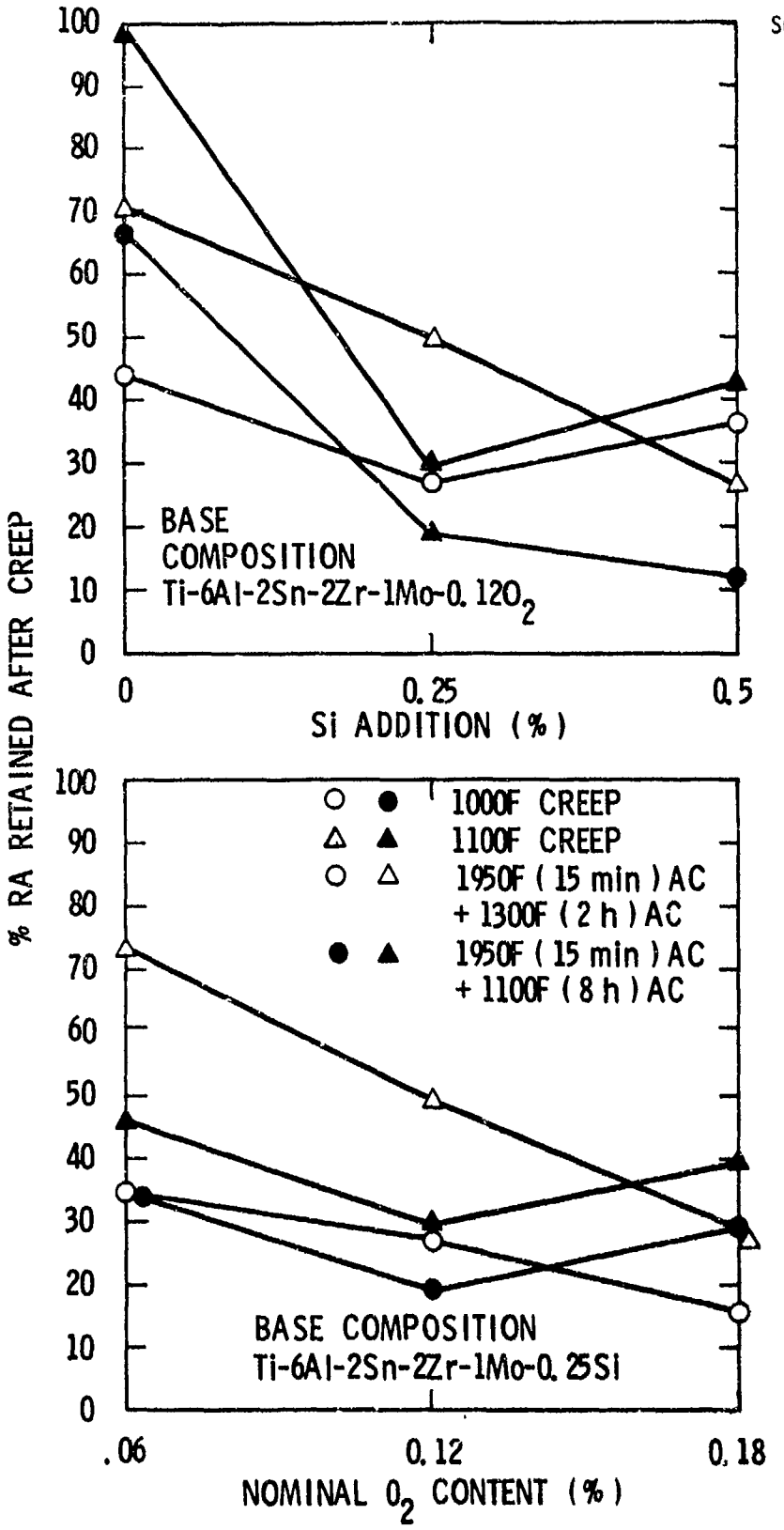

Figure 56 Percent retained ductility (RA) after creep exposure for 100 lb. ingot materials.

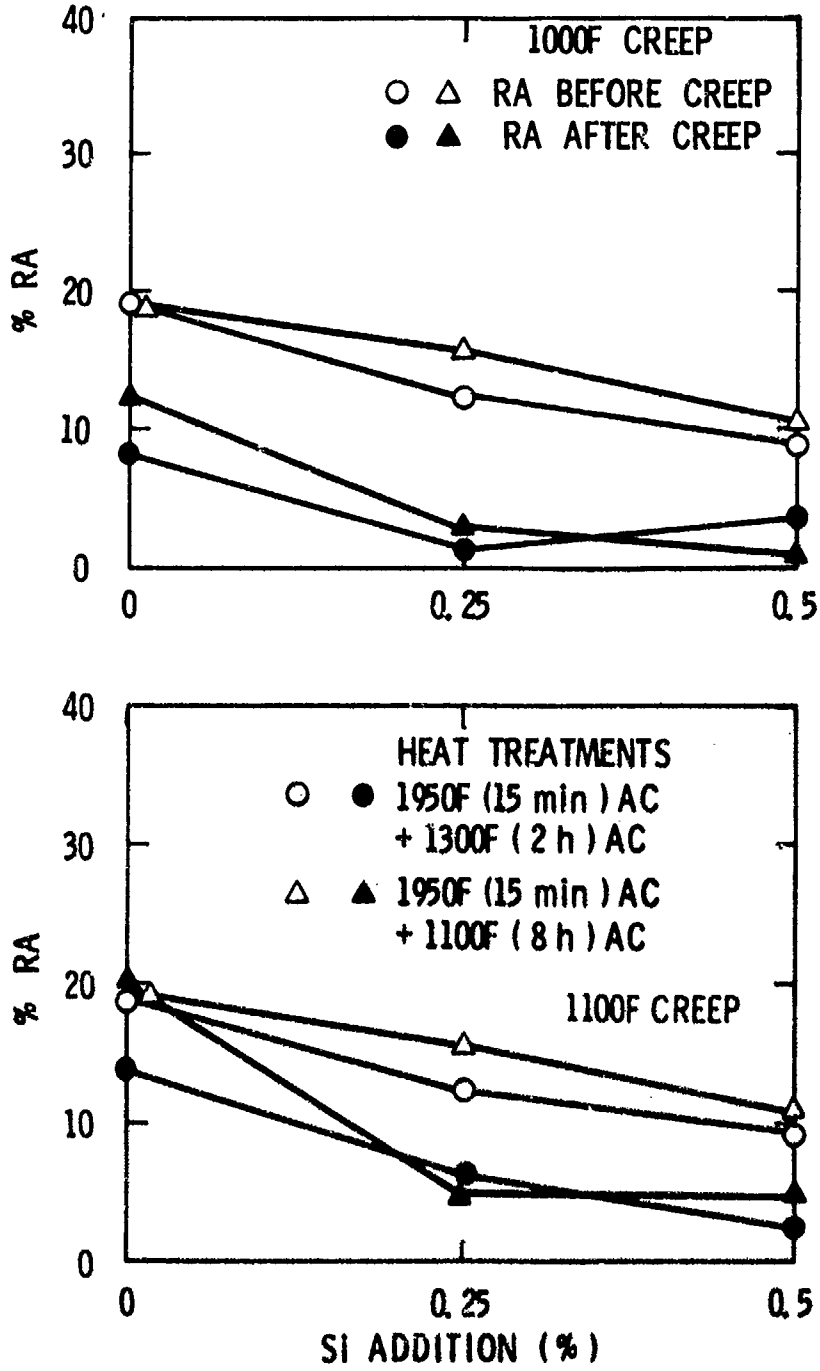

Figure 57 Effects of creep exposure on ductility (RA) of 100 lb. ingot materials of base composition Ti-6Al-2Sn-2Zr-1Mo-0.12 O_2 with additions of Si.

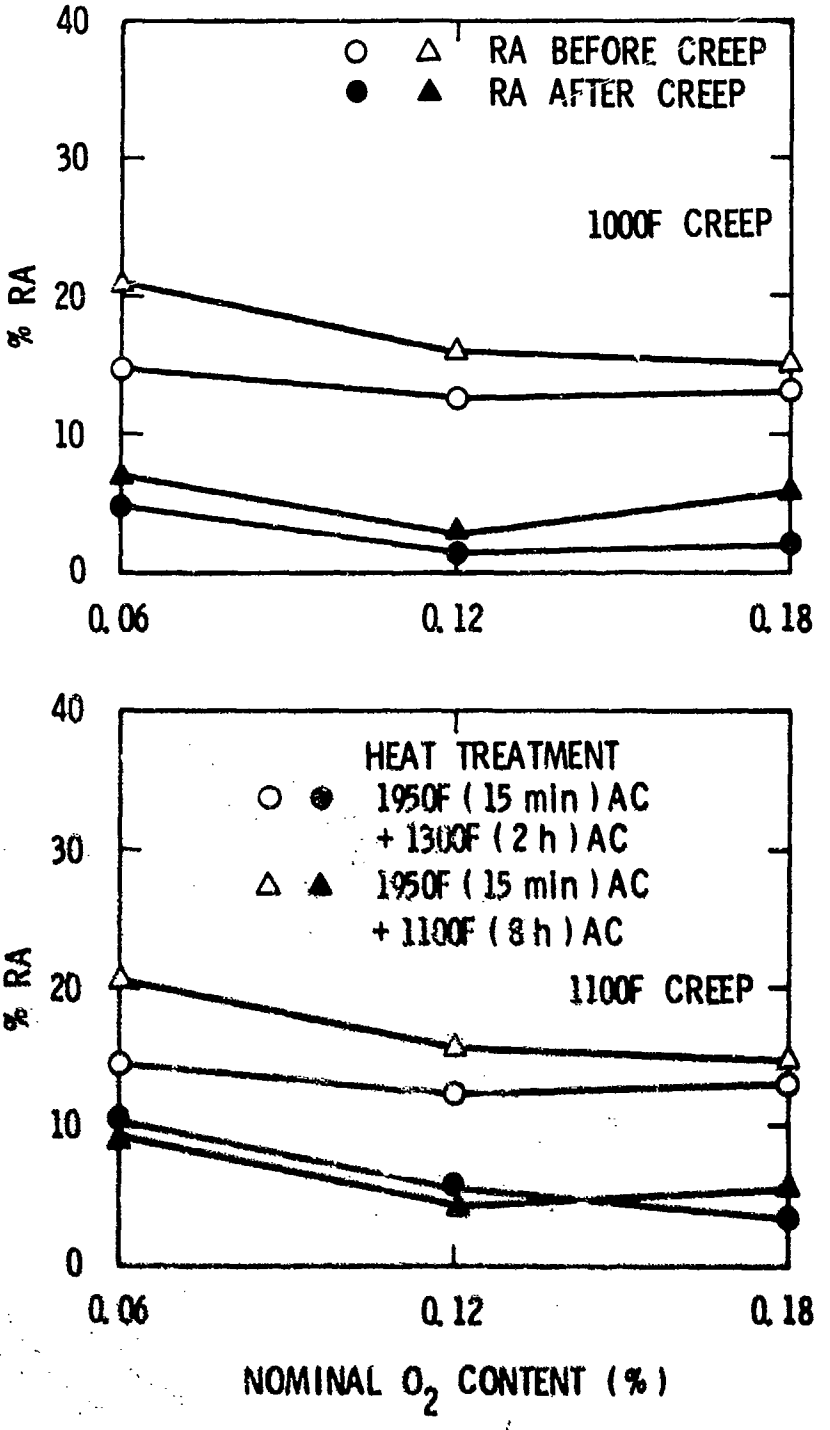

Figure 58 Effects of creep exposure on ductility (RA) of 100 lb. ingot materials of base composition Ti-6Al-2Sn-2Zr-1Mo-0.25Si with additions of O_2.

Figure 59 Structure of the Ti-6Al-2Sn-2Zr-1Mo-0.5Si button melt slow cooled and quenched from 1775F (1241K).

Figure 60 Same as Fig. 59 except quenched from 1750F (1227K).

Figure 61 Same as Fig. 59 except quenched from 1600F (1144K). Note large silicide particles.

Figure 62 Structure of the Ti-6Al-2Sn-2Zr-1Mo-2Bi (actual Bi content 1.32%) alloy slow cooled and quenched from 1775F (1241K).

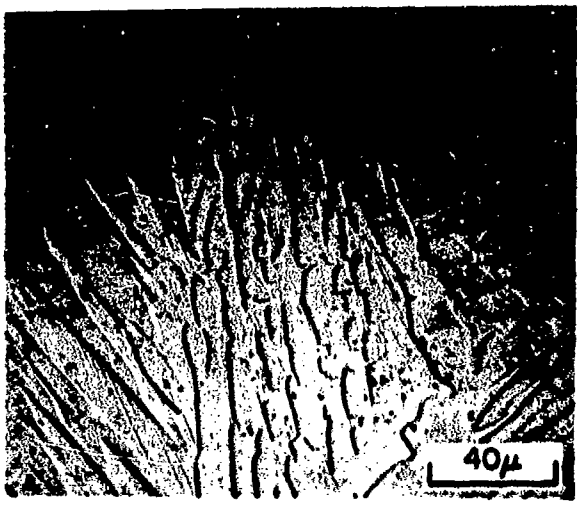

Figure 63 Same as Fig. 62 except quenched from 1750F (1227K).

Figure 64 Same as Fig. 62 except quenched from 1650F (1172K).

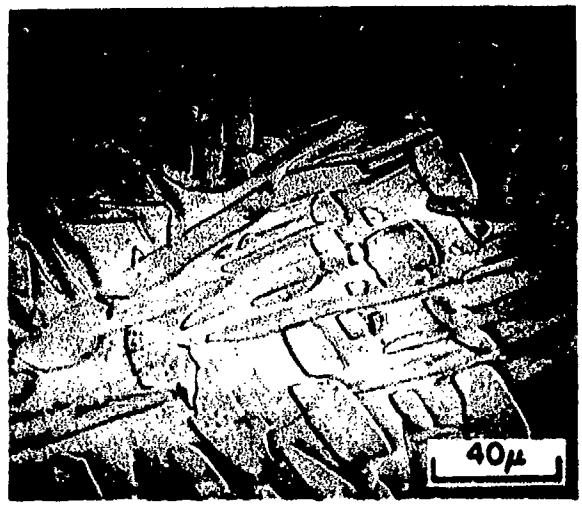

Figure 65 Structure of the Ti-6Al-2Sn-2Zr-1Mo-1Fe button melt slow cooled and quenched from 1725F (1214K).

Figure 66 Same as Fig. 65 except quenched from 1675F (1186K).

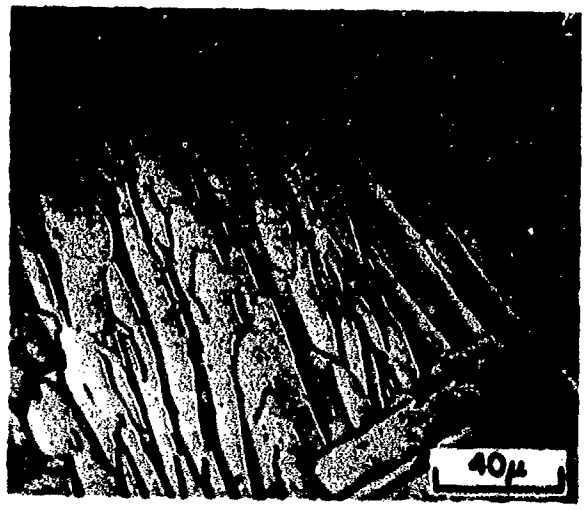

Figure 67 Same as Fig. 65 except quenched from 1550F (1116K).

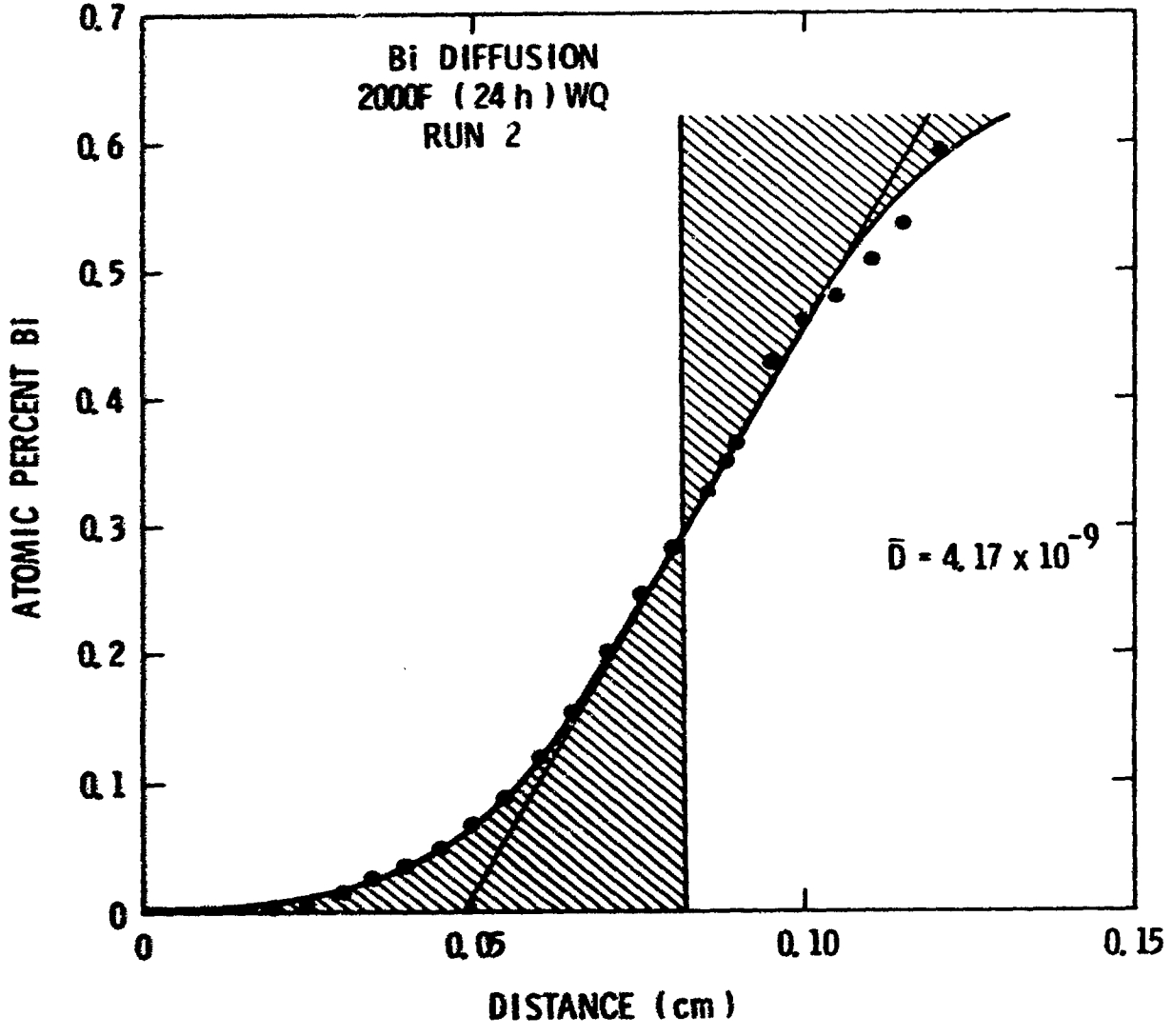

Figure 68 Concentration vs. distance for a Bi diffusion couple created at 2000F (1366K) for 24 hrs

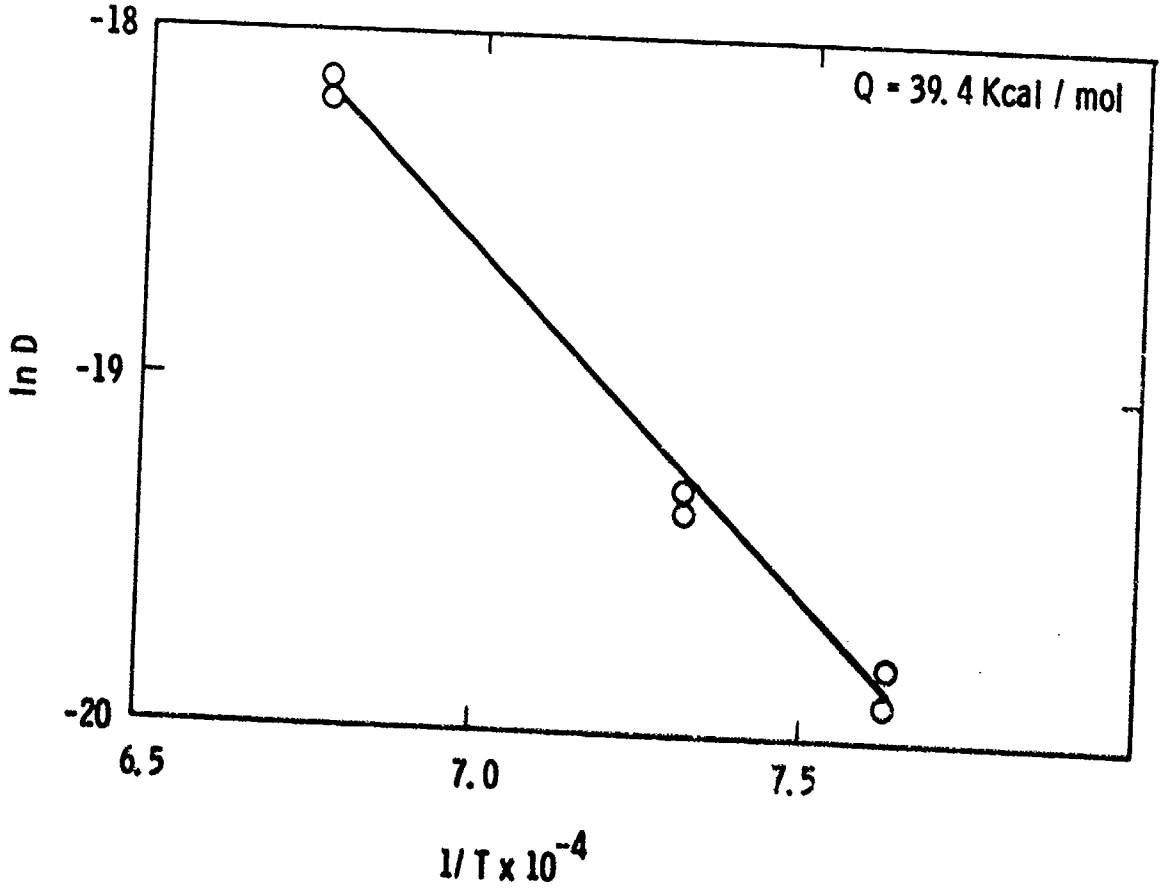

Figure 69 Arrhenius plot of diffusion data for Bi.

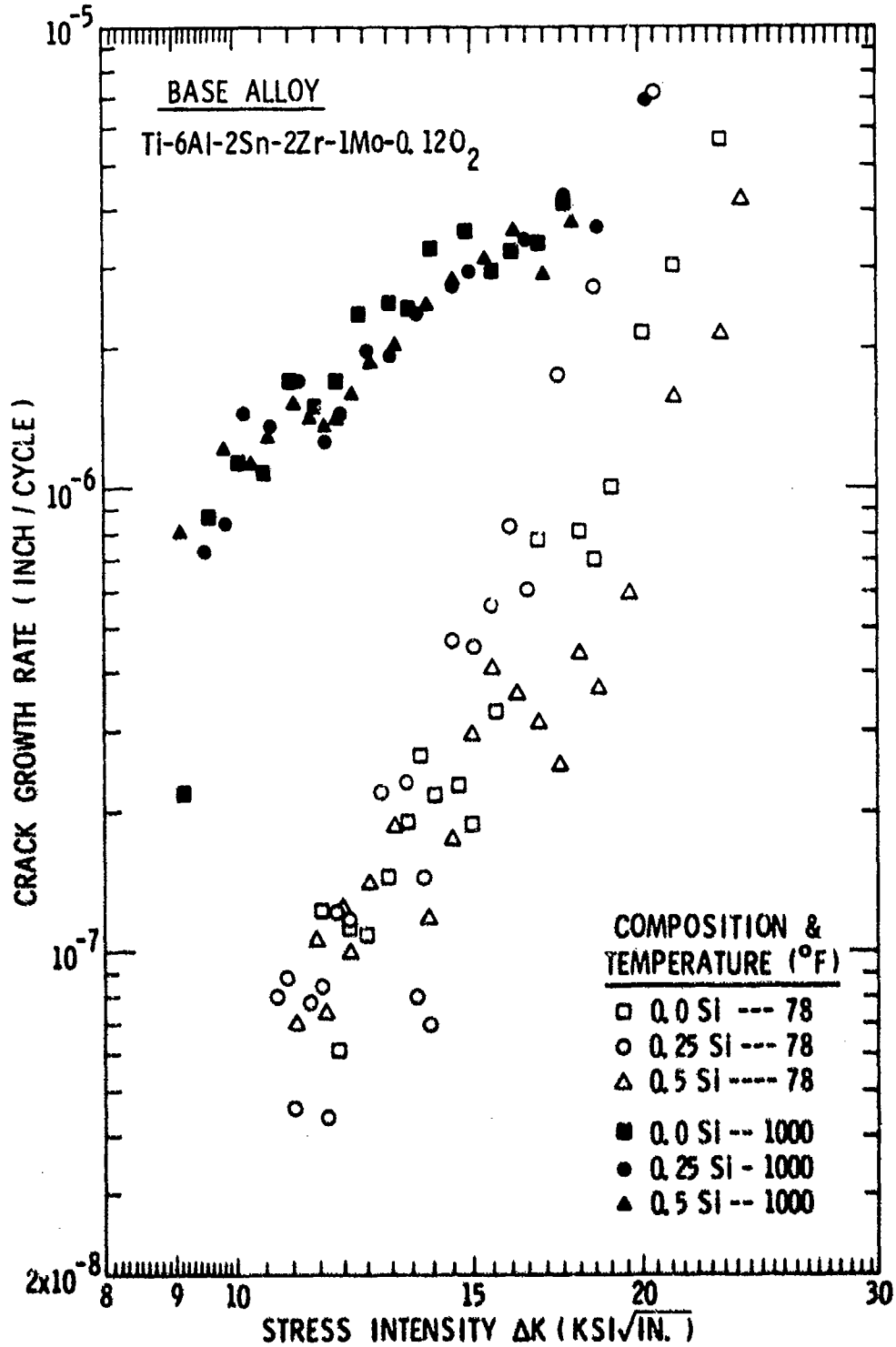

Figure 70 Fatigue crack growth rate of Ti-6Al-2Sn-2Zr-1Mo-.12O_2 at 78 and 1000F (298 and 811K) as a function of Si additions and stress intensity.

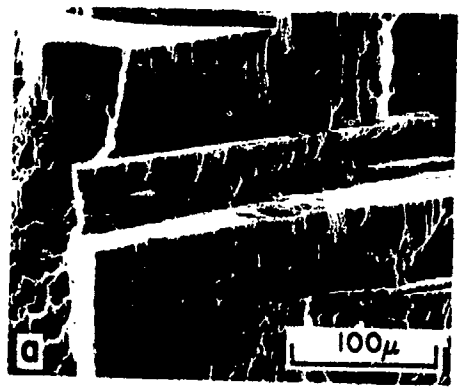

Figure 71 Fractography of fatigue fracture surfaces of Ti-6Al-2Sn-2Zr-1Mo-.12O_2 at da/dN ≅ $3x10^{-7}$ in/cycle with the following additions of Si, a) None, b) 0.25, and c) 0.5.

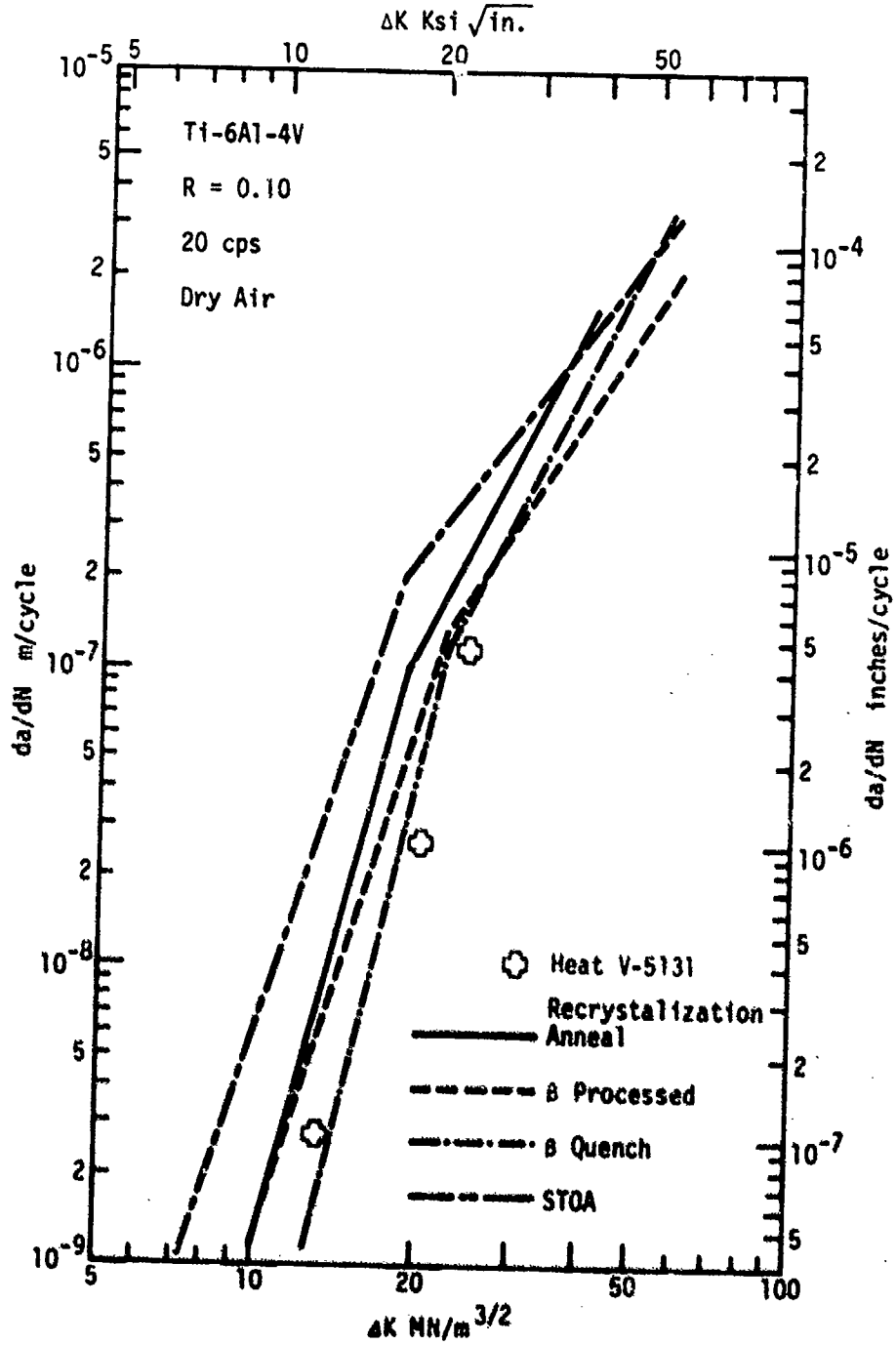

Figure 72 Comparison of fatigue crack growth rate of Ti-6Al-4V[12] and Heat V-5131 (Ti-6Al-2Sn-2Zr-1Mo-.12O_2-.25Si) at 78F (298K).

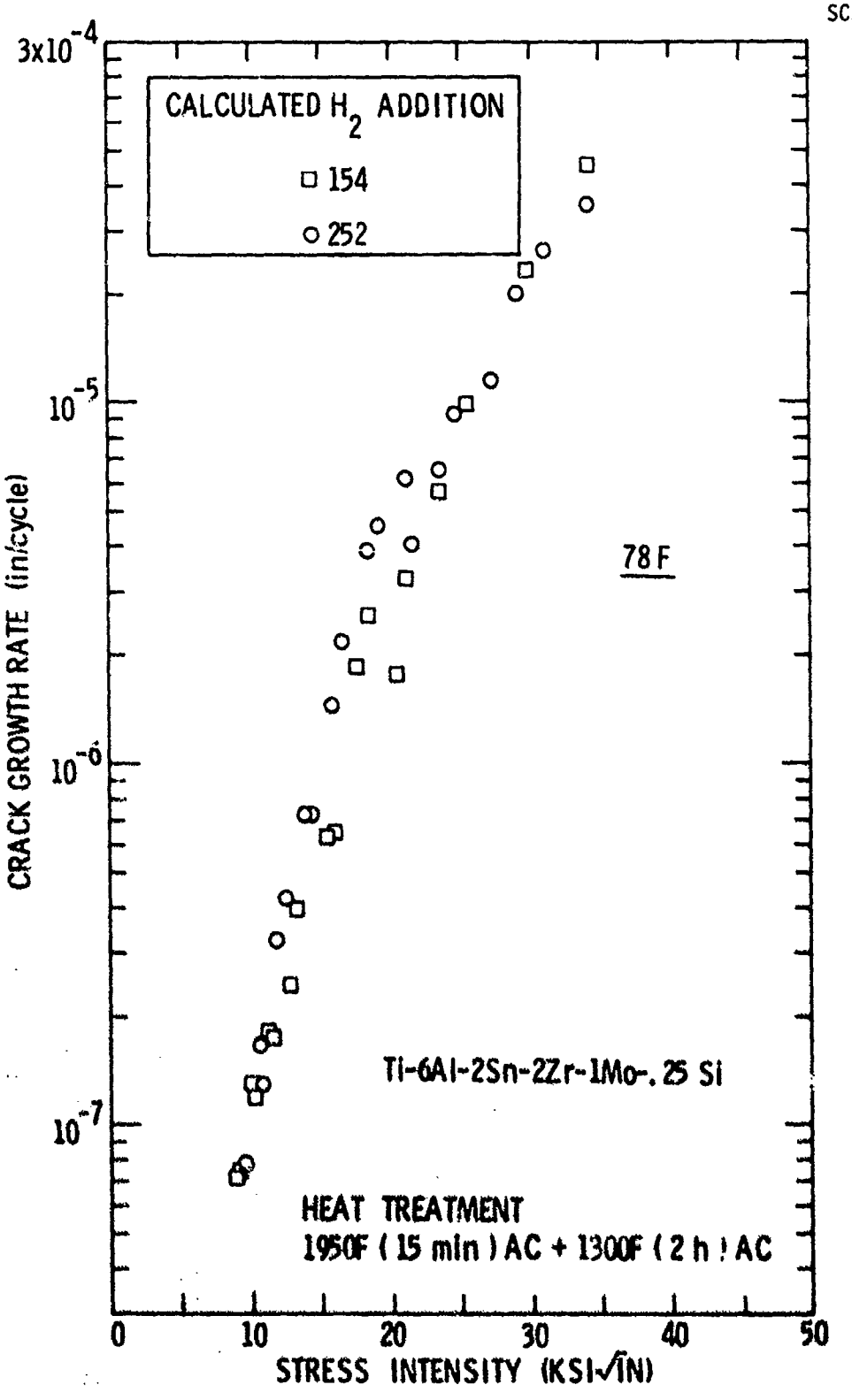

Figure 73 Fatigue crack growth rate at 78F in 100 lb. ingot material of composition Ti-6Al-2Sn-2Zr-1Mo-.25Si with additions of hydrogen.

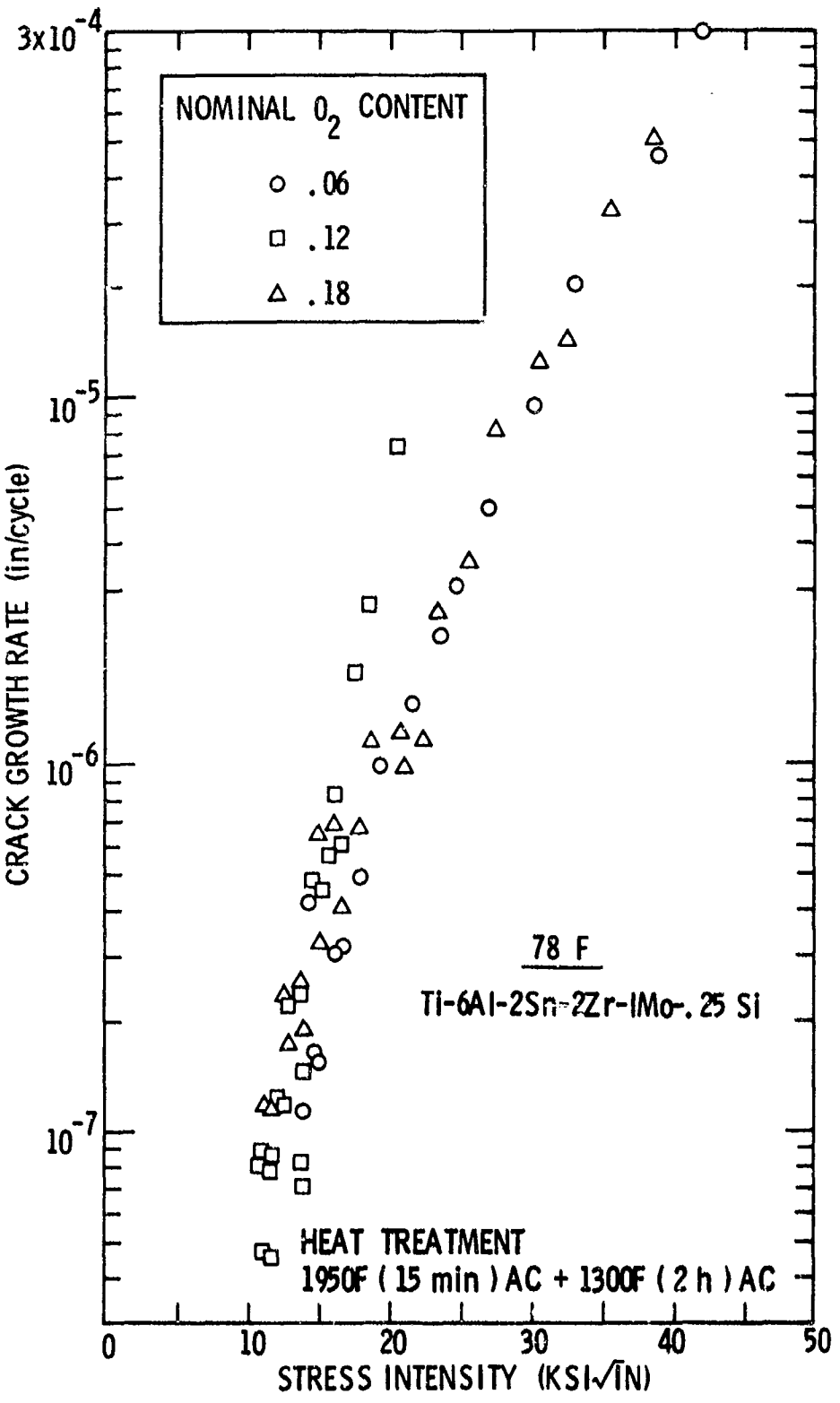

Figure 74 Fatigue crack growth rate at 78F in 100 lb. ingot material of composition Ti-6Al-2Sn-2Zr-1Mo-.25Si with additions of oxygen.

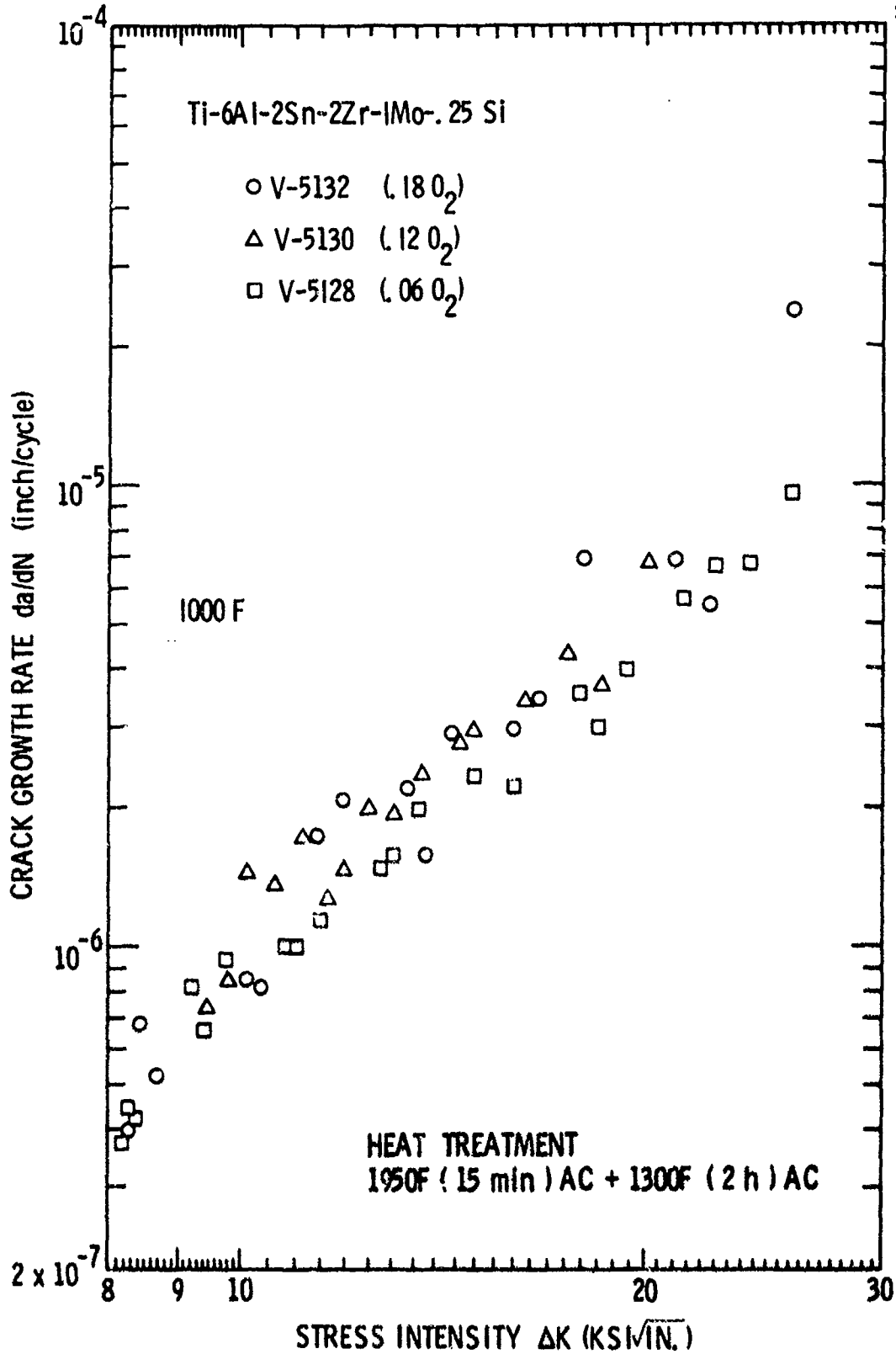

Figure 75 Fatigue crack growth rate of Ti-6Al-2Sn-2Zr-1Mo-.25Si at 1000F (811K) as a function of oxygen content and stress intensity.

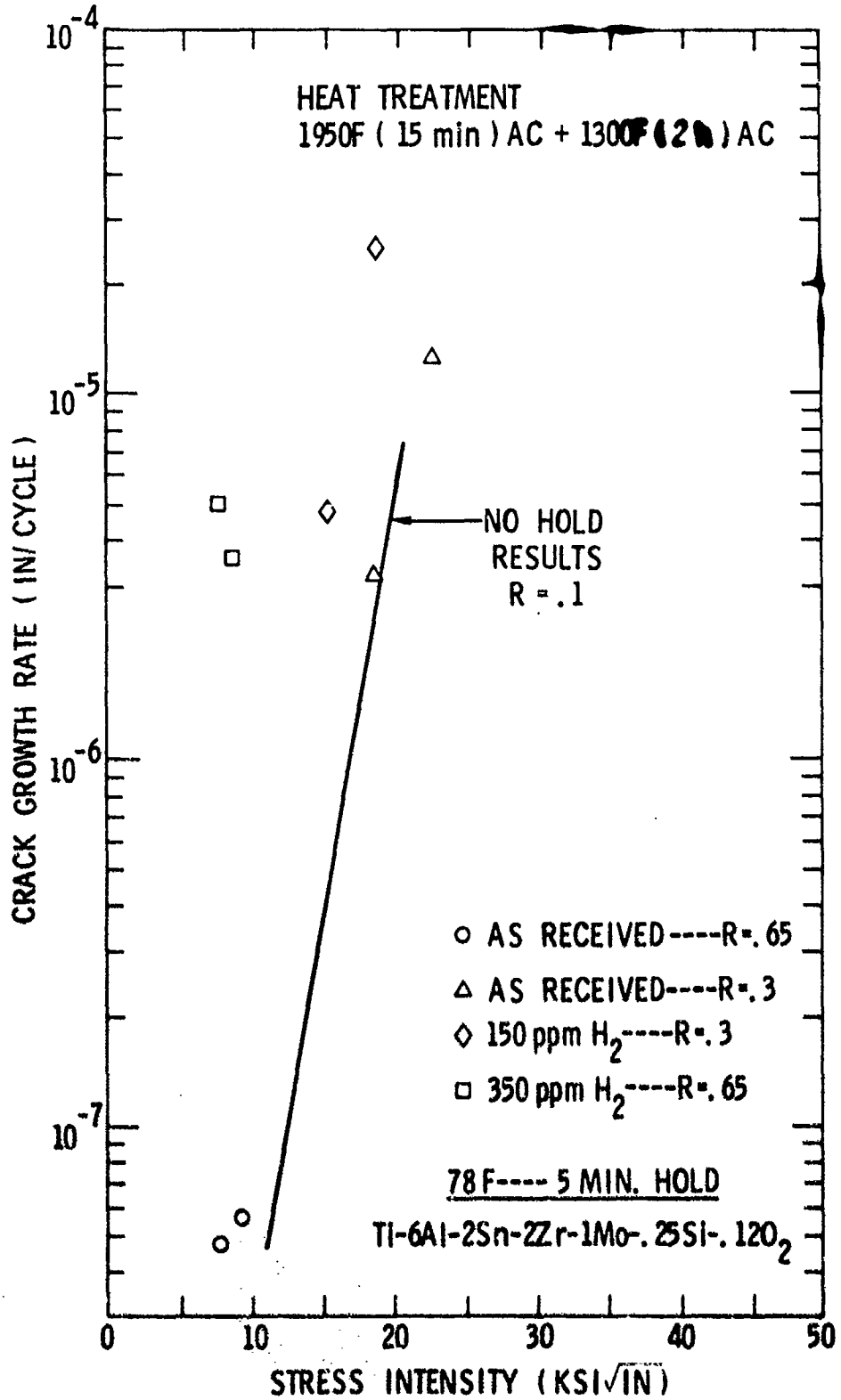

Figure 76 Fatigue crack growth rate of Ti-6Al-2Sn-2Zr-1Mo-.25Si-.120_2 at 78°F (298K) with 5-minute hold times at maximum load as a function of hydrogen content and R ratio.

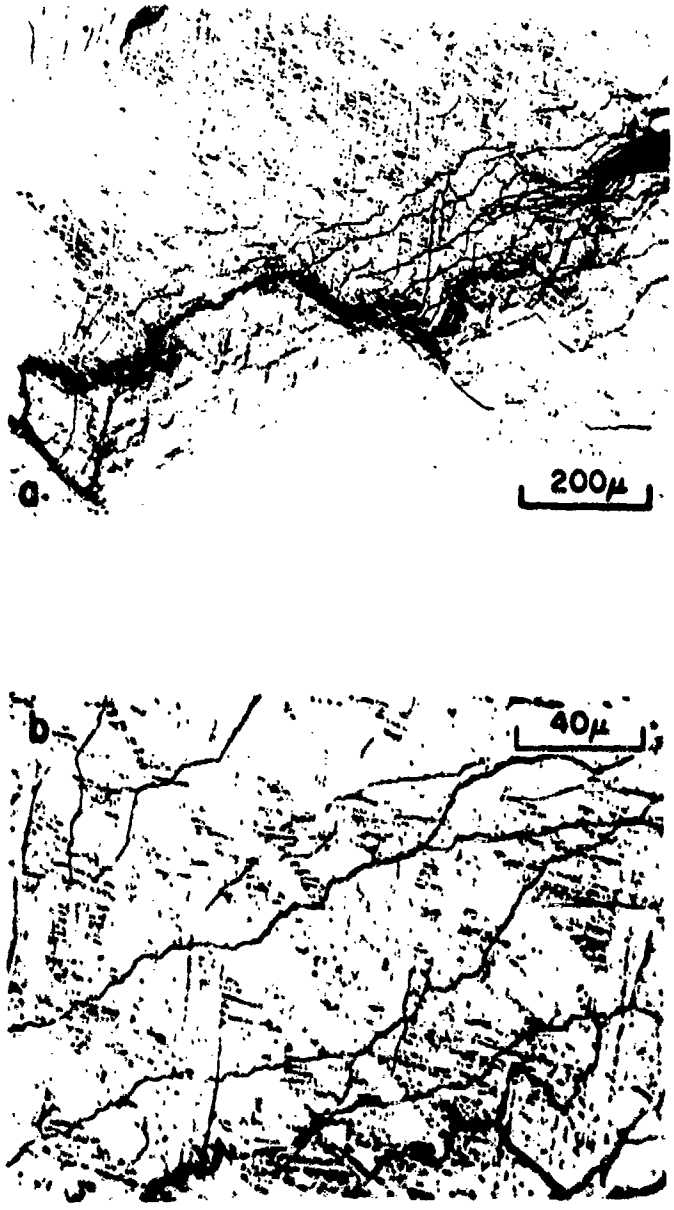

Figure 77 Optical microscopy illustrating the crack path in Ti-6Al-2Sn-2Zr-1Mo-.25Si-.12O_2 created by fatigue loading with superimposed 5-minute hold periods at the maximum load; a) low magnification, and b) high magnification.

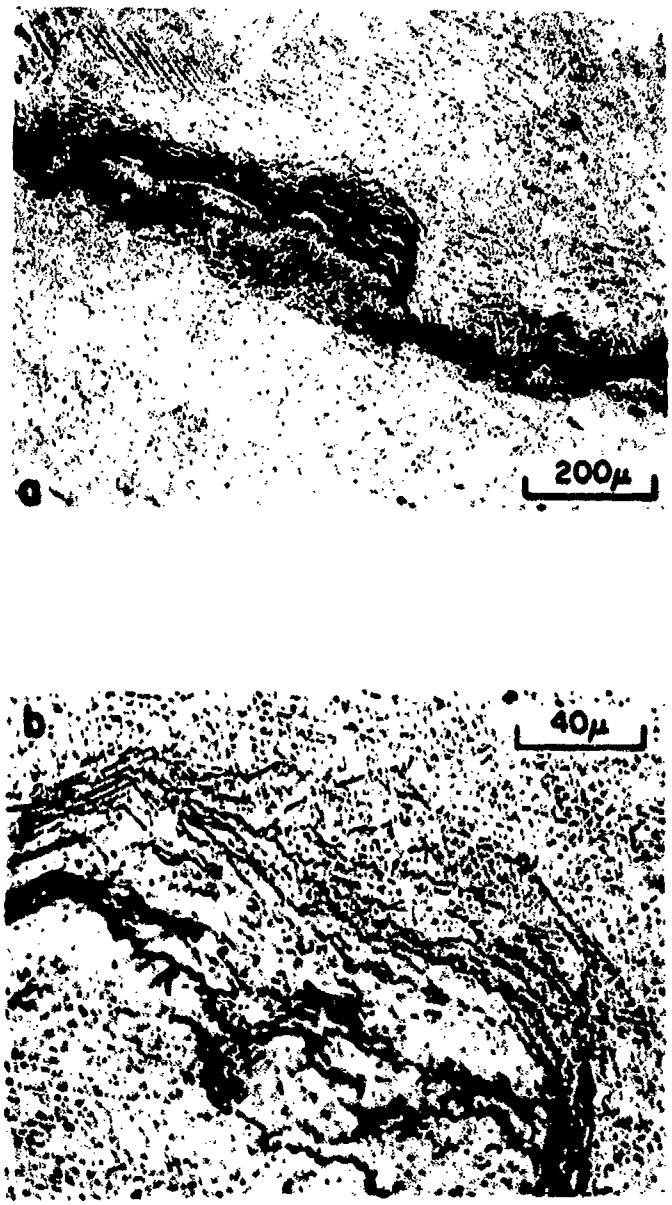

Figure 78 Optical microscopy illustrating the crack path in Ti-6Al-2Sn-2Zr-1Mo-.25Si-.12 O_2 + 350 ppm H created by fatigue loading with superimposed 5-minute hold periods at the maximum load; a) low magnification and b) high magnification.

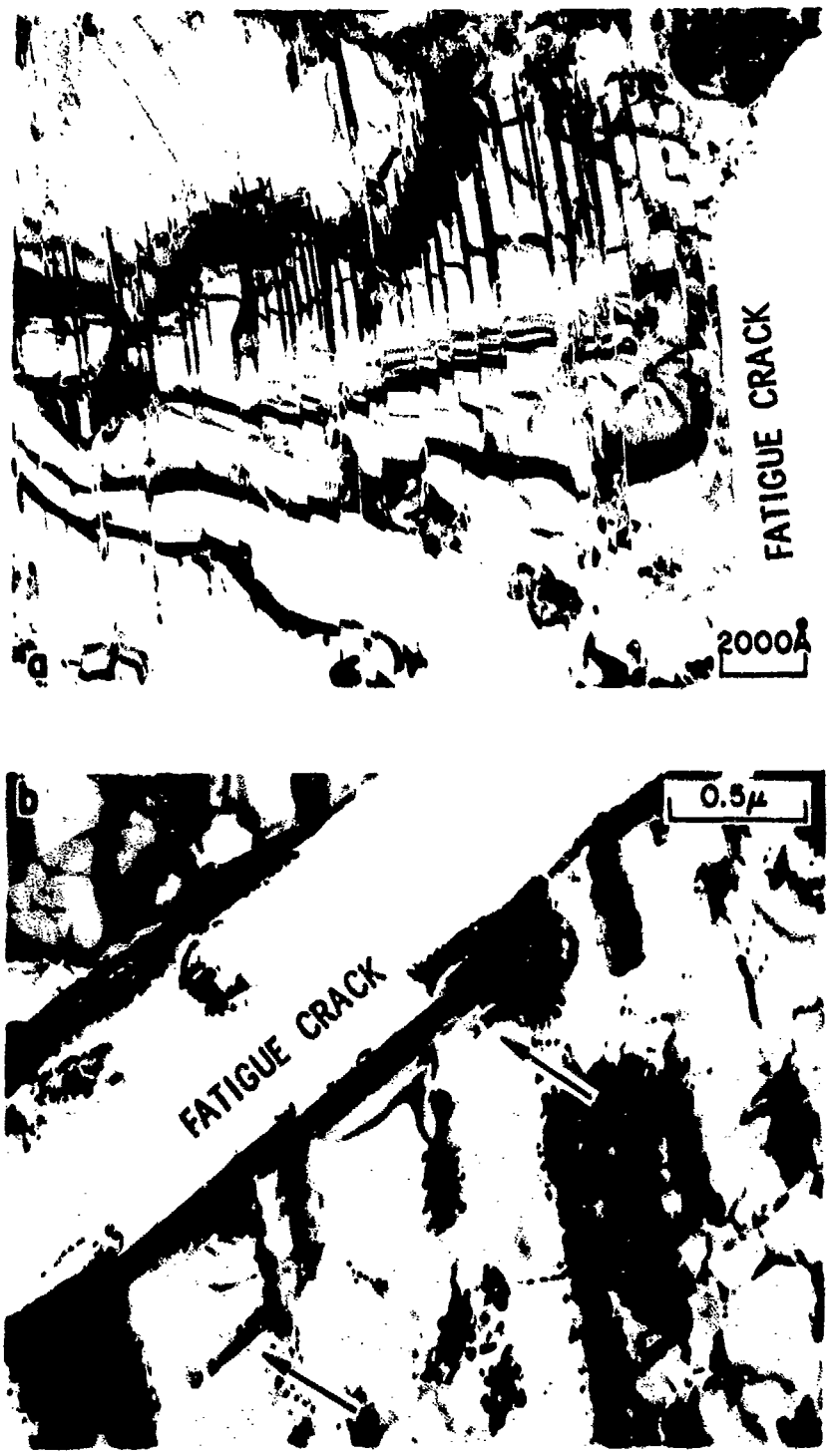

Figure 79 (a and b) Transmission electron microscopy illustrating the parallel orientation of fatigue cracks and basal hydrides.

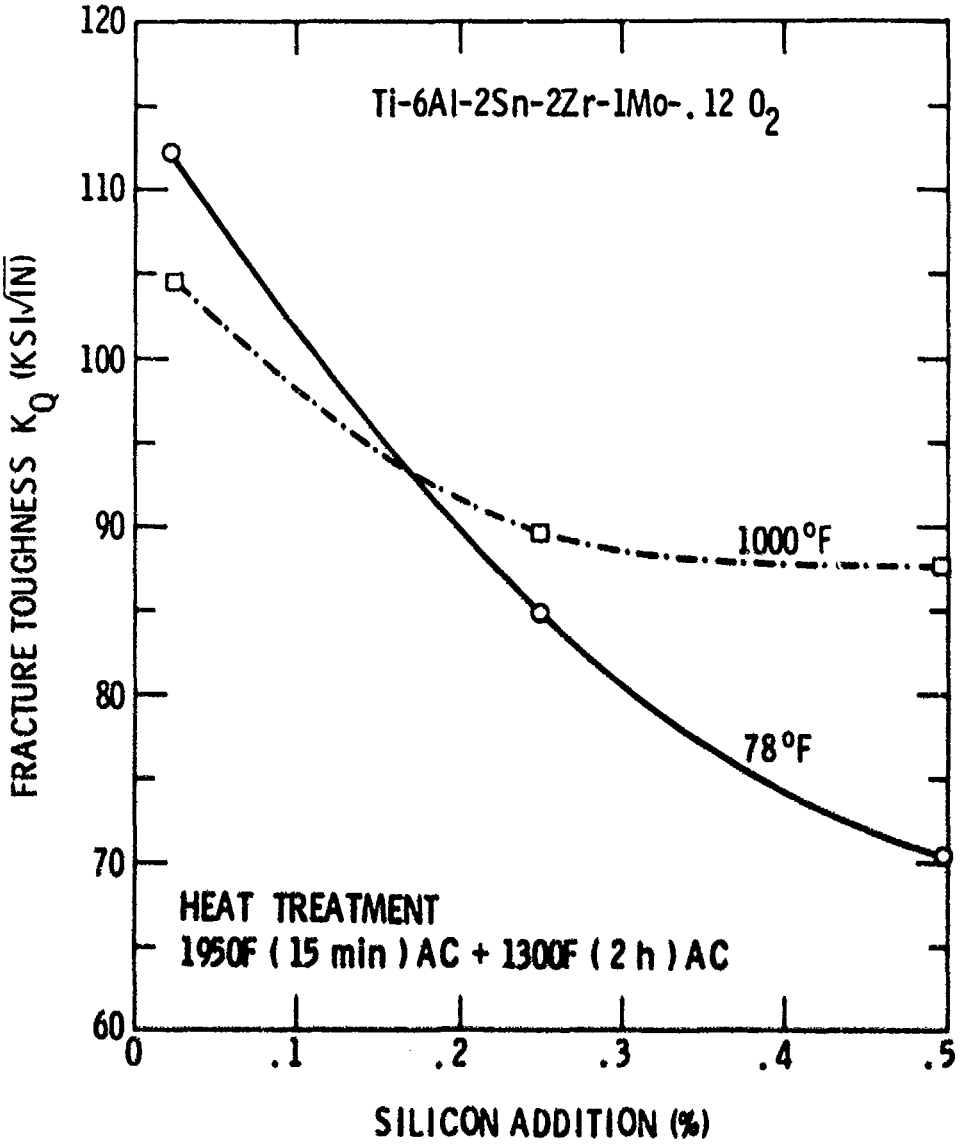

Figure 80 Fracture toughness of Ti-6Al-2Sn-2Zr-1Mo-.12 O_2 at 78 and 1000F (298 and 811K) as a function of Si additions.

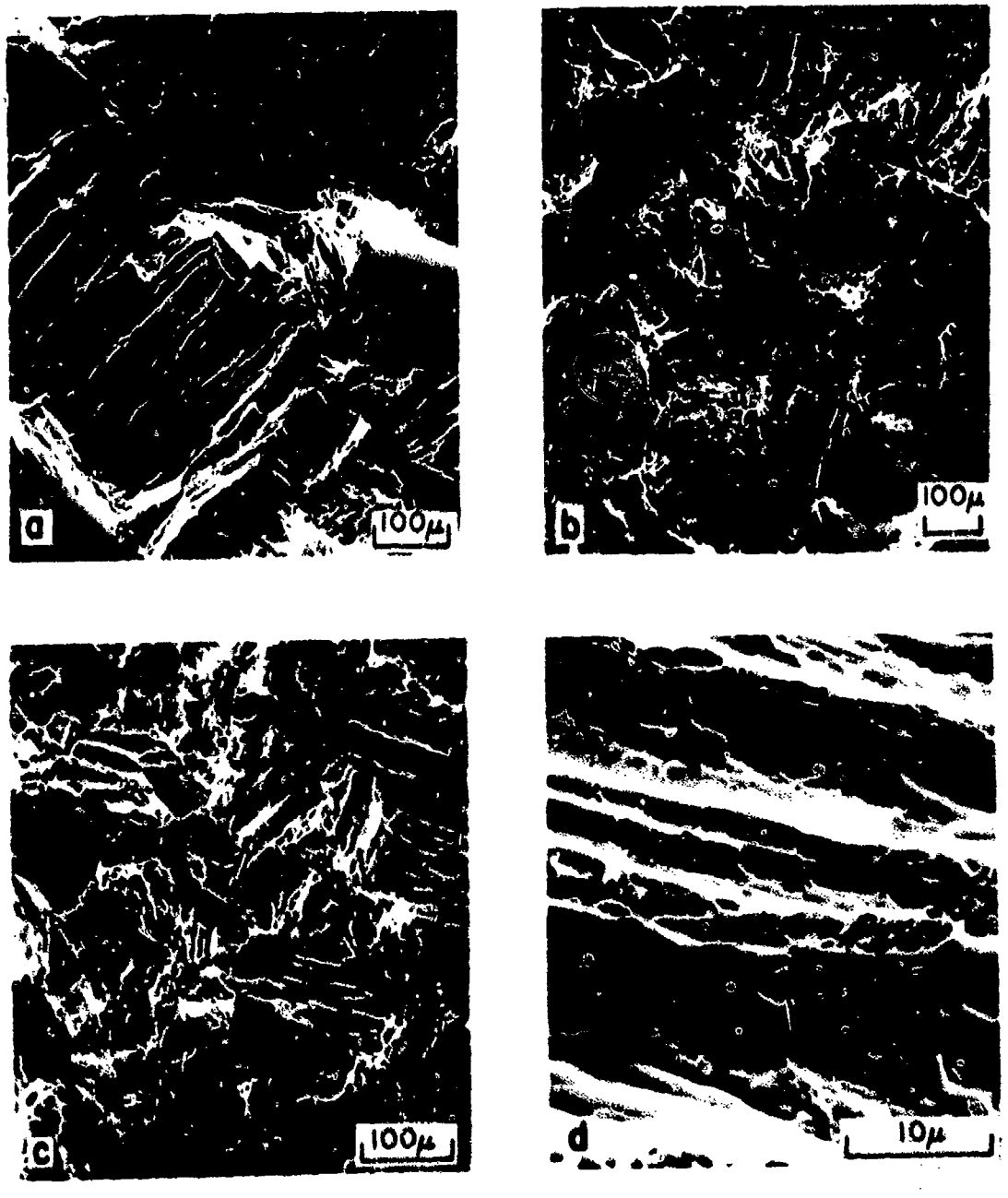

Figure 81 Fractography of fracture toughness specimens of composition Ti-6Al-2Sn-2Zr-1Mo-.12O_2 with the following additions of Si, a) .25, b) None, c and d) .5.

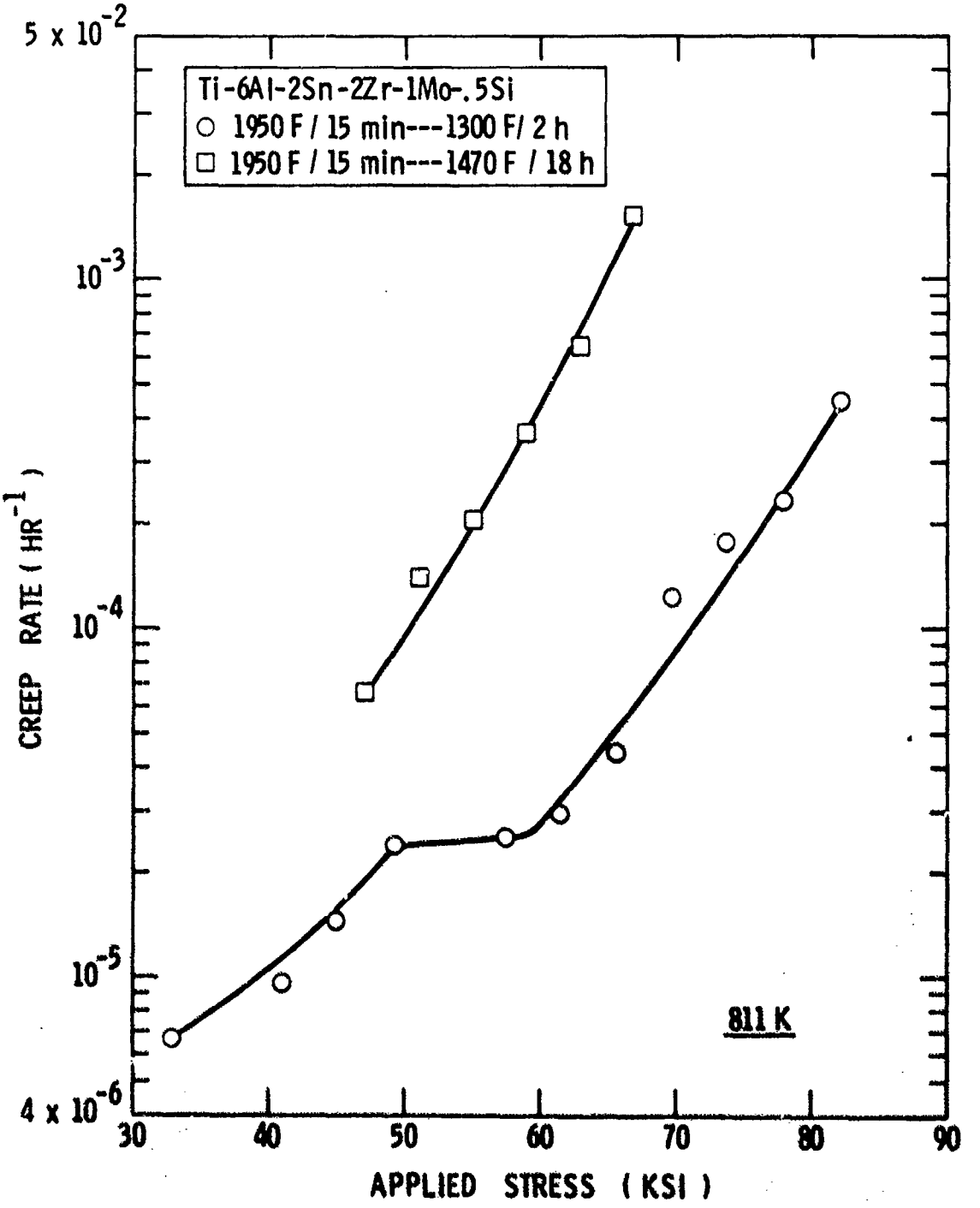

Figure 82 Creep rate at 1000F for 100 lb. ingot material of composition Ti-6Al-2Sn-2Zr-1Mo-.5Si for two heat treatments.

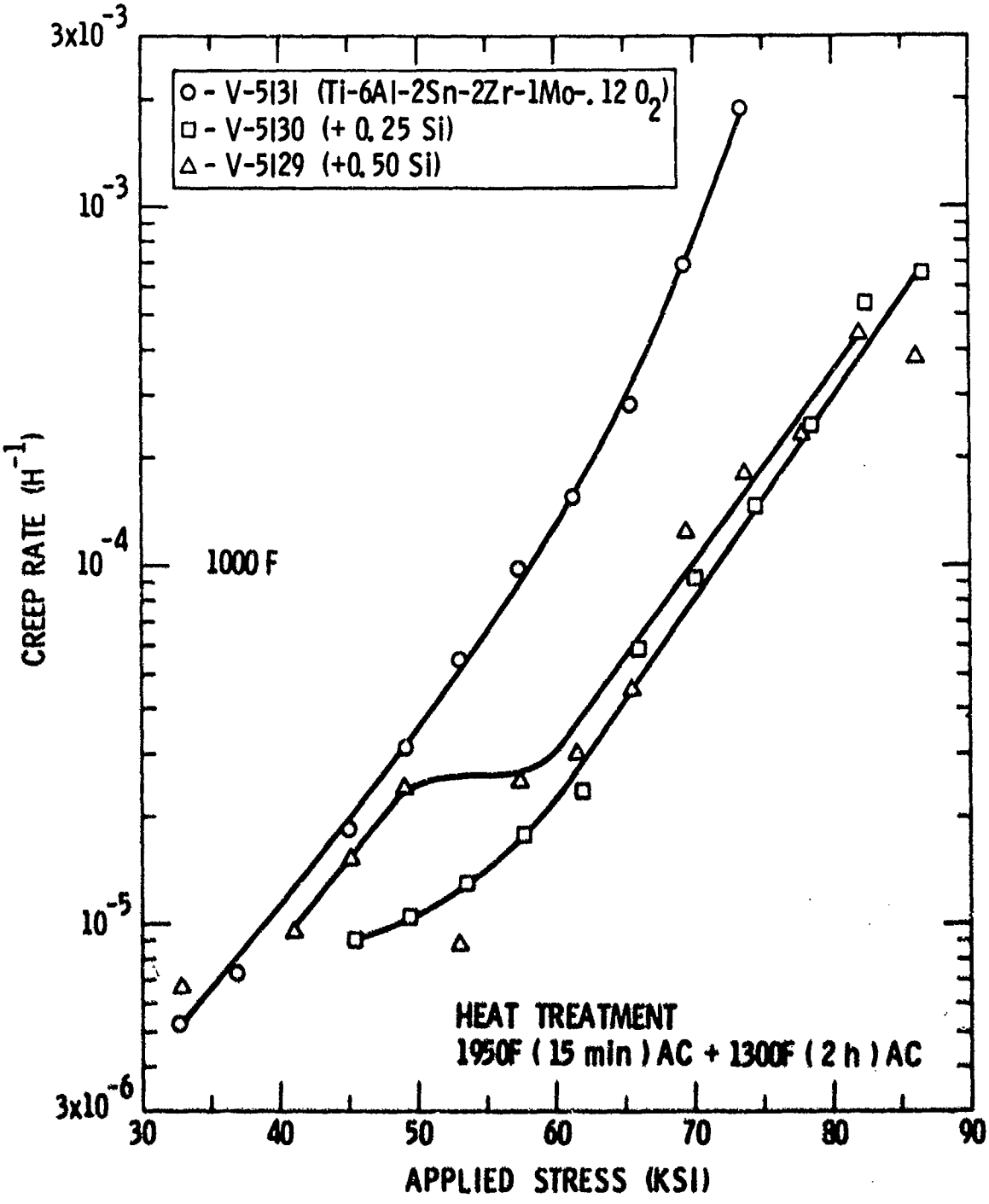

Figure 83 Creep rate as a function of applied stress at 1000F for 100 lb. ingot materials of composition Ti-6Al-2Sn-2Zr-1Mo-.12 O_2 with additions of Si.

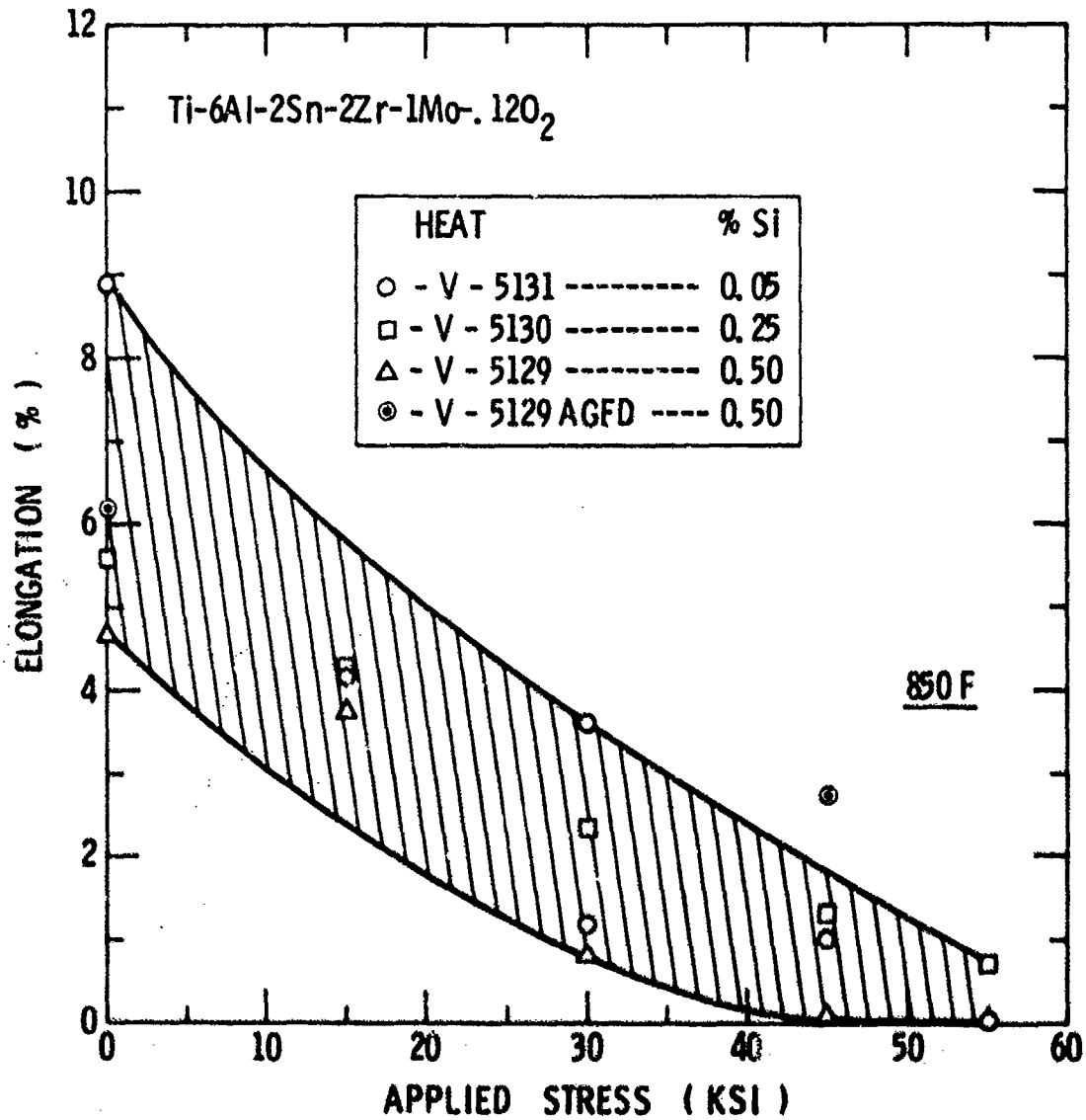

Figure 84 Residual elongation in 100 lb. ingot materials of base composition Ti-6Al-2Sn-2Zr-1Mo after exposure to a hot salt stress corrosion environment at 850F as a function of Si content, heat treatment and applied stress during exposure.

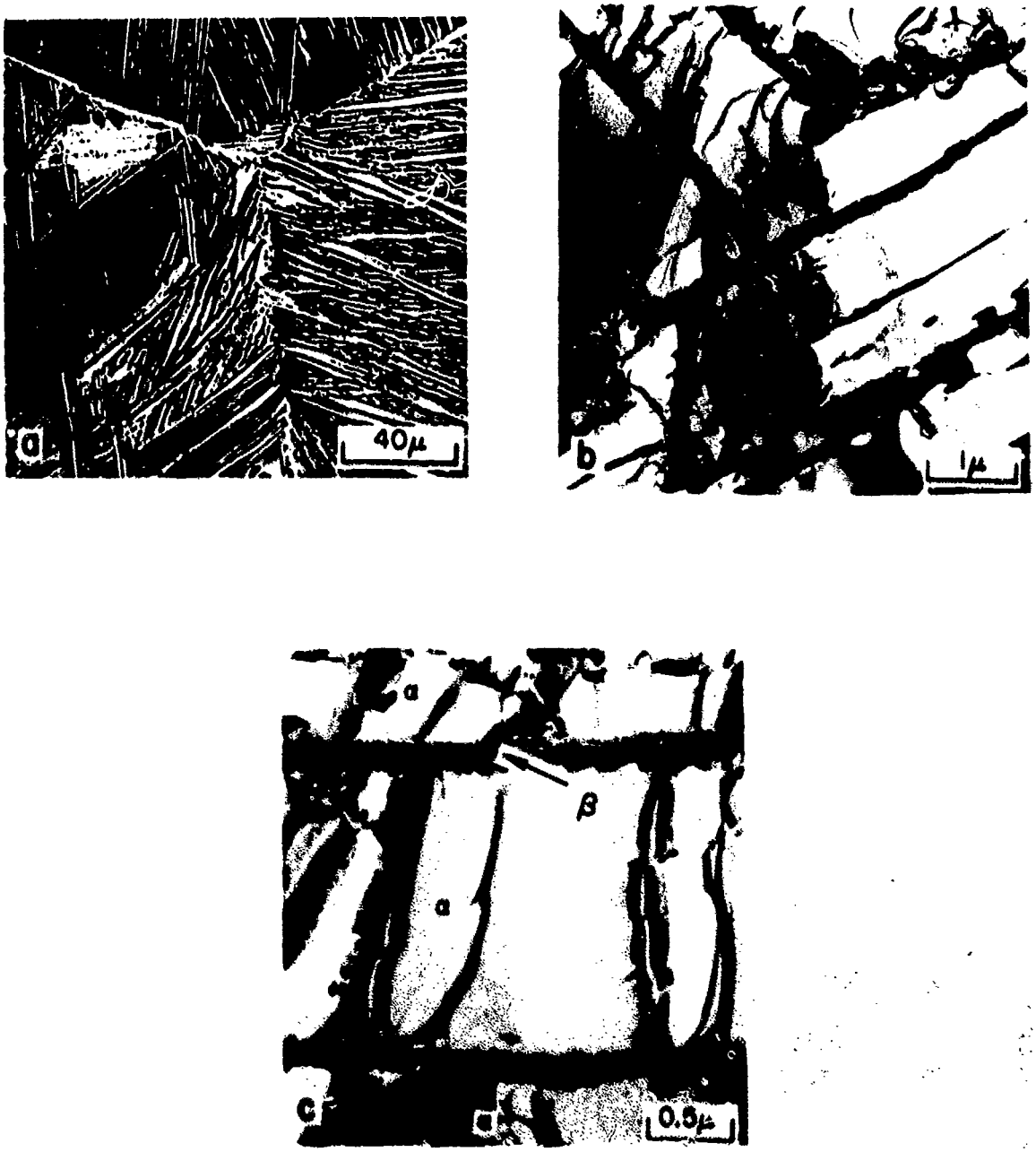

Ti-6Al-2Sn-2Zr-1Mo

Figure 85 Microstructure of Heat B-2650, base alloy Ti-6Al-2Sn-2Zr-1Mo; (a) optical micrograph, (b) and (c) transmission electron microscopy.

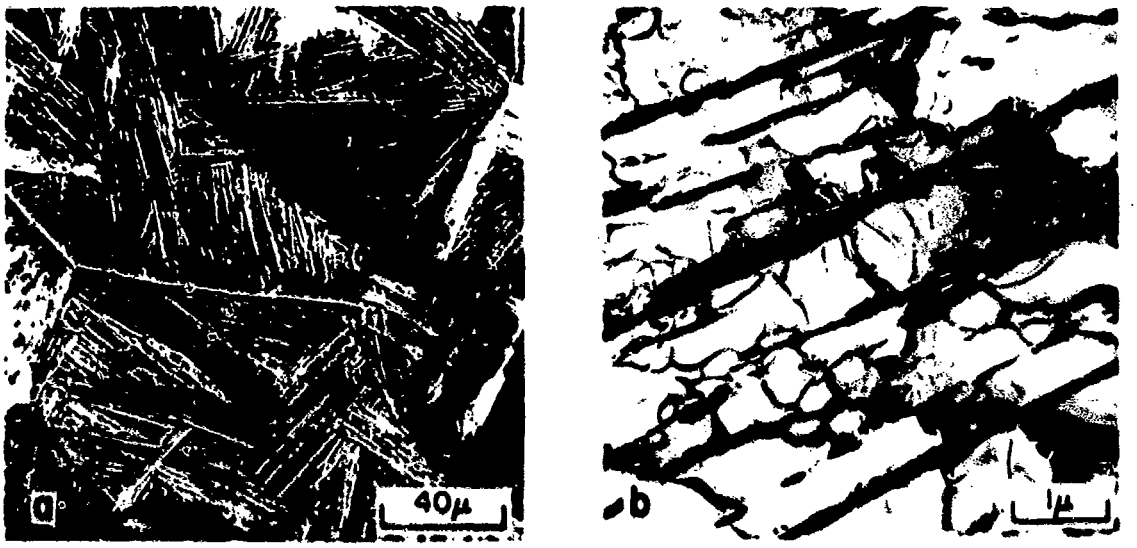

Ti-6Al-2Sn-2Zr-1Mo-0.1Si

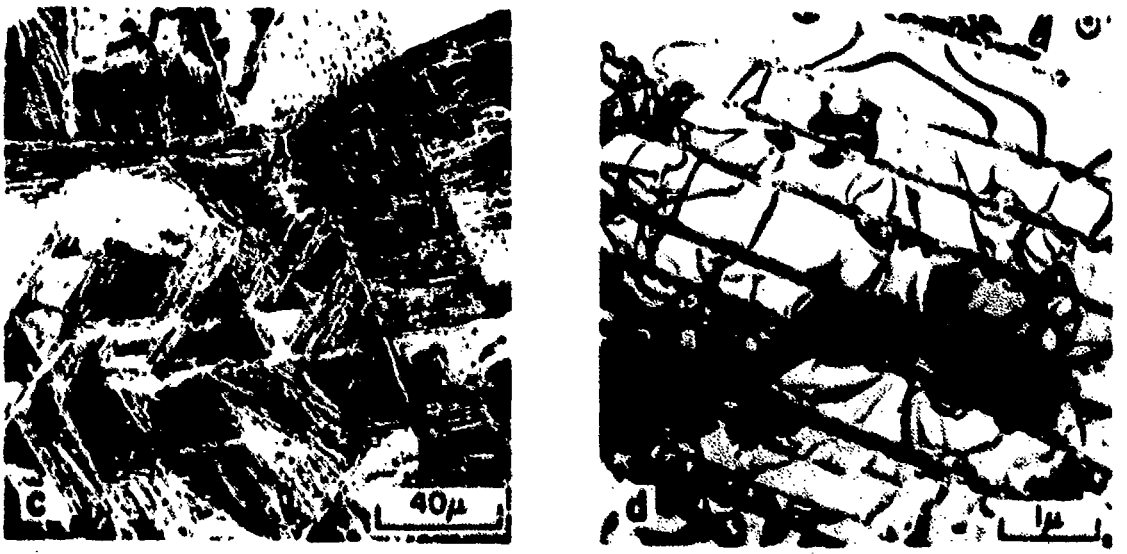

Ti-6Al-2Sn-2Zr-1Mo-0.25Si

Figure 86 (a) and (b) Optical and transmission electron microscopy, respectively, of Heat B-2652, alloy addition of 0.1 Si. (c) and (d) Optical and transmission electron microscopy, respectively, of Heat B-2654, alloy addition of 0.25 Si.

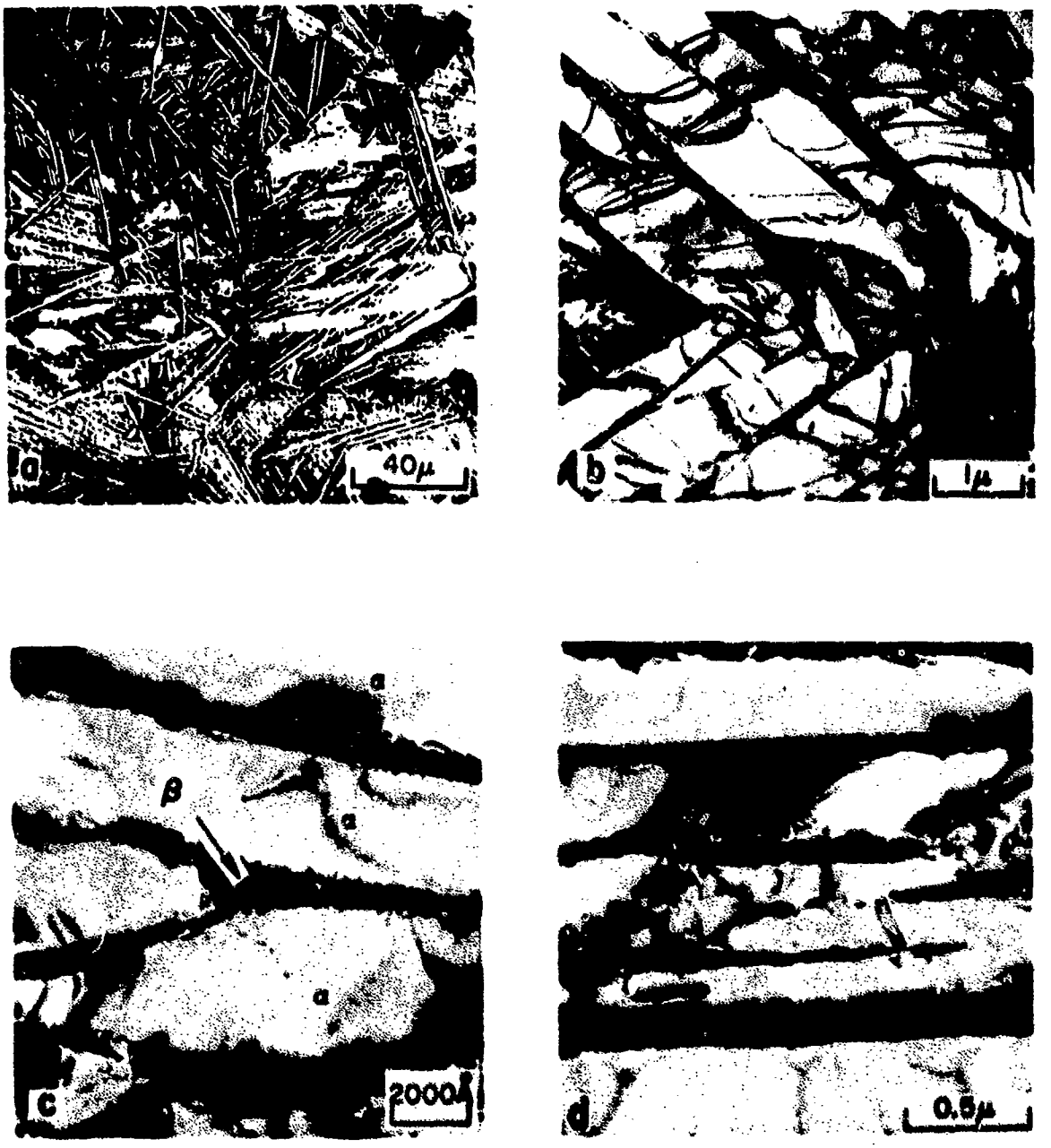

Ti-6Al-2Sn-2Zr-1Mo-0.5Si

Figure 87 Microstructure of Heat B-2656, alloy addition of 0.5 Si: (a) optical micrograph, (b), (c) and (d) transmission electron microscopy. (a), (b) and (c) alloy aged at 1300°F (2 Hrs.), (d) alloy aged at 1100°F (8 Hrs.).

Ti-6Al-2Sn-2Zr-1Mo-0.25Bi

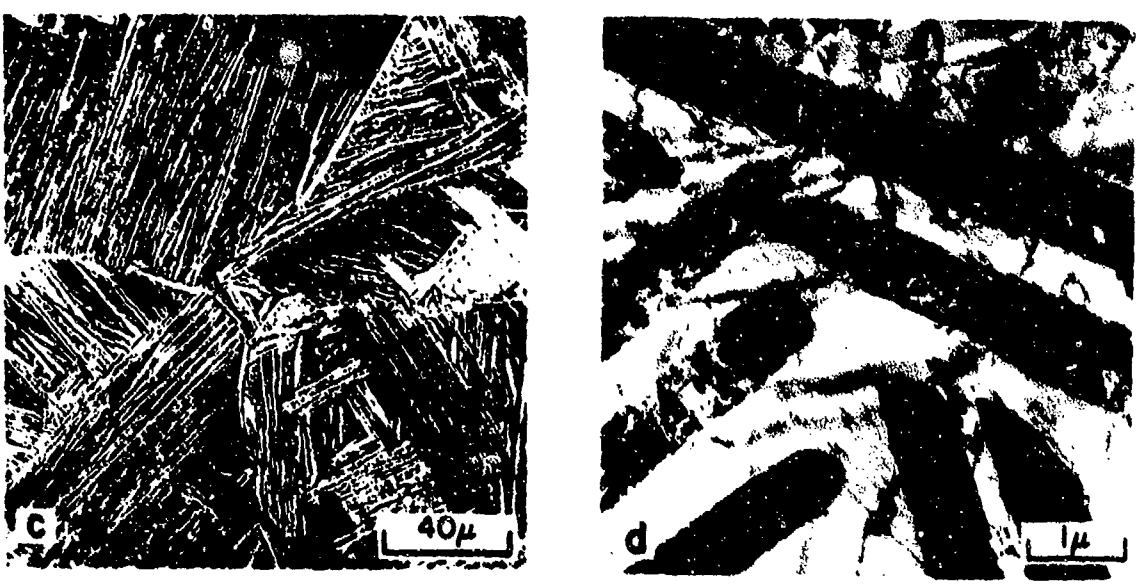

Ti-6Al-2Sn-2Zr-1Mo-0.5Bi

Figure 88 (a) and (b) Optical and transmission electron microscopy, respectively, of Heat B-2658, alloy addition of 0.25 Bi. (c) and (d) Optical and transmission electron micruscopy, respectively, of Heat B-2660, alloy addition of 0.50 Bi.

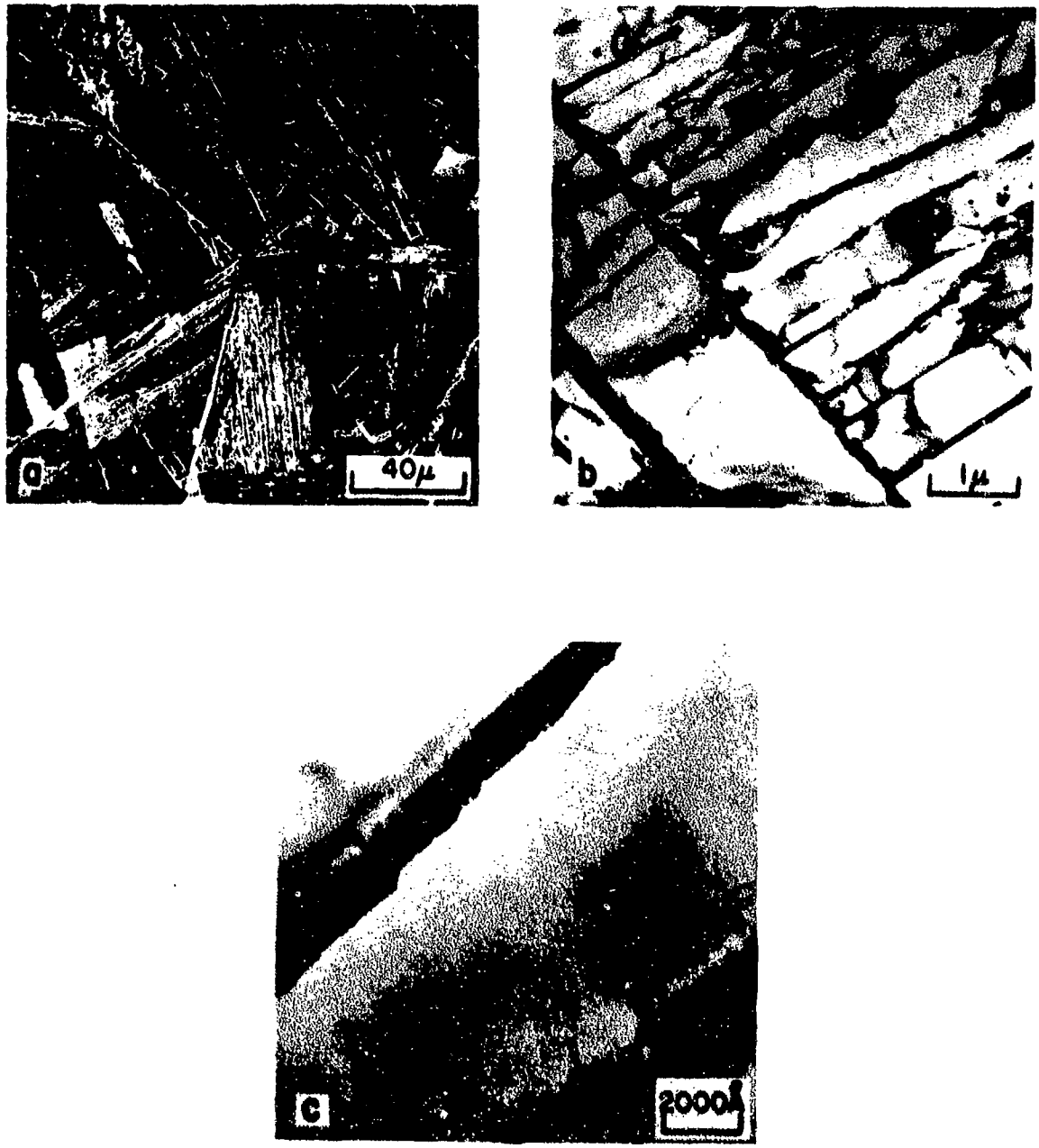

Ti-6Al-2Sn-2Zr-1Mo-1.0Bi

Figure 89 Microstructure of Heat B-2662, alloy addition of 1.0 Bi; (a) optical micrograph, (b) and (c) transmission electron microscopy.

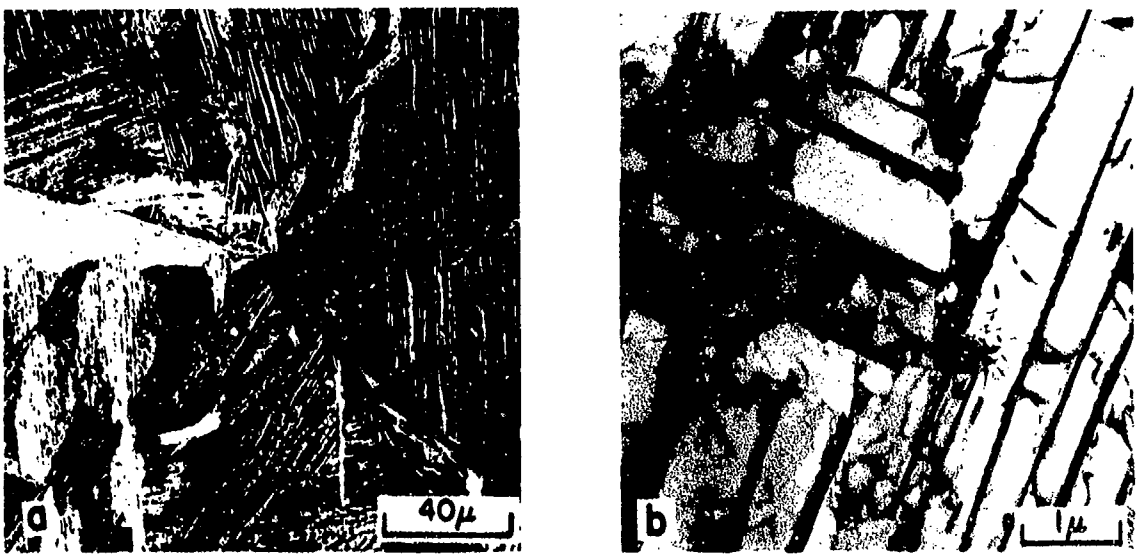

Ti-6Al-2Sn-2Zr-1Mo-2.0Bi

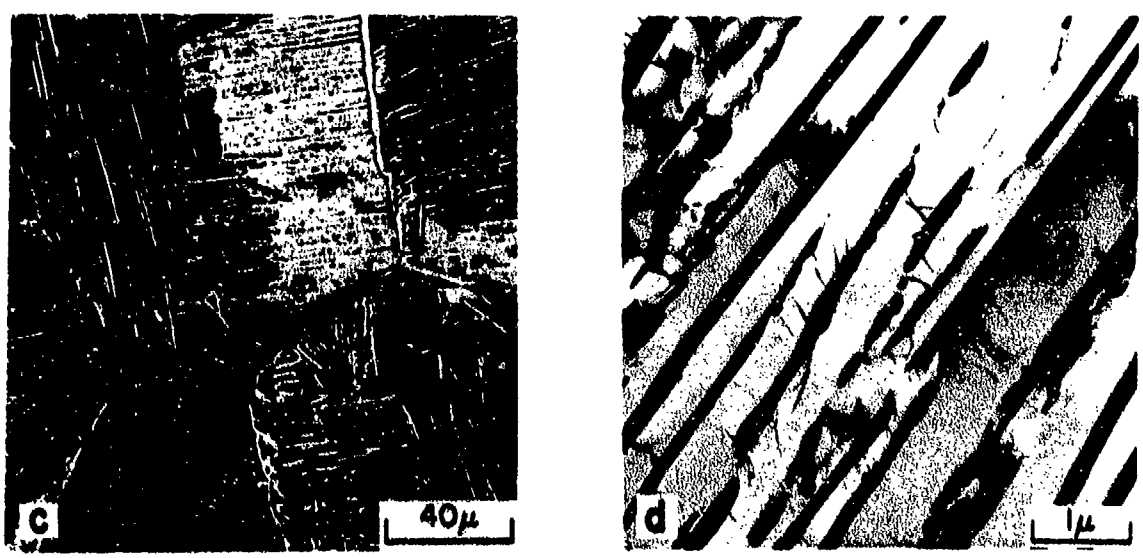

Ti-6Al-2Sn-2Zr-1Mo-0.15Fe

Figure 90 (a) and (b) Optical and transmission electron microscopy, respectively, of Heat B-2664, alloy addition of 2.0 Bi. (c) and (d) Optical and transmission electron microscopy, respectively, of Heat B-2666, alloy addition of 0.15 Fe.

Ti-6Al-2Sn-2Zr-1Mo-0.25Fe

Figure 91 Microstructure of Heat B-2668, alloy addition of 0.25 Fe; (a) optical micrograph, (b) and (c) transmission electron microscopy.

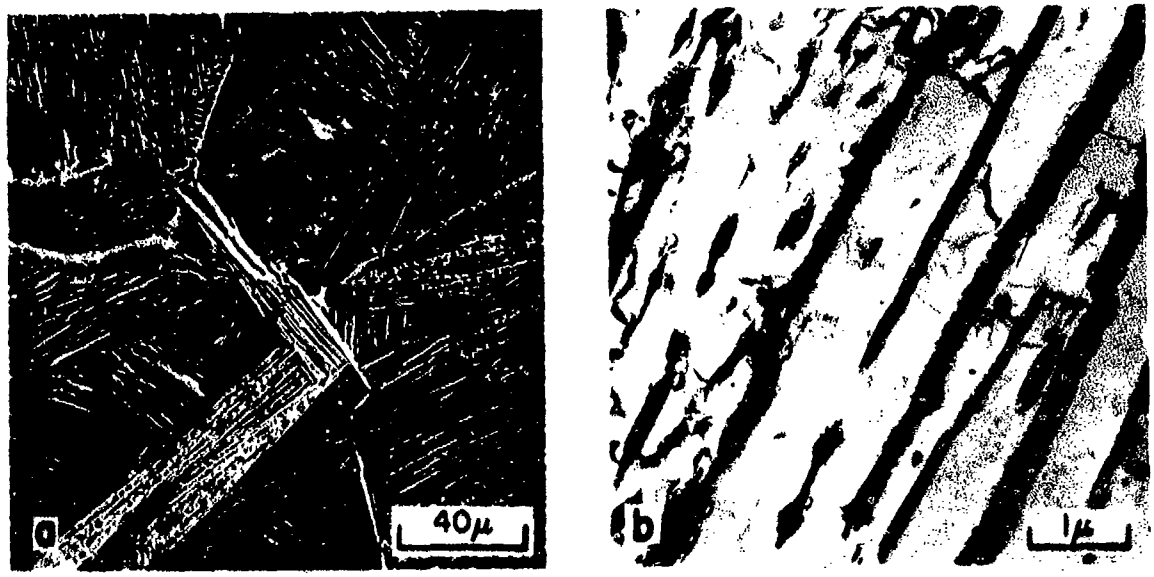

Ti-6Al-2Sn-2Zr-1Mo-0.5Fe

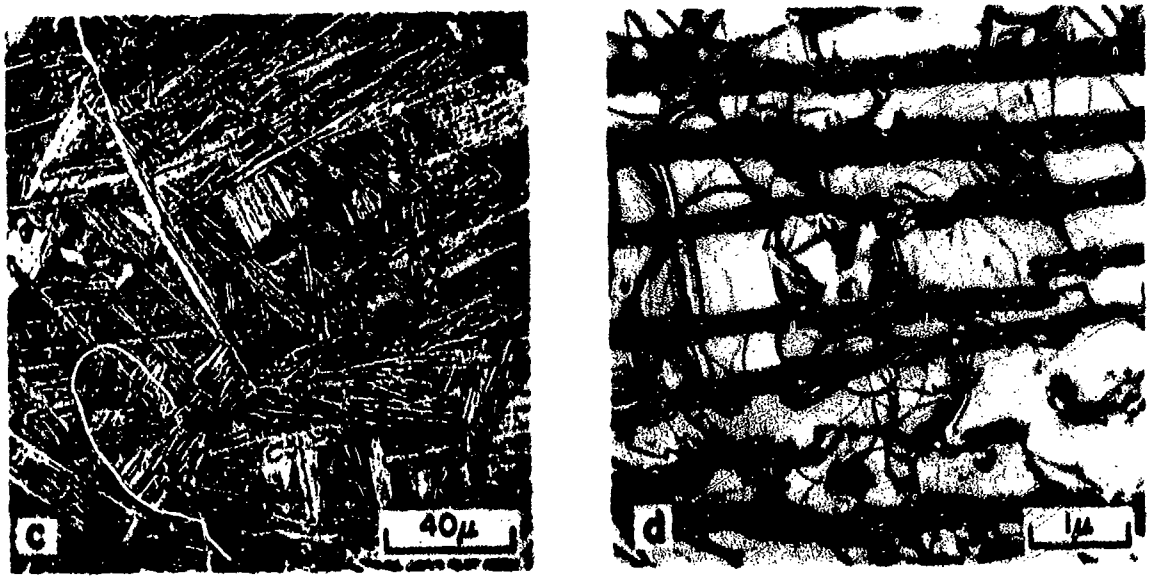

Ti-6Al-2Sn-2Zr-1Mo-1.0Fe

Figure 92 (a) and (b) Optical and transmission electron microscopy, respectively, of Heat B-2670, alloy addition of 0.5 Fe. (c) and (d) Optical and transmission electron microscopy, respectively, of Heat B-2672, alloy addition of 1.0 Fe.

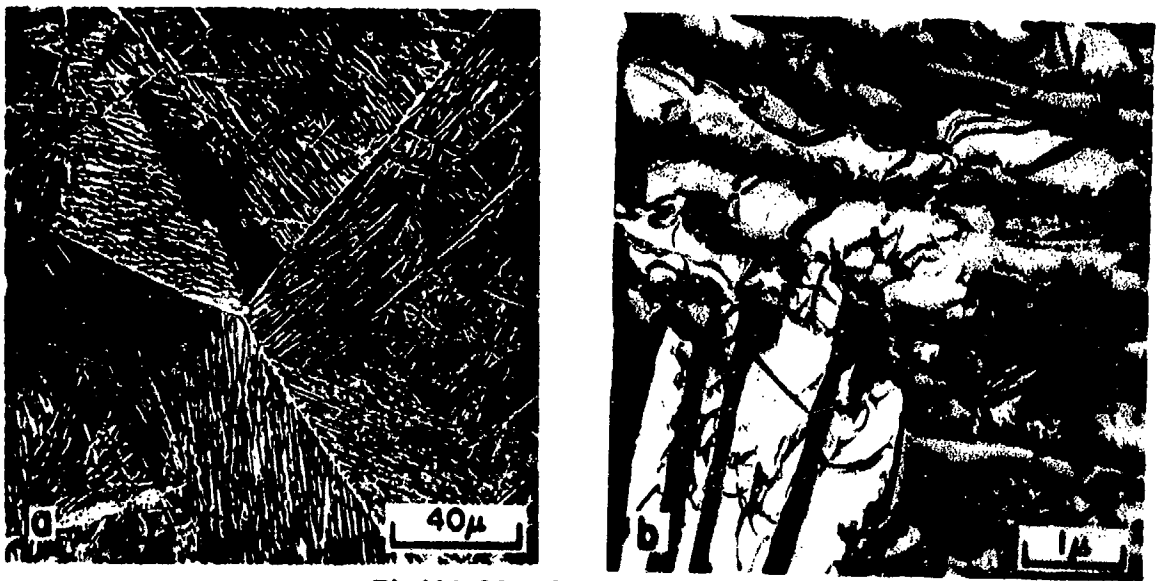

Figure 93 (a) and (b) Optical and transmission electron microscopy, respectively, of Heat B-2674, alloy addition of 2.0 Fe. (c) and (d) Optical and transmission electron microscopy, respectively, of Heat B-2676, alloy addition of 0.005 S.

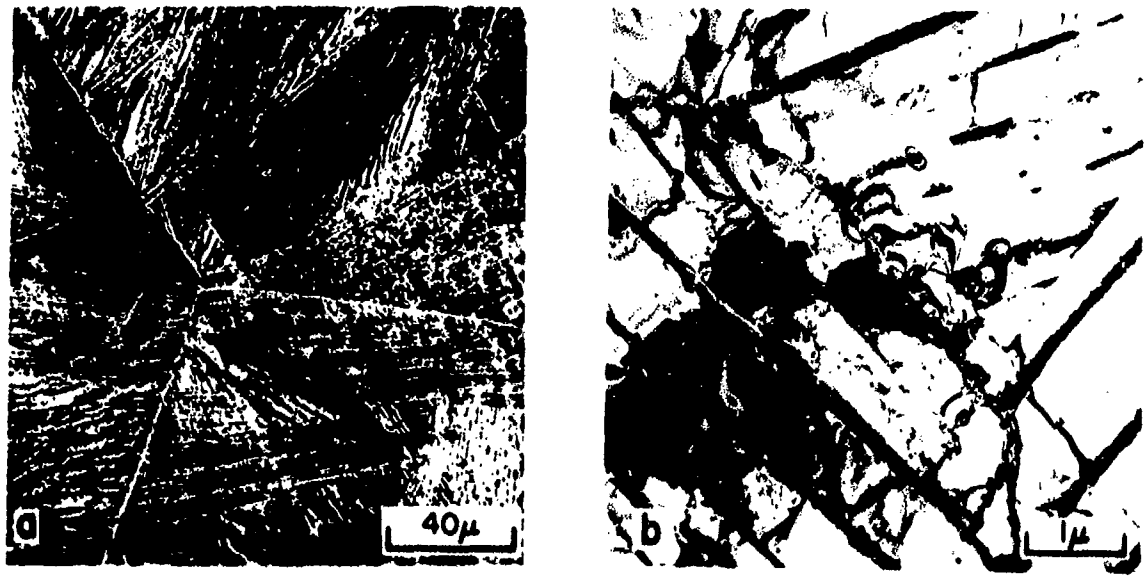

Ti-6Al-2Sn-2Zr-1Mo-0.010S

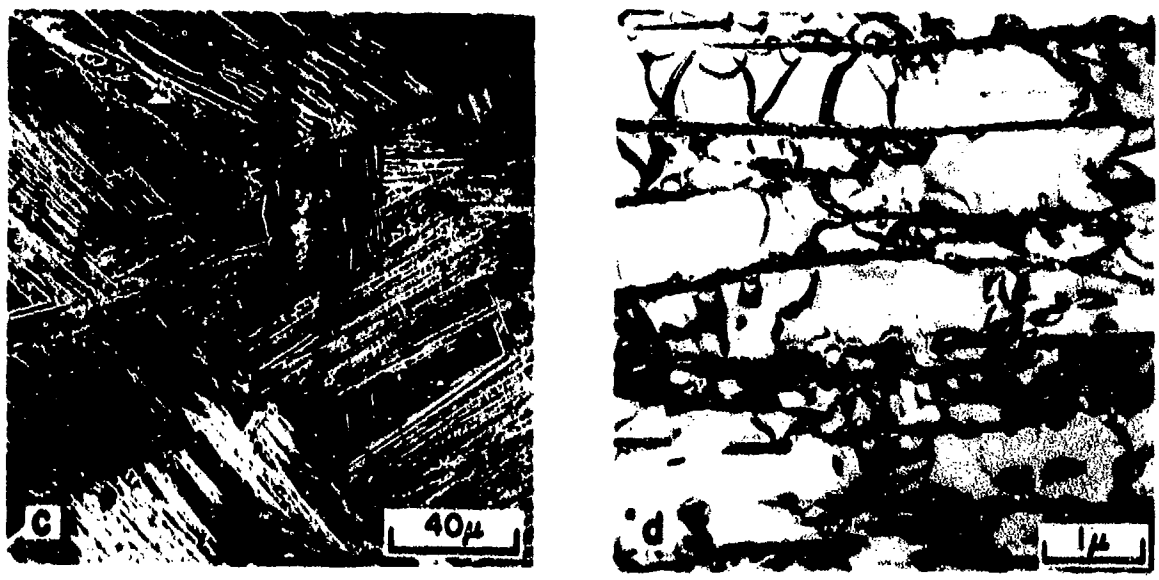

Ti-6Al-2Sn-2Zr-1Mo-0.020S

Figure 94 (a) and (b) Optical and transmission electron microscopy, respectively, of Heat B-2678, alloy addition of 0.010 S. (c) and (d) Optical and transmission electron microscopy, respectively, of Heat B-2680, alloy addition of 0.020 S.

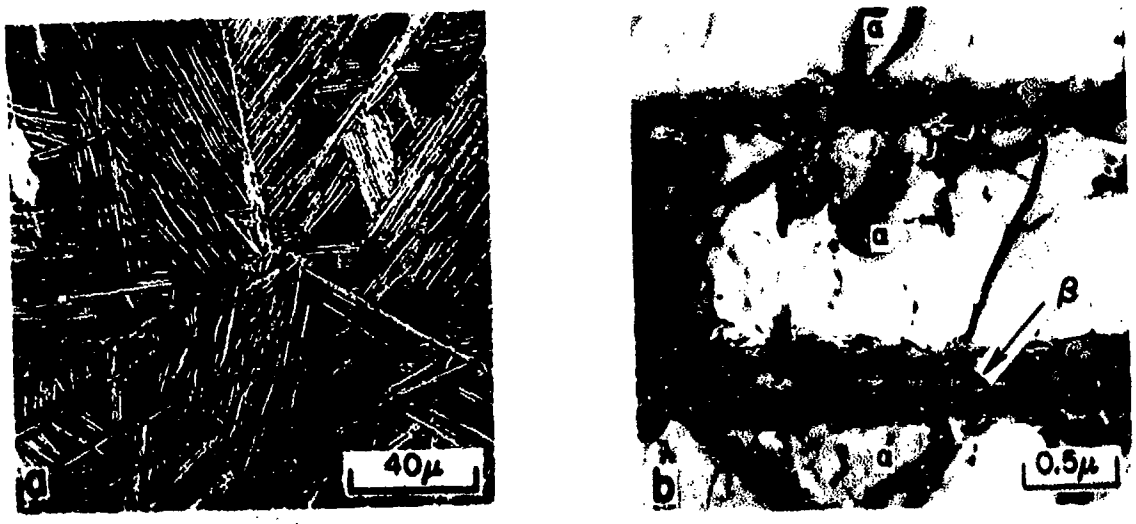

Ti-6Al-2Sn-2Zr-1Mo-.25Si-.25Fe

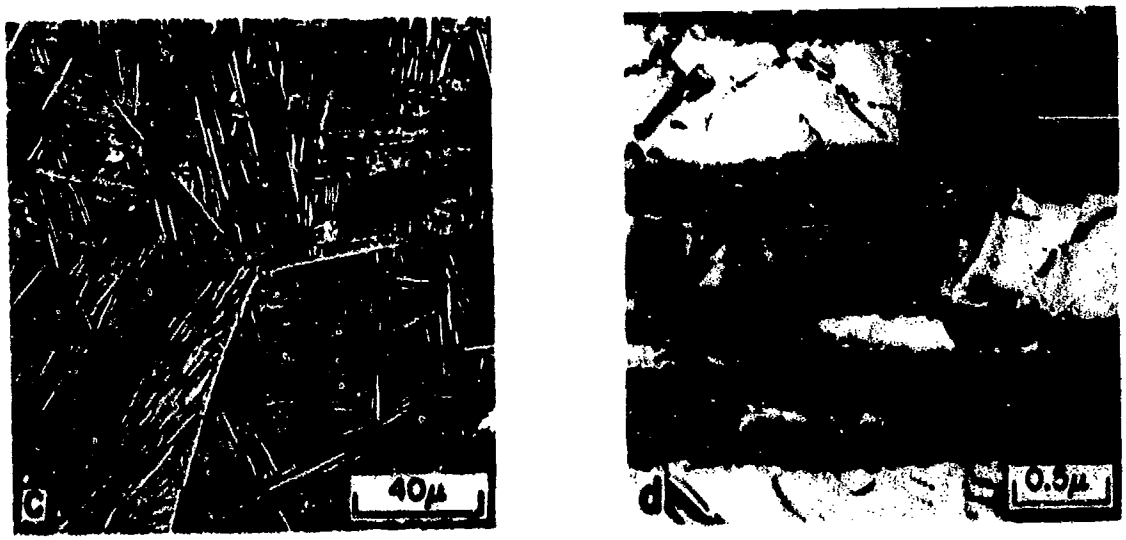

Ti-6Al-2Sn-2Zr-1Mo-.25Si-.5Fe

Figure 95 (a) and (b) Optical and transmission electron microscopy, respectively, of Heat B-2987, alloy additions of 1Mo-.25Si-.25Fe. (c) and (d) Optical and transmission electron microscopy, respectively, of Heat B-2989, alloy additions of 1Mo-.25Si-.5Fe.

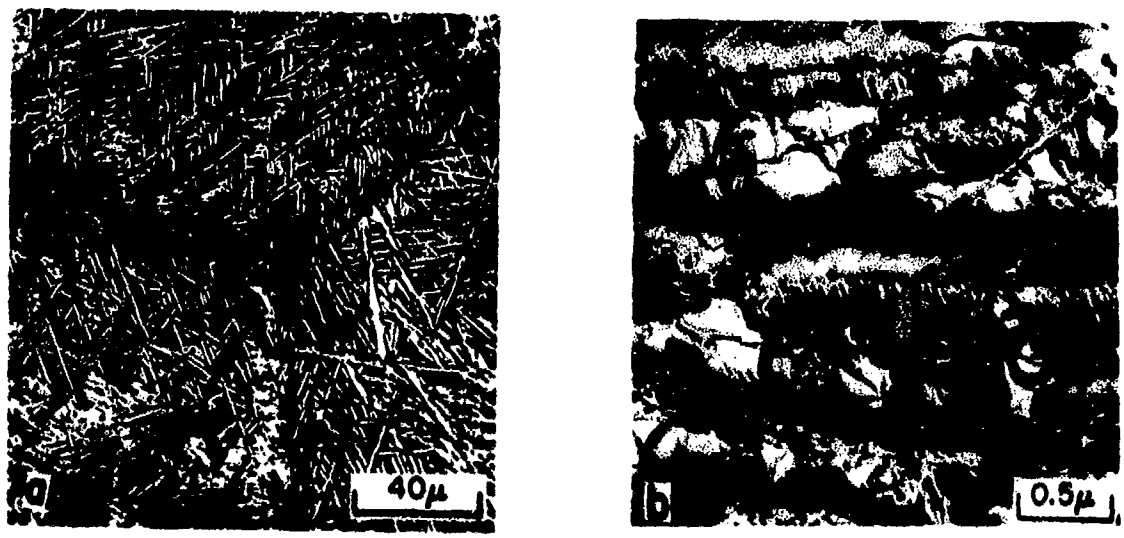

Ti-6Al-2Sn-2Zr-1Mo-.25Si-2.0Fe

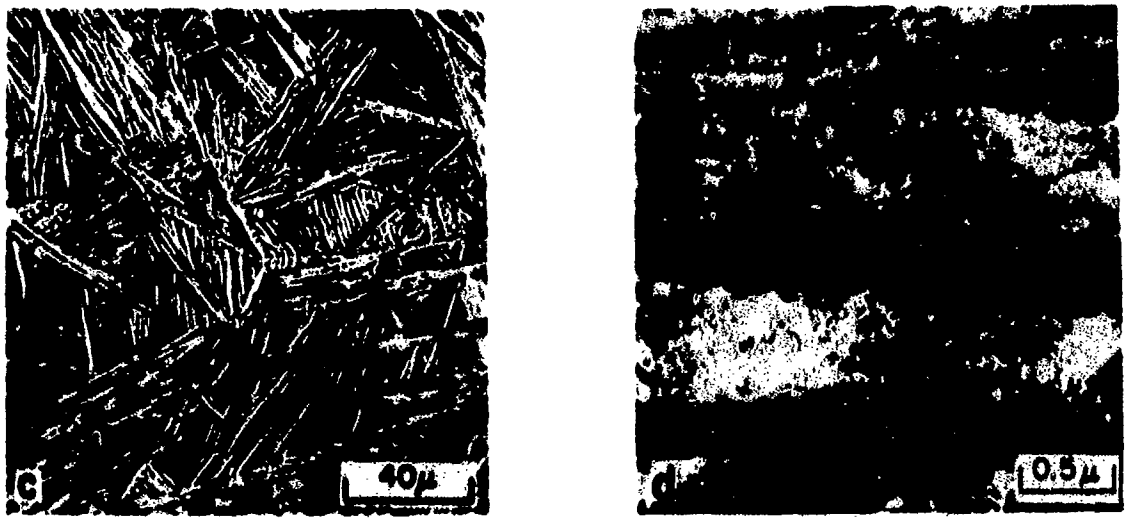

Ti-6Al-2Sn-2Zr-1Mo-.5Si-.25Fe

Figure 96 (a) and (b) Optical and transmission electron microscopy, respectively, of Heat B-2991, alloy additions of 1Mo-.25Si-2.0Fe. (c) and (d) Optical and transmission electron microscopy, respectively, of Heat B-2993, alloy additions of 1Mo-.5Si-.25Fe.

Ti-6Al-2Sn-2Zr-1Mo-.5Si-.5Fe

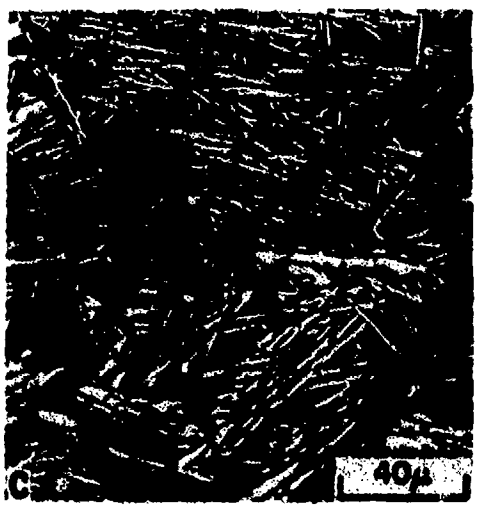

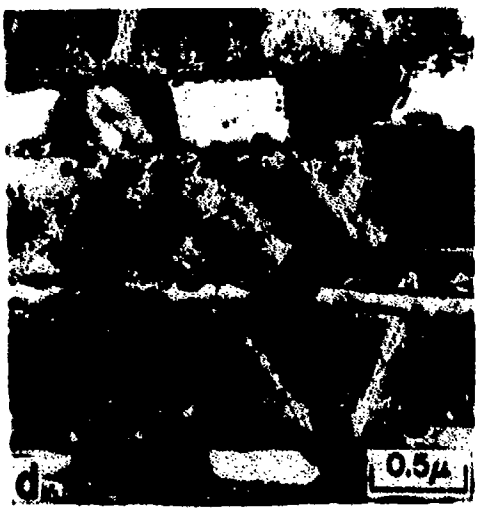

Ti-6Al-2Sn-2Zr-1Mo-.5Si-2.0Fe

Figure 97 (a) and (b) Optical and transmission electron microscopy, respectively, of Heat B-2995, alloy additions of 1Mo-.5Si-.5Fe. (c) and (d) Optical and transmission electron microscopy, respectively, of Heat B-2997, alloy additions of 1Mo-.5Si-2.0Fe.

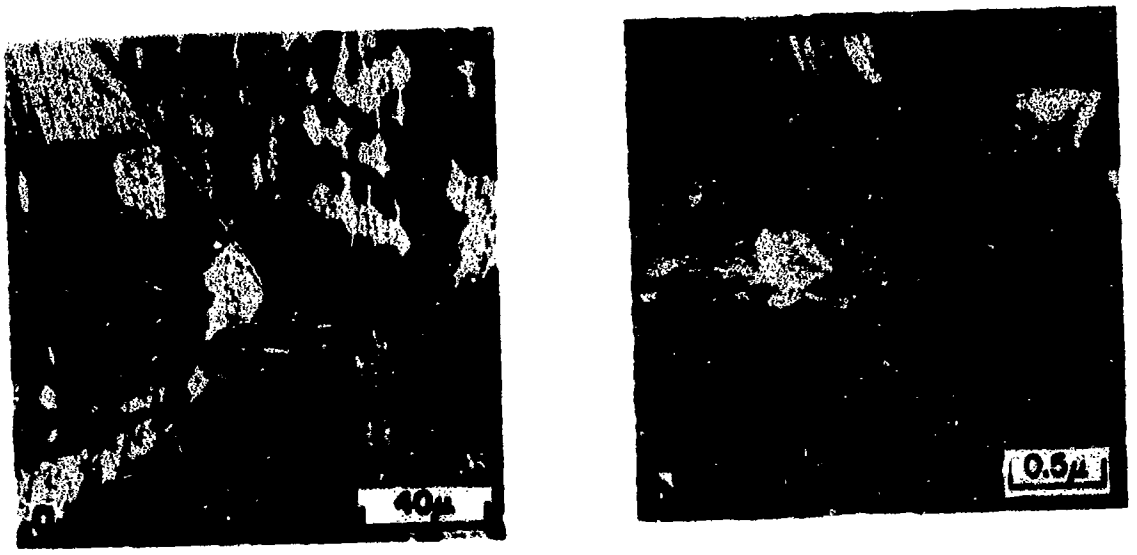

Ti-6Al-2Sn-2Zr-1Mo-.005S-.25Fe

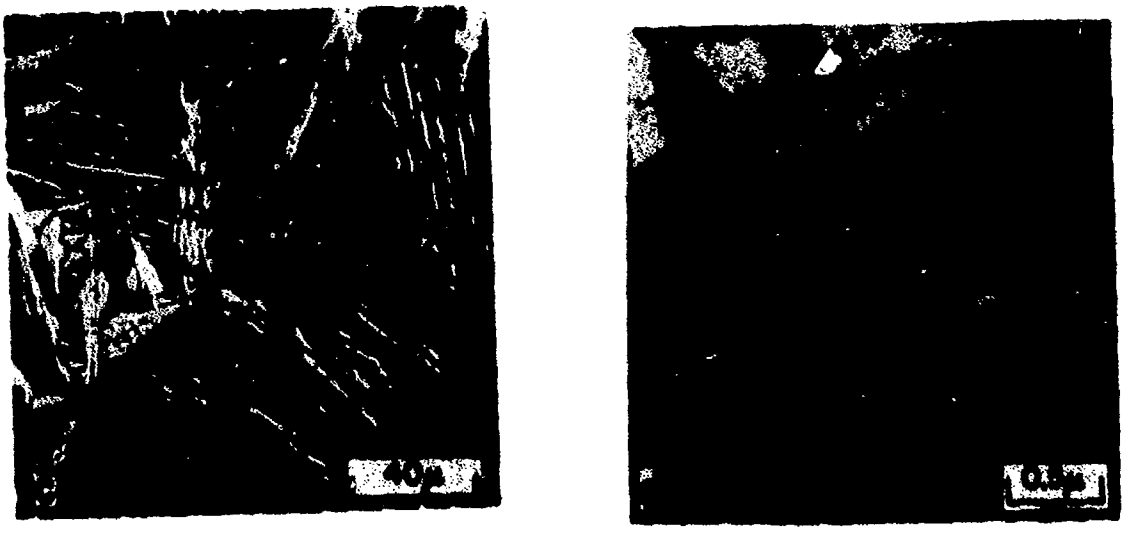

Ti-6Al-2Sn-2Zr-1Mo-.005S-.5Fe

Figure 98 (a) and (b) Optical and transmission electron microscopy, respectively, of Heat B-3080, alloy additions of 1Mo-.005S-.25Fe. (c) and (d) Optical and transmission electron microscopy, respectively, of Heat B-3082, alloy additions of 1Mo-.005S-.5Fe.

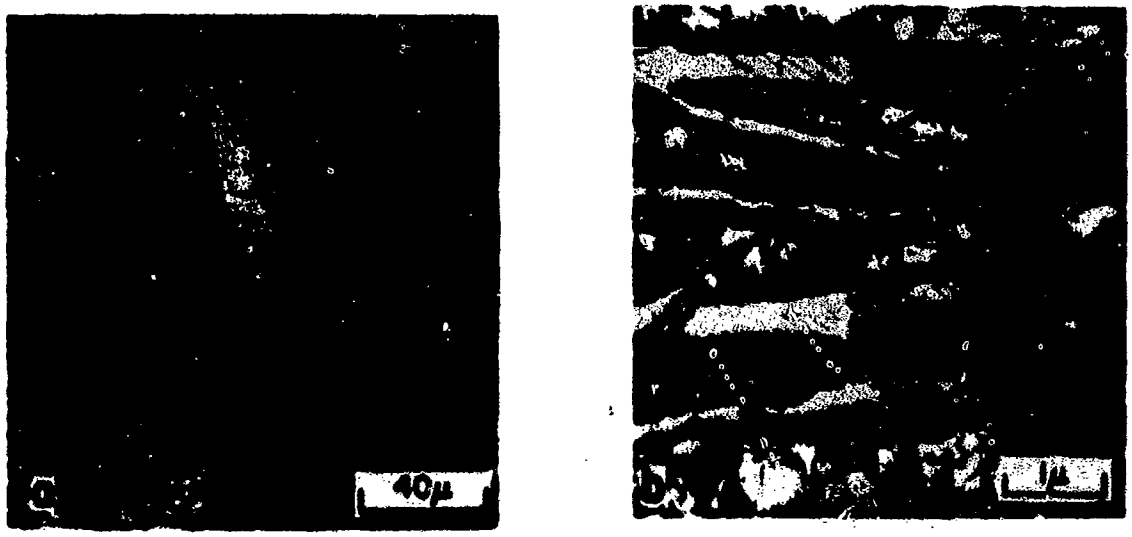

Ti-6Al-2Sn-2Zr-1Mo-.005S-2.0Fe

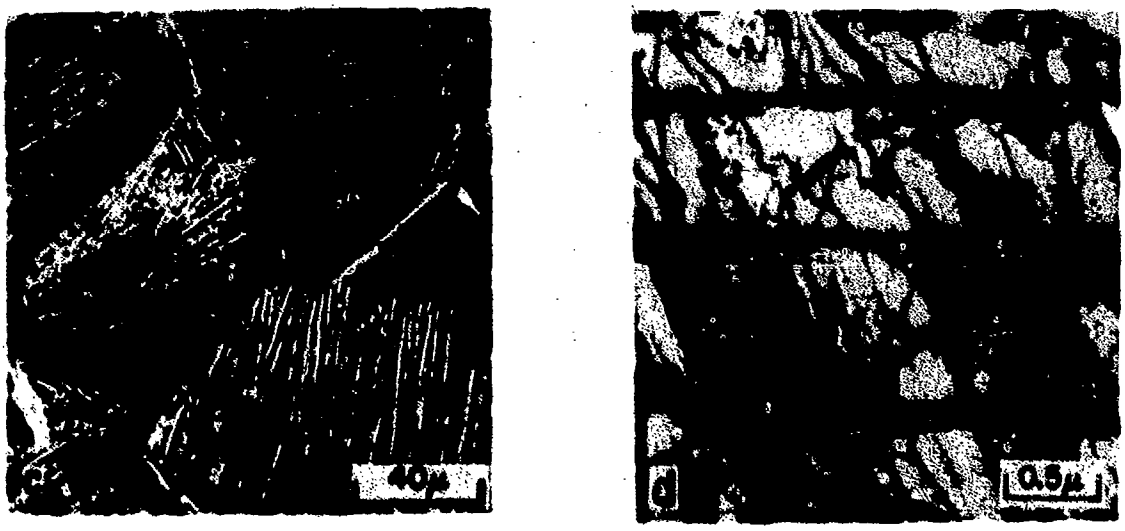

Ti-6Al-2Sn-2Zr-1Mo-.02S-.25Fe

Figure 99 (a) and (b) Optical and transmission electron microscopy, respectively, of Heat B-3009, alloy additions of 1Mo-.005S-2.0Fe. (c) and (d) Optical and transmission electron microscopy, respectively, of Heat B-3062, alloy additions of 1Mo-.02S-.25Fe.

Ti-6Al-2Sn-2Zr-1Mo-.02S-.5Fe

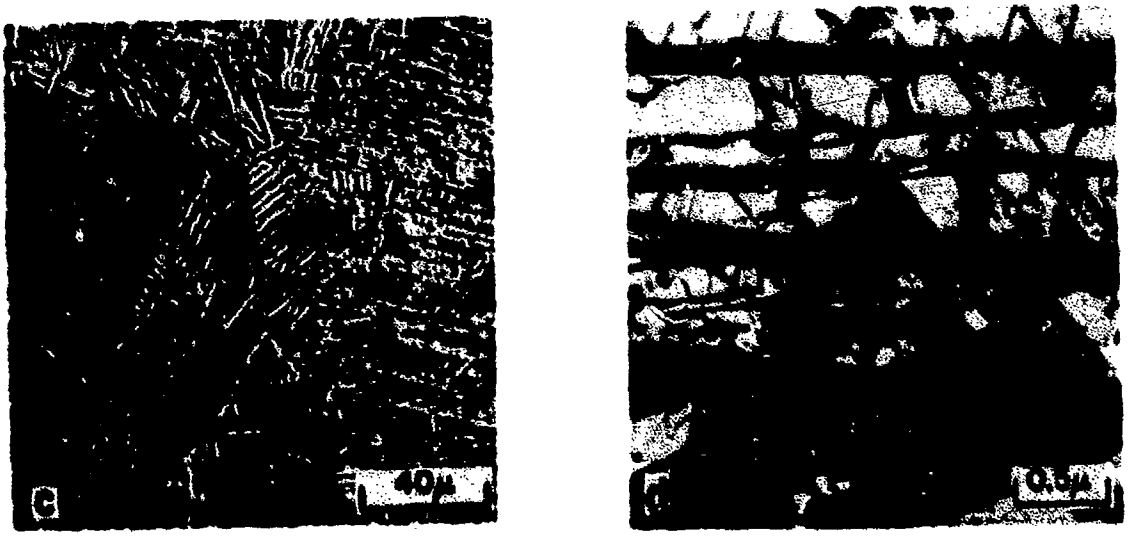

Ti-6Al-2Sn-2Zr-1Mo-.02S-2.0Fe

Figure 100 (a) and (b) Optical and transmission electron microscopy, respectively, of Heat B-3064, alloy additions of 1Mo-.02S-.05Fe. (c) and (d) Optical and transmission electron microscopy, respectively, of Heat B-3066, alloy additions of 1Mo-.02S-2.0Fe.

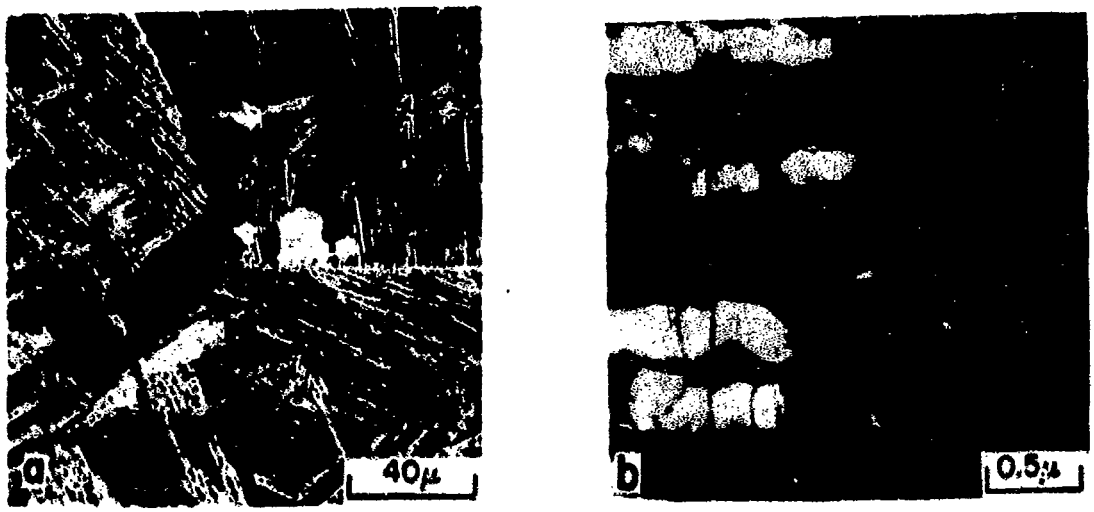

Ti-6Al-2Sn-2Zr-1Mo-.$12O_2$

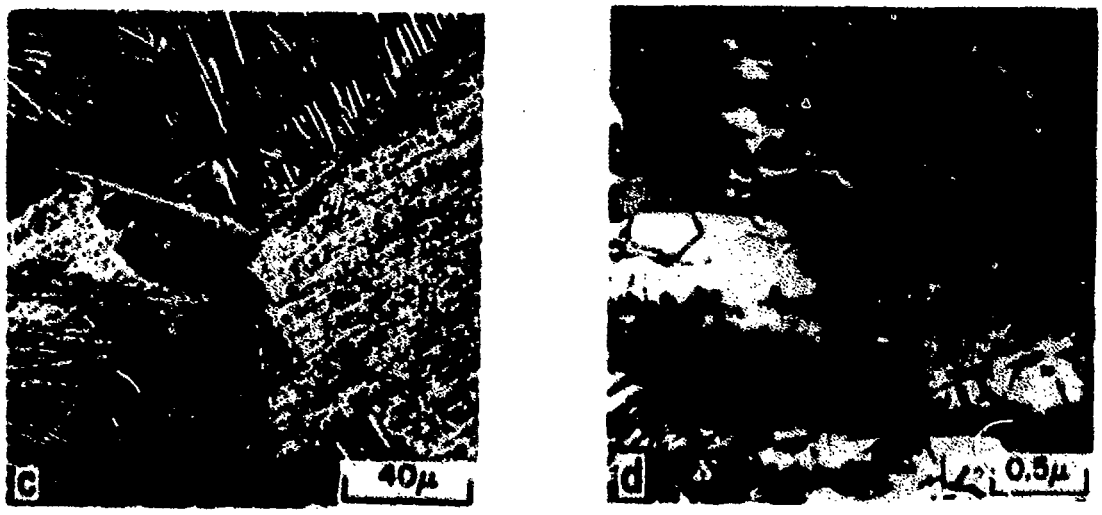

Ti-6Al-2SN-2Zr-1Mo-.$12O_2$-.25Si

Figure 101 (a) and (b) Optical and transmission electron microscopy, respectively, of Heat B-3011, alloy additions of 1Mo-.$12O_2$. (c) and (d) Optical and transmission electron microscopy, respectively, of Heat B-3013, alloy additions of 1Mo-.$12O_2$-.25Si.

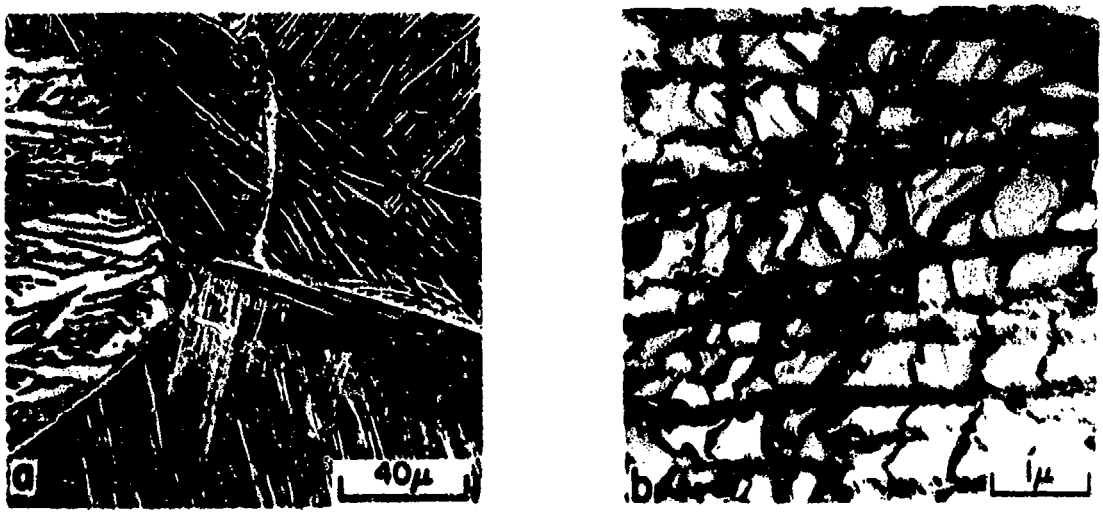

Ti-6Al-2Sn-2Zr-1Mo-.$12O_2$-.5Si

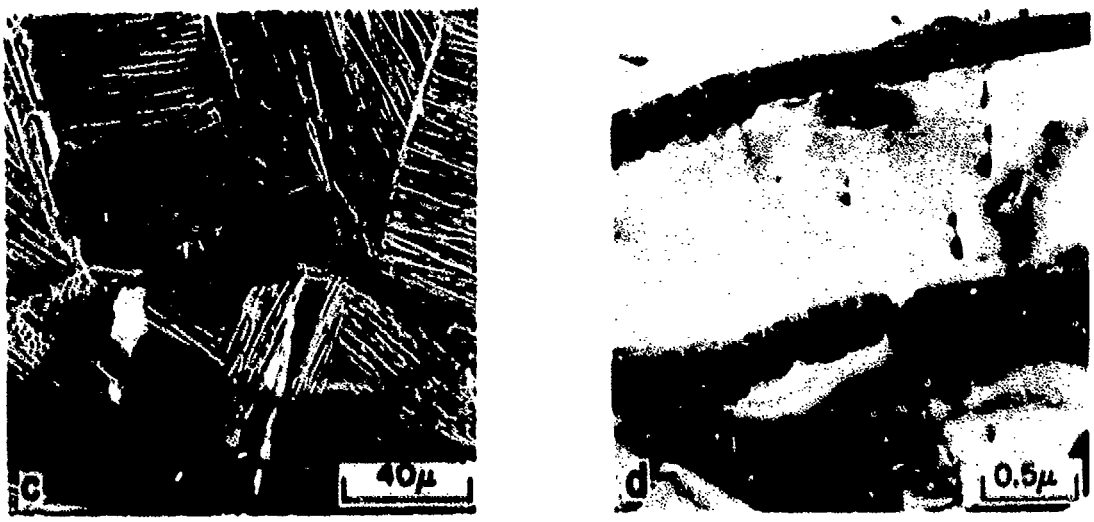

Ti-6Al-2Sn-2Zr-1Mo-.$18O_2$

Figure 102 (a) and (b) Optical and transmission electron microscopy, respectively, of Heat B-3015, alloy additions of 1Mo-.$12O_2$-.5Si. (c) and (d) Optical and transmission electron microscopy, respectively, of Heat B-3017, alloy additions of 1Mo-.$18O_2$.

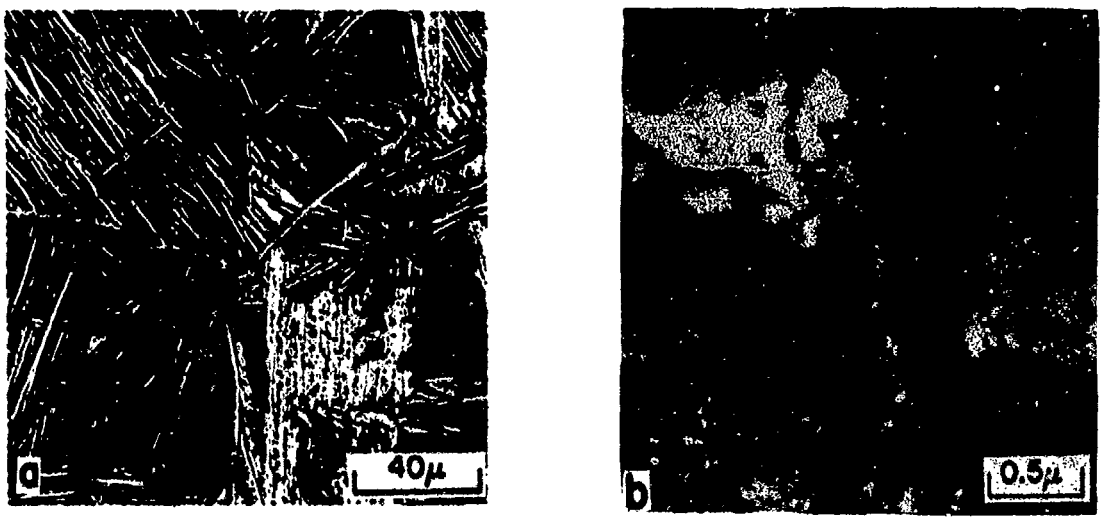

Ti-6Al-2Sn-2Zr-1Mo-.$18O_2$-.25Si

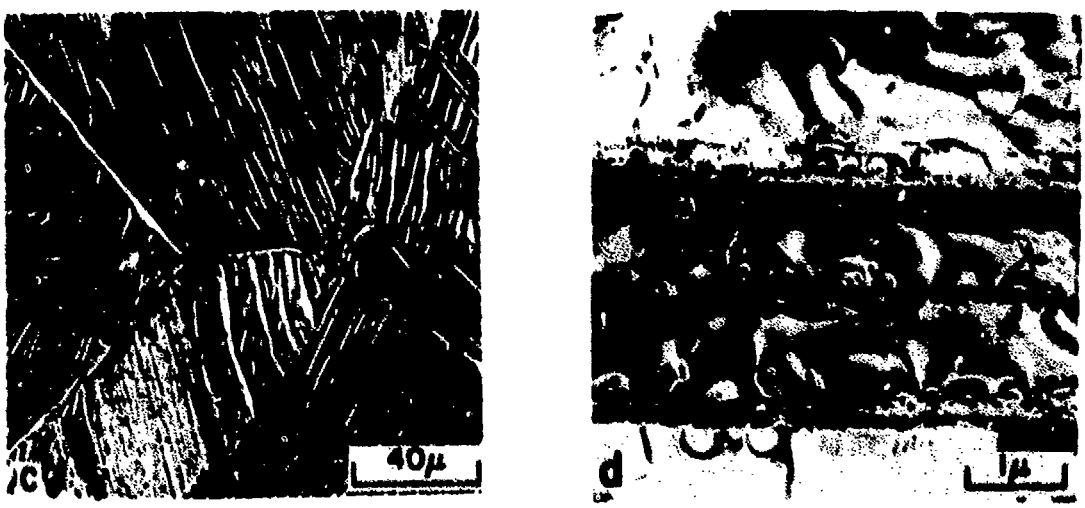

Ti-6Al-2Sn-2Zr-1Mo-.$18O_2$-.5Si

Figure 103 (a) and (b) Optical and transmission electron microscopy, respectively, of Heat B-3019, alloy additions of 1Mo-.$18O_2$-.25Si. (c) and (d) Optical and transmission electron microscopy, respectively, of Heat B-3021, alloy additions of 1Mo-.$18O_2$-.5Si.

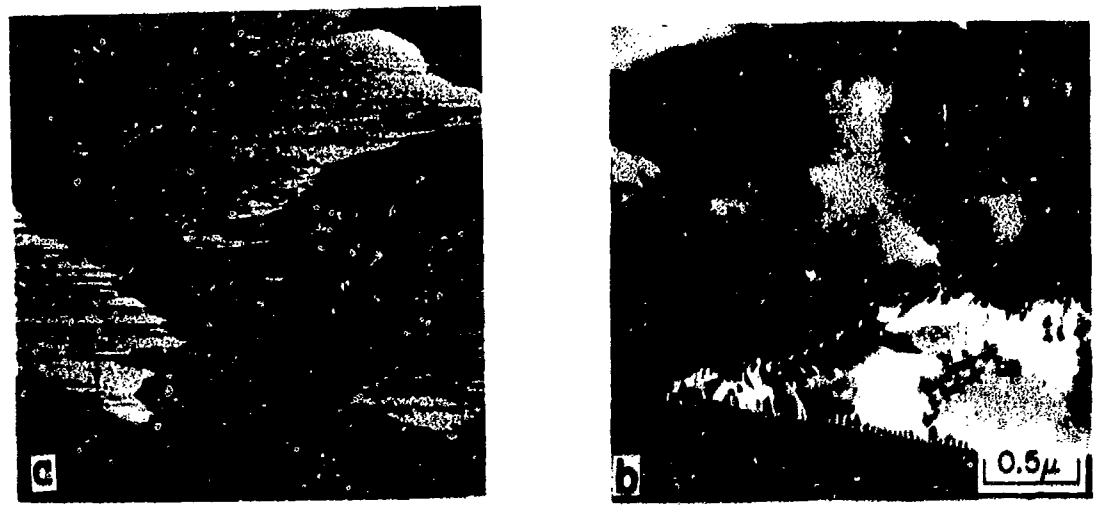

Ti-6Al-2Sn-2Zr

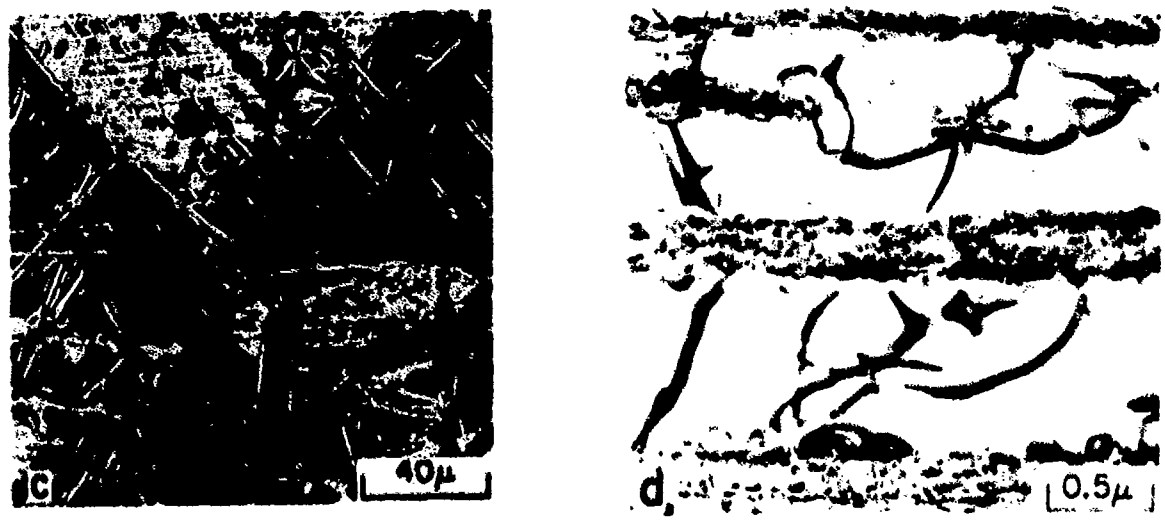

Ti-6Al-2Sn-2Zr-2Mo

Figure 104 (a) and (b) Optical and transmission electron microscopy, respectively, of Heat B-3023, with no alloying additions. (c) and (d) Optical and transmission electron microscopy, respectively, of Heat B-3025, with an alloy addition of 2Mo

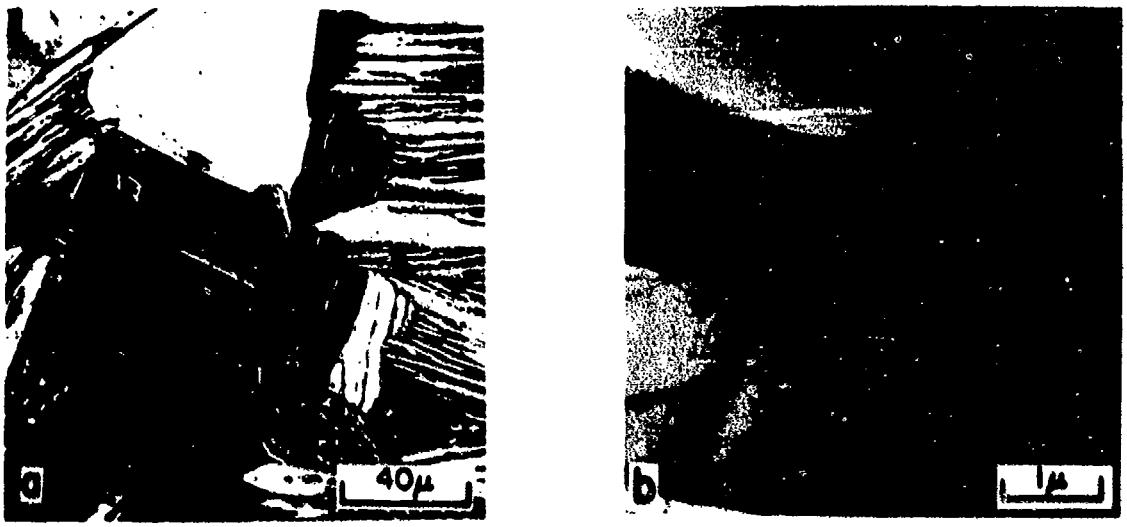

Ti-6Al-2Sn-2Zr-.25Si

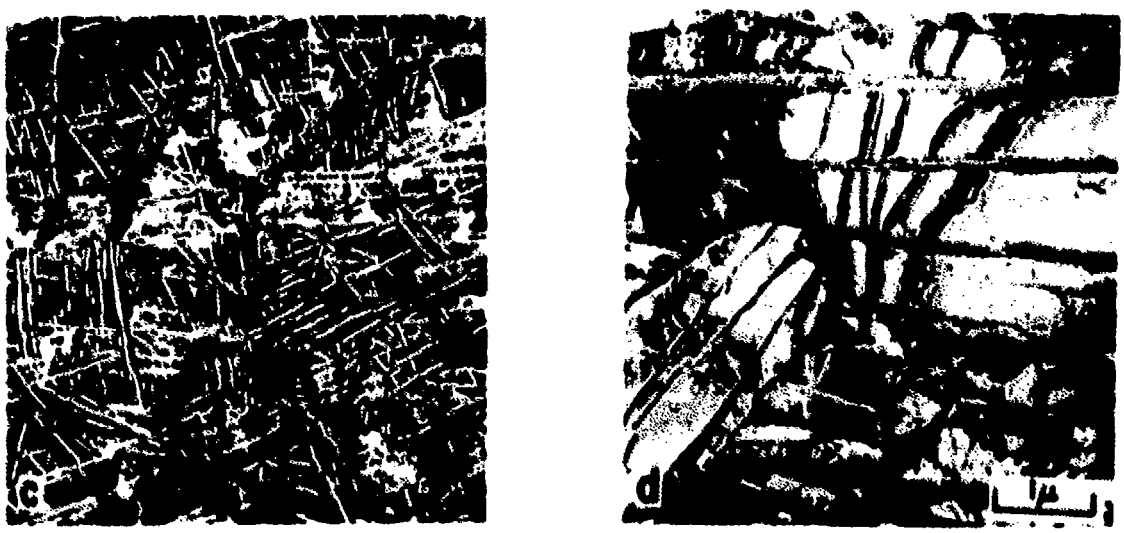

Ti-6Al-2Sn-2Zr-2Mo-.25Si

Figure 105 (a) and (b) Optical and transmission electron microscopy, respectively, of Heat B-3027, alloy addition of .25Si. (c) and (d) Optical and transmission electron microscopy, respectively, of Heat B-3051, alloy additions of 2Mo-.25Si.

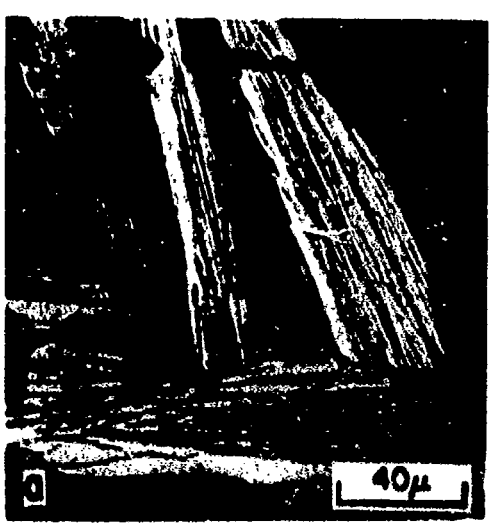

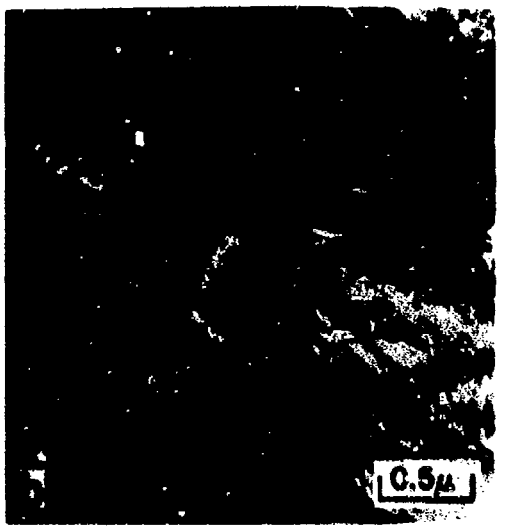

Ti-6Al-2Sn-2Zr-.5Si

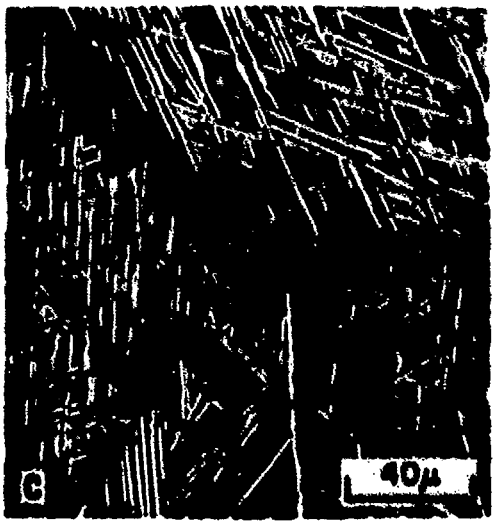

Ti-6Al-2Sn-2Zr-2Mo-.5Si

Figure 106 (a) and (b) Optical and transmission electron microscopy, respectively, of Heat B-3031, with an alloy addition of .5Si. (c) and (d) Optical and transmission electron microscopy, respectively, of Heat B-3033, alloy additions of 2Mo-.5Si.

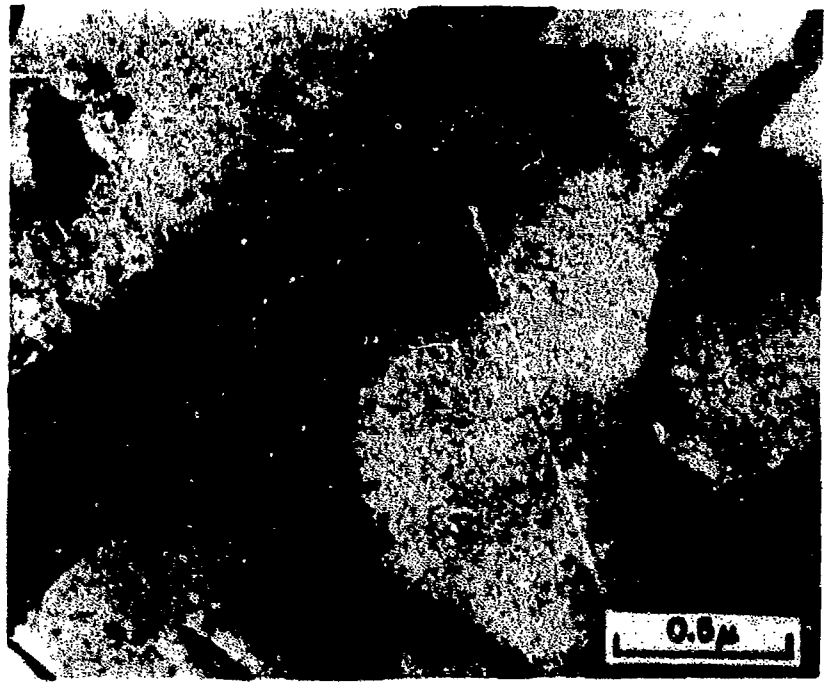

Figure 107 Ti-6Al-2Sn-2Zr-1Mo-1Fe alloy (1300°F age) showing complete absence of precipitation on dislocations.

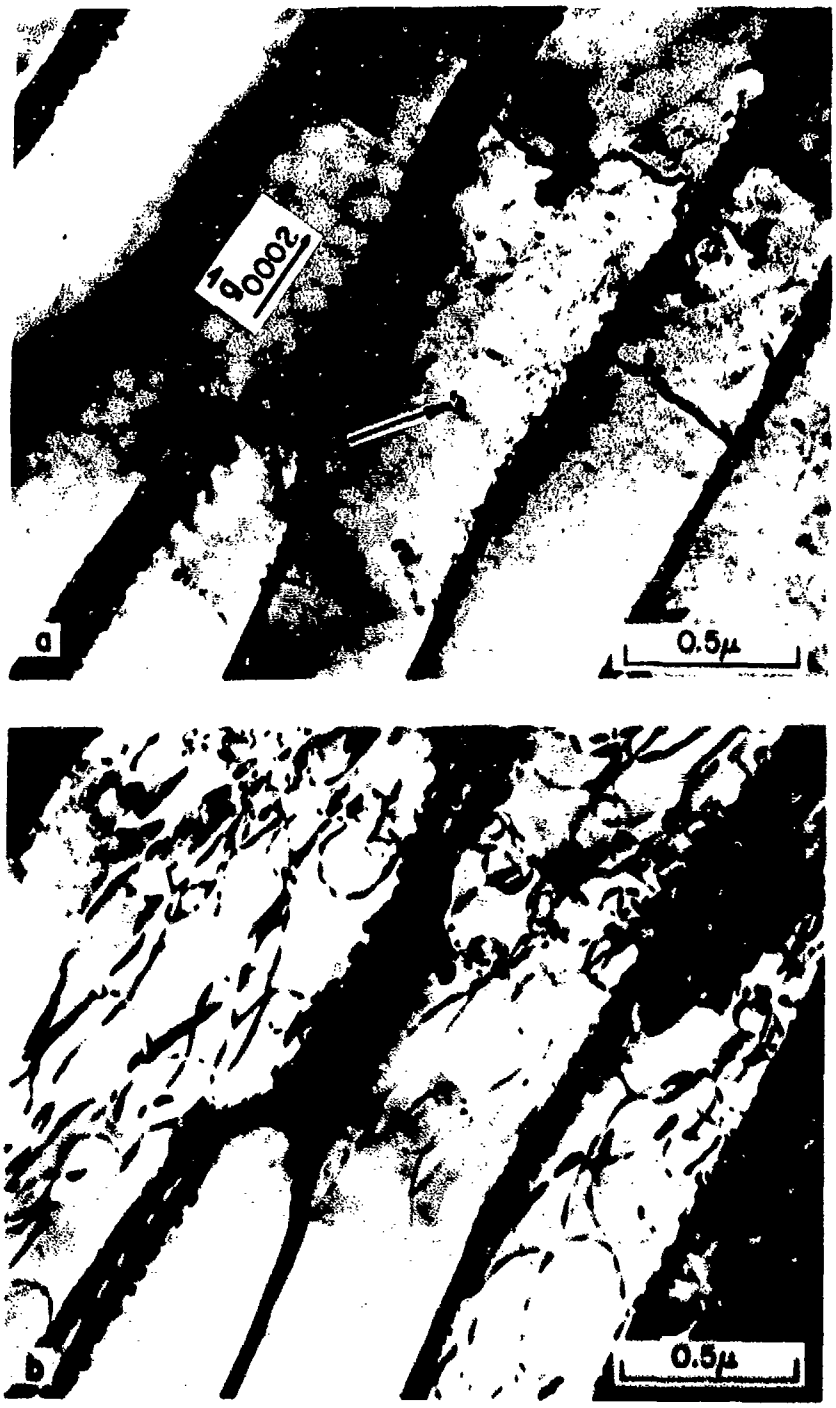

Figure 103 Ti-6Al-2Sn-2Zr-1Mo-.05Si alloy (1300°F age) strained 1.5% at 1000°F at an average strain rate of 6×10^{-4} hr^{-1} showing (a) precipitates on dislocations and strong residual contrast near arrow imaged with 0002 reflection to show only $\vec{c}+\vec{a}$ dislocations and precipitates, (b) same area imaged with a $10\bar{1}1$ reflection showing both $\vec{a}$ and $\vec{c}+\vec{a}$ dislocations.

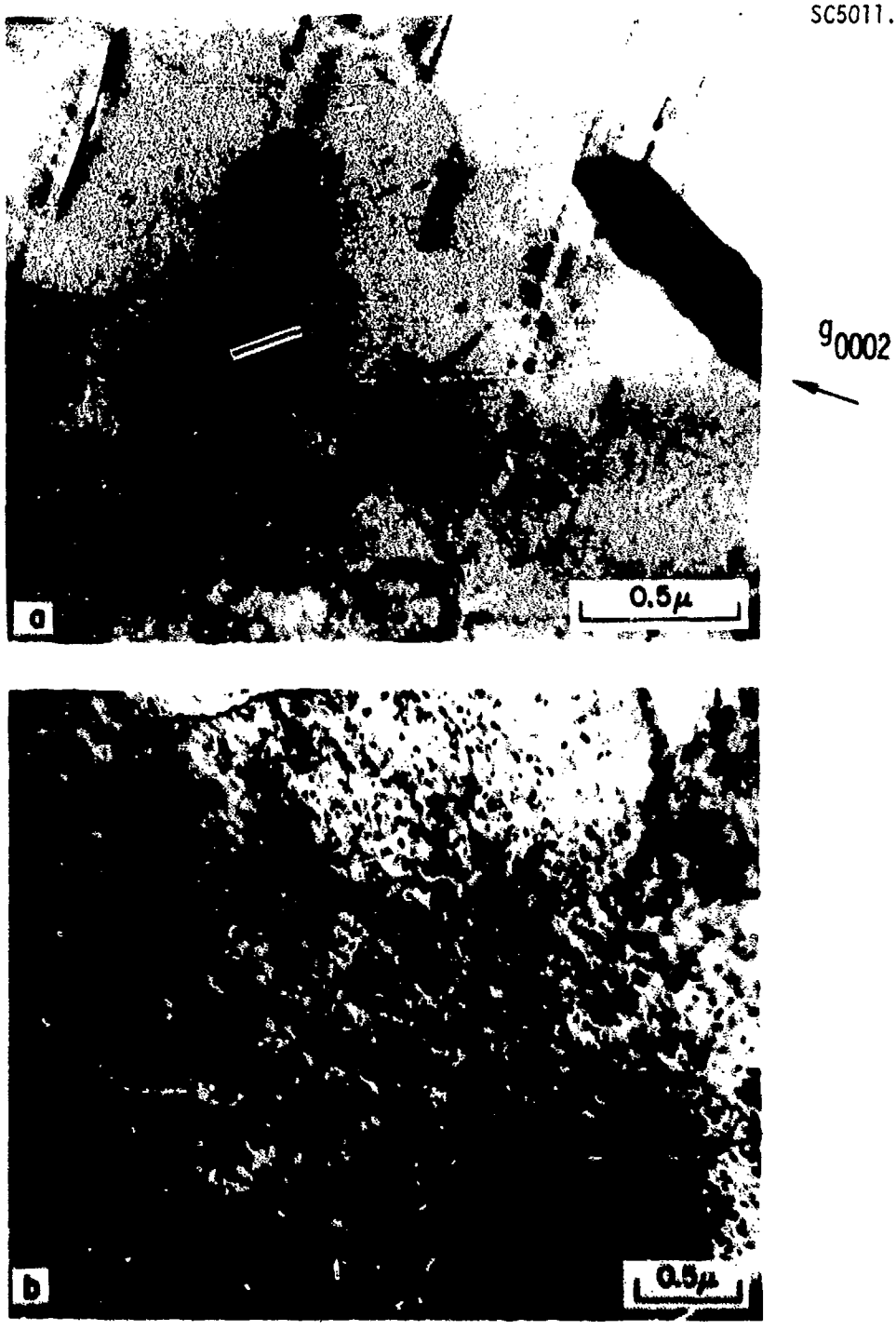

Figure 109 Ti-6Al-2Sn-2Zr-1Mo-0.5Si alloy heat treated at 1900F/15 min AC and 1100F/8 hr AC after a creep strain of 2.24% at an average strain rate of 1×10^{-4} hr^{-1} showing (a) high magnification image and (b) low magnification image; low contrast features are precipitates on dislocations imaged with a 0002 reflection (arrowed in (a))

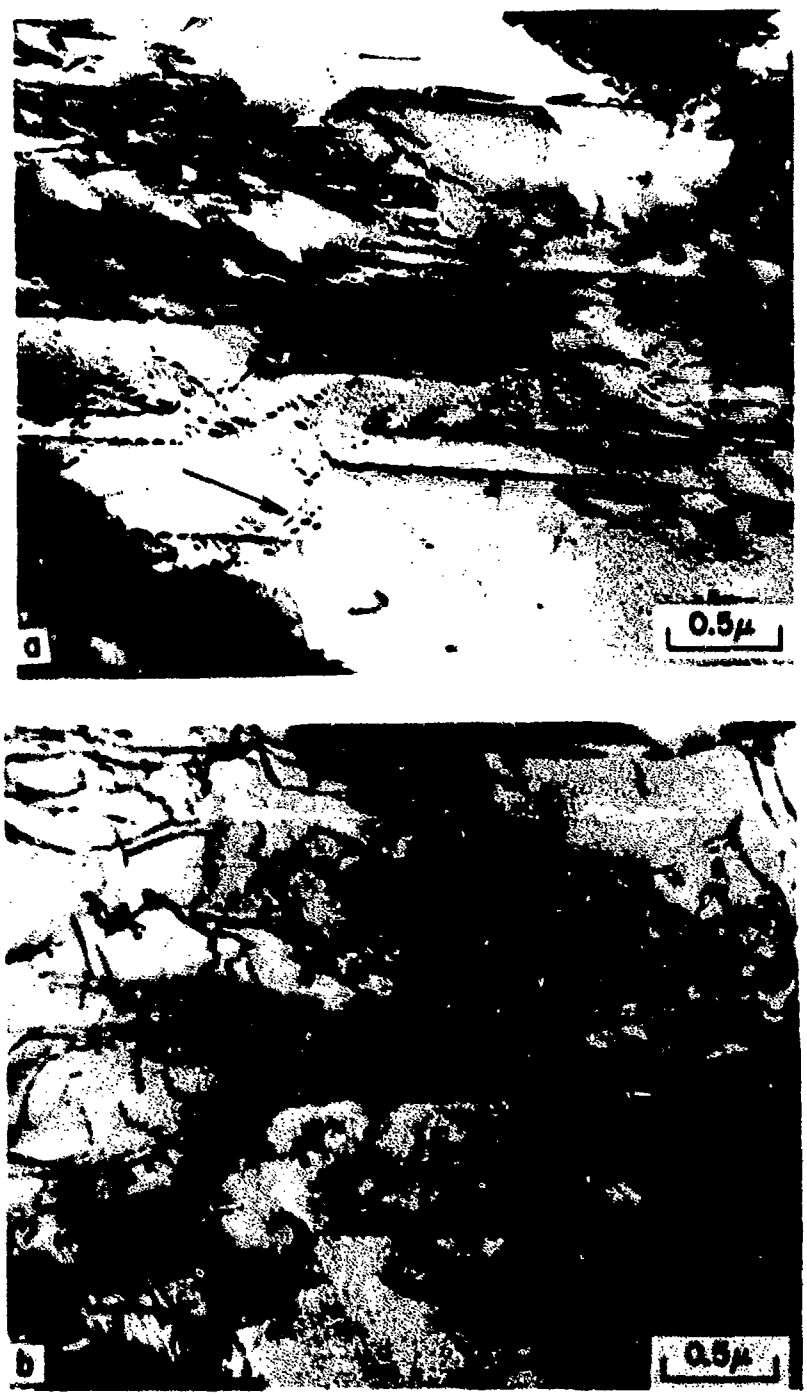

Figure 110 Ti-6Al-2Sn-2Zr-1Mo-0.5Si alloy (aged 1300°F) after a creep strain of 0.2 percent at an average strain rate of 2×10^{-5} hr^{-1}. Arrow shows an example of precipitation of Si on dislocations.

References

1. Parris, W.M., and Russell, H.A., "A New Titanium Alloy for Elevated Temperature Application," in Titanium Science and Technology, Jaffee and Burte, Eds. Plenum Press, New York, 1973, p. 2219.
2. Russo, P.A., Seagle, S.R., and Bomberger, H.B., "Development of a 900F Titanium Alloy," AFML-TR-70-125.
3. Redden, T.K., and Shamblen, C.E., "900F Titanium Alloy Development," AFML-TR-70-168.
4. Anthony, K.C., "Composition and Structure of Silicide Precipitate in Complex Titanium (6Al-3Sn-3Zr)-Silicon Alloys," Trans. Met. Soc. of AIME, Vol. 242, p. 1454, July (1968).
5. Paton, N.E., and Mahoney, M.W., "Creep of Titanium-Silicon Alloys," Met. Trans., Vol. 7A, p. 1685 (1976).
6. Rosenberg, H.W., "Alloying Ti for High Temperature Use - Critical Review," Titanium Science and Technology, Jaffee and Burte, Eds., Plenum Press, New York, 1973.
7. Flower, H.M., Swann, P.R., and West, D.R.F., Met. Trans. Vol. 2, p. 3289 (1971).
8. Annual Book of ASTM Standards, Part 31, p. 960 (1973).
9. Brownlee, K.A., "Industrial Experimentation," pp. 52-54.
10. Mahoney, M.W., and Paton, N.E., "Investigation of Basic Creep Mechanisms," Final Report on Contract No. N00019-75-C-0104, September 1975.
11. Cahn, R.W. (editor), Physical Metallurgy, John Wiley and Sons, New York, 1965, p. 806.
12. Chesnutt, J.C., Frandsen, J.D., Thompson, A.W., and Williams, J.C., "Influence of Metallurgical Factors on the Fatigue Crack Growth Rate in Alpha-Beta Titanium Alloys," Quarterly Report on Contract F33615-74-C-5067, for October 1 to December 31, 1974.

13. Mahoney, M.W., and Paton, N.E., "The Influence of Gas Environments on Fatigue Crack Growth Rates in Types 316 and 321 Stainless Steel," Nuclear Tech., p. 290, Vol. 23, Sept. 1974.

14. James. L.A., "Fatigue-Crack Propagation in Austenitic Stainless Steels," Atomic Energy Review, Vol. 14, p. 37, No. 1 (1976).

15. Paton, N.E., and Spurling, R.A., "Hydride Habit Planes in Titanium-Aluminum Alloys," Met. Trans., Vol. 7A, p. 1769 (1976).

16. Mahoney, M.W., and Tetelman, A.S., "Effect of Microstructure on the Hot Salt Stress Corrosion Susceptibility of Titanium Alloys," Met. Trans., Vol. 7A, p. 1549 (1976).

17. Petersen, V.C., "Hot-Salt Stress-Corrosion of Titanium," Journal of Metals, p. 40, April 1971.

18. Rhodes, C.G., and Paton, N.E., "The Influence of Microstructure on Mechanical Properties in Ti-3Al-8V-6Cr-4Mo-4Zr (Beta-C)," submitted to Met. Trans.

•U.S. Government Printing Office: 1977 — 787-001/134